The Aerobic Cyclase Involved in (Bacterio)chlorophyll Biosynthesis

Guangyu Chen

A thesis submitted for the degree of Doctor of Philosophy

Department of Molecular Biology and Biotechnology

University of Sheffield

September 2016

Summary

Photosynthesis is essential for almost all life on Earth. Chlorophylls are essential for photosynthesis and are modified tetrapyrrole molecules containing a centrally chelated magneiusm ion and a unique isocyclic E ring. The formation of the E ring is catalysed by the magnesium-protoporphyrin IX monomethyl ester cyclase (the cyclase). Two fundamentally distinct types of the cyclase exist in photosynthetic organisms, utilising an oxygen atom from either water (the anaerobic cyclase) or molecular oxygen (the aerobic cyclase). The aerobic cyclase has remained an enigma for over 65 years and it was proposed to be a multi-subunit enzyme. The first subunit was identified in the purple bacterium *Rubrivivax gelatinosus* and designated as AcsF, which is the catalytic subunit and contains a di-iron binding motif. AcsF is conserved across all phototrophs that possess an aerobic cyclase. Ycf54 was identified as a possible second subunit in the cyanobacterium *Synechocystis* sp. PCC6803 and is conserved in all oxygenic phototrophs. Previous studies suggested that there are more, unknown subunits required for the aerobic cyclase.

This thesis focuses on studying the subunit composition of aerobic cyclase with extensive genetic engineering conducted in several photosynthetic bacteria. *Rhodobacter sphaeroides*, one of the principal model organisms to study bacterial photosynthesis, was shown to harbour a functional aerobic cyclase. BciE was subsequently identified to be the second aerobic cyclase subunit in this organism. Complementation profiles in a *Rubrivivax gelatinosus* mutant lacking both the anaerobic and aerobic cyclases lead to the identification of three classes of aerobic cyclase as represented by the enzymes from *Rhodobacter sphaeroides* (AcsF + BciE), *Rubrivivax gelatinosus* (AcsF) and *Synechocystis* sp. PCC6803 (AcsF + Ycf54), respectively. The distribution of BciE and Ycf54 across phototrophs is well correlated with the evolutionary history of the AcsF proteins. A suppressor screen conducted with a Ycf54-lacking mutant of *Synechocystis* sp. PCC6803 did not reveal any additional subunit of aerobic cyclase. Likewise, transposon mutagenesis performed in a *Rubrivivax gelatinosus* mutant lacking the anaerobic cyclase did not uncover any new subunit of aerobic cyclase. The aerobic cyclase activity was demonstrated *in vivo* with an *Escherichia coli* strain expressing the *Rubrivivax gelatinosus* AcsF protein, providing conclusive evidence that no additional subunit is required for the aerobic cyclase. Finally, the core pathway of chlorophyll biosynthesis, from protoporphyrin IX to chlorophyllide *a*, was successfully constructed in *Escherichia coli*.

To my Mum

Acknowledgements

First, I would like to thank my supervisor Professor Neil Hunter FRS for his continued support and advice throughout the four years I have been with the lab. He demonstrates to me every day how to be a great scientist; passion, dedication, hard work and collaboration. Thanks for leading me to the way of scientific thinking. Thanks for his warm hospitality for inviting me to his house several times.

I would like to thank Dr Wei Huang for introducing me to Neil for my PhD study. Thanks for his efforts to make my PhD study in UK real. Thanks for all his encouraging words and Chinese meal treats, which helped me a lot during my first two years of PhD.

I would like to thank Dr Daniel Canniffe for teaching me all the experimental techniques, all the inspirational discussions, showing me the proper scientific writing in English and helping me through lots of difficult times during my PhD. I have learnt so much and will learn more from him. Thanks for assuring me when I had serious self-doubt. Thanks for answering my requests no matter how busy he was, including my very late request of reviewing Chapter 7 of this thesis. I am really appreciated for all his help and support.

Thanks to Dr Andrew Hitchcock for all his advice and help whenever I asked since he joined this group. Thanks to Dr Roman Sobotka for his collaboration with me in the suppressor mutant work and all the 'transport service' during my visit in Trebon. Thanks to Dr John Olsen for his great engineering skills to 'rescue' me. Thanks to Dr Paul Davison for his patience to answer my endless questions. Thanks to Drs Sarah Hollingshead, Pu Qian, Jack Chidgey, Cvetelin Vasilev, Michael Cartron, Phil Jackson for their help during my PhD. Thanks to Elizabeth Martin and Dr Amanda Brindley for keeping things running in the lab. Thanks to everyone in Hunter's group. I enjoyed all the lab meals, beer drinking, pool competitions…

My PhD study was funded by a University of Sheffield Scholarship, which I am really grateful for.

I would like to thank my parents and sister for all their love, support and understanding throughout the four years. I haven't been home often and wasn't there when I was needed. I have missed lots of important family events. I hope in the end I did not make a wrong decision to go abroad for PhD study.

Table of Contents

Chapter 4 Identification of three classes of aerobic cyclase involved in (bacterio)chlorophyll biosynthesis _____ 101

Table of figures

Chapter 5

Chapter 6

Chapter 7

Table of tables

Chapter 7

Abbreviations

$\Delta G°'$	standard free energy change at pH 7
2D	two-dimensional
AA	amino acid residues
AAA+	ATPase associated with a variety of cellular activities
ABA	abscisic acid
AcsF	aerobic cyclisation system Fe-containing subunit
ALA	δ-aminolevulinic acid
ALAS	ALA synthase
Arabidopsis	*Arabidopsis thaliana*
ATP[γ-S]	adenosine 5'-[γ-thio]triphosphate
B-	bacterio
bch-	gene for bacteriochlorophyll biosynthesis
BLAST	basic local alignment search tool
Bpheid	bacteriopheophorbide
C.	*Chlamydomonas*
cfu	colony-forming units
Chl	chlorophyll
chl-	gene for chlorophyll biosynthesis
Chlide	chlorophyllide
CN	clear-native
CoA	Coenzyme A
Copro'gen	coproporphyrinogen III
COR	Chlide *a* oxidoreductase
CPO	Copro'gen oxidase
CTAB	cetyltrimethylammonium bromide
cyclase	Mg-protoporphyrin IX monomethyl ester cyclase
Deutero	deuteroporphyrin IX
DMSO	dimethyl sulfoxide
DPOR	light-independent (dark-operative) PChlide reductase
DV	divinyl
DVR	divinyl reductase
Dxs	1-deoxy-D-xylulose 5-phosphate synthase
E.	*Escherichia*
EDTA	ethylenediaminetetraacetic acid
EM	electron microscopy
EPR	electron paramagnetic resonance
GG	geranylgeraniol
GluTR	Glu-tRNA reductase
Glu-tRNA	glutamyl-tRNA
GSA	glutamate-1-semialdehyde
GSAM	GSA 2,1-aminomutase
GUN	genomes uncoupled
HE	hydroxyethyl
hem-	gene for haem biosynthesis
HEPES	2-[4-(2-hydroxyethyl)piperazin-1-yl]ethanesulfonic acid
HMB	hydroxymethylbilane
HPLC	high performance liquid chromatography
IPTG	isopropyl β-D-1-thiogalactopyranoside
JTT	Jones-Taylor-Thornton

K_d	dissociation constant	*Rba.*	*Rhodobacter*
K_m	Machaelis constant	RED	reductases, epimerases, and dehydrogenases
LB	Luria-Bertani		
LCAA	low chlorophyll accumulation A	rpm	revolutions per minute
		Rvi.	*Rubrivivax*
MES	2-morpholin-4-ylethanesulfonic acid	SAH	*S*-adenosyl-L-homocysteine
MgP	Mg-protoporphyrin IX	SAM	*S*-adenosyl-L-methionine
MgPME	Mg-protoporphyrin IX monomethyl ester	SDS	sodium dodecyl sulfate
		SNP	single-nucleotide polymorphism
MV	monovinyl		
MW	molecular weight	SOC	super optimal broth with catabolite repression
NMR	nuclear magnetic resonance		
		spp.	species
NTRC	NADPH-dependent thioredoxin reductase C	STE	sodium-Tris-EDTA
		Synechocystis	*Synechocystis* sp. PCC6803
OD	optical density		
od-	oxygen-dependent	*T.*	*Thermosynechococcus*
oi-	oxygen-independent	TAE	Tris-acetate-EDTA
ORF	open reading frame	TBS	Tris-buffered saline
PAGE	polyacrylamide gel electrophoresis	TE	Tris-EDTA
		TES	N-Tris(hydroxymethyl) methyl-2-aminoethanesulfonic acid
PBG	pyrrole porphobilinogen		
PBGD	PBG deaminase		
PBGS	PBG synthase		
PChlide	protochlorophyllide	TIM	triosephosphate isomerase
PGC	photosynthesis gene cluster		
		Tris	Tris(hydroxymethyl)amin omethane
PLP	pyridoxal 5'-phosphate		
POR	light-dependent NADPH:PChlide oxidoreductase	UROD	Uro'gen decarboxylase
		Uro'gen	uroporphyrinogen III
		UROS	Uro'gen synthase
		V	vinyl
PP	pyrophosphate	WRKY	Trp-Arg-Lys-Tyr protein domain
PPO	Proto'gen oxidase		
Proto	protoporphyrin IX		
Proto'gen	protoporphyrinogen IX	WT	wild type
PS	photosystem	ycf	hypothetical chloroplast open reading frame
psi	pounds per square inch		
PVDF	polyvinylidene fluoride		
RATE	random amplification of transposon ends		

Chapter 1

Introduction

1.1 Photosynthesis

Photosynthesis is the biological process by which solar energy is harvested and converted to a chemical form that can be stored and used to power life. Photosynthesis is essential for almost all life on Earth by maintaining the oxic atmosphere, supplying all organic compounds, and providing most of the energy. Only chemolithoautotrophs are independent from photosynthesis. Two fundamentally different types of photosynthesis are known so far: one operates via rhodopsins, which are light-driven proton or chloride pumps; the other carries out (bacterio)chlorophyll ((B)Chl)-dependent light harvesting and photochemistry. The latter is called (B)Chl-type photosynthesis and organisms carrying out this process are called chlorophototrophs accordingly.

(B)Chl-type photosynthesis is dominant on Earth and can be represented by the following general equation, first proposed by van Niel (1962):

$$2H_2A + CO_2 \xrightarrow{hv} (CH_2O) + H_2O + 2A$$

where, with the input of light energy (hv), hydrogen is transferred from the donor H_2A to CO_2 to form organic compound or carbohydrate (CH_2O) with the by-product A from oxidation of H_2A. Photosynthesis can be classified as oxygenic and anoxygenic types, depending on whether O_2 is produced in the process. Oxygenic photosynthesis is performed by plants, algae and cyanobacteria, whilst all phototrophic bacteria excluding the cyanobacteria carry out anoxygenic photosynthesis. Anoxygenic photosynthesis is able to utilise various compounds other than H_2O as the electron donor including hydrogen sulfide, elemental sulfur, thiosulfate, molecular hydrogen, ferrous ion, nitrite, and small organic compounds such as acetate and succinate.

Photosynthesis consists of two sets of reactions. In the first set of reactions, traditionally called the light reactions, light energy is captured, transferred and utilised to energise an electron from a (B)Chl pigment in the reaction centre. The high-energy electron then flows down an electron transport chain and is finally used to reduce $NADP^+$ to produce NADPH. A proton gradient is generated during the electron transport, which is used to drive ATP

synthesis. The second sets of reactions, known as the dark reactions, fix carbon via conversion of CO_2 to organic compounds, consuming ATP and NADPH, the products of the light reactions.

1.2 Photosynthetic organisms

Among the three domains of life, chlorophototrophs are identified within the *Bacteria* and *Eukarya* domains. The *Archaea* domain only contains bacteriorhodopsin-type photosynthesis, which is mechanistically different from (B)Chl-based photosynthesis, the topic of this thesis. Algae and plants are the two groups of eukaryotic organisms that are capable of photosynthesis. Despite the huge diversity of the *Bacteria* domain, only seven bacterial phyla have been reported to contain photosynthetic organisms (Zeng *et al.*, 2014): *Cyanobacteria*, *Proteobacteria*, *Chlorobi*, *Chloroflexi*, *Firmicutes*, *Acidobacteria*, and *Gemmatimonadetes*. The characteristics of each group of prokaryotic phototrophs are compared in **Table 1.1**.

Table 1.1 Characteristics of known groups of phototrophic prokaryotes[a]

Phototrophic bacteria	Phylum	Main pigments	Carbon fixation pathway	Reaction centre	Discovery
Cyanobacteria	Cyanobacteria	Chl *a/b/d/f*[b], carotenoids, phycobilins	Reductive pentose phosphate cycle	Types I, Type II	19th century
Purple bacteria	*Proteobacteria*	BChl *a/b*[c], carotenoids	Reductive pentose phosphate cycle	Type II	19th century
Green sulfur bacteria	*Chlorobi*	BChl *a/c/d/e*, carotenoids	Reductive tricarboxylate acid cycle	Type I	Early 20th century
Filamentous anoxygenic phototrophs	*Chloroflexi*	BChl *a/c*, carotenoids	3-hydroxypropionate bi-cycle	Type II	Pierson and Castenholz, 1974
Heliobacteria	*Firmicutes*	BChl *g*, carotenoids	Absent	Type I	Gest and Favinger, 1983
Chloroacidobacteria[d]	*Acidobacteria*	BChl *a/c*, carotenoids	Absent	Type I	Bryant *et al.*, 2007
Gemmatimonadetes[e]	*Gemmatimonadetes*	BChl *a*, carotenoids	Absent	Type II	Zeng *et al.*, 2014

[a] Modified from Zeng *et al.* (2014).

[b] Most only contain Chl *a*. Prochlorophytes also contain Chl *b*. Some types also contain Chl *d* or *f*.

[c] Either BChl *a* or *b*, not both in a species.

[d] Only one species has been isolated so far, *Chloracidobacterium thermophilum* B.

[e] Only one species has been isolated so far, *Gemmatimonas* sp. AP64.

The quality and intensity of light in different environments can be significantly variable. Phototrophs have adapted to utilise the available portions of the solar spectrum in their natural habitat. The absorption spectra of some groups of photosynthetic bacteria are shown in **Figure 1.1**. BChl-containing photosynthetic bacteria can use light in the near infrared region (700~1000 nm), which is not utilised by Chl-containing oxygenic phototrophs.
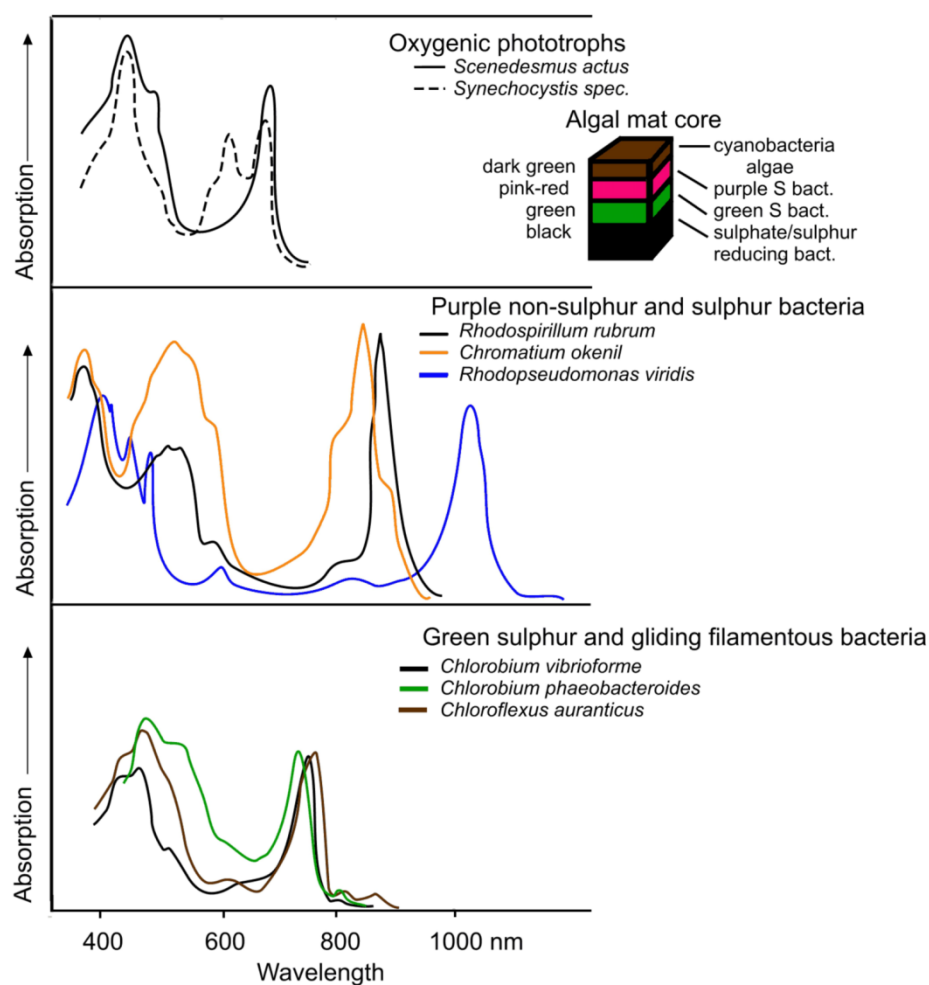
Figure 1.1 Absorption spectra of some groups of photosynthetic bacteria

Heliobacteria, *Chloroacidobacteria* and *Gemmatimonadetes* are not included. A schematic diagram of a representative algal mat core is shown at the right side of the spectra of oxygenic phototrophs. Shown are from Canniffe (2010).

1.2.1 Algae and plants

Algae are a large, diverse and polyphyletic group of photosynthetic eukaryotes. Algae carry out oxygenic photosynthesis in their chloroplasts, which ultimately derived from an engulfed cyanobacterium in a single primary endosymbiosis. The three subgroups of algae derived directly from a single primary endosymbiotic event are the green algae, the red algae and the

glaucophytes (Archibald, 2005). The evolution of all other algae involved secondary endosymbiotic events, in which a primary chloroplast-containing alga became incorporated within a non-photosynthetic eukaryote (Archibald, 2005). As the likely progenitors of plants, the green algae have been extensively studied. *Chlamydomonas* (*C.*) *reinhardtii*, a unicellular green alga, is widely used as a model organism to study many biological processes including photosynthesis.

Plants are multicellular eukaryotes derived from the green algae. They conduct oxygenic photosynthesis in their chloroplasts. As with the green algae, plants contain Chl *b* in addition to Chl *a*, which together serve as the main accessory pigments in light-harvesting complexes. Plants can be divided into the non-vascular (mosses, hornworts and liverworts) and the vascular (seed plants and ferns) forms. Seed plants can be divided into the gymnosperms (naked seeds) and the angiosperms (enclosed seeds; the flowering plants). Ferns reproduce via spores. Belonging to the flowering plants, *Arabidopsis thaliana* (*Arabidopsis*) is a popular model organism for studying plant biology.

1.2.2 Cyanobacteria

Cyanobacteria utilise Chl for photosynthesis and are the only phylum of photosynthetic prokaryotes that conducts oxygenic photosynthesis. Most cyanobacteria contain only Chl *a* and bilins, which are found in the light-harvesting antenna complexes. Chls *b, c, d* and *f* are also found in some species of cyanobacteria (Blankenship, 2014). It is generally accepted that chloroplasts of eukaryotic organisms originated from a cyanobacterial ancestor by endosymbiotic events. Cyanobacteria share remarkable similarity with plastids in the photosynthetic apparatus and Chl biosynthesis, making their study of great importance for understanding eukaryotic photosynthesis. *Synechocystis* sp. PCC6803 (*Synechocystis*) is one of the most well studied species of cyanobacteria. A detailed description of *Synechocystis* is given in Section 1.3.1.

1.2.3 Purple bacteria

Purple bacteria belong to the bacterial phylum *Proteobacteria* and they perform anoxygenic photosynthesis. They are extraordinarily versatile regarding metabolism and are widely distributed in nature. Many of these bacteria exhibit a purple colour, resulting from a combination of the blue colour from BChl and the red/orange colour from carotenoids (Blankenship, 2014). Purple phototrophs contain BChl *a* or BChl *b*, but not both and contain most of their photosynthesis-associated genes in a small region of the genome, namely the

photosynthesis gene cluster (PGC) (Swingley *et al.*, 2009). Most of them conduct photosynthesis only under anaerobic conditions when light is available. Under photosynthetic conditions, the cytoplasmic membrane of purple bacteria invaginates to form the so-called intracytoplasmic membranes, containing the photosynthetic apparatus. Purple bacteria have been extensively studied as model organism for bacterial photosynthesis, such as *Rhodobacter sphaeroides* 2.4.1 (*Rba. sphaeroides*) and *Rhodobacter capsulatus* SB1003 (*Rba. capsulatus*). These two species together with another purple bacterium, *Rubrivivax gelatinosus* IL144 (*Rvi. gelatinosus*), are described in detail in Sections 1.3.2, 1.3.3 and 1.3.4. It is noteworthy that another group of purple bacteria, the aerobic anoxygenic phototrophs, conduct photosynthesis only under aerobic conditions and requires organic carbon for growth.

1.2.4 Green sulfur bacteria

Green sulfur bacteria are a group of phototrophs in the bacterial phylum *Chlorobi*. Unlike purple bacteria, green sulfur bacteria are metabolically inflexible as they are obligately anaerobic and strictly photoautotrophic. They fix CO_2 via the reductive tricarboxylic acid cycle, instead of the Calvin-Benson-Bassham cycle (Fuchs *et al.*, 1980a; Fuchs *et al.*, 1980b). Most members of green sulfur bacteria utilise sulfide, thiosulfate, elemental sulfur, and molecular hydrogen as electron donors, while some can also oxidise ferrous ion (Frigaard and Dahl, 2009). They contain highly organised light-harvesting antenna structures known as chlorosomes consisting mostly of aggregated BChl *c*, *d* or *e*, with small amounts of BChl *a* and protein components (Frigaard and Bryant, 2006). Chlorosomes are highly efficient at capturing light, which allow green sulfur bacteria to live in environments with extremely low light. Chlorosomes are attached to the cytoplasmic side of the membrane via the BChl *a*-containing Fenna-Matthews-Olson complex, which mediates energy transfer between chlorosomes and membrane-embedded reaction centres (Olson, 2004). Green sulfur bacteria have type-I (FeS-type) reaction centres containing BChl *a* and also a small amount of Chl *a* esterified with Δ2,6-phytadienol (Kobayashi *et al.*, 2000). *Chlorobium tepidum* has been used as a model organism for studying green sulfur bacteria.

1.2.5 Filamentous anoxygenic phototrophs

Filamentous anoxygenic phototrophs belong to the bacterial phylum *Chloroflexi*. They uniquely display filamentous morphology, as indicated by the name, and also gliding motility (Hanada and Pierson, 2006). They are usually isolated from thermophilic environments. In

contrast to green sulfur bacteria, they are metabolically versatile with the capability to perform aerobic respiration, photoautotrophic and photoheterotrophic growth (Blankenship, 2014). They are the only known group of bacteria that fix CO_2 via the 3-hydroxypropionate cycle for autotrophic growth (Strauss and Fuchs, 1993). They contain BChl *a* and BChl *c*. They are so-called 'chimeric organisms' because, like the green sulfur bacteria, they contain chlorosomes, but employ integral membrane antenna complexes and type-II (quinone-type) reactions centres, which resemble those found in purple bacteria (Blankenship and Matsuura, 2003; Hanada and Pierson, 2006). *Chloroflexus aurantiacus* is the most entensively studied species among filamentous anoxygenic phototrophs.

1.2.6 *Heliobacteria*

Heliobacteria are members of *Firmicutes*, which is the fifth bacterial phylum found to contain phototrophs. They are the only known Gram-positive phototrophic bacteria. *Heliobacteria* are obligate anaerobes and are incapable of photoautotrophic growth (Gest and Favinger, 1983). BChl *g* is uniquely utilised by heliobacteria as the major photosynthetic pigment (Gest and Favinger, 1983). In adddtion, 8^1-hydroxy Chl *a*, with a farnesyl tail, is also present in their reaction centres (van de Meent *et al*., 1991). *Heliobacteria* contain type-I (FeS-type) homodimeric reaction centres but do not contain chlorosomes or intracytoplasmic membranes or have an autotrophic carbon fixation pathway (Gest and Favinger, 1983; Heinnickel and Golbeck, 2007). Thus, they are considered to have the simplest photosynthetic apparatus among all bacterial phototrophs.

1.2.7 *Chloroacidobacteria*

The isolation of '*Candidatus* Chloracidobacterium thermophilum' from microbial mats of a hot spring made *Acidobacteria* the sixth bacterial phylum that contains members of phototrophs (Bryant *et al*., 2007). An axenic culture of the strain was established and the name *Chloracidobacterium thermophilum* B was finally given (Tank and Bryant, 2015). It synthesises BChl *a*, BChl *c*, Chl *a* and an epimer of Zn-BChl *a* (Garcia Costas *et al*., 2012; Tsukatani *et al*., 2012). As an aerobe, it surprisingly contains chlorosomes and type-I (FeS-type) homodimeric reaction centres (Garcia Costas *et al*., 2012; Tsukatani *et al*., 2012).

1.2.8 *Gemmatimonadetes*

Very recently, *Gemmatimonadetes* has been documented as the seventh bacterial phylum containing phototrophs (Zeng *et al.*, 2014). The only known phototrophic bacterium belonging to this phylum, *Gemmatimonas* sp. AP64, is a semiaerobic photoheterotroph and

contains BChl *a* and type-II (quinone-type) reaction centres (Zeng *et al.*, 2014). A 42.3 kb PGC is present in the genome of this strain, which was suggested to be acquired from purple bacteria via horizontal gene transfer (Zeng *et al.*, 2014).

1.3 Model organisms used in this study

1.3.1 *Synechocystis* sp. PCC6803

The cyanobacterium *Synechocystis* was first isolated by R. Kunisawa (University of California at Berkeley, USA) in 1968 and subsequently deposited in the Pasteur Culture collection of Cyanobacteria (PCC) (Stanier *et al.*, 1971). It is possible and convenient to perform genetic manipulations in *Synechocystis* since it is naturally transformable and is able to integrate exogenous DNA into its genome through homologous recombination (Grigorieva and Shestakov, 1982). The isolation of glucose tolerant strains of *Synechocystis* has enabled mutant construction under photoheterotrophic conditions (Rippka *et al.*, 1979; Williams, 1988). Most importantly, *Synechocystis* is the first photosynthetic organism with an available genomic seqeuence (Kaneko *et al.*, 1996). As a result of all these advantages, *Synechocystis* has been a very popular model organism for studying many biological processes especially for photosynthesis research. *Synechocystis* contains multiple copies of its genome and the most recent determination shows 7~11 copies per cell (Tichy *et al.*, 2016). Such a characteristic may be beneficial for conducing suppressor screens, but also requires careful handling of *Synechocytis* strains to avoid unnecessary generation of mutations.

1.3.2 *Rhodobacter sphaeroides*

The purple phototrophic bacterium, *Rba. sphaeroides* belongs to the α-3 subgroup of *Alphaproteobacteria* and exhibits extraordinary metabolic versatility. *Rba. sphaeroides* is capable of utilising energy from aerobic respiration, anaerobic respiration, photosynthesis and fermentation, and utilising both organic and inorganic carbon sources (Madigan and Jung, 2009). Genetic manipulations can be easily performed in *Rba. sphaeroides* and the genome seqeuence has been available since 2001 (Mackenzie *et al.*, 2001; Kontur *et al.*, 2012). *Rba. sphaeroides*, as a typical photosynthetic bacterium, conducts anoxygenic photosynthesis under anaerobic conditions when light is available. Most of the photosynthesis-associated genes in *Rba. sphaeroides* are within the 40.7 kb PGC (Naylor *et al.*, 1999). The facultative growth of *Rba. sphaeroides* allows genes involved in photosynthesis to be inactivated and studied by mutagenesis. The *Rba. sphaeroides* photosystem (PS) is relatively simple and

comprises only the quinone-type reaction centres that receive excitation energy from light-harvesting 2 and 1 antenna complexes. All these characteristics make *Rba. sphaeroides* an important model organism to study aspects of photosynthesis that include the formation, function, regulation and structure of PS. In particular, many BChl biosynthetic genes have been identified and studied in *Rba. sphaeroides*.

1.3.3 *Rhodobacter capsulatus*

Another purple phototrophic bacterium, *Rba. capsulatus* also belongs to the α-3 subgroup of *Alphaproteobacteria* and is a close relative to *Rba. sphaeroides*. It is also widely used as a model organism for studying bacterial photosynthesis. *Rba. capsulatus* does not possess the *acsF* gene, which encodes the catalytic subunit of the aerobic magnesium-protoporphyrin IX monomethyl ester cyclase (cyclase), as indicated by its genomic sequence (Strnad *et al*., 2010). In this study, *Rba. capsulatus* was included as a host for testing the aerobic cyclase activity from heterologously produced protein.

1.3.4 *Rubrivivax gelatinosus*

Rvi. gelatinosus is a purple phototrophic bacterium belonging to the *Betaproteobacteria*. The genomic sequence of this strain has been reported by Nagashima *et al*. (2012). Although *Rvi. gelatinosus* may not be employed as extensively as *Rba. sphaeroides* or *Rba. capsulatus* to study photosynthesis, the fact that the first gene encoding an aerobic cyclase, *acsF*, was identified first in this organism highlights its special importance in aerobic cyclase research (Pinta *et al*., 2002). As a facultative phototrophic organism, *Rvi. gelatinosus* can live without photosynthesis, making disruption of the BChl biosynthesis pathway not lethal. Unlike *Rba. sphaeroides*, *Rvi. gelatinosus* has a marked activity of aerobic cyclase and inactivation of aerobic cyclase has an apparent phenotype. Transposon mutagenesis in this organism has been demonstrated to be feasible (Vanzin *et al*., 2010; Steunou *et al*., 2013; Azzouzi *et al*., 2013). Thus, genes associated with aerobic cyclase are possible to be identified by conducting transposon mutagenesis in *Rvi. gelatinosus* combined with an appropriate phenotype screen.

1.4 Overview of (bacterio)chlorophyll biosynthesis

(B)Chls are essential cofactors for photosynthesis and involved in both light harvesting and photochemistry. They are cyclic tetrapyrrole molecules with a centrally chelated magnesium ion and a unique isocyclic E ring. Only 5 types of Chls are currently known to be present in oxygenic phototrophs: Chl *a* (including divinyl-Chl *a*), Chl *b* (including divinyl-Chl *b*), Chl *c*, Chl

d and Chl *f* (Chen, 2014). Only 7 types of BChls have been identified in anoxygenic phototrophs, BChls *a*, *b*, *c*, *d*, *e*, *f*, and *g* (Blankenship, 2014). Chl *a* and BChl *a* are the most widely distributed Chls and BChls in photosynthetic organisms, respectively. Their chemical structures and absorption spectra in methanol are shown in **Figure 1.2**. BChl *a* differs from Chl *a* through an acetyl group at the C-3 position and a reduced ring B. The reduction of the B ring causes a blue-shift of the Soret band and a red-shift of the Q_y band, extending the absorption of BChl *a* into the ultraviolet and infrared ranges, which are not absorbed strongly by Chl *a*.
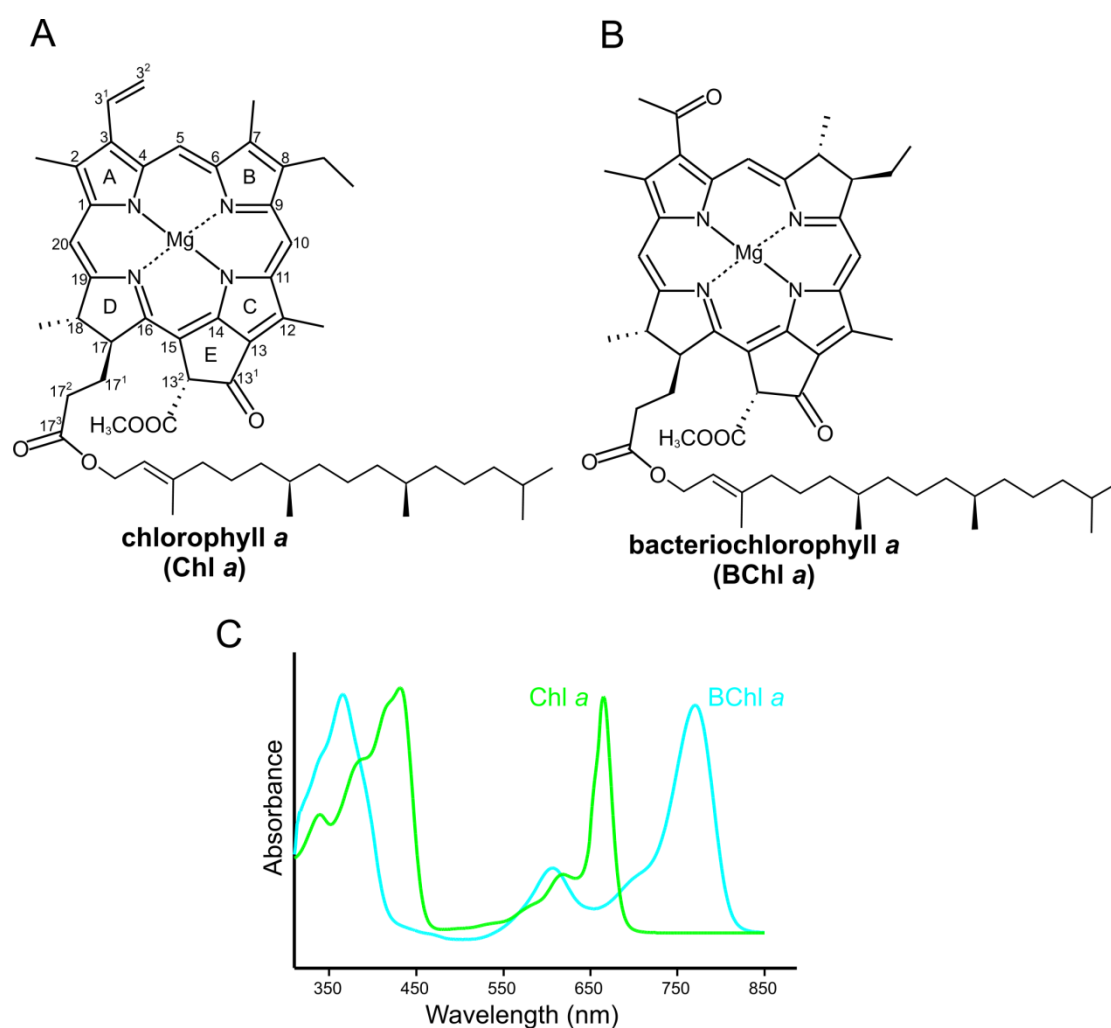
Figure 1.2 Structures of chlorophyll *a* and bacteriochlorophyll *a*

(**A**) Structure of Chl *a*. The carbon skeleton is numbered according to the IUPAC system. The four tetrapyrrole rings and the fifth isocyclic ring are lettered from A to E. The numbering and lettering systems applies to all Chl-type pigments. (**B**) Structure of BChl *a*. (**C**) Absorption spectra of Chl *a* and BChl *a* in methanol.

The (B)Chl biosynthetic pathway is relatively complicated and consists of a series of enzymatic steps. Several (B)Chl biosynthetic intermediates are shared by the biosynthesis of other naturally occurring tetrapyrrole molecules including haems, vitamin B_{12}, sirohaem, cofactor F_{430} and bilins, as displayed in **Figure 1.3**. These intermediates are δ-aminolevulinic acid (ALA), uroporphyrinogen III (Uro'gen) and protoporphyrin IX (Proto). ALA is the common and committed precursor for all tetrapyrrole biosynthesis. Uro'gen lies at the first branch point where the pathways of sirohaem, vitamin B_{12}, cofactor F_{430} and Proto diverge from each other. Proto is the second branch point where it can chelate either a magnesium ion for (B)Chl biosynthesis or ferrous ion for haem biosynthesis. Bilins are linear, open-chain tetrapyrrole molecules and are synthesised as haem derivatives. The whole (B)Chl biosynthetic pathway can be divided into the formation of ALA, the steps from ALA to protoporphyrin IX (Proto), the core pathway of (B)Chl biosynthesis, the unique steps for BChl biosynthesis and the phytylation of (bacterio)chlorophyllide (Chlide).
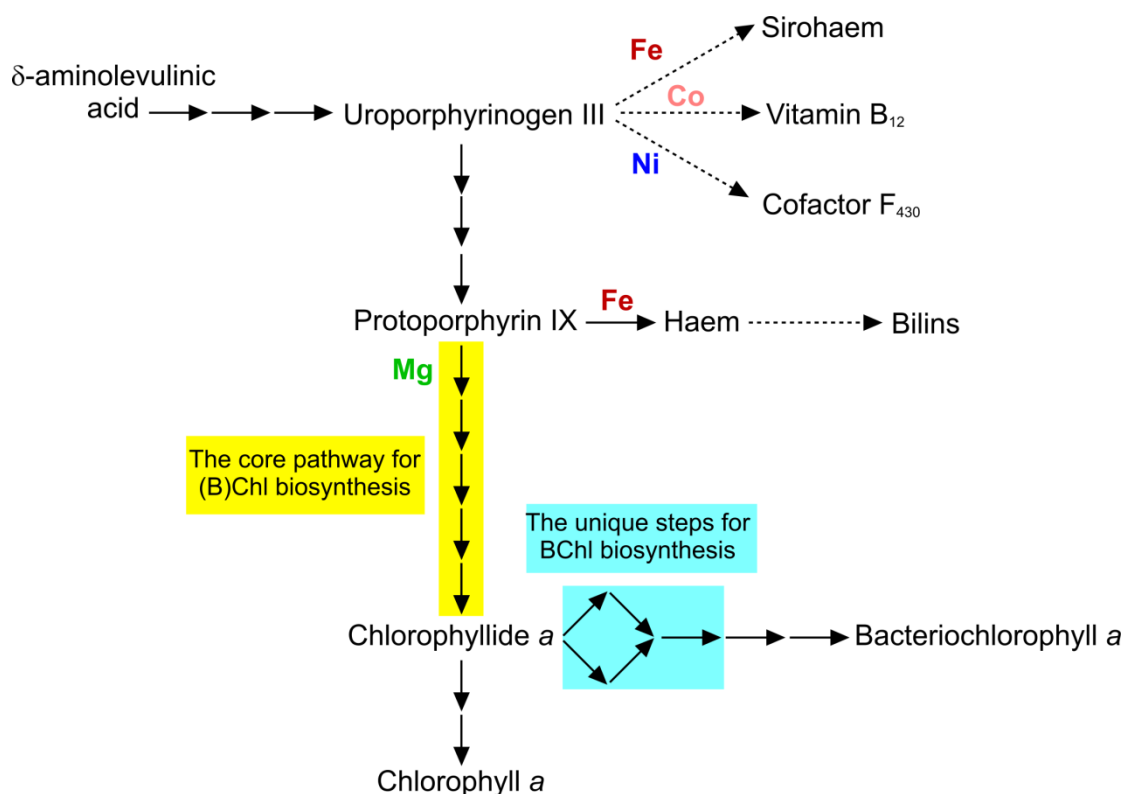
Figure 1.3 Outline of tetrapyrrole biosynthesis from δ-aminolevulinic acid
The individual biosynthetic steps for sirohaem, vitamin B_{12}, cofactor F_{430} and bilins are not shown. Arrows with solid lines represent single enzymatic steps. The core pathway for (B)Chl biosynthesis is highlighted in yellow. The unique steps for BChl biosynthesis are highlighted in blue.

1.5 Formation of δ-aminolevulinic acid

ALA is the first committed substrate for tetrapyrrole biosynthesis and can be synthesised in nature via two different routes, known as the Shemin pathway and the C_5-pathway (**Figure 1.4**). The Shemin pathway, found in animals, fungi, yeast and α-proteobacteria, produces ALA from the condensation of glycine and succinyl-CoA catalysed by the enzyme δ-aminolevulinic acid synthase (ALAS). In plants, algae, archaea and most bacteria (except for α-proteobacteria), the C_5-pathway is utilised to synthesise ALA from glutamyl-tRNA (Glu-tRNA) via two steps catalysed by Glu-tRNA reductase (GluTR) and glutamate-1-semialdehyde 2,1-aminomutase (GSAM) (Oh-hama, 1995).
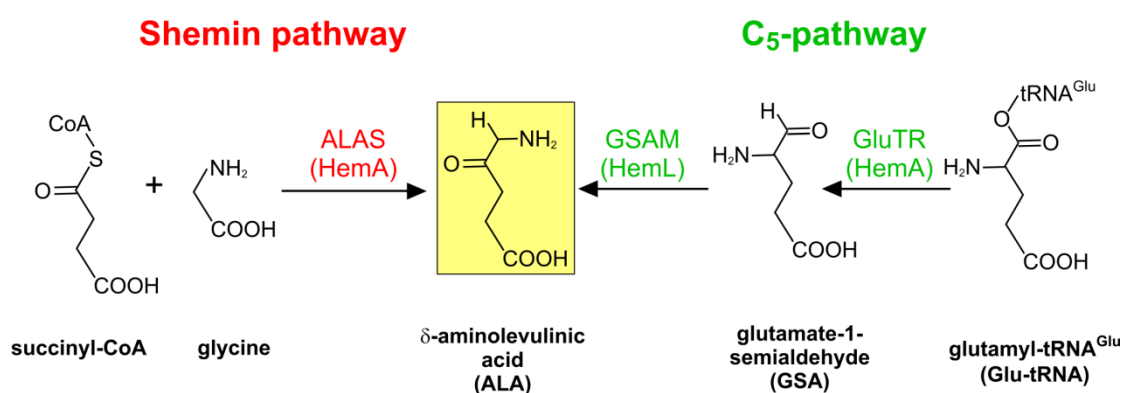
Figure 1.4 The biosynthesis of δ-aminolevulinic acid

In the Shemin pathway, ALA synthase (ALAS) catalyses the condensation of succinyl-CoA and glycine to form ALA. In the C_5-pathway, ALA is synthesised via two steps catalysed by glutamyl-tRNA reductase (GluTR) and glutamate-1-semialdehyde 2,1-aminomutase (GSAM).

1.5.1 Shemin pathway

The Shemin pathway, in which ALA is produced from the condensation of glycine and succinyl-CoA with the release of CO_2 and free coenzyme A, was first identified and biochemically characterised mainly by the Shemin and Neuberger groups (Shemin and Kumin, 1952; Neuberger and Scott, 1953; Shemin and Russell, 1953; Kikuchi *et al.*, 1958; Gibson *et al.*, 1958). ALAS activity was first demonstrated using extracts from *Rba. sphaeroides* and *Rhodospirillum rubrum* (Kikuchi *et al.*, 1958). Purification of ALAS revealed in *Rba. sphaeroides* there are two isoforms of the enzyme, which were differentially induced under various conditions (Tuboi *et al.*, 1970a; Tuboi *et al.*, 1970b; Fanica-Gaignier and Clement-Metral, 1973b). The first ALAS encoding gene, termed as *hemA*, was cloned from *Rba. capsulatus* (Biel *et al.*, 1988). In *Rba. sphaeroides*, *hemA* and *hemT* were identified to encode

the two ALAS isozymes and found to be involved in the genetic control of photosynthetic apparatus (Neidle and Kaplan, 1993a; Neidle and Kaplan, 1993b). Mammals also contain two ALAS isozymes, one for housekeeping and the other for high level of haem production in erythrocytes (Bishop *et al.*, 1990).

ALAS requires pyridoxal 5'-phosphate (PLP) as a cofactor and belongs to the α-oxoamine synthase subfamily within the α-family of PLP-dependent enzymes (Fanica-Gaignier and Clement-Metral, 1973a; Nandi, 1978; Alexander *et al.*, 1994). ALAS has an ordered bi-bi mechanism, with glycine binding before succinyl-CoA, and then CoA being released before ALA (Fanica-Gaignier and Clement-Metral, 1973a). ALAS is highly unusual as almost all the α-family of PLP-dependent enzymes cleave a single α-carbon bond of the substrate, whereas ALAS cleaves two. The catalytic cycle of ALAS has been proposed as follows. PLP binds covalently to an active site lysine via an internal aldimine, which is displaced by the formation of an external aldimine between the incoming glycine and PLP. Then the pro-*R* proton of glycine is removed by the active site lysine leading to the formation of a quinonoid intermediate, which is subsequently condensed with succinyl-CoA to form a 2-amino-3-keto adipate intermediate. Decarboxylation of this intermediate with a proton cleaves the external aldimine, resulting in the release of the product, ALA (Heinemann *et al.*, 2008; Layer *et al.*, 2010). The crystal structures of *Rba. capsulatus* ALAS, in its free form or in complex with glycine or succinyl-CoA, have been solved and reveal a tightly interlocked homodimer with each monomer consisting of three domains (Astner *et al.*, 2005). The active site pockets are deeply buried in each monomer and allow for a tight coordination of the cofactor PLP, and the substrates glycine and succinyl-CoA. The active site pocket is connected to the enzyme surface by a channel (Astner *et al.*, 2005).

1.5.2 C$_5$-pathway

Investigation of the formation of ALA in plants by ^{14}C-labelling experiments led to the discovery of an alternative ALA synthesis route in which the intact five-carbon skeleton of glutamate is converted to ALA (Beale and Castelfranco, 1974b; Beale *et al.*, 1975). This alternative ALA synthesis route was thus named as the C$_5$-pathway. The involvement of a tRNA cofactor in the C$_5$-pathway was discovered in the mid-1980s (Huang *et al.*, 1984). In the C$_5$-pathway, Glu-tRNA synthetase catalyses the ligation of glutamate to tRNA^{Glu}, resulting in the formation of Glu-tRNA that can serve as a substrate for both protein synthesis and tetrapyrrole biosynthesis. GluTR catalyses the reduction of Glu-tRNA to form glutamate-1-

semialdehyde (GSA), a labile intermediate in the C_5-pathway. GSA is then subjected to intramolecular rearrangement catalysed by GSAM to form ALA.

The *hemA* gene encoding GluTR from *Methanopyrus kandleri* was cloned and overexpressed in *E. coli*. The purified recombinant GluTR is a tetramer with a native MW of 190 kD and requires NADPH for activity. Without NADPH, GluTR hydrolyses Glu-tRNA to release glutamate (Moser *et al.*, 1999). Later, the crystal structure of GluTR from this organism was solved in complex with the inhibitor glutamycin, which displays an unusual V-shaped dimeric structure with each monomer constituting one leg of the V-shape (Moser *et al.*, 2001). The structure model reveals an extensive protein-tRNA interface and supports a thioester-mediated reduction process. The highly conserved Cys48 of GluTR nucleophilically attacks the aminoacyl bond of Glu-tRNA resulting in a highly reactive thioester intermediate. Then this thioester is reduced via hydride transfer from NADPH to form GSA. A GluTR-tRNA^{Glu}-GSAM model complex generated by structure docking reveals that GSA can leave GluTR via a "back door" of the glutamate recognition pocket and directly channel to the active site of GSAM (Moser *et al.*, 2001).

GSAM, encoded by the *hemL* gene, belonging to the α-family of PLP-dependent enzymes, converts GSA to ALA in an intramolecular transamination reaction. The catalytic mechanism of GSAM includes enzyme-bound diaminovalerate as a central intermediate (Pugh *et al.*, 1992; Contestabile *et al.*, 2000). The first crystal structure of GSAM from *Synechococcus* with a substrate analogue was solved and revealed an asymmetric dimer structure (Hennig *et al.*, 1997). Structural analysis of the trapped catalytic intermediates of GSAM reveals an active-site "gating loop", which undergoes a dramatic conformational change during catalysis and is open in one subunit while closed in the other, suggesting negative cooperativity between the allosteric pair (Stetefeld *et al.*, 2006). However, the structure of *Thermosynechococcus* (*T.*) *elongatus* GSAM in its PLP-bound form reveals a symmetric homodimer, thus challenges the previously proposed negative cooperativity between monomers of the enzyme (Schulze *et al.*, 2006). The crystal structure of *Bacillus subtilis* GSAM is also a symmetric homodimer (Ge *et al.*, 2010). In addition, GSAM is structurally related to ALAS and ALAS may thus have evolved from the more ancient GSAM (Schulze *et al.*, 2006).

The synthesis of ALA by the C_5 pathway requires the close coordination of GluTR and GSAM due to the highly reactive nature of GSA. Substrate channelling between GluTR and GSAM has been proposed based on the structures of GluTR and GSAM (Moser *et al.*, 2001; Schulze *et al.*, 2006). *In vitro* and *in vivo* experiments with *E. coli* and *C. reinhardtii* have confirmed that

GluTR and GSAM do form a physical and functional complex (Luer *et al.*, 2005; Nogaj and Beale, 2005).

1.6 From δ-aminolevulinic acid to protoporphyrin IX

All tetrapyrrole biosynthesis starts from the universal precursor ALA. **Figure 1.5** shows the biosynthetic pathway from ALA to protoporphyrin IX (Proto). Two ALA molecules are condensed to form the pyrrole porphobilinogen (PBG) by PBG synthase (PBGS). Four PBG molecules are then condensed to produce the linear tetrapyrrole hydroxymethylbilane (HMB) by PBG deaminase (PBGD). The cyclisation of HMB results in the first cyclic tetrapyrrole intermediate Uro'gen catalysed by Uro'gen synthase (UROS). Uro'gen is then decarboxylated to form coproporphyrinogen III (Copro'gen) by Uro'gen decarboxylase (UROD). Copro'gen is oxidatively decarboxylated by Copro'gen oxidase (CPO) to produce protoporphyrinogen IX (Proto'gen). Finally, Proto'gen is oxidised to give Proto by Proto'gen oxidase (PPO) (Willows and Kriegel, 2009; Layer *et al.*, 2010).
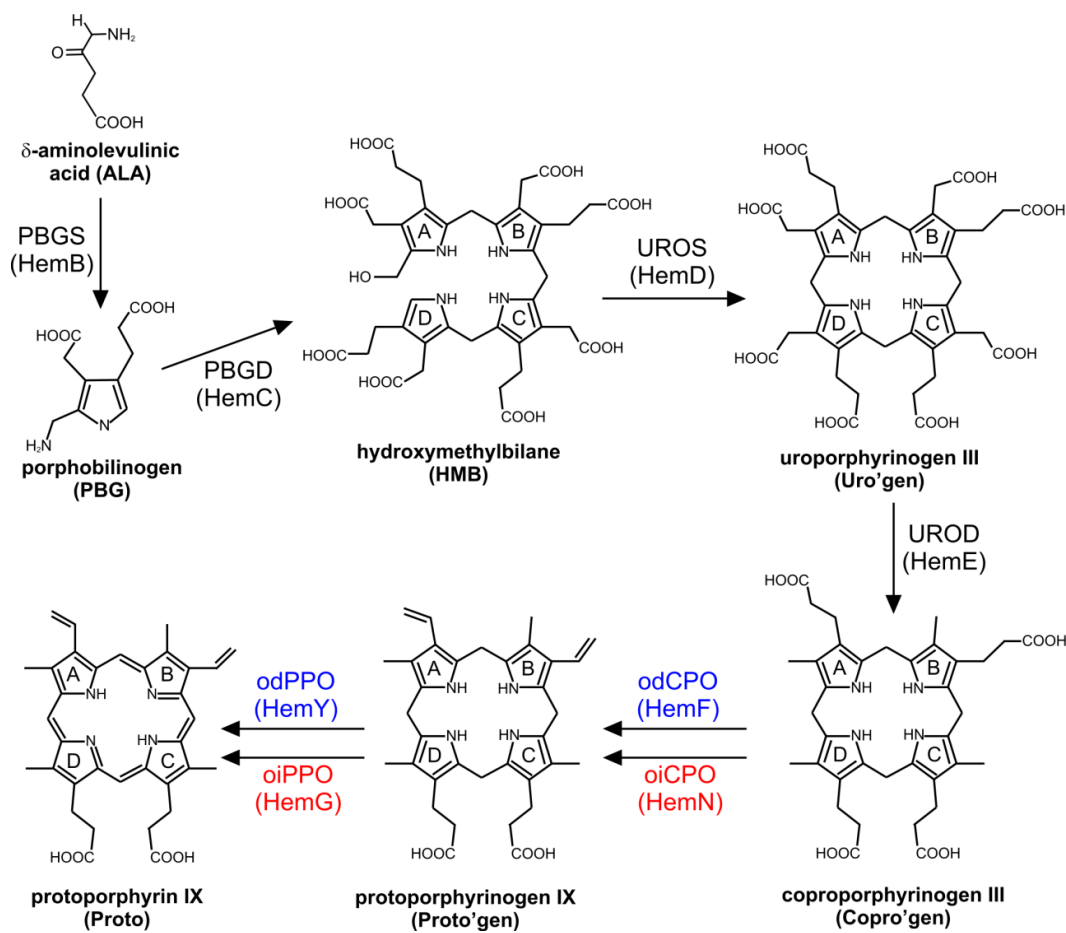
Figure 1.5 From δ-aminolevulinic acid to protoporphyrin IX

Abbreviations for enzymes: PBGS, porphobilinogen synthase; PBGD, porphobilinogen deaminase; UROS, uroporphyrinogen III synthase; UROD, uroporphyrinogen III decarboxylase; odCPO, oxygen-dependent coproporphyrinogen III oxidase; oiCPO, oxygen-independent coproporphyrinogen III oxidase; odPPO, oxygen-dependent protoporphyrinogen IX oxidase; and oiPPO, oxygen-independent protoporphyrinogen IX oxidase.

1.6.1 Porphobilinogen synthase

PBGS, also known as ALA dehydratase, catalyses the asymmetric condensation of two ALA molecules to form PBG, the first pyrrole molecule in the pathway, with the release of two H_2O molecules. Early biochemical characterisation of PBGS was performed by the Nandi and Shemin group with the purified enzyme from *Rba. sphaeroides*. The *Rba. sphaeroides* PBGS exhibits many features of an allosteric enzyme and some monovalent cations can act as the allosteric effectors (Nandi *et al.*, 1968). In the presence of allosteric effectors, the protein associates into a mixture of monomers, dimers and trimers (Nandi and Shemin, 1968b). Based on enzyme assays with the *Rba. sphaeroides* PBGS, a catalytic model was proposed which involves the formation of a Schiff base, an aldol condensation and the elimination of

the elements of water (Nandi and Shemin, 1968a). Single-turnover experiments with purified PBGS from human erythrocytes showed that the first ALA molecule bound to the enzyme provides the "propionate" half of PBG, while the second ALA molecule forms the "acetate" half of PBG (Jordan and Gibbs, 1985). The corresponding substrate binding sites of PBGS are termed as the P-site and A-site, respectively.

PBGS, encoded by the *hemB* gene, usually functions as an homooctamer with the exception of the hexameric *Rba. capsulatus* enzyme (Bollivar *et al*., 2004). Although PBGS enzymes from different organisms share a high degree of sequence similarity, different metal dependency allows PBGS to be divided into two main groups, the Zn-dependent PBGS present in mammals, yeast, some bacteria including *E. coli* and cyanobacteria, and the Mg-dependent PBGS found in plants, algae and some other bacteria (Beale, 1999). In addition, some but not all Zn-dependent PBGS, such as the *E. coli* PBGS, are stimulated by Mg ion (Mitchell and Jaffe, 1993; Jaffe *et al*., 1995). Unlike other PBGS, the *Rba. capsulatus* PBGS does not require any metal ion for function and is a hexamer (Nandi and Shemin, 1973; Bollivar *et al*., 2004).

The first crystal structure of PBGS was from the yeast enzyme and is a homooctamer in which each monomer adopts an $(\alpha/\beta)_8$ or TIM-barrel fold with a 39-residue N-terminal arm (Erskine *et al*., 1997). All eight active sites are on the surface of the octamer and contain Lys210 and Lys263. Lys263 forms a Schiff base with the P-site substrate. The two lysine chains are close to the zinc binding sites one of which is formed by Cys133, Cys135 and Cys143 and the other is formed by Cys234 and His142 (Erskine *et al*., 1997). The substrate binding, metal coordination and catalysis of Mg-dependent PBGS have been defined more clearly with the crystal structure of *E. coli* PBGS, and also there is a third metal binding site close to the active site flap, which may be involved in the stimulatory effect of Mg ions (Erskine *et al*., 1999). The first crystal structure of Mg-dependent PBGS was solved from *Pseudomonas aeruginosa* (Frankenberg *et al*., 1999). The homooctameric enzyme consists of four asymmetric dimers in which one monomer is different from the other by having a "closed" and an "open" active site pocket. Although no metal ions are found in the active sites, a Mg^{2+} ion is bound to the closed form of the monomer at a site remote from the active site, which may explain the allosteric role of Mg^{2+} in the conformational difference between the closed form and active form (Frankenberg *et al*., 1999). All these structural features of *Pseudomonas aeruginosa* PBGS are shared by the structure of *Chlorobium vibrioforme* PBGS, which is also a Mg^{2+}-dependent PBGS (Coates *et al*., 2004).

1.6.2 Porphobilinogen deaminase

PBGD, also known as HMB synthase, catalyses the polymerisation of four PBG molecules to form the linear tetrapyrrole, HMB. The ^{13}C NMR spectroscopic studies demonstrated that HMB is an intermediate between PBG and Uro'gen and free HMB rapidly cyclises spontaneously and irreversibly to form uroporphyrinogen I, which is physiologically irrelevant (Jordan *et al.*, 1979; Burton *et al.*, 1979; Battersby *et al.*, 1979). The assembly of four PBG occurs in a unidirectional order starting from ring A with sequential addition of ring B, C and finally ring D (Battersby *et al.*, 1979; Jordan and Seehra, 1979). The intermediates mono-, di-, tri- and tetra-pyrroles of the reaction are covalently bound to the PBGD before being released as HMB (Jordan and Berry, 1981; Battersby *et al.*, 1983). Dipyrromethane, a PBG dimer, was identified as the cofactor for PBGD and is covalently linked to the enzyme through a cysteine (Jordan and Warren, 1987; Hart *et al.*, 1987; Jordan *et al.*, 1988; Scott *et al.*, 1989). The free α-position of this cofactor interacts with the incoming substrate PBG to give the covalently bound enzyme-intermediate complex (Warren and Jordan, 1988). There is a transient protein bound hexapyrrole from which the HMB tetrapyrrole is cleaved off leaving the dipyrromethane cofactor intact for next tetrapolymerisation (O'Brian and Thony-Meyer, 2002).

Site-specific mutagenesis studies of the *E. coli* PBGD encoded by the *hemC* gene have revealed several of the conserved arginine residues in the catalytic cleft of the enzyme involved in the assembly of the cofactor, and the initiation and elongation of the tetrapyrrole chain (Lander *et al.*, 1991; Jordan and Woodcock, 1991). The crystal structure of *E. coli* PBGD has been solved and reveals a monomer consisting of three equally sized α/β domains (Louie *et al.*, 1992).The large active-site cleft is located at the interface between domains I and II. The dipyrromethane cofactor is covalently attached to Cys243 on a loop of the domain III and positioned by extensive salt-bridges and hydrogen-bonds within the active-site cleft. The enzyme also exhibits a high degree of interdomain flexibility which may be necessary for repositioning the cofactor and enzyme-intermediate complexes during chain elongation (Louie *et al.*, 1992; Louie *et al.*, 1996). The crystal structure of human PBGD has also been solved (Gill *et al.*, 2009). Despite the insertion of loop regions, the structure of human PBGD shares many features with that of *E. coli* PBGD (Gill *et al.*, 2009).

1.6.3 Uroporphyrinogen III synthase

UROS catalyses the cyclisation of HMB and the inversion of the D ring to form Uro'gen, the asymmetric III isomer of uroporphyrinogen. HMB is unstable and is spontaneously cyclised to the non-physiological product uroporphyrinogen I unless UROS is present to convert it to Uro'gen. Bogorad (1958) reported the first purification and enzyme assay of UROS from wheat germ and it was designated as uroporphyrinogen isomerase in this paper. Then around twenty years later, HMB was discovered to be an intermediate between PBG and Uro'gen and act as a substrate for UROS (Burton *et al.*, 1979; Jordan *et al.*, 1979). Although many reaction schemes were proposed, few stood for a long time. The reaction mechanism proposed by Mathewson and Corwin (1961) which involves a spirocyclic intermediate has been supported by both experiments and theoretical calculations (Spivey *et al.*, 1996; Silva and Ramos, 2008). In this reaction scheme, dehydration of HMB results in the first azafulvene intermediate, which then reacts with the substituted α-position of ring D to yield a spirocyclic pyrrolenine. Spirocyclic pyrrolenine is cleaved to generate a second azafulvene intermediate that finally cyclises to Uro'gen (Shoolingin-Jordan, 1995; Layer *et al.*, 2010).

UROS, encoded by the *hemD* gene, has been purified as a monomer with a molecular weight of around 30 kD, from multiple organisms including *E. coli* (Alwan *et al.*, 1989), *Euglena gracilis* (Hart and Battersby, 1985) and mammals (Kohashi *et al.*, 1984; Tsai *et al.*, 1988). As the overall sequence similarity between UROS homologues across species is low, simple BLAST search to identify UROS genes is not applicable (Heinemann *et al.*, 2008). Instead, it is practical to perform functional complementation of known *hemD* mutants with the genomic DNA library or cDNA library from the organism under investigation. In this way, the *Arabidopsis* UROS encoding gene was identified (Tan *et al.*, 2008).

The crystal structure of human UROS has been determined and reveals a monomeric protein consisting of two α/β domains connected by a two-strand anti-parallel β-ladder (Mathews *et al.*, 2001). The active site is located in the large open cleft between the two domains. The inherent interdomain flexibility was observed and was suggested to be important in the catalytic cycle. Site-specific mutagenesis of the highly conserved residues with titratable side chains demonstrated that the reaction mechanism does not require acid/base catalysis (Mathews *et al.*, 2001). The crystal structures of *Thermus thermophilus* UROS in its ligand-free and Uro'gen-bound forms have also been reported (Schubert *et al.*, 2008). The overall fold of the *Thermus thermophilus* UROS is similar to the human UROS despite the interdomain linker is much less ordered than that of the human UROS. Uro'gen binds at the interface between

the two domains and the binding induces domain closure. Uro'gen adopts a highly puckered "two-up, two-down" configuration, where rings A and C are pointing in one direction and rings B and D are pointing in the opposite direction. A conserved tyrosine residue, reported previously to be important for the enzyme activity (Roessner *et al.*, 2002), is potentially positioned to facilitate the hydration of HMB to initiate the reaction (Schubert *et al.*, 2008).

Uro'gen is the first macrocyclic intermediate and first branch point of the tetrapyrrole biosynthesis pathway, where Uro'gen can be directed down one of the two routes: methylation at positions 2 and 7 of Uro'gen directs the synthesis towards sirohaem, cofactor F_{430} and vitamin B_{12}, while decarboxylation at positons 2, 7, 12 and 18 of Uro'gen catalysed by Uro'gen decarboxylase leads to the synthesis of haem and (B)Chl (Warren and Scott, 1990).

1.6.4 Uroporphyrinogen III decarboxylase

UROD catalyses the sequential decarboxylation of the four acetate side chains of Uro'gen to yield Copro'gen. The UROD activity was first demonstrated using an enzyme preparation from erythrocytes (Mauzerall and Granick, 1958). Regarding the substrate specificity, UROD is flexible as it accepts uroporphyrinogen I and III as well as all 14 possible intermediates between Uro'gen and Copro'gen (Jackson *et al.*, 1976; Smith *et al.*, 1979). UROD activity was shown to be inhibited by divalent metal ions and -SH reagents (Kawanishi *et al.*, 1983; de Verneuil *et al.*, 1983; Straka and Kushner, 1983). It was demonstrated that the decarboxylation reaction is random with an excess of substrate, whereas decarboxylation is orderded under physiological conditions, starting with the acetate side chain of ring D, followed by A, B and finally C (Lash, 1991; Luo and Lim, 1993; Jones and Jordan, 1993). Analysis of mutant yeast UROD enzymes suggested there is a single active site in the enzyme (Chelstowska *et al.*, 1992).

The crystal structures of human UROD revealed a homodimer in which each monomer consists of a $(\beta/\alpha)_8$-barrel with a deep active site cleft formed by loops at the C-terminal ends of the barrel strands (Whitby *et al.*, 1998). Many conserved residues cluster at the catalytic cleft, including the six invariant polar residues, Arg37, Arg41, Asp86, Tyr164, Ser219 and His339 (Whitby *et al.*, 1998). The crystal structure of tobacco UROD displays a broken $(\beta/\alpha)_8$-barrel fold with seven parallel β-strands forming a circular β-barrel and a similar catalytic cleft as human UROD structure (Martins *et al.*, 2001). The two monomers in the dimeric enzyme are oriented head-to-head with the active site clefts facing each other at the interface. The presence of Pro26 (numbering in recombinant mature tobacco UROD) proceeding residues

Pro27-Trp29 causes the disruption of the β-barrel by impairing their β-strand conformation (Martins *et al.*, 2001). Later on, the crystal structures of human UROD in complex with its coproporphyrinogen products were solved by using a novel enzymatic approach to generate highly oxygen-sensitive porphyrinogen substrate *in situ* (Phillips *et al.*, 2003). The UROD product adopts a domed conformation that lies against a collar of conserved hydrophobic residues, which enables the formation of hydrogen-bonds between Asp86 and the pyrrole NH groups. The central coordination geometry of Asp86 allows the initial substrates and the various partially decarboxylated intermediates to be bound with equivalent activating interactions, supporting a single active site hypothesis (Phillips *et al.*, 2003). In addition, the conserved arginine residues within the active site accommodate the negatively charged substrate rather than precisely orienting the substrate, which explains the substrate flexibility of UROD (Layer *et al.*, 2010). The single active site hypothesis was further confirmed by the observations of the engineered UROD protein with two subunits connected by a flexible linker (Phillips *et al.*, 2009). The crystal structure of *Bacillus subtilis* UROD, encoded by the *hemE* gene, has also been reported with a variation of two loops compared with eukaryotic UROD (Fan *et al.*, 2007).

1.6.5 Coproporphyrinogen III oxidase

CPO catalyses the oxidative decarboxylation of the propionate side chains at positions 3 and 8 of Copro'gen to vinyl groups to yield Proto'gen. Two structurally and mechanistically unrelated CPOs are found in nature. One requires molecular oxygen as terminal electron acceptor, referred as the O_2-dependent CPO (odCPO), and is present in both prokaryotes and eukaryotes. The other is the O_2-independent CPO (oiCPO) of which the physiological electron acceptor is still unknown although $NADP^+$ can be used as an electron acceptor *in vitro* (Layer *et al.*, 2010). The oiCPO is mainly found in bacteria but also in some eukaryotes.

The partial purification and *in vitro* enzyme assays of the odCPO from bovine, rat and yeast, has been reported since 1961 (Sano and Granick, 1961; del Batlle *et al.*, 1965; Poulson and Polglase, 1974). The *in vitro* activity of the odCPO was also demonstrated in various bacteria including *Rba. sphaeroides*, *E. coli* and *Rhizobium japonicum* (Tait, 1969; Jacobs *et al.*, 1970; Jacobs *et al.*, 1971; Keithly and Nadler, 1983). It appears that the odCPO enzymes from different species vary in metal requirement since the bovine, human and yeast enzymes do not require any metal (Yoshinaga and Sano, 1980a; Medlock and Dailey, 1996; Labbe, 1997), whereas the mouse enzyme requires Cu^{2+} and the *E. coli* enzyme (HemF) requires Mn^{2+} (Kohno *et al.*, 1996; Breckau *et al.*, 2003). The reaction occurs stepwise via a tri-propionate

porphyrinogen intermediate, harderoporphyrinogen, with the decarboxylation of the 3-propionate side chain prior to that of the 8-propionate side chain of Copro'gen (Cavaleiro *et al.*, 1974; Elder *et al.*, 1978; Jackson *et al.*, 1980; Yoshinaga and Sano, 1980b). ^{2}H- and ^{3}H-labelling experiments revealed the decarboxylation of the propionate group only involves the loss of the pro-*R* hydrogen atom at the β-position (Zaman *et al.*, 1972; Zaman and Akhtar, 1976; Seehra *et al.*, 1983). The overall stereochemistry of the reaction is an antiperiplanar elimination of proton and CO_2 (Battersby *et al.*, 1975). Two reaction mechanisms have been proposed, the Arigoni model involving an oxygen-dependent hydroxylation step (Lee *et al.*, 2005) and the Lash model which involves the formation of a 2*H*-pyrrole peroxide anion (Lash *et al.*, 2005). According to both mechanisms, H_2O_2 is generated during the odCPO catalysis, which has been demonstrated with *E. coli* enzyme (Breckau *et al.*, 2003). Quantum chemical computations seem to favor the Lash model (Silva and Ramos, 2008).

The crystal structures of yeast and human odCPO have been solved and both reveal a homodimer with each monomer consisting of a central flat seven-stranded β-sheet sandwiched by α-helices (Phillips *et al.*, 2004; Lee *et al.*, 2005). The dimeric assembly is formed by helix packing and a short isolated strand forming a β-ladder with its counterpart in the partner subunit. One monomer rotates relative to the second by around 40° to create an intersubunit interface that is closed to two independent active sites (Phillips *et al.*, 2004; Lee *et al.*, 2005). The open and closed conformations of the active-site cleft of yeast odCPO have been captured and in the closed conformation, a substrate-sized cavity is buried by a helix which forms a lid over the active site (Phillips *et al.*, 2004).

The oiCPO activity was first demonstrated in cell-free extracts prepared from *Rba. sphaeroides* under anaerobic conditions with nicotinamide nucleotides, ATP and methionine (Tait, 1969; Tait, 1972). Although structurally and catalytically unrelated to odCPO, oiCPO is analogous to odCPO in that only the pro-*S* hydrogen atom at the β-position of propionate group is involved in the reaction and harderoporphyrinogen is the reaction intermediate (Seehra *et al.*, 1983; Rand *et al.*, 2010). The oiCPO encoding genes, named as *hemN*, have been identified in various bacteria including the cyanobacterium *Synechocystis* (Coomber *et al.*, 1992; Xu *et al.*, 1992; Xu and Elliott, 1994; Troup *et al.*, 1995; Lieb *et al.*, 1998; Fischer *et al.*, 2001; Goto *et al.*, 2010). The *E. coli* HemN was purified anaerobically as a monomeric protein which contains a conserved CXXXCXXC motif to bind an oxygen-sensitive [4Fe-4S] cluster (Layer *et al.*, 2002). HemN requires *S*-adenosyl-L-methionine (SAM), NAD(P)H and

additional cytoplasmatic components for activity and belongs to the Radical SAM protein superfamily (Sofia *et al.*, 2001).

The crystal structure of *E. coli* HemN reveals a monomeric, two-domain protein (Layer *et al.*, 2003). The larger N-terminal catalytic domain consists of a curved, 12-stranded β-sheet and is decorated at its outer surface by α-helices. The core of N-terminal domain resembles an incomplete TIM-barrel consisting of six (β/α) repeats rather than eight found in true TIM-barrel. HemN contains three cofactors, a [4Fe-4S] cluster and two SAM molecules, which are bound close to each other within the active-site pocket of the catalytic domain. Three of the four Fe ions of the [4Fe-4S] cluster are coordinated via three conserved cysteine residues, Cys62, Cys66 and Cys69 of the CXXXCXXC motif. A juxtaposed SAM coordinates the fourth Fe ion through its amide nitrogen and carboxylate oxygen. Unexpectedly, HemN binds a second SAM molecule adjacent to the first SAM (Layer *et al.*, 2003). SAM was identified as a co-substrate for HemN catalysis and two SAM molecules are consumed for the formation of one Proto'gen (Layer *et al.*, 2005). A mechanism for HemN catalysis can be proposed based on the solved crystal structure of HemN in combination with Mössbauer and EPR spectroscopic studies (Layer *et al.*, 2003; Layer *et al.*, 2005; Layer *et al.*, 2006; Layer *et al.*, 2010). An electron is transferred from the reduced [4Fe-4S] cluster to SAM, resulting in homolytic cleavage of SAM into methionine and a 5'-deoxyadenosyl radical. This radical then abstracts the pro-*S* hydrogen atom at the β-position of the propionate group resulting in the formation of an allylic substrate radical (Layer *et al.*, 2006). The catalytic cycle finishes at the elimination of CO_2 and transfer of the remaining electron to a terminal electron acceptor.

1.6.6 Protoporphyrinogen IX oxidase

PPO catalyses the six-electron oxidation (aromatisation) of Proto'gen to form Proto, a fully conjugated and coloured tetrapyrrole. Although this reaction can readily occur non-enzymatically, it was demonstrated that an enzyme, PPO, is required under physiological conditions (Sano and Granick, 1961; Porra and Folk, 1961; Porra and Folk, 1964; Jacobs and Jacobs, 1981; O'Brian and Thony-Meyer, 2002). There are multiple structurally unrelated types of PPO found in nature: the oxygen-dependent PPO, encoded by the *hemY* gene, is present in eukaryotes and some bacteria including *Bacillus subtilis*, *Myxococcus xanthus* and *Aquifex aeolicus*; the oxygen-independent PPO, encoded by the *hemG* gene, is found in many *Gammaproteobacteria* including *E. coli*; in most cyanobacteria, the majority of *Proteobacteria* and *Bacteroidetes*, a third type of PPO was identified and the encoding gene was designated

as *hemJ*; there is at least one as-yet unidentified type of PPO in some species from *Bacteroidetes* and *Chlorobi* (Kato *et al*., 2010; Layer *et al*., 2010).

HemY contains non-covalently bound flavin adenine dinucleotide (FAD) as a cofactor and is a member of the FAD superfamily that also includes monoamine oxidase and phytoene desaturase (Dailey and Dailey, 1998). HemY uses molecular oxygen as the terminal electron acceptor. The native eukaryotic HemY proteins were purified to homogeneity from bovine, barley, mouse and yeast, with PPO activity demonstrated by *in vitro* assays (Siepker *et al*., 1987; Jacobs and Jacobs, 1987; Ferreira and Dailey, 1988; Camadro *et al*., 1994; Camadro and Labbe, 1996). All the eukaryotic HemY proteins are membrane-associated homodimers and are strongly inhibited by the diphenyl ether herbicide acifluorfen (AF). The eukaryotic enzymes cannot utilise Copro'gen as substrate. The bacterial HemY proteins were overexpressed in *E. coli*, purified to homogeneity and characterised (Dailey and Dailey, 1996; Corrigall *et al*., 1998; Wang *et al*., 2001). Both the *Myxococcus xanthus* and *Aquifex aeolicus* HemY proteins are similar to eukaryotic enzymes except the *Aquifex aeolicus* enzyme is a monomer. However, the *Bacillus subtilis* HemY differs from other HemY proteins as it is monomeric, cytoplasmic, able to utilise Copro'gen as substrate (Hansson and Hederstedt, 1994), and is resistant to AF. The crystal structure of tobacco mitochondrial HemY with a phenylpyrazole inhibitor has been solved and reveals a loosely associated dimer with each monomer consisting of three lobes: a FAD-binding domain of the *p*-hydroxybenzoate-hydrolase fold, a substrate-binding domain that encloses a narrow active site cavity beneath the FAD and an α-helical membrane-binding domain (Koch *et al*., 2004). The crystal structure of *Myxococcus xanthus* HemY in its ligand-free form and AF-bound form have also been reported (Corradi *et al*., 2006). The structure of *Myxococcus xanthus* HemY is similar to that of tobacco HemY regarding the overall topology, but the charge distribution and crystal packing are different (Corradi *et al*., 2006). The unique properties of the *Bacillus subtilis* HemY have been explained on the basis of the crystal structure of the enzyme complexed with AF (Qin *et al*., 2010).

The oxygen-independent PPO is less well-characterised and has mainly been studied with the *E. coli* enzyme. The *E. coli* enzyme was shown to be linked to the anaerobic respiratory chain and use alternative terminal electron acceptors such as nitrate or fumarate (Jacobs and Jacobs, 1975; Jacobs and Jacobs, 1976). The *E. coli* gene responsible for the PPO activity was cloned, sequenced and named as *hemG* (Sasarman *et al*., 1979; Sasarman *et al*., 1993). HemG is a member of the long chain flavodoxins and contains flavin mononucleotide as a cofactor.

The *E. coli* HemG has been overexpressed, purified and characterised (Boynton *et al.*, 2009). The purified *E. coli* HemG was shown to have a menadione-dependent PPO activity conveyed by the long chain insertion loop (Boynton *et al.*, 2009).

The absence of a *hemY* or *hemG* homologue in most archaea and many other bacteria including cyanobacteria suggests these organisms possess a as-yet unidentified type of PPO (Panek and O'Brian, 2002). Kato *et al.* (2010) identified the gene that is responsible for the PPO activity in *Synechocystis* by *in vitro* mutagenesis combined with functional complementation. This gene, slr1790, was subsequently designated as *hemJ*. The homologue of Slr1790 from *Rba. sphaeroides* was overexpressed in *E. coli* and the recombinant protein was shown to have PPO activity (Kato *et al.*, 2010). An independent study identified the *hemJ* gene in *Acinetobacter baylyi* ADP1 by bioinformatic search and experimental techniques (Boynton *et al.*, 2011). The *hemJ* homologue has been found in most cyanobacteria, the majority of *Proteobacteria* and *Bacteroidetes*. However, some species have PPO activity but do not contain a *hemY, hemG* or *hemJ* homologue, indicating there is at least one as-yet unidentified PPO encoding gene (Kato *et al.*, 2010).

Proto is at the second branch point in tetrapyrrole biosynthesis pathway, where haem biosynthesis and (B)Chl biosynthesis split. The fate of Proto is determined by two enzymes: ferrochelatase catalyses the insertion of ferrous iron into Proto to complete haem biosynthesis; whereas magnesium chelatase (Mg-chelatase) catalyses the insertion of magnesium into Proto to form magnesium-protoporphyrin IX (MgP), the first committed intermediate of (B)Chl biosynthesis. Although both ferrochelatase and Mg-chelatase catalyse a metal chelation reaction, they are structurally and mechanistically unrelated. Ferrochelatase is encoded by a single gene, *hemH*, and catalyses the energetically favorable insertion of iron into Proto without the requirement of ATP. Mg-chelatase is described in detail in the following section.

1.7 The core pathway of (bacterio)chlorophyll biosynthesis

All Chls and BChls can be synthesised from the hub intermediate, chlorophyllide *a* (Chlide *a*), which is produced from Proto by the core pathway of (B)Chl biosynthesis as shown in **Figure 1.6** (Chew and Bryant, 2007b). Mg-chelatase catalyses the insertion of magnesium ion into the Proto macrocycle to form MgP, determining the fate of the porphyrin molecule for (B)Chl biosynthesis. In oxygenic phototrophs, the Gun4 protein interacts with Mg-chelatase and

stimulates the reaction. The next step is the methylation of the C13 propionate side chain of MgP to form magnesium-protoporphyrin IX monomethyl ester (MgPME), catalysed by the MgP methyltransferase. Then the converstion of MgPME into 3, 8-divinyl protochlorophyllide *a* (DV PChlide *a*) via the formation of an isocyclic E ring is catalysed by an oxygen-dependent or oxygen-independent MgPME cyclase. The reduction of the D ring is catalysed by the PChlide reductase, which exists in two structural unrelated forms in nature. The reduction of the 8-vinyl group is catalysed by the divinyl reductase (DVR). This reaction can occur at different stages in the pathway and several types of DVR have been identified. After these 5 steps, the resulting Chlide *a* can be utilised to synthesise various types of (B)Chls depending on the organism.
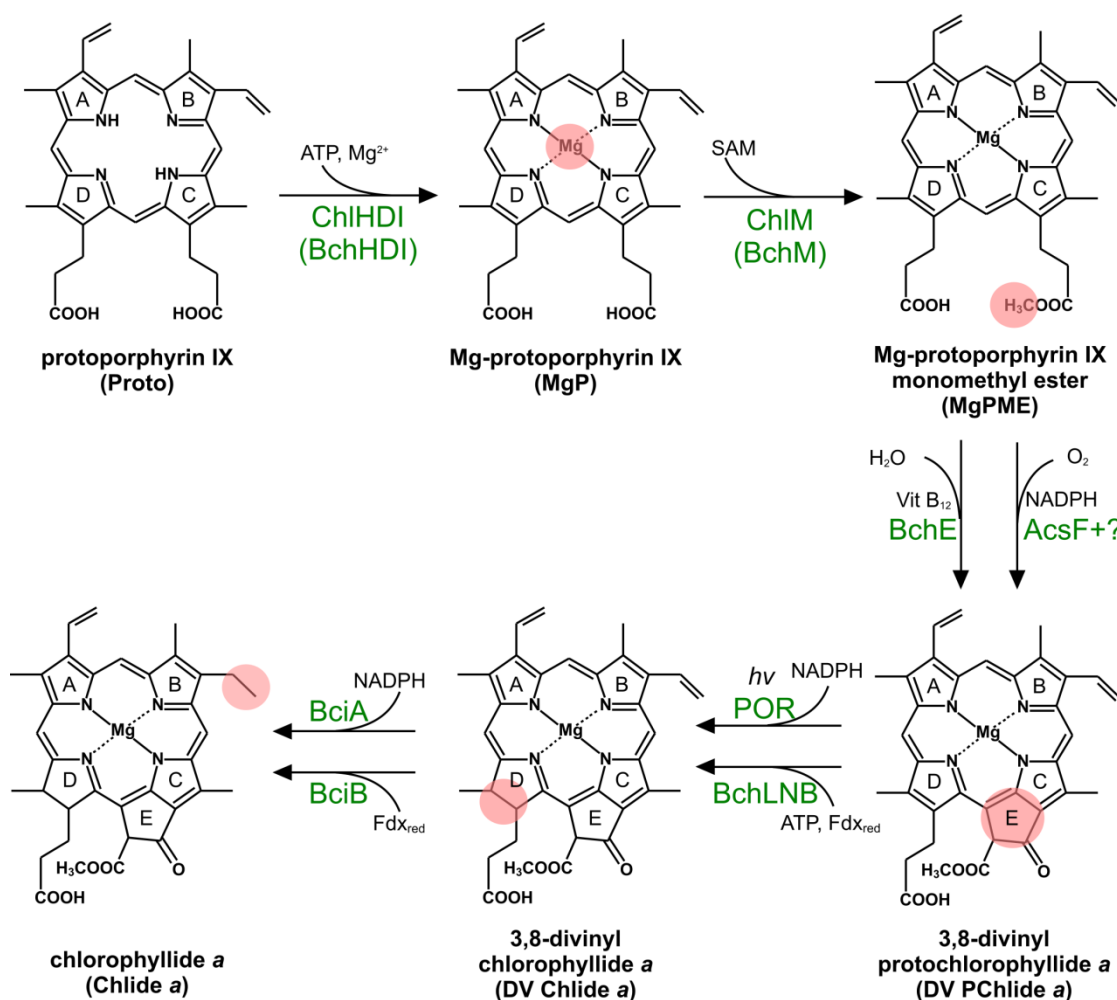
Figure 1.6 The core pathway of (bacterio)chlorophyll biosynthesis

For each step, the subunit composition of the enzyme, non-tetrapyrrole substrate, and required cofactors are shown on reaction arrows. The group modified by each step is marked by pink shading. Shown are based on Chew and Bryant (2007b).

1.7.1 Magnesium-protoporphyrin IX chelatase

The first committed step of (B)Chl biosynthesis is the insertion of magnesium into the Proto macrocycle to form MgP, catalysed by Mg-chelatase. Mg-chelatase is one of the two most extensively studied enzymes involved in (B)Chl biosynthesis. Despite catalyzing a superficially similar reaction as ferrochelatase, Mg-chelatase is completely different from ferrochelatase regarding the enzyme composition, reaction requirement and catalytic mechanism (Beale, 1999). Due to the difficulty of removing H_2O molecules coordinated to the Mg^{2+} (Fleischer *et al.*, 1964; Hambright, 1975), Mg chelation is energetically unfavourable and was demonstrated to require ATP (Pardo *et al.*, 1980).

Early biochemical work demonstrated Mg-chelatase activity in isolated etioplasts from cucumber and whole cells of *Rba. sphaeroides* (Gorchein, 1972; Gorchein, 1973; Smith and Rebeiz, 1977; Pardo *et al.*, 1980; Fuesler *et al.*, 1984; Walker and Weinstein, 1991a). The synthesis of MgP was proved to be an enzymatic reaction (Smith and Rebeiz, 1977). Mg-chelatase activity was abolished when cucumber etioplasts or *Rba. sphaeroides* cells were broken (Gorchein, 1973; Walker and Weinstein, 1991a). Richter and Rienits (1982) showed the synthesis of MgP using membranes of cucumber etioplasts, but the synthesis rate was too low to be significant. Mg-chelatase activity was only observed in the presence of ATP (Gorchein, 1973; Pardo *et al.*, 1980; Walker and Weinstein, 1991a). The first true *in vitro* Mg-chelatase assay conducted with fractions of lysed pea chloroplasts resolved the activity into soluble and membrane-bound components (Walker and Weinstein, 1991b). Broken and reconstituted cucumber etioplasts were unable to maintain Mg-chelatase activity, which was shown to be caused by an inactive membrane component (Walker and Weinstein, 1991b). However, Lee *et al.* (1992) showed that if the cucumber etioplasts were lysed in the presence of Proto, ATP and Mg^{2+}, the membrane fraction from lysed etioplasts alone is capable of synthesizing MgP. This particular lysis method may stabilize the entire Mg-chelatase complex which is localised in the membrane fraction (Walker and Willows, 1997). Later on, cell-free Mg-chelatase activity was demonstrated in *Rba. sphaeroides* and *Rba. capsulatus* (Gorchein, 1997).

Genetic work with *Rba. sphaeroides* and *Rba. capsulatus* identified three genes, *bchH*, *bchI* and *bchD*, to be responsible for the Mg chelation (Coomber *et al.*, 1990; Bollivar *et al.*, 1994b). *In vitro* Mg-chelatase assays using lysates of *E. coli* overexpressing the *bchH*, *bchI* and *bchD* genes of *Rba. sphaeroides* further confirmed that BchH, BchI and BchD were the necessary and sufficient components of Mg-chelatase (Gibson *et al.*, 1995). The homologous genes have

been identified and termed as *chlH* (*Xantha-f* in barley), *chlI* (*Xantha-h* in barley) and *chlD* (*Xantha-g* in barley) in Chl-containing phototrophs including *Arabidopsis* (Koncz *et al.*, 1990), *Antirrhinum majus* (Hudson *et al.*, 1993), *Synechocytis* (Jensen *et al.*, 1996b), barley (Jensen *et al.* 1996a; Kannangara *et al.*, 1997; Petersen *et al.*, 1999) and tobacco (Papenbrock *et al.*, 1997). The *Synechocystis* Mg-chelatase encoding genes were overexpressed in *E. coli*, resulting in a functional enzyme *in vitro* (Jensen *et al.*, 1996b). Mg-chelatase activity was also reconstituted from recombinant yeast strains overexpressing tobacco Mg-chelatase encoding genes (Papenbrock *et al.*, 1997).

Large quantities of Mg-chelatase proteins can be produced in heterologous expression systems and subsequently purified, allowing extensive biochemical and structural analysis. The Mg-chelatases from *Synechocystis*, *Rba. sphaeroides* and *Rba. capsulatus* have been studied in greatest detail and all enzymes absolutely require ATP, Mg^{2+} and a suitable porphyrin substrate for activity. In all three cases a significant lag phase of the reaction was observed and can be reduced by pre-incubating BchI/ChlI and BchD/ChlD with ATP and Mg^{2+} (Willows *et al.*, 1996; Willows and Beale, 1998), with an additional pre-incubation of ChlH with Proto, ATP and Mg^{2+} for *Synechocystis* Mg-chelatase (Jensen *et al.*, 1998). The occurrence of a lag phase indicates that an enzyme activation step preceded the insertion of the metal ion (Walker and Weinstein, 1994). The activation step involves BchI/ChlI and BchD/ChlD and requires the presence of hydrolysable ATP or adenosine 5'-[γ-thio]triphosphate (ATP[γ-S]) (Walker and Weinstein, 1994). The magnesium insertion step also requires ATP, which cannot be replaced by ATP[γ-S] (Walker and Weinstein, 1994).

The K_m values of *Synechocystis* Mg-chelatase for ATP, Mg^{2+} and Proto have been determined as 0.49 mM, 4.9 mM and 1.25 μM, respectively (Jensen *et al.*, 1998). The K_m value for Mg^{2+} is much higher than that of ATP, suggesting free Mg^{2+} is also required in addition to the Mg^{2+} bound to ATP ($MgATP^{2-}$) (Jensen *et al.*, 1998). Free Mg^{2+} has positive cooperativity on Mg-chelatase as well as acting as a substrate (Reid and Hunter, 2004). It has been demonstrated that the reaction catalysed by Mg-chelatase requires hydrolysis of ~15 $MgATP^{2-}$ *in vitro* and that the magnesium insertion step is energetically unfavourable, with a $\Delta G°'$ of 25~33 kJ/mol (Reid and Hunter, 2004). Many Mg-chelatase assays were conducted using an alternative porphyrin substrate, deuteroporphyrin IX (Deutero) because it is more soluble in water than Proto. The K_m value of *Synechocystis* Mg-chelatase for Deutero is estimated to be 3.20 μM, which is higher than that for Proto (Reid and Hunter, 2004).

The three subunits of Mg-chelatase, BchH/ChlH, BchI/ChlI and BchD/ChlD, have predicted molecular masses of 120~155 kD, 37~46 kD and 60~87 kD, respectively (Beale, 1999). The H subunit shares homology with CobN subunit of cobalt chelatase, and all three Mg-chelatase subunits are similar to the counterparts of nickel chelatase (Walker and Willows, 1997). The H subunit has been found to be the porphyrin-binding subunit because of the following observations: Overexpressed BchH binds Proto in *E. coli* (Gibson *et al*., 1995); BchH binds Proto in an approximate molar ratio of 1:1 to form a stable complex which can survive throughout purification (Willows *et al*., 1996; Willows and Beale, 1998); and pre-incubation of ChlH with Proto, ATP and Mg^{2+} can significantly reduce the lag phase of Mg-chelatase reaction (Jensen *et al*., 1998). The porphyrin-binding property of the H subunit has been studied using Deutero with *Rba. sphaeroides* BchH and *Synechocystis* ChlH (Karger *et al*., 2001). The binding process does not require Mg^{2+} or ATP or the I or D subunits. The K_d values for Deutero binding to *Rba. sphaeroides* BchH and *Synechoccystis* ChlH were determined as 1.22 ± 0.42 μM and 0.53 ± 0.12 μM, respectively. Deutero is subjected to nonplanar distortion of the macrocycle upon binding to the H subunit (Karger *et al*., 2001). Hansson and Kannangara (1997) reported the ATPase activity of the H subunit, but this was found later to be an artefact resulted from a contaminating *E. coli* protein (Sirijovski *et al*., 2006). Besides, ChlH from *Synechocystis* was shown to stimulate the activity of MgP methyltransferase (ChlM), the next enzyme in Chl biosynthesis pathway, by accelerating the formation and breakdown of an intermediate in the catalytic cycle of ChlM (Shepherd *et al*., 2005).

The BchH subunit from *Rba. capsulatus* was analysed by single-particle electron microscopy (EM) and a three-lobed structure was revealed at a resolution of 25 Å (Sirijovski *et al*., 2008). The binding of Proto involves both the N- and C-terminal of BchH, causes a distinct conformational change in two of three lobes and protects BchH from degradation (Sirijovski *et al*., 2008). The cyanobacterial ChlH is a large cage-like assembly adjoining by a small, globular N-terminal domain, determined by single-particle EM and small-angle X-ray scattering at a resolution of ~30 Å (Qian *et al*., 2012). The caged structure of ChlH, which is not in BchH, has been proposed to be responsive to the intracellular environment of oxygenic phototrophs (Qian *et al*., 2012). The crystal structure of *Synechocystis* ChlH was solved at a resolution of 2.5 Å, providing the molecular basis for the substrate channelling during the reaction (Chen *et al*., 2015a). As shown by the solved structure, ChlH is composed of six domains (I~VI), with domains III~VI to form the cage-like assembly, and with domains I and II to form the N-terminal "head" and "neck" regions. At the interface between domains III and

V, there is an internal pocket whose size is large enough to engulf a porphyrin ligand (Chen *et al.*, 2015a).

The I and D subunits are both members of the 'ATPase associated with a variety of cellular activities' (AAA[+]) family of ATPases (Neuwald *et al.*, 1999; Fodje *et al.*, 2001). At the activation step of the reaction, the I and D subunits interact with MgATP to form the I-D-MgATP complex, which does not require ATP hydrolysis (Gibson *et al.*, 1999; Jensen *et al.*, 1999; Jensen *et al.*, 2000). The I subunit is the active ATPase component of Mg-chelatase, whereas the D subunit is not (Jensen *et al.*, 1999). The I subunit only catalyses the hydrolysis of ATP when an additional Mg^{2+} is bound (Reid *et al.,* 2003) and the catalysis is via an enzyme-phosphate complex (Adams and Reid, 2012). In addition, the ATPase activity of the I subunit is repressed in the presence of the D subunit (Jensen *et al.*, 1999). The crystal structure of BchI from *Rba. capsulatus* has been solved at a resolution of 2.1 Å (Fodje *et al.*, 2001). The structure reveals an N-terminal AAA[+] module containing nucleotide-binding site and a C-terminal helical domain. Sequence analysis revealed that BchD contains a C-terminal integrin I domain, a proline-rich acidic linker domain and an N-terminal AAA[+] module. The C-terminal integrin I domain of BchD was suggested to be involved in the interaction with BchI and BchH during the catalytic cycle. The proline-rich linker domain has been proposed to bind to the positively charged groove on the surface of BchI (Fodje *et al.*, 2001). The N-terminal AAA[+] domain of ChlD from *Synechocytis* has been shown to allosterically regulate Mg^{2+} and MgATP binding of Mg-chelatase (Adams and Reid, 2013). Very recently, it has been demonstrated that the C-terminal domain of *Synechocytis* ChlD is responsible for Mg^{2+} cooperativity upon Mg-chelatase, in which five Glu residues play a major role (Brindley *et al.*, 2015).

AAA[+] proteins often form oligomeric complexes. Single-particle EM demonstrated that in the presence of ATP, ChlI from *Synechocystis* forms heptameric rings and BchI forms hexameric rings (Reid *et al.,* 2003; Willows *et al.*, 2004). BchD from *Rba. capsulatus* was shown to form ATP-independent hexameric structures which were proposed to serve as a platform for the assembly of the BchI subunits (Axelsson *et al.*, 2006). The *Rba. capsulatus* BchI and BchD form stable complexes which have been revealed as ~660 kD bipartite hexamers at a resolution of 7.5 Å by single-particle EM (Elulund *et al.*, 2008). Furthermore, reconstructions of BchI-BchD complex with ATP, ADP and the nonhydrolysable ATP analog, AMP-PNP, have demonstrated that the ATP hydrolysis is coupled with substantial conformational changes in the BchI-BchD complex and suggested the C-terminal integrin I domain of BchD transmits conformational changes of BchI to BchD (Lundqvist *et al.*, 2010).

A model of the catalytic cycle of Mg-chelatase has been proposed (**Figure 1.7**) (Masuda, 2008; Heyes and Hunter, 2009). At the activation step, six I subunits and six D subunits interact with MgATP to form the I-D-MgATP complex, which is a two-tiered hexameric ring structure. In this complex, the ATPase activity of I subunit is inhibited by the binding of the C-terminal integrin I domain of D subunit. Meanwhile, the H subunit binds to Proto and most likely also Mg^{2+} to form the Mg-H-Proto complex. At the chelation step, the Mg-H-Proto complex reacts with the I-D-MgATP complex to form a transient holoenzyme complex. Magnesium insertion proceeds with the hydrolysis of ATP. After the formation of MgP, the holoenzyme complex disassembles and the subunits can be recharged with their ligand/ligands for next catalytic cycle.
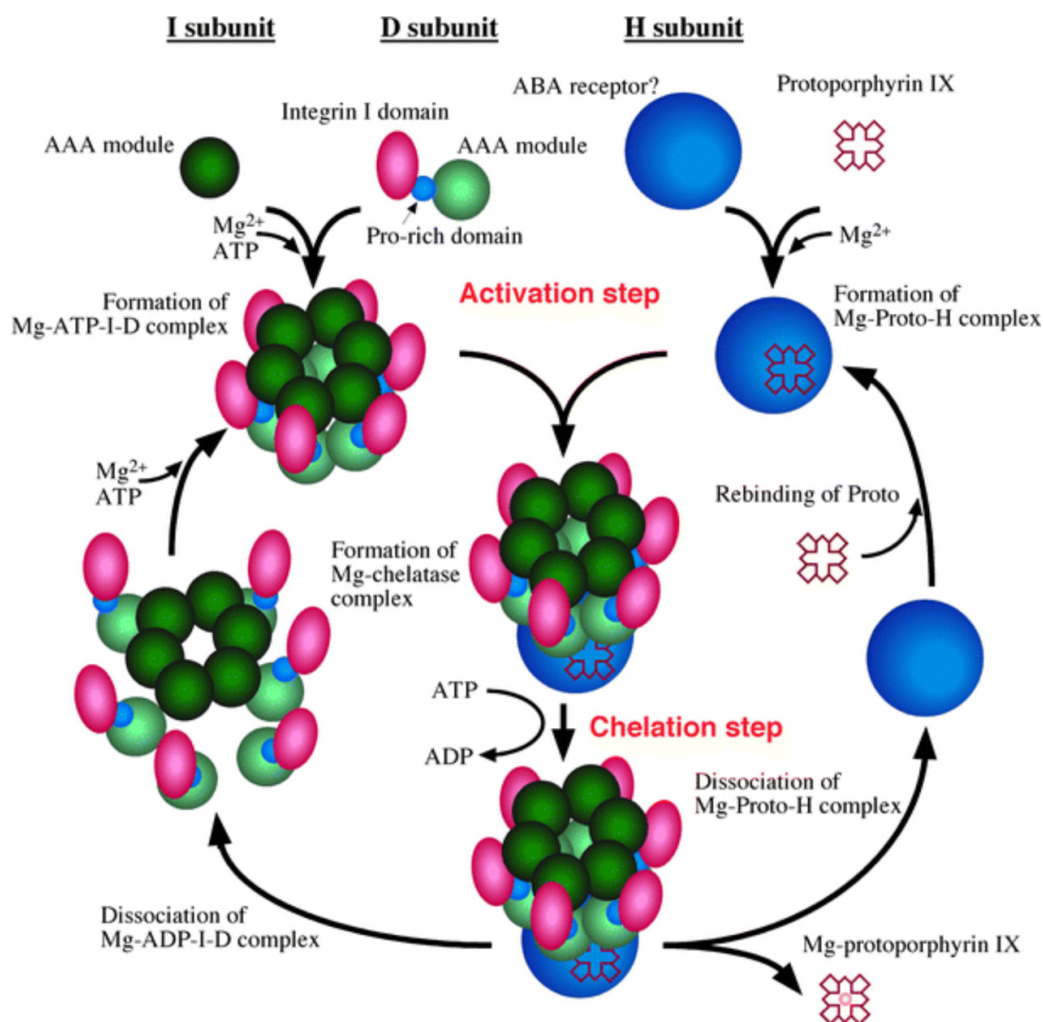
Figure 1.7 Proposed model of the catalytic cycle of Mg-chelatase

Activation step: the subunits I and D form a complex with MgATP. The H subunit forms a complex with Proto and Mg^{2+}. Chelation step: a transient Mg-chelatase holoenzyme complex is formed. Mg insertion is driven by the hydrolysis of ATP. The complex then disassembles and the subunits are ready for the next catalytic cycle. Shown are from Masuda (2008).

In addition to its enzymatic function as a subunit of Mg-chelatase, ChlH has some other functions. In higher plants, ChlH plays a key role in plastid-to-nucleus signal transduction (Mochizuki *et al.*, 2001; Surpin *et al.*, 2002; Strand *et al.*, 2003; Nott *et al.*, 2006). In *Arabidopsis*, ChlH was identified to specifically bind abscisic acid (ABA) and mediate ABA signalling as a positive regulator in seed germination, post-germination growth and stomatal movement, through antagonizing a group of WRKY transcription repressors (Shen *et al.*, 2006; Wu *et al.*, 2009; Shang *et al.*, 2010). The role of *Arabidopsis* ChlH in ABA signalling has been confirmed by another research group studying of ABA-mediated plant responses to drought conditions (Legnaioli *et al.*, 2009). However, there are still some arguments in the literature concerning the function of ChlH in ABA signalling (Muller and Hansson, 2009; Tsuzuki *et al.*, 2011). In *Synechocystis*, ChlH has been proposed to be an anti-sigma factor for SigE and to repress sugar catabolic pathways (Osanai *et al.*, 2005; Osanai *et al.*, 2009).

GUN4

GUN4 (genomes uncoupled 4) was originally discovered in a search for *Arabidopsis* mutants which are defective in plastid-to-nucleus signalling (Susek *et al.*, 1993). The *GUN4* gene product was shown to bind the substrate and product of Mg-chelatase, and activate Mg-chelatase by binding to ChlH (Mochizuki *et al.*, 2001; Larkin *et al.*, 2003). The homologues of *GUN4* appear to be only present in oxygenic phototrophs including cyanobacteria and photosynthetic eukaryotes. An *Arabidopsis GUN4* mutant contains reduced Chl level compared to WT (Mochizuki *et al.*, 2001). Inactivation of the *gun4* gene in *Synechocystis* impairs Mg-chelatase activity, resulting in decreased Chl level and the inability to grow photoautotrophically (Sobotka *et al.*, 2008). A *gun4* insertion mutant of *C. reinhardtii* contains only 50% of Chl as WT and accumulates Proto (Formighieri *et al.*, 2012). In addition, GUN4 has been proposed to be involved in the posttranslational regulation of ALA and Chl biosynthesis in plants (Peter and Grimm, 2009).

Biochemical and structural characterisation of Gun4 has provided much more information to understand the mechanism of Gun4. It was demonstrated *in vitro* that Gun4 dramatically increases the efficiency of the Mg-chelatase reaction and reduces the threshold Mg^{2+} concentration required for activity at low porphyrin concentration (Davison *et al.*, 2005). By altering the response of Mg-chelatase to Mg^{2+} at physiologically relevant concentrations, Gun4 has been proposed to act as a molecular switch *in vivo* to control the activity of Mg-chelatase (Davison *et al.*, 2005). It has been suggested that GUN4 may activate ChlH in a different mechanism from cyanobacterial Gun4 as the eukaryotic GUN4 requires its unique C-

terminal extension for activation (Zhou *et al*., 2012). The crystal structures of ligand-free Gun4 from *T. elongatus* and *Synechocystis* both show a highly helical, and two-domain structure with a hand-shaped fold for porphyrin binding (Davison *et al*., 2005; Verdecia *et al*., 2005). The structures of porphyrin-bound Gun4 reveals that the binding of porphyrin causes significant conformational changes in Gun4, resulting in the formation of a porphyrin-binding pocket that is not apparently present in the structures of porphyrin-free Gun4 (Chen *et al*., 2015b).

1.7.2 Mg-protoporphyrin IX methyltransferase

MgP methyltransferase catalyses the methyl transfer from SAM to the C13 propionate side chain of MgP. The methylation is thought to be indispensable to protect the propionate group from spontaneous decarboxylation during the next step of (B)Chl biosynthesis (Beale, 1999). This reaction is considered to be similar to other methyltransferase reactions and not to play a marked role in the regulation of the biosynthesis pathway (Bollivar, 2006). As the spectroscopic features of the tetrapyrrole substrate and product are identical, it is impossible to conduct a simple spectroscopic assay (Bollivar, 2006). Instead, the activity of the methyltransferase can be measured by coupled assays, chromatographic assays or radiometric assays.

Early biochemical studies demonstrated the methyltransferase activity in isolated chromatophores from *Rba. sphaeroides* and isolated chloroplasts from maize (*Zea mays*) by using ^{14}C-methyl-labelled SAM as the methyl donor (Tait and Gibson, 1961; Gibson *et al*., 1963; Radmer and Bogorad, 1967). The *Rba. sphaeroides* enzyme was shown to have some specificity for the tetrapyrrole substrate: zinc- and calcium-protoporphyrin IX are substrates for the enzyme, while ferrous, ferric, manganous, manganic and metal-free protoporphyrins are not (Gibson et al., 1963).

The methyltransferase is encoded by a single gene and was designated as *bchM* in BChl-containing phototrophs and *chlM* in Chl-containing phototrophs. The *bchM* genes from *Rba. sphaeroides* and *Rba. capsulatus* were cloned, sequenced and overexpressed in *E. coli* producing the functional methyltransferase of which the activity was confirmed by *in vitro* enzyme assay (Gibson and Hunter, 1994; Bollivar *et al*., 1994a). By complementation of a *bchM* mutant of *Rba. capsulatus*, Smith *et al*. (1996) identified the *chlM* gene from *Synechocystis*. The first plant methyltransferase encoding gene was identified from *Arabidopsis* and the enzyme was found to be located in both chloroplast envelope and

thylakoid membranes (Block *et al.*, 2002). The cloning and expression studies of tobacco *CHLM* gene were reported by Alawady *et al*. (2005) and they revealed the posttranslational activation of methyltransferase during greening and light/dark-cycles.

Kinetic studies have been performed using the recombinant *Synechocystis* ChlM protein purified from *E. coli*: steady-state kinetic study revealed the reaction proceeds via a ternary complex which is formed by random binding of substrates to the enzyme; transient kinetic analysis demonstrated the presence of an enzyme isomerisation step that precedes the binding of MgP and the formation of an intermediate during the reaction (Shepherd *et al.*, 2003; Shepherd and Hunter, 2004). An enzyme-coupled continuous spectrophotometric assay for the methyltransferase has been developed by enzymatically converting the non-porphyrin product *S*-adenosyl-L-homocysteine (SAH) to hypoxanthine, which can be monitored by a decrease in absorbance at 265 nm (McLean and Hunter, 2009). This rapid and continuous methyltransferase assay allows more accurate measurement of the enzyme activity compared with HPLC-based discontinuous assays (McLean and Hunter, 2009). Recently, the crystal structures of the SAM- and SAH-bound *Synechocystis* ChlM have been solved (Chen *et al*., 2014). Based on the structures, a catalytic model for *Synechocystis* ChlM was proposed: the C13 propionate group of MgP is properly positioned by Tyr-28 and His-139 at the active site to facilitate a direct methyl transfer from SAM to MgP; two "arm" regions present in the enzyme may modulate binding and release of substrates/products to and from the active site through conformational changes (Chen *et al*., 2014).

The interaction between methyltransferase and the H subunit of Mg-chelatase has been demonstrated by multiple researchers (Hinchigeri *et al.,* 1997; Alawady *et al.,* 2005; Shepherd *et al.*, 2005; Johnson and Schmidt-Dannert, 2008). Actually, BchH was mistakenly assigned as the methyltransferase due to the close relation between the chelation and methyl transfer reaction (Gorchein *et al*., 1993). *Rba. capsulatus* BchH protein was shown to be able to activate BchM (Hinchigeri *et al*., 1997). Using purified recombinant *Synechocystis* ChlH and ChlM proteins, Shepherd *et al.* (2005) demonstrated that ChlH can dramatically accelerate the formation and breakdown of an intermediate in the catalytic cycle of ChlM and is thus directly involved in the reaction chemistry. The tobacco CHLM is stimulated in the presence of CHLH and the physical interaction between these two proteins was confirmed by yeast two-hybrid system (Alawady *et al*., 2005). Substrate channelling between methyltransferase and Mg-chelatase, which may reduce the phototoxicity of free MgP, has been suggested but not tested yet (Bollivar, 2006; Masuda, 2008). In addition, plant CHLM was also linked to

other tetrapyrrole synthesis step: lower CHLM activity leads to reduced magnesium chelatase activity and ALA synthesis rate, but increased ferrochelatase activity (Alawady and Grimm, 2005).

1.7.3 Mg-protoporphyrin IX monomethyl ester cyclase

The conversion of MgPME into DV PChlide *a* is catalysed by MgPME cyclase. The isocyclic ring (E ring) formation causes a red-shifted colour change, from red to green (**Figure 1.8 A**). This cyclisation reaction makes (B)Chls unique from other tetrapyrroles, without which our world would look like an infrared photograph as shown in **Figure 1.8 B** (kindly provided by Ed Thompson). Although being studied for over 65 years, the cyclisation reaction remains the least understood step in the Chl biosynthesis pathway. The active enzyme has never been completely purified either from a native or a recombinant system.
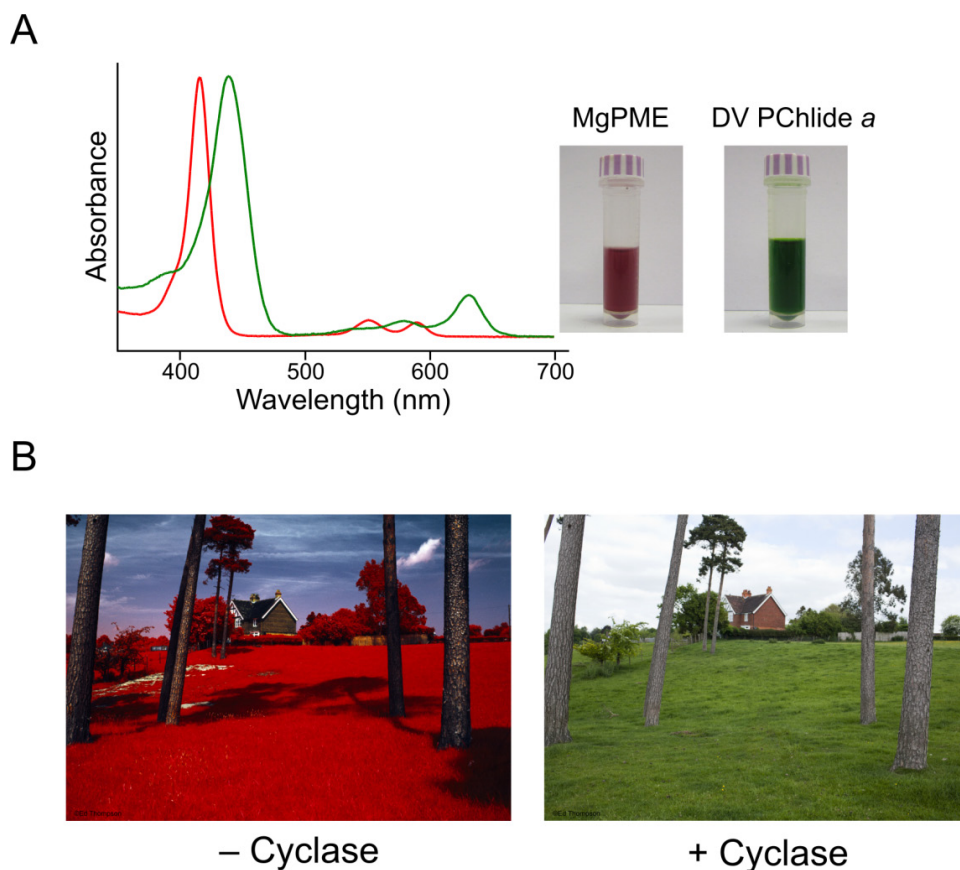
Figure 1.8 The dramatic colour change catalysed by Mg-protoporphyrin IX monomethyl ester cyclase

(**A**) The appearances and absorption spectra of the substrate (MgPME) and the product (DV PChlide *a*) of the reaction catalysed by the cyclase. (**B**) Infrared photograph versus normal photograph, illustrating the effect made by the cyclase. The photographs were kindly provided by Ed Thompson.

Granick (1948) first proposed the isocyclic ring may be formed in a way similar to the β-oxidation of fatty acids, which is by the β-oxidation of 13-methyl propionate group of MgPME, via 13^1-13^2 acrylate, 13^1-hydroxy, 13^1-keto intermediates. The 13^1-hydroxy and 13^1-keto intermediates were confirmed using reconstituted organelle-free cyclase system prepared from developing cucumber chloroplasts (Wong *et al.*, 1985; Wong and Castelfranco, 1985). Further study with this system showed the 13^1-13^2 acrylate was inactive as a substrate for the cyclisation and the 13^1-hydroxy intermediate is formed in an asymmetric hydroxylation reaction (Walker *et al.*, 1988). Thus, the original scheme proposed by Granick was modified by omitting the 13^1-13^2 acrylate, as shown in **Figure 1.9**.

Mg-protoporphyrin IX monomethyl ester (MgPME) → **13^1-hydroxy intermediate** → **13^1-keto intermediate** → **3,8-divinyl protochlorophyllide *a* (DV PChlide *a*)**
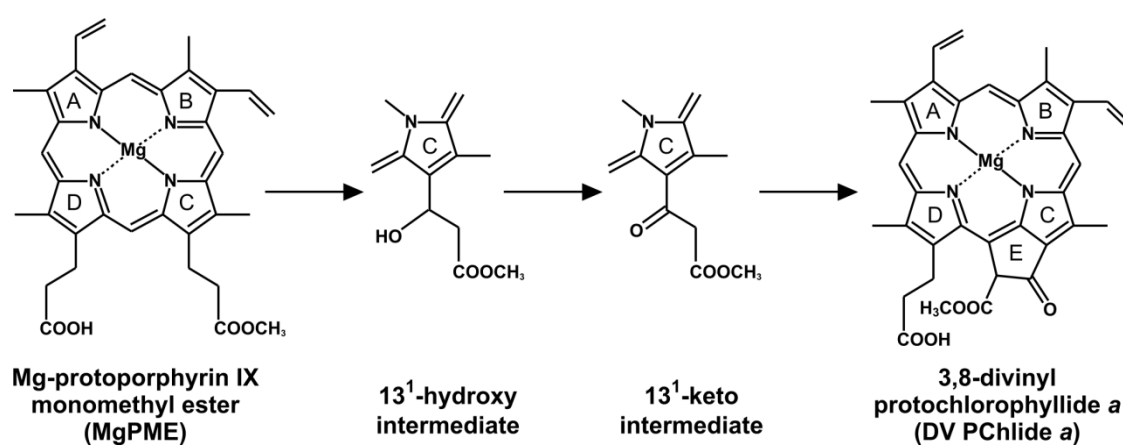
Figure 1.9 The intermediates of Mg-protoporphyrin IX monomethyl ester cyclase reaction
MgPME is converted into DV PChlide *a* via 13^1-hydroxy and 13^1-keto intermediates.

The first clue to the oxygen requirement of the cyclase was from *in vivo* observations on plants grown under O_2 deficiency: (1) plants contained less Chl but accumulated MgPME; (2) when fed with ALA in the dark, plants accumulated much less PChlide but much more MgPME (Spiller *et al.*, 1982). Furthermore, cyclase assays conducted with isolated etioplasts from cucumber cotyledons and wheat shoots showed O_2 was absolutely required for cyclase activity (Chereskin and Castelfranco, 1982; Chereskin *et al.*, 1982; Nasrulhaq-Boyce *et al.*, 1987). By conducting $^{18}O_2$-labelling experiments with detached cucumber cotyledons, Walker *et al.* (1989) established the oxygen atom in the isocyclic ring comes from molecular oxygen. Cyclase systems from the green alga *C. reinhardtii* and the cyanobacterium *Synechocystis* also require O_2 for activity as shown by *in vitro* cyclase assay (Bollivar and Beale, 1995; Bollivar and Beale, 1996).

Duggan and Gassman (1974) found that etiolated bean (*Phaseolus vulgaris*) leaves accumulated large amounts of MgPME when treated with iron chelators, and this effect was

also observed in etiolated tissues of corn (*Zea mays*), cucumber (*Cucumis sativus*) and pea (*Pisum sativum*). Their results were confirmed by Spiller *et al*. (1982) who found that plants grown under iron deficiency had less Chl content and accumulated MgPME. Although Chereskin and Castelfranco (1982) failed to either demonstrate or rule out the iron requirement in cyclase assay with isolated cucumber etioplasts, they still supported the proposal that a Fe-dependent oxygenase was involved in the cyclase reaction. Another group working on wheat etioplasts obtained clear evidence for the iron requirement and they found that only hydrophobic chelators were effective inhibitors of the cyclase reaction, indicating that the iron-dependent reaction occurred on the inside of plastid membrane (Nasrulhaq-Boyce *et al*., 1987). Bollivar and Beale (1996) showed that the cyclase from both eukaryotic and prokaryotic phototrophs requires Fe^{2+} for activity, which cannot be replaced with other metal ions including Zn^{2+}, Fe^{3+}, Cu^{2+} and Mn^{2+}. In addition, inhibitor studies on the cyclase excluded the possible involvement of iron-sulfur proteins or hemoproteins (Chereskin *et al*., 1982; Bollivar and Beale, 1996).

Chereskin *et al*. (1982) found cyclase activity could be stimulated by addition of NADPH or $NADP^+$ in isolated cucumber plastids but they admitted that this stimulation was variable in their hands. By using a reconstituted cyclase system from cucumber plastids, Wong and Castelfranco (1984) investigated the effects of pyridine nucleotides in detail and they found, (1) only the reduced pyridine nucleotides (NADPH and NADH) can activate the reconstituted system; (2) at low concentration (<2 mM), NADPH was more effective than NADH. The same research group then found sugar phosphates (glucose-6-phosphate and 6-phosphogluconate) alone could activate the reconstituted cyclase system probably through a protein-bound NADPH pool which was vulnerable to NADPH competitors or NADPH depletion systems (Whyte and Castelfranco, 1993). The dependence on NADPH was also observed in the cyclase systems from wheat etioplasts, *C. reinhardtii* chloroplasts and *Synechocystis* (Nasrulhaq-Boyce *et al*., 1987; Bollivar and Beale, 1995; Bollivar and Beale, 1996).

Besides these three key findings (requirements of O_2, Fe, and NADPH) of the cyclase system, several other properties regarding inhibitor studies and substrate specificity are noteworthy. The eukaryotic cyclase system was proved to be insensitive to inhibitors of iron-sulfur proteins, hemoproteins, copper proteins and flavoproteins (Chereskin *et al*., 1982; Whyte and Castelfranco, 1993; Bollivar and Beale, 1996); but extremely sensitive to artificial electron acceptors (Chereskin *et al*., 1982), and benzoquinone or benzoquinol (Whyte and Castelfranco, 1993). This enzyme system requires essential sulfhydryls (Wong and

Castelfranco, 1984; Fuesler *et al*., 1984; Wong and Castelfranco, 1985) and essential disulfides (Wong and Castelfranco, 1985) for function. Reactive oxygen quenchers, such as catalase and ascorbate, can significantly increase cyclase activity (Bollivar and Beale, 1996). This enzyme system also exhibits some substrate specificity. Zinc protoporphyrin monomethyl ester as well as MgPME, but not copper or nickel or metal-free protoporphyrin monomethyl ester, are substrates (Nasrulhaq-Boyce *et al*., 1987). The 13^1-hydroxy and 13^1-keto MgPME intermediates as proposed in Granick's scheme can be a substrate but only one of the two enantiomers of 13^1-hydroxy MgPME works (Walker *et al.*, 1988). Both 8-vinyl and 8-ethyl MgPME can be substrates while the vinyl at position 3 cannot be replaced with an ethyl (Wong and Castelfranco, 1985; Nasrulhaq-Boyce *et al*., 1987; Walker *et al.*, 1988).

The first attempt at biochemical purification of cyclase enzyme was reported by Wong and Castelfranco (1984), which was performed using a lysate of developing chloroplasts from cucumber. The cucumber cyclase enzyme was resolved into a high-speed supernatant fraction which could be enriched by $(NH_4)_2SO_4$ precipitation, and a membrane pellet fraction. Further purification conducted by the same group revealed several properties of the soluble and membrane fractions: (1) solubilisation of the pellet fraction appeared to be not possible; (2) the membrane fraction requires heavy-metal ions for function; (3) the cyclase soluble protein(s) is over 30 kD and does bind to porphyrin but not NADPH; (4) the optimum pH of the reconstituted cyclase is 9.0; (5) the cyclase soluble protein(s) can be purified 40-fold by $(NH_4)_2SO_4$ fractionation and hydrophobic-interaction (phenyl-Sepharose) chromatography (Walker *et al.*, 1991). A different group reported the purification of the cyclase enzyme from *C. reinhardtii* chloroplasts and *Synechocystis* (Bollivar and Beale, 1996). Interestingly, they found the cyclase in *C. reinhardtii* only requires the membrane fraction for activity and further attempts to purify the membrane fraction again failed. However, the cyclase from *Synechocystis* requires both the soluble and membrane fractions. The membrane fraction was able to be solubilised by the detergent *n*-octyl-β-D-glucoside and partially purified 3-fold by dye-affinity (Red-agarose) and ion-exchange (DEAE-cellulose) chromatography (Bollivar and Beale, 1996).

The cyclase step belongs to the core pathway to synthesise Chlide *a*, the universal precursors of all (B)Chls. Many anoxygenic photosynthetic bacteria, such as *Rba. sphaeroides* and *Rba. capsulatus*, synthesise BChls under anaerobic conditions, which implies the existence of the second type of cyclase different from the oxygen-dependent enzyme utilised by oxygenic phototrophs. The gene encoding the anaerobic or oxygen-independent cyclase was first

identified in *Rba. sphaeroides* via analysing a mutant (N6) which cannot synthesise BChl but excretes MgPME, and this gene was designated as *bchE* (Hunter and Coomber, 1988). The homologue of *bchE* was then identified in *Rba. capsulatus* (Yang and Bauer, 1990; Bollivar *et al.*, 1994b). By observing the phenotypes and conducting *in vivo* cyclase assays in cobalamin-requiring mutants of *Rba. capsulatus*, Gough *et al.* (2000) demonstrated cobalamin was a cofactor of the anaerobic cyclase and they proposed an adenosyl radical mediated reaction for the anaerobic cyclase (**Figure 1.10**). Recently, two genes from *Cyanothece* sp. PCC7425 and PCC7822 were identified as the cyanobacteria *bchE* homologues as they can complement *Rba. capsulatus bchE*-lacking mutant (Yamanashi *et al.*, 2015).
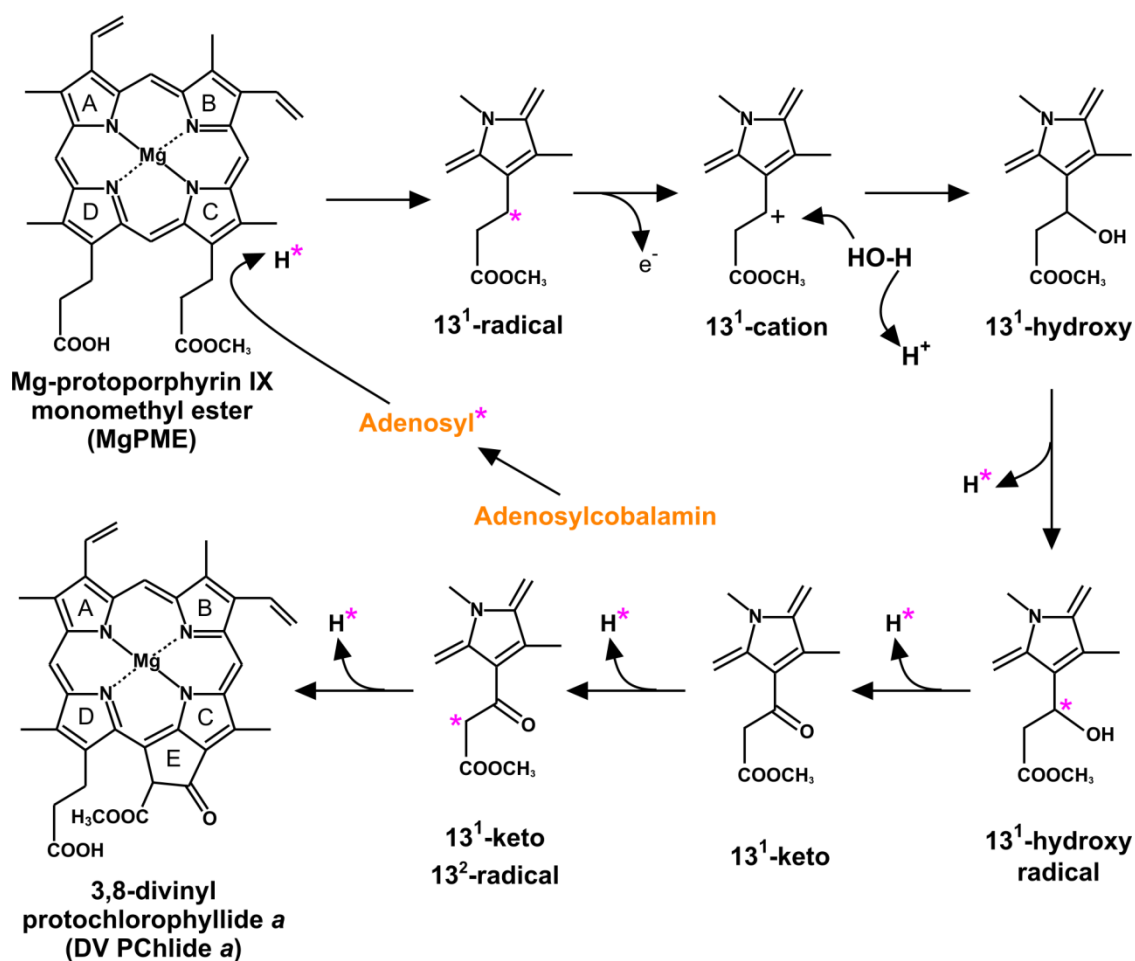
Figure 1.10 The proposed radical reaction mechanism for the anaerobic cyclase

The anaerobic cyclase requires a cobalamin (vitamin B_{12}) cofactor. Adenosylcobalamin forms the adenosyl radical, which attacks MgPME to form 13^1-radical of MgPME. Withdrawal of an electron leads to the formation of the 13^1-cation of MgPME, which is subsequently attacked by a hydroxyl ion to form the 13^1-hydroxy of MgPME. Four hydrogen atoms are withdrawn successively to give the final product DV PChlide *a*. Radicals are marked by an asterisk. Modified from Gough *et al.* (2000).

Although early biochemical approaches revealed several important features of the aerobic cyclase, the genetic identity of this enzyme had remained elusive until Pinta *et al*. (2002) identified the first subunit of aerobic cyclase from *Rubrivivax gelatinosus* (*Rvi. gelatinosus*). They found that *orf358*, a previously unidentified ORF, played a crucial role in the aerobic cyclase reaction, and the protein encoded by *orf358* contained a diiron binding motif (E-x_n-E-x-x-H-x_n-E-x_n-E-x-x-H) (Berthold and Stenmark, 2003). Thus, they designated *orf358* as *acsF* (aerobic cyclisation system Fe-containing subunit). Homologues of AcsF are widespread in photosynthetic organisms from bacteria to eukaryotes.

Here only the homologues that have been confirmed by experiments, rather than only sequence similarity, are mentioned. *C. reinhardtii* has two AcsF homologues, Crd1 and Cth1, which were first shown to be involved in the maintenance of PSI and light-harvesting complex I, and then their functions were narrowed down to the aerobic cyclase (Moseley *et al.*, 2000; Moseley *et al.*, 2002; Allen *et al.*, 2008). CHL27 is the only AcsF homologue in *Arabidopsis*; *CHL27* knock-down mutants were defective in Chl biosynthesis at the cyclase step and CHL27 was shown to be located on both the envelope and thylakoid membranes (Tottey *et al*., 2003; Bang *et al*., 2008). As the genome sequence of barley (*Hordeum vulgare* L.) is not available even now, studies of the enzymes in Chl biosynthesis are limited to analyses of the relevant barley mutants. Rzeznicka *et al.* (2005) demonstrated the barley *xantha-l* and *viridis-k* mutants that accumulate MgPME were deficient in the membrane components of the aerobic cyclase. All the *xantha-l* mutants were found to have mutations in one gene, the *acsF* homologue in barley, which was named accordingly as *Xantha-l*. The *Xantha-l* gene in the *viridis-k* mutants is intact; thus, the authors proposed that the aerobic cyclase requires at least three components, a soluble subunit, a membrane subunit encoded by *Xantha-l* and another membrane subunit encoded by *Viridis-k* (Rzeznicka *et al*., 2005). Sll1214, as one of the two AcsF homologues found in *Synechocystis*, was shown to be essential for the cyclase reaction; the other AcsF homologue, Sll1874, was demonstrated to be involved in certain conditions (Minamizaki *et al*., 2008; Peter *et al*., 2009). The AcsF protein was found to be quite abundant in the chlorosomes of *Chloroflexus aurantiacus* under anaerobic conditions, which indicates the function of AcsF in this organism may be irrelevant to other phototrophs (Tang *et al*., 2009).

It is noteworthy that the cyclase exists as isozymes in *C. reinhardtii* and cyanobacteria. Crd1 and Cth1, the two AcsF homologues in *C. reinhardtii*, are expressed reciprocally: the level of Crd1 is increased under copper-deficient or hypoxia conditions; whereas Cth1 accumulates

under copper-sufficient and oxygen-sufficient conditions (Moseley *et al.*, 2000; Moseley *et al.*, 2002; Allen *et al.*, 2008). The function of Crd1 cannot be fully bypassed by misexpression of Cth1 (Moseley *et al.*, 2002). The copper-responsive regulation is achieved by a copper-responsive element located upstream of *Crd1* gene and alternative transcription of *Cth1* gene (Moseley *et al.*, 2002; Allen *et al.*, 2008). As with *C. reinhardtii*, there are two *acsF*-like genes in *Synechocystis*, *sll1214* (designated as *cycI*) and *sll1874* (designated as *cycII*). Although Minamizaki *et al.* (2008) managed to fully segregate Δ*cycII* mutants under aerobic conditions and Δ*cycI* only under micro-oxic conditions, Peter *et al.* (2009) only obtained the fully segregated Δ*cycII* but not Δ*cycI* even under mixotrophic low-light and low-oxygen conditions. Despite the difference in the construction of Δ*cycI*, both papers demonstrated CycI was the sole cyclase under aerobic conditions while CycI works together with CycII under micro-oxic or low-oxygen conditions (Minamizaki *et al.*, 2008; Peter *et al.*, 2009). All these findings suggest that the isozymes of cyclase are ecoparalogues, paralogous proteins catalysing the same chemical reaction but optimised for different conditions (Sanchez-Perez *et al.*, 2008; Allen *et al.*, 2008).

Following the identification of AcsF as the first subunit of aerobic cyclase, another potential component was discovered in *Synechocystis* and tobacco. Ycf54 (Slr1780) was found to be an interaction partner of CycI and CycII in *Synechocystis* by *in vivo* pull-down experiments using FLAG-CycI and FLAG-CycII as bait, separately (Hollingshead *et al.*, 2012). This interaction was authenticated by a co-purification of FLAG-Ycf54 with CycI. The partial *ycf54* mutant contains a significantly reduced level of Chl but accumulates a very high level of MgPME. In a screen for genes associated with Chl deficiency in tobacco, *LCAA* (abbreviation of low chlorophyll accumulation A) was identified and the antisense mutants of this gene were shown to be impaired at the cyclase step (Albus *et al.*, 2012). *In vivo* bimolecular fluorescence complementation assays revealed LCAA localised in chloroplasts, where it physically interacts with CHL27 and also forms homodimers. Sequence alignment shows that LCAA is a tobacco homologue of Ycf54. Ycf54/LCAA is conserved in all eukaryotic phototrophs and cyanobacteria; both Hollingshead *et al.* (2012) and Albus *et al.* (2012) proposed that Ycf54/LCAA is an additional subunit or at least a critical factor for the stability and activity of aerobic cyclase. Recently, Bollivar *et al.* (2014) argued that Ycf54/LCAA is not a soluble but a membrane component of the cyclase based on *in vitro* barley cyclase assays, which is surprising since Ycf54/LCAA is localised in both the soluble and membrane fractions of *Synechocystis* and tobacco (Hollingshead *et al.*, 2012; Albus *et al.*, 2012).

The existence of two fundamentally different forms of cyclase was first confirmed by ^{18}O-labelling experiments which demonstrated the oxygen atom of the 13^1-oxo group of BChl in *Rba. sphaeroides* is derived from H_2O, whereas in *Roseobacter denitrificans* it is from O_2 (Porra *et al.*, 1996). Porra *et al.* (1998) then found both an oxygenase-type and a hydratase-type cyclase exist in *Rhodovulum sulfidophilum*, which belongs to the facultative aerobic bacteria. The coexistence of two types of cyclase was also demonstrated in *Rvi. gelatinosus* by a genetic approach: an anaerobic type encoded by the *bchE* gene is functional under photosynthetic or low-oxygen conditions, and an aerobic type of which one subunit is encoded by the *acsF* gene is active under high-oxygen conditions (Pinta *et al.*, 2002; Ouchane *et al.*, 2004). The current knowledge regarding the cyclase is summarised in **Figure 1.11**. A study on the origin and distribution of cyclase revealed the coexistence of BchE and AcsF is well conserved in facultative aerobic phototrophs, and suggested that BchE in phototrophic Proteobacteria is an ancient form of cyclase while AcsF may be acquired from cyanobacteria (Boldareva-Nuianzina *et al.*, 2013).
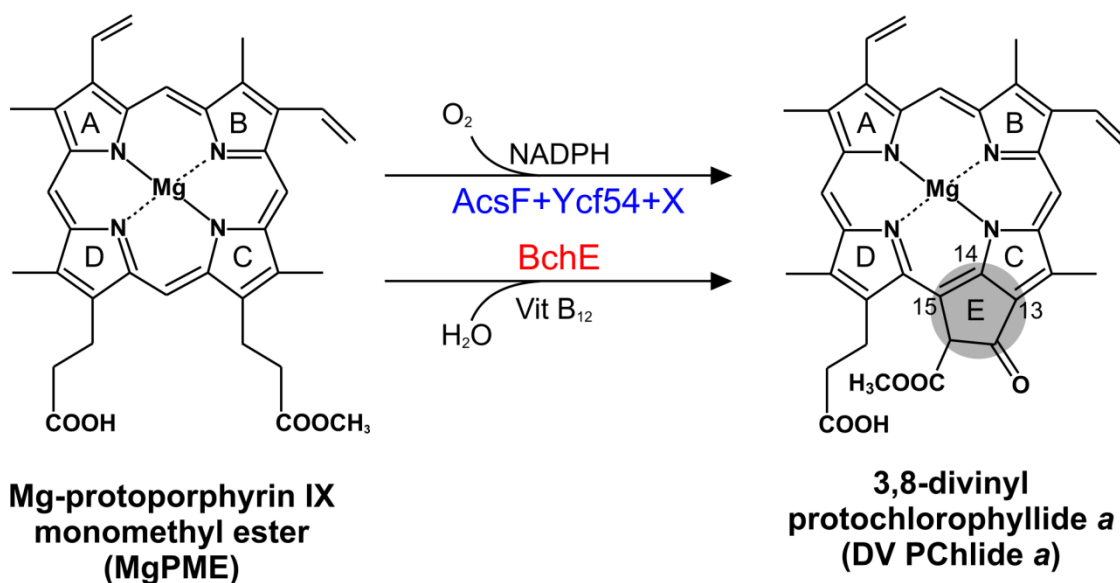
Figure 1.11 The aerobic and anaerobic Mg-protoporphyrin IX monomethyl ester cyclase reactions

Two fundamentally different types of cyclase are utilised by phototrophs. The aerobic cyclase utilises molecular oxygen as a substrate and is a multi-subunit enzyme consisting of two known subunits (AcsF and Ycf54) and some unknown subunit(s) (X). The anaerobic cyclase utilises water as a substrate and is encoded by the *bchE* gene.

The aerobic cyclase reaction can generate reactive oxygen species which are potentially harmful to the cyclase system. *In vitro* cyclase assays conducted with lysed *C. reinhardtii*

chloroplasts demonstrated that catalase and ascorbate can significantly stimulate the reaction by extinguishing reactive oxygen species (Bollivar and Beale, 1996). Stenbaek *et al*. (2008) showed that an H_2O_2-scavenging system, which consists of NTRC (abbreviation of NADPH-dependent thioredoxin reductase C) and 2-Cys peroxiredoxins, is required to protect aerobic cyclase, especially during darkness or chloroplast biogenesis. Their experimental evidence is that the *Arabidopsis ntrc* mutant is disturbed in Chl biosynthesis probably at the cyclase step; NTRC and 2-Cys peroxiredoxins can stimulate the *in vitro* barley cyclase reaction, similar to other H_2O_2-scavenging systems, like catalase. Recently, Steccanella *et al*. (2015) proposed an inspired catalytic scheme for aerobic cyclase involving a dynamic plastoquinone pool based on their analysis of *Arabidopsis* and barley mutants which have a perturbed plastoquinone pool. These findings, together with the fact that no NADPH-binding domain is present in the known aerobic cyclase subunits, evoke the necessity to reconsider the role of NADPH in aerobic cyclase system. NADPH may not be directly involved in the catalytic reaction as a cofactor, but rather it could protect the cyclase system through an NADPH-dependent H_2O_2-scavenging system.

1.7.5 Protochlorophyllide reductase

PChlide is converted to Chlide *a* via the reduction of the C17-C18 double bond of the D ring catalysed by PChlide reductase. Two types of structurally unrelated PChlide reductases have been identified in phototrophs. One is light-dependent NADPH:PChlide oxidoreductase (POR) which is a single-subunit enzyme and belongs to the "RED" (Reductases, Epimerases, and Dehydrogenases) superfamily of enzymes (Wilks and Timko, 1995). The other is light-independent (dark-operative) PChlide reductase (DPOR) which is a multi-subunit enzyme and requires ATP and ferredoxin for catalysis (Fujita and Bauer, 2000; Nomata *et al*., 2005). All Chl-containing organisms have both POR and DPOR except for the angiosperms (flowering plants) which only contain POR, while BChl-containing bacteria appear to only possess DPOR except for the phototrophic α-proteobacterium *Dinoroseobacter shibae* DFL12 which was discovered to contain a functional POR (Suzuki and Bauer, 1995b; Kaschner *et al*., 2014).

Light-dependent protochlorophyllide reduction

POR is one of two most extensively studied enzymes involved in the (B)Chl biosynthesis pathway. This is mainly because POR is one of the only two enzymes known to require light for catalysis; the other enzyme is DNA photolyase (Sancar and Sancar, 1987). The light requirement of POR provides researchers with a unique opportunity to investigate catalysis at

low temperatures and on ultrafast timescales that are impossible for most enzyme-catalysed reactions (Heyes and Hunter, 2005).

POR plays an important role in the greening of angiosperms and is a major target for photosynthesis regulation (Bollivar, 2006). Plant etioplasts have the characteristic paracrystalline tubular membranes known as prolamellar bodies which contain POR as the major protein constituent (Murakami *et al.*, 1985; Dehesh and Ryberg, 1985). In the prolamellar bodies, POR exists in a ternary complex with NADPH and PChlide (Lebedev and Timko, 1998). Upon illumination PChlide is converted to Chlide by POR followed by the disintegration of POR-pigment complexes and the dispersion of prolamellar bodies (Heyes and Hunter, 2009). During this process, a shift in the absorbance maximum of Chlide, known as the Shibata shift (Shibata, 1957), can be observed. POR activity was demonstrated *in vitro* using isolated etioplast membranes from barley, maize, oat and runner bean (Griffiths, 1975; Griffiths, 1978; Oliver and Griffiths, 1980; Oliver and Griffiths, 1982). Griffiths (1975, 1978) showed the first direct evidence for the NADPH requirement in POR reaction. Apel *et al*. (1980) reported the purification of barley POR from solubilised prolamellar bodies to apparent homogeneity. The purified enzyme was shown to be active by *in vitro* assays and was proposed to be composed of a single subunit which has a molecular weight of 36 kD determined by SDS-PAGE (Apel *et al.*, 1980).

POR-encoding genes have been cloned from a variety of organisms including barley (Schulz *et al.*, 1989), oat (Darrah *et al.*, 1990), *Arabidopsis* (Benli *et al.*, 1991), pea (Spano *et al.*, 1992), wheat (Teakle and Griffiths, 1993) and *Synechocystis* (Suzuki and Bauer, 1995b). The POR encoding genes can be heterologously expressed in *E. coli* resulting in active POR enzymes demonstrated by *in vitro* assays (Schulz *et al.*, 1989; Benli *et al.*, 1991; Knaust *et al.,* 1993). Overexpressing POR in *E. coli* as a fusion with maltose binding protein or hexahistidine greatly simplifies the process to obtain highly pure POR, which provide a good opportunity to characterise POR both functionally and structurally (Martin *et al.*, 1997; Townley *et al.*, 1998; Lebedev and Timko, 1999; Heyes *et al.*, 2000).

A combination of substrate analogues, site-directed mutagenesis, steady-state kinetics and multiple forms of spectroscopy has been applied to study the mechanism of the POR catalytic cycle (Heyes and Hunter, 2005). NMR studies using 4*R* and 4*S* ^{3}H-labelled isomers of NADPH demonstrated that a hydride from the *pro-S* face of NADPH is delivered to the C17 of PChlide and that the C18 is protonated by water or an active site acid (Begley and Young, 1989). By aligning POR with other proteins belonging to the short-chain alcohol dehydrogenase family,

two highly conserved residues, Tyr275 and Lys279 (numbering of pea POR), were identified and confirmed to be essential for POR activity (Wilks and Timko, 1995). The proton at the C18 of PChlide is derived from Tyr275, while Lys279 lowers the pKa of Tyr275 to facilitate the deprotonation of the phenolic group of Tyr275 (Wilks and Timko, 1995). Studies using PChlide analogues have revealed the substrate specificity for POR: modifications of the side chains at ring A and ring B are allowed; the central magnesium ion can be replaced by a zinc ion; analogues with different side chains at ring D or ring E are not accepted (Klement *et al*., 1999). Griffiths *et al*. (1996) demonstrated the reaction proceeds through a single-photon mechanism.

Using recombinant POR from *Synechocystis* and *T. elongatus* BP-1, the catalytic steps of the POR reaction have been studied in great detail by characterising the intermediates of the reaction with various types of spectroscopy at low temperature. The complete catalytic cycle of POR can be described as follows (**Figure 1.12**): a POR-NADPH-PChlide complex is formed, which is the rate-limiting step in the overall reaction (Heyes *et al*., 2008); the initial photochemical step proceeds via a charge transfer complex, occurring below 200 K (Heyes *et al*., 2002; Heyes *et al*., 2006); two dark steps involve the formation of the POR-Chlide-NADP$^+$ complex and the release of the NADP$^+$ from the complex, which only occur above the "glass transition" temperature (~200 K) of proteins (Heyes *et al*., 2003b; Heyes and Hunter, 2004); another two dark steps involve NADPH-binding and Chlide-release events, which occur above 260 K (Heyes and Hunter, 2004). In addition, the reaction dynamics have been studied by femtosecond pump-probe spectroscopy after initiation with a 50 femtosecond laser pulse (Heyes *et al*., 2003a). It has been shown that the reaction occurs on an ultrafast timescale, which appears to be complete within 400 picoseconds (Heyes *et al*., 2003a).

The structure of POR has not been solved. POR is a member of the "RED" superfamily of proteins. The crystal structures of several members of this superfamily have been used as a template to construct a homology model of POR from *Synechocystis* (Townley *et al.,* 2001). This model proposes a central parallel β-sheet comprised of seven β-strands surrounded by nine α-helices. An insertion of 33 residues between the fifth and sixth α-helices makes POR unique in the "RED" superfamily, of which the function is still unclear. NADPH binds to the N-terminus of POR, which contains a glycine-rich GXXXGXG motif termed as the Rossmann fold. Homology models of POR from barley share structural features with the model of POR from *Synechocystis* (Buhr *et al.,* 2008).
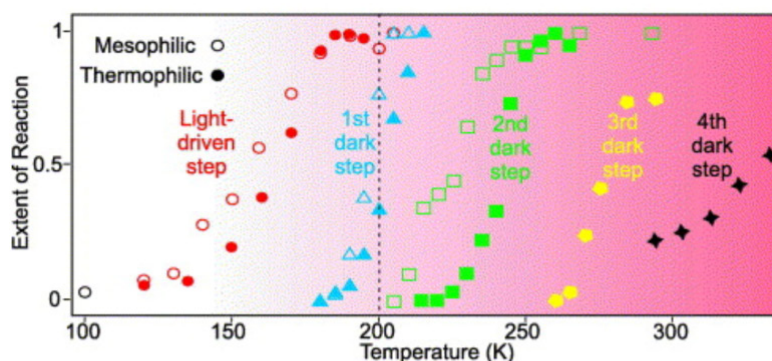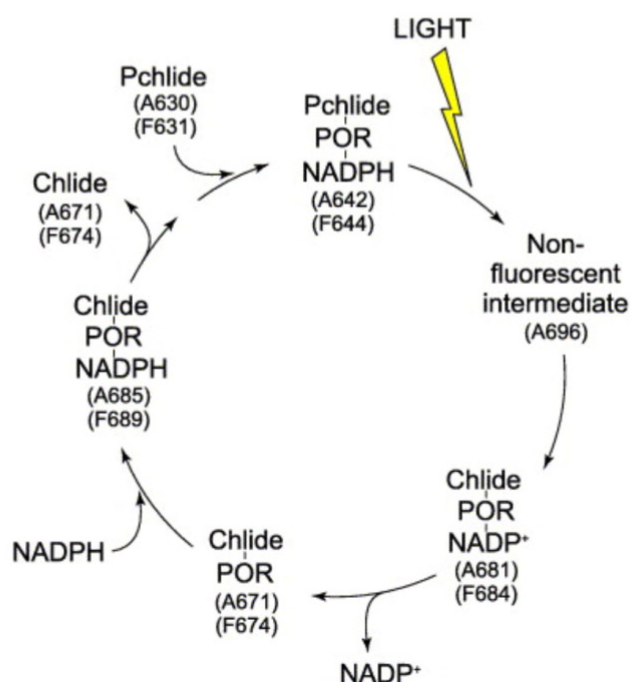
Figure 1.12 The catalytic steps for light-dependent reduction of protochlorophyllide *a*

(**A**) Temperature dependence of the catalytic steps of mesophilic and thermophilic POR (Heyes *et al*., 2002; Heyes *et al*., 2003b; Heyes and Hunter, 2004). (**B**) The catalytic cycle of POR. The intermediates were identified by using a thermophilic variant of POR (Heyes and Hunter, 2004). Shown are from Heyes and Hunter (2005).

In angiosperms, three different isoforms of POR have been identified so far and are named PORA, PORB and PORC (Holtorf *et al*., 1995; Armstrong *et al*., 1995; Oosawa *et al*., 2000), all of which are differentially regulated by light and developmental state. PORA performs a specialised function restricted to the initial stage of greening while PORB is present and functional throughout the life of the plant (Armstrong *et al*., 1995; Lebedev and Timko, 1998).

PORC, only found in *Arabidopsis* to date, is expressed only in the light and is regulated by light intensity (Oosawa *et al.*, 2000; Su *et al.*, 2001). In contrast, oxygenic phototrophs which contain DPOR, such as cyanobacteria and algae, only contain one form of POR (Schoefs and Franck, 2003; Masuda and Takamiya, 2004).

Light-independent protochlorophyllide reduction

All photosynthetic organisms except angiosperms contain DPOR, which enables these organisms to synthesise (B)Chl in the dark. Genetic studies in *Rba. capsulatus* demonstrated that DPOR is encoded by three genes, *bchL*, *bchN*, and *bchB* (Yang and Bauer, 1990; Burke *et al.*, 1993a; Bollivar *et al.*, 1994b). Homologous genes in Chl-containing organisms are termed as *chlL*, *chlN* and *chlB*. The sequences of the three subunits of DPOR show significant similarities to the three subunits of nitrogenase, a well-characterised enzyme catalysing the reduction of dinitrogen to ammonia (Fujita and Bauer, 2000).

Biochemical approaches that had been used to study nitrogenase were applied to analyse DPOR. Fujita and Bauer (2000) demonstrated the DPOR activity using purified protein subunits from *Rba. capsulatus*. Two of the three subunits (BchL and BchN) were expressed as S-tag fusion proteins for affinity purification. The third subunit (BchB) was co-purified with the BchN protein, indicating that BchN and BchB form a tight complex. DPOR activity is dependent on the presence of all three subunits, ATP and dithionite, strongly supporting that DPOR is a "nitrogenase-like" enzyme (Fujita and Bauer, 2000). Further biochemical analysis of the *Rba. capsulatus* DPOR revealed that ferredoxin functions as an electron donor and the enzyme is comprised of a BchL homodimer (L-protein) as a reductase component which contains an oxygen-sensitive [4Fe-4S] cluster, and a BchN-BchB heterotetramer (NB-protein) as the catalytic component which contains oxygen-tolerant [4Fe-4S] clusters (Nomata *et al.*, 2005; Nomata *et al.*, 2006; Nomata *et al.*, 2008). The subunits of DPOR from *Chlorobium tepidum* have been heterologously overproduced in *E. coli* and purified to homogeneity (Brocker *et al.,* 2008). The K_m values of PChlide, ATP and dithionite were determined using the recombinant wild-type DPOR from *Chlorobium tepidum*. Four ATP molecules are required for each catalytic cycle. By analysing 23 mutant DPOR enzymes, the residues essential to DPOR activity were identified: Cys97 and Cys131 (numbering in *Chlorobium tepidum* DPOR) of the L-protein (BchL$_2$) coordinate an intersubunit [4Fe-4S] cluster; Lys10 and Leu126 of the BchL$_2$ are crucial to ATP-driven electron transfer from BchL$_2$; Three cysteines (Cys21, Cys46 and Cys103) from BchN and one cysteine (Cys94) from BchB in the NB-protein ((BchN-BchB)$_2$) coordinate a second intersubunit [4Fe-4S] cluster (Brocker *et al.,* 2008).

The crystal structure of the L-protein from *Rba. capsulatus* was determined with bound MgADP to 1.6 Å resolution (Sarma *et al.*, 2008). The L-protein of DPOR shares overall structural similarity with the Fe protein of nitrogenase, including the [4Fe-4S] cluster and the nucleotide binding sites. However, the charge of the docking site of the L-protein with the NB-protein is significantly distinct from that of the Fe protein, which may serve to guarantee the exclusive interactions with their partner proteins (Sarma *et al.*, 2008). Crystal structures of the NB-protein from *Rba. capsulatus* were solved both in the PChlide-bound and PChlide-free forms at 2.3 Å and 2.8 Å resolutions, respectively (Muraki *et al.*, 2010). The overall structure is similar to that of the MoFe protein of nitrogenase. Each catalytic BchN-BchB subunit contains one PChlide and one [4Fe-4S] cluster (NB-cluster) coordinated uniquely by one aspartate and three cysteines. The spatial arrangement of the NB-cluster and PChlide is almost identical to that of the P-cluster (the iron-sulfur cluster in MoFe protein) and FeMo-cofactor in the nitrogenase MoFe protein (Muraki *et al.*, 2010). Based on the structures of the L-protein and NB-protein, the reaction mechanism of DPOR can be proposed as follows: the L-protein transfers two electrons from ferredoxin to the NB-protein, coupled with hydrolysis of four ATP molecules; the NB-protein catalyses *trans*-specific reduction of the C17 = C18 double bond of PChlide in which the C17-propionate of PChlide donates a proton for the C18 and an aspartate from BchB donates a proton for the C17, concomitant with transfer of two electrons from the NB-protein to PChlide (Muraki *et al.*, 2010).

Why are two completely different enzymes utilised to catalyse the same reaction? To answer this question, the different oxygen sensitivity of POR and DPOR needs to be considered. The L-protein of DPOR is highly sensitive to oxygen (Nomata *et al.*, 2006; Yamamoto *et al.*, 2009), whereas POR is entirely insensitive to oxygen since it functions in oxygenic phototrophs. The transition of the Earth's anaerobic atmosphere to aerobic atmosphere in which DPOR is not able to function may cause a selection pressure on phototrophs due to the photooxidative damage coming with the accumulation of PChlide. The evolution of POR may have arisen from this selection pressure (Reinbothe *et al.*, 2010). A similar explanation may apply to the adoption of the oxygen-dependent MgPME cyclase (Boldareva-Nuianzina *et al.*, 2013).

1.7.6 Divinyl reductase

Chl can be classified into two groups: 3, 8-divinyl (DV) Chl and 3-monovinyl (MV) Chl. DVR catalyses the conversion of the 8-vinyl group of the tetrapyrrole to an ethyl group. This reaction is believed to be essential since almost all of the oxygenic phototrophs contain MV Chl with the exceptions being *Prochlorococcus* spp., which contain DV Chl *a* and *b* as the

photosynthetic pigments (Chisholm *et al*., 1992; Goericke and Repeta, 1992). The exact stage of the DV reduction in the (B)Chl biosynthesis pathway is unclear as many MV and DV Chl precursors have been found in plants and algae (Rebeiz *et al.,* 1994). To make it more complicated, the proportions of MV and DV Chl precursors in higher plants have been shown to be variable depending on the plant species, the age of the plant and environmental conditions (Tripathy and Rebeiz, 1986; Tripathy *et al.,* 1988; Shioi and Takamiya, 1992). The MV and DV pools of different Chl precursors evoke the possibility that two Chl biosynthesis routes are used to independently synthesise MV Chl and DV Chl (Rebeiz *et al.,* 1994). Two theories regarding the identity of DVR can be proposed: one is that there are multiple unique DVRs using different DV tetrapyrroles as substrate; the other is that there is only one DVR which is able to utilise multiple DV tetrapyrroles as substrate but with different reaction rates for different substrates (Heyes and Hunter, 2009).

Tripathy and Rebeiz (1988) reported the partial conversion of exogenous DV PChlide to MV PChlide in barley plastids, which was not observed in cucumber plastids. The first *in vitro* DVR assay was conducted with isolated etioplast membranes from cucumber, corn and barley (Parham and Rebeiz, 1992; Parham and Rebeiz, 1995). DVR activity was shown to be strictly dependent on NADPH and to be specific for DV Chlide but not DV PChlide, suggesting two different DVRs may be involved in the reduction of DV PChlide and DV Chlide (Parham and Rebeiz, 1992). Kolossov and Rebeiz (2001) achieved an overall 20-fold purification of the DVR enzyme from barley etioplasts.

In *Rba. capsulatus*, a *bchJ* mutant was found to accumulate DV PChlide but still be able to synthesise BChl (Bollivar *et al.*, 1994b). Further analysis of this *bchJ* mutant and a *bchJ/bchL* double mutant revealed that *bchJ* appears to be involved in the 8-vinyl reduction (Suzuki and Bauer, 1995a). Chew and Bryant (2007a) showed that the *Chlorobaculum tepidum bchJ* mutant produces MV (B)Chls although secretes large amounts of DV PChlide into the growth medium, suggesting that BchJ is not a DVR, but may play a role in substrate channelling in (B)Chl biosynthesis. Canniffe *et al*., (2013) mutated the *bchJ* gene in *Rba. sphaeroides* and similar results were achieved as those with *Chlorobaculum tepidum*.

Two groups independently isolated the first DVR encoding gene, AT5G18660, by characterising *Arabidopsis* mutants that accumulate DV Chl (Nakanishi *et al.*, 2005; Nagata *et al.*, 2005). The cell extracts from *E. coli* overexpressing the AT5G18660 gene catalysed the conversion of DV Chlide to MV Chlide (Nagata *et al.*, 2005). Homologues of the AT5G18660 gene are found in higher plants, green algae, some green sulfur bacteria, some purple

bacteria and *Synechococcus* spp., but not in red algae or filamentous anoxygenic phototrophs or fresh-water cyanobacteria (Chew and Bryant, 2007; Ito *et al*., 2008). The homologous DVR-encoding gene in phototrophic bacteria was renamed as *bciA* (Chew and Bryant, 2007a). The functions of the DVR homologues in *Chlorobaculum tepidum*, rice (*Oryza sativa*) and *Rba. sphaeroides* have been confirmed by genetic mutation (*Chlorobaculum tepidum*, rice and *Rba. sphaeroides*), genetic complementation (*Rba. sphaeroides*) and recombinant DVR assays (*Chlorobaculum tepidum* and rice) (Chew and Bryant, 2007a; Wang *et al*., 2010; Canniffe *et al.,* 2013).

The existence of at least one non-BciA DVR is indicated by the fact that many cyanobacteria utilise MV Chl as photosynthetic pigments even though they do not contain *bciA* homologues. A *Synechocystis* gene, slr1923, was independently identified to be essential for 8-vinyl reduction in this organism by two groups (Ito *et al.*, 2008; Islam *et al*., 2008). Mutants of this gene only synthesise DV Chl and cannot grow under high light conditions (Ito *et al.*, 2008; Islam *et al*., 2008). Homologues of the slr1923 gene are present in many other cyanobacteria, higher plants, green algae, some green sulfur bacteria, some purple bacteria and some filamentous anoxygenic phototrophs (Ito *et al.*, 2008; Islam *et al*., 2008). The slr1923 homologue in the green sulfur bacterium *Chloroherpeton thalassium*, designated as *bciB*, was recombinantly purified from *E. coli* and characterised (Saunders *et al.*, 2013). The recombinant BciB binds two [4Fe-4S] clusters and a FAD cofactor, and was demonstrated by *in vitro* assays to be a ferredoxin-dependent DVR (Saunders *et al.*, 2013).

Plant and green algal genomes contain homologues of both *bciA* and *bciB*, and most cyanobacterial genomes only contain homologues of one gene, either *bciA* or *bciB*. However, in the marine cyanobacterium *Acaryochloris marina*, both *bciA* and *bciB* homologues were found in the genome and demonstrated to be functional and active (Chen *et al.*, 2016b). These two *Acaryochloris marina* genes are able to complement a Δ*bciB* strain of *Synechocystis* (Chen *et al.*, 2016b). It has been hypothesised that there exists a third type of DVR in phototrophic bacteria since *Roseiflexus* spp. produce MV (B)Chl but have neither *bciA* nor *bciB* (Ito *et al*., 2008). Canniffe *et al*. (2013) showed that *Rba. sphaeroides* utilises at leaset two types of DVR based on the observation that a Δ*bciA* strain of this organism can still produce MV BChl. Since *Rba. sphaeroides* does not have *bciB*, this study indicates the existence of a third or fourth type of DVR, depending on whether the non-BciA enzyme in *Rba. sphaeroides* is related to the unknown DVR in *Roseiflexus* spp. (Saunders *et al.*, 2013).

Wang *et al*. (2013) systematically conducted *in vitro* DVR assays using four recombinant BciA-type DVRs from higher plants and five DV substrates including MgP, MgPME, PChlide *a*, Chlide *a* and Chl *a*. The rice and maize DVRs were found to be able to utilise all five DV substrates, while the *Arabidopsis* and cucumber DVRs can convert three of them, namely MgPME, PChlide *a* and Chlide *a*. Based on the results of the *in vitro* assays together with the observation that rice plants with inactivated *DVR* gene accumulate only DV Chls and intermediates, the conclusion was drawn that a single DVR with broad substrate specificity is responsible for the reduction of the 8-vinyl groups of various Chl intermediates in higher plants, but DVR homologues differ between species regarding substrate preferences and catalytic activities (Wang *et al*., 2013). *In vivo* study has also demonstrated both BciA from *Rba. sphaeroides* and BciB from *Synechocystis* prefer DV Chlide *a* as their substrate (Canniffe *et al*., 2014).

1.8 The steps unique to bacteriochlorophyll biosynthesis

For the synthesis of BChl *a*, three additional steps occur before the addition of an isoprenoid tail (**Figure 1.13**); these reactions modify rings A and B of Chlide *a* to form bacteriochlorophyllide (BChlide) *a*, which are unique to purple and green bacteria. These steps were identified by characterising the BChl intermediates excreted from mutants of *Rba. sphaeroides* (Richards and Lascelles, 1969). The enzymes involved in these steps are as follows: Chlide *a* oxidoreductase (COR) catalyses the reduction of the C7=C8 double bond of ring B; 3-vinyl (3V)BChlide *a* hydratase is responsible for the hydroxylation of the 3V group; and 3-hydroxyethyl (3HE) BChlide *a* dehydrogenase converts the 3-hydroxyethyl (3HE) group to a 3-acetyl group. The order of the two steps catalysed by COR and 3V BChlide *a* hydratase was shown to be interchangeable by the isolation of a BChl intermediate, 3V BChlide *a* (Pudek and Richards, 1975).
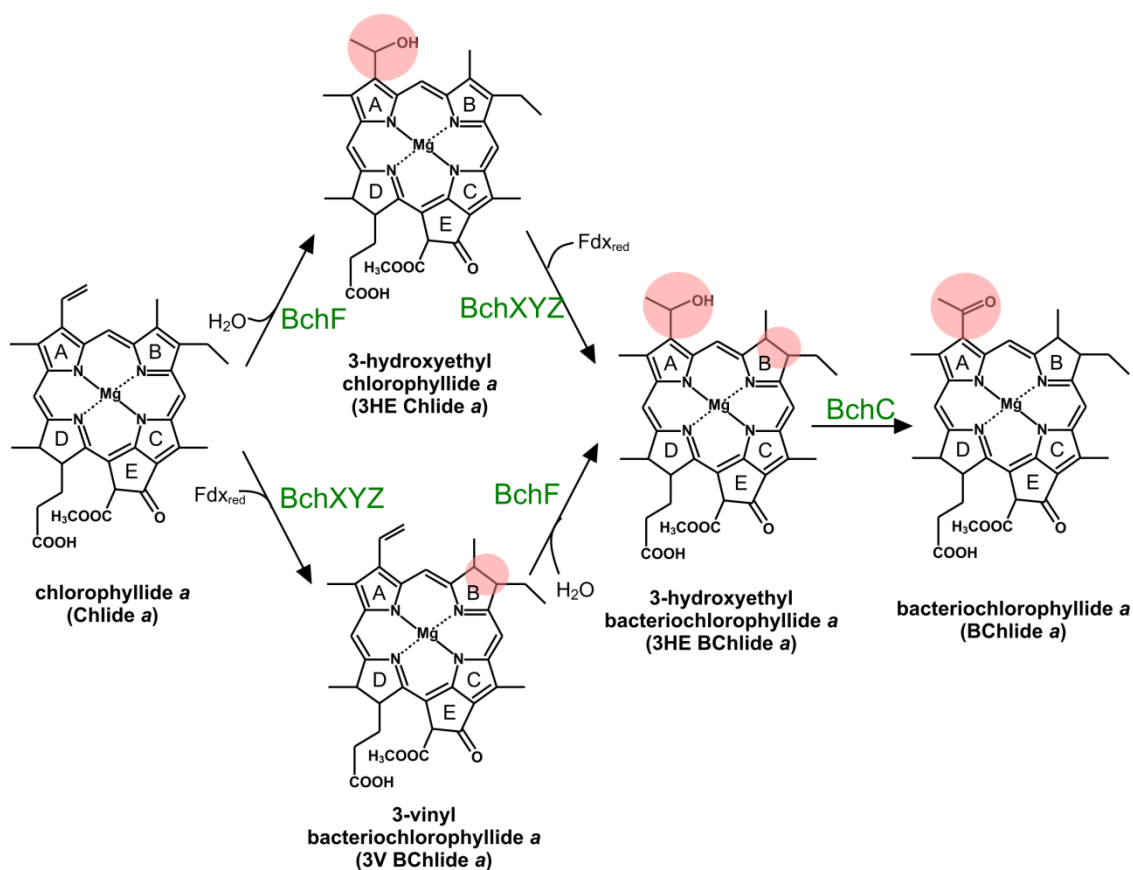
Figure 1.13 The steps unique to bacteriochlorophyll biosynthesis

The steps between Chlide *a* and 3HE BChlide *a*, catalysed by BchF (3V BChlide *a* hydratase) and BchXYZ (Chlide *a* oxidoreductase), are interchangeable. BchC (3HE BChlide *a* dehydrogenase) then catalyses the conversion of 3HE BChlide *a* into BChlide *a*. The group modified by each step is marked by pink shading. Modified from Chew and Bryant (2007b), and Heyes and Hunter (2009).

COR, as a second nitrogenase-like enzyme in (B)Chl biosynthesis, shares great similarities with DPOR, not only in the reaction chemistry but also in the enzyme composition (Nomata *et al*., 2006). Genetic studies of *Rba. sphaeroides* and *Rba. capsulatus* revealed the three genes, *bchX*, *bchY* and *bchZ*, encode COR (Hunter and Coomber, 1988; Burke *et al*., 1993b; McGlynn and Hunter, 1993; Bollivar *et al*., 1994b). The *Rba. capsulatus* COR was reconstituted with purified BchX and BchY-BchZ proteins using identical biochemical approaches that were applied to reconstitute DPOR and as expected COR requires ATP and dithionite for activity, as for DPOR (Nomata *et al*., 2006). Furthermore, the recombinant COR from *Roseobacter denitrificans* was used to study the substrate binding and catalytic mechanism of COR (Kiesel *et al*., 2015). COR is able to use substrates with modifications on rings A, C and E, but modifications of the C17-propionate group are not accepted. The presence of a [4Fe-4S] cluster in the $(BchX)_2$ and a second [4Fe-4S] cluster in the $(BchY/BchZ)_2$ was revealed by EPR

experiments. The second iron-sulfur cluster is ligated by four cysteines, different from the three cysteines/one aspartate ligation pattern in DPOR. The ternary COR holoenzyme can be trapped with the ATP transition-state analog ADP·AlF$_4^-$, indicating that the initial electron transfer events of COR catalysis resemble DPOR and nitrogenase (Kiesel *et al.*, 2015). Phylogenetic analysis of the BchX, BchL and nitrogenase Fe proteins implied that the duplication of the genes encoding nitrogenase gave rise to the ancestral DPOR, which reduced its substrate twice to form a bacteriochlorin. Subsequent duplication of the genes encoding this reductase allowed the two copies to specialise toward reduction of PChlide and Chlorin, allowing the appearance of Chl (Burke *et al.*, 1993c). This implication is supported to some extent by the observation that the photosynthetic growth of *Synechocytis* was arrested by superoxide generated by the heterologously expressed COR (Kim *et al.*, 2008; Kim *et al.*, 2009).

A hydratase mechanism for the formation of the 3-acetyl group of BChl *a* was demonstrated by ^{18}O-labelling and mass spectrometry (Porra *et al.*, 1996). The *bchF* gene was shown to encode the enzyme that catalyses the hydration of the 3V group (Burke *et al.*, 1993a; Bollivar *et al.*, 1994b). Biochemical characterisation of this enzyme has only been reported very recently (Lange *et al.*, 2015). Heterologous overexpression of *Chlorobaculum tepidum* BchF revealed an integral transmembrane protein that can be isolated by detergent solubilisation. The isolated recombinant BchF was shown to be able to convert Chlide *a* to 3HE Chlide *a* (Lange *et al.*, 2015).

The oxidation of the 3HE group to form a 3-acetyl group is catalysed by a dehydrogenase, which is encoded by the *bchC* gene (Wellington and Beatty, 1989; McGlynn and Hunter, 1993). Similar to BchF, biochemical information on BchC has only become available very recently (Lange *et al.*, 2015). The *Chlorobaculum tepidum* BchC was overexpressed in *E. coli* and subsequently purified as a soluble protein-NAD$^+$ complex. *In vitro* assays using artificial substrates broadened the substrate specificity of BchC: modification of the E ring is tolerated; the central magnesium ion can be omitted or replaced with a zinc ion; and a non-reduced B ring is also accepted. This broad substrate specificity of BchC, together with a DPOR-BchF-BchC pathway reconstitution assay, indicates a new branched route for the synthesis of BChl *a* (Lange *et al.*, 2015). In addition, BchC was shown to be an unusual zinc-independent dehydrogenase specifically using NAD$^+$ as a redox cofactor, in accordance with the assignment of BchC to a newly defined family of the medium-chain dehydrogenase/reductase superfamily (Lange *et al.*, 2015; Hedlund *et al.*, 2010).

1.9 The phytylation of (bacterio)chlorophyllide

The last step of (B)Chl synthesis is the addition of phytol, which is a C_{20} isoprenoid alcohol, to the C17 propionate side chain of BChlide *a* or Chlide *a* (**Figure 1.14**). The phytyl tail makes (B)Chl highly hydrophobic, which is crucial for the assembly and function of (B)Chl within light-harvesting and rection centre complexes. It has been suggested that the phytyl tail is formed in two steps: the esterification of BChlide *a* or Chlide *a* with geranylgeraniol (GG) pyrophosphate (PP) and the three successive reductions of the attached GG moiety. The esterification is catalysed by (B)Chl synthase and GG reductase is responsible for the reduction of the GG moiety.
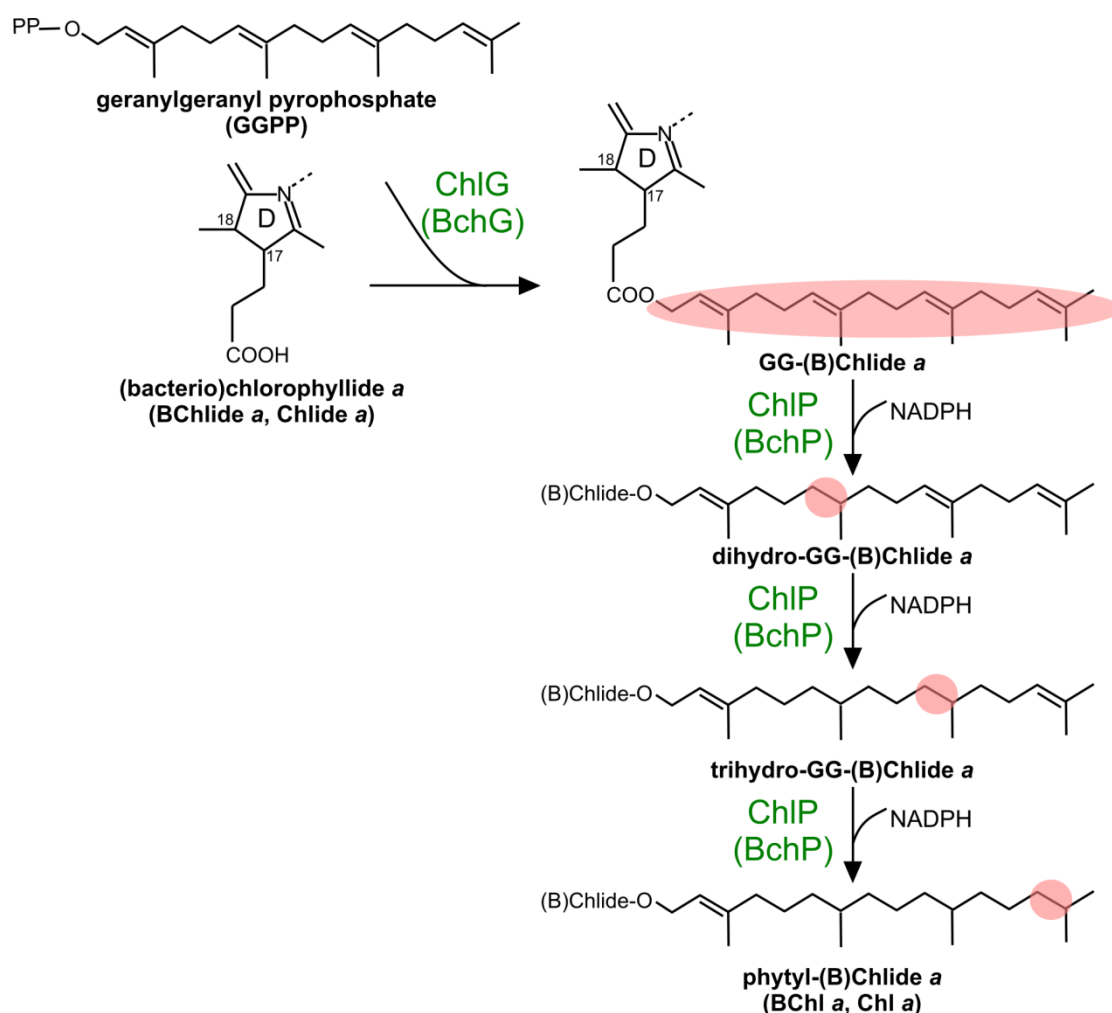
Figure 1.14 The phytylation of (bacterio)chlorophyllide

The phytylation of BChlide *a* to produce BChl *a* is catalysed by BchG and BchP, whilst ChlG and ChlP catalyse the conversion of Chlide *a* into Chl *a*. The group modified by each step is marked by pink shading. Modified from Heyes and Hunter (2009).

Early biochemical approaches with etioplasts from oat (*Avena sativa*) seedlings and spinach chloroplasts revealed the location and substrate specificity of Chl synthase (Rüdiger *et al*., 1980; Soll *et al*., 1983). Genetic studies showed that *bchG* encodes BChl synthase in *Rba. sphaeroides* and *Rba. capsulatus* as mutations of this gene accumulate BChlide *a* and lack BChl *a* (Coomber *et al*., 1990; Bollivar *et al*., 1994c). Further confirmation comes from the successful BChl synthase assays using extracts from *E. coli* overexpressing *Rba. capsulatus* BchG (Oster *et al*., 1997). Homologues of BchG were found in other (B)Chl-containing organisms and (B)Chl synthase activities were demonstrated with the recombinant enzymes from *Synechocytis* (Oster *et al*., 1997), *Arabidopsis* (Oster and Rüdiger, 1997), *Rba. sphaeroides* (Addlesee *et al*., 2000) and *Avena sativa* (Schmid *et al*., 2001). (B)Chl synthase is able to use either GGPP or phytyl PP with a preference varied in different organisms: the enzyme from oat etioplasts and the recombinant enzyme from *Arabidopsis* favour the use of GGPP, while the enzyme from spinach chloroplasts and the recombinant enzymes from *Synechocystis* and *Rba. capsulatus* prefer phytyl PP (Rüdiger *et al*., 1980; Soll *et al*., 1983; Oster *et al.*, 1997; Oster and Rüdiger, 1997). However, these preferences need to be considered with caution as they may be simulated by the variations of the *in vitro* assay conditions (Schmid *et al*., 2001).

(B)Chl synthases also exhibit a high degree of specificity for the tetrapyrrole substrate. ChlG from Chl-containing organisms can only utilise Chlide *a* but not BChlide *a*, whilst BchG from BChl-producing organisms can only utilise BChlide *a* but not Chlide *a* (Benz and Rüdiger, 1981; Oster *et al.*, 1997; Oster and Rüdiger, 1997). Competitive inhibitions of the ChlG of *Synechocytis* by BChlide *a* and the BchG of *Rba. sphaeroides* by Chlide were observed, suggesting a structural similarity between the active sites of ChlG and BchG (Kim *et al*., 2010). The Ile44 of *Synechocystis* ChlG and Phe28 of *Rba. sphaeroides* BchG were found to be responsible for the tetrapyrrole susbstrate specificity based on the experimental evidence that the ChlG Ile44Phe mutant has BchG activity, while the BchG Phe28Ile mutant has ChlG activity (Kim *et al.,* 2016).

It has been suggested that Chl synthase may play a role in the assembly of Chl-protein complexes as free Chls are expected to be phototoxic (Bollivar, 2006). Recently, *Synechocystis* FLAG-tagged ChlG was shown to be present in a complex with the high-light-inducible protein HliD, the Ycf39 protein and the YidC/Alb3 insertase (Chidgey *et al*., 2014). This observation provides evidence for the physical linkage between the Chl biosynthesis and PS apoprotein synthesis (Chidgey *et al*., 2014).

Generally, (B)Chlide *a* is esterified with GGPP and followed by the reduction of the GG moiety, although it has been observed that the order of esterification and reduction can be different depending on growth stages and substrate availabilities (Rüdiger, 1987). The utilisation of GG as esterifying alcohol was demonstrated by the isolation of GG-PChlide from dark grown barley leaves (Liljenberg, 1974), the observation of an intermediate between Chlide and Chl (Ogawa *et al.*, 1974), and the detection of BChl molecules esterified with GG, dihydro-GG and tetrahydro-GG in purple bacteria (Shioi and Sasa, 1984). GG reductase catalyses the reductions of the three C=C bonds of the GG moiety using NADPH as the electron donor (Benz *et al.*, 1980). The enzyme was found to be encoded by a single gene, *bchP*, in *Rba. capsulatus* (Bollivar *et al.*, 1994c). The *Synechocystis* homologue gene *chlP* was functionally assigned and found to be able to partially complement a *bchP* mutant of *Rba. sphaeroides* (Addlesee *et al.*, 1996). *In vitro* GG reductase assays have been reported using lysates of *E. coli* overexpressing the enzymes from *Arabidopsis* (Keller *et al.*, 1998) and *Rba. sphaeroides* (Addlesee and Hunter, 1999). The enzyme from *Arabidopsis* was shown to be a multifunctional enzyme as it is able to reduce free GGPP as well as GG-Chlide *a*, suggesting this enzyme may be shared by the Chl, tocopherol and phylloquinone pathways (Keller *et al.*, 1998).

The hydrogenation of the GG moiety has been demonstrated to be important or even indispensible for the stability of PS. The *Rba. capsulatus bchP* mutant exhibits severely impaired photosynthetic growth ability due to a reduced steady-state level of PS (Bollivar *et al.*, 1994c). In *Synechocystis*, a mutant with an inactivated *chlP* gene was found to be unable to grow photoautotrophically resulting from the instability and rapid degradation of the PS, which is proposed to be caused by the increased rigidity of the GG-Chl with three additional C=C bonds (Shpilyov *et al.*, 2005; Shpilyov *et al.*, 2013).

1.10 Aims of this study

The foregoing review shows that the cyclase step is the least understood component of (B)Chl biosynthesis. Accordingly, the aim of this study is to further our understanding of the aerobic cyclase, which catalyses the oxygen-dependent conversion of magnesium-protoporphyrin IX monomethyl ester to 3, 8-divinyl protochlorophyllide *a*. The intention is to address the following questions:

- Does *Rba. sphaeroides* possess a functional aerobic cyclase?
- Can the aerobic cyclase encoding gene from an anoxygenic phototroph (for example, *Rvi. gelatinosus*) complement the loss of the aerobic cyclase encoding gene in an oxygenic phototroph (for example, *Synechocystis*)? Is the reciprocal exchange of enzymes possible?
- Is there any unknown subunit required for the aerobic cyclase?
- Is there any difference among aerobic cyclases from various organisms?
- Can the aerobic cyclase activity be assayed *in vivo* using an expression host that does not possess an aerobic cyclase?

Chapter 2

Materials and Methods

2.1 Standard buffers, reagents and media

All buffers were prepared in ultrapure water (resistivity = 18.2 MΩ cm at 25°C) made by a NANOpure Diamond water purification system (Barnstead). Solutions for DNA work were autoclaved at 15 psi at 121°C for 20 min. If required, heat-labile reagents were sterilised by passing through 0.2 μm filters. All reagents were purchased from Sigma-Aldrich or Thermo Fisher Scientific unless stated otherwise. Growth media were made in deionised water following the recipes listed in **Table 2.1** and sterilised by autoclaving at 15 psi at 121°C for 20 min. Heat-labile solutions such as vitamins and antibiotics were added to growth media cooled to below 50°C.

2.2 *E. coli* strains and plasmids

All *E. coli* strains used are listed in **Table 2.2**. All plasmids used are listed in **Table 2.3**. *E. coli* strains were grown in LB medium. If required, antibiotics were added at the following concentrations: kanamycin at 30 μg ml^{-1}, ampicillin at 100 μg ml^{-1} and chloramphenicol at 34 μg ml^{-1}. *E. coli* strains were stored at -70°C in 25% (v/v) glycerol in LB.

2.2.1 Chemically competent *E. coli* cells

JM109 chemically competent cells (>10^7 cfu μg^{-1}) were purchased from Promega and were used for molecular cloning. Other chemically competent *E. coli* strains were prepared as follows. Cells were streaked out from glycerol stock onto LB agar plates supplemented with appropriate antibiotic if required. The plates were incubated overnight at 37°C. A single colony was inoculated into 5 ml of LB medium, which was incubated at 37°C with shaking at 230 rpm. 1 ml of the overnight culture was inoculated into 50 ml of LB medium in a 250 ml Erlenmeyer flask. The incubation was performed at 37°C with shaking at 230 rpm until OD$_{600}$ of the culture reached ~0.5. The cells were then harvested in a pre-chilled 50 ml Falcon tube by centrifugation at 4,000 g for 10 min. The cell pellet was washed sequentially with 25 ml of ice-cold 0.1 M MgCl$_2$ solution and 25 ml of ice-cold 0.1 M CaCl$_2$ solution. Finally, the cell pellet was resuspended in 1 ml of 0.1 M CaCl$_2$, 20% (v/v) glycerol solution. The suspension was aliquoted in 50 μl, flash frozen in liquid nitrogen and stored at -70°C.

2.2.2 Transformation of *E. coli* using heat shock

A 50 μl aliquot of chemically competent *E. coli* cells was thawed on ice. Approximately 100 ng of plasmid DNA or 5 μl of ligation solution was added to the competent cells. The cells and DNA were mixed by flicking the tube gently. The mixture was incubated on ice for 20 min and then was subjected to heat shock at 42°C for 45 s. After 2 min incubation on ice, 500 μl of SOC medium (see **Table 2.1**) was added and the cell suspension was incubated at 37°C with shaking at 230 rpm for 1 hr. Then the cells were pelleted down and resuspended in 50 μl of LB medium and plated out onto LB agar medium containing the appropriate antibiotic. The plates were incubated overnight at 37°C.

2.2.3 Preparation of electrocompetent *E. coli* cells

A single colony from a freshly streaked out plate was inoculated into 10 ml of LB medium, which was incubated at 37°C with shaking at 230 rpm. The overnight culture was inoculated into 500 ml of LB medium in a 2 L Erlenmeyer flask. The incubation was performed at 37°C with shaking at 230 rpm until OD_{600} of the culture reached ~0.5. The culture was incubated on ice with shaking for 30 min and then harvested by centrifugation at 5,000 g at 4°C for 30 min. The cell pellet was resuspended in 500 ml of ice-cold sterile 10% (v/v) glycerol and the suspension was pelleted down at 5,000 g at 4°C for 30 min. The cell pellet was resuspended in 250 ml of ice-cold sterile 10% (v/v) glycerol and the suspension was pelleted down at 5,000 g at 4°C for 30 min. The cell pellet was resuspended in 30 ml of ice-cold sterile 10% (v/v) glycerol and transferred to an ice-cold sterile 50 ml Falcon tube. The suspension was pelleted down at 5,000 g at 4°C for 30 min. The cell pellet was resuspended in 1 ml of ice-cold sterile 10% (v/v) glycerol. The suspension was aliquoted in 50 μl, flash frozen in liquid nitrogen and stored at -70°C.

2.2.4 Electroporation of *E. coli*

A 50 μl aliquot of electrocompetent *E. coli* cells was thawed on ice. 1 μl of 10-fold diluted ligation solution was added to the competent cells and the resulting mixture was transferred to a chilled electroporation cuvette (0.1 cm gap, BioRad). Electroporation was performed using the MicroPulser (BioRad) with the program Ec1 (voltage = 1.8 kV, pulse length = ~5 ms). After electroporation, 500 μl of SOC medium was immediately added to the cuvette and the cell suspension was incubated at 37°C with shaking at 230 rpm for 1 hr. Then the cells were pelleted down, resuspended in 50 μl of LB medium, and plated out onto LB agar medium containing the relevant antibiotic. The plates were incubated overnight at 37°C.

2.3 Purple bacteria strains

All purple bacterial strains used are listed in **Table 2.4**. All plasmids used for mutant construction and gene expression are listed in **Table 2.3**. Recipes of growth media were shown in **Table 2.1**. Strains were grown in the dark at 30°C in the described medium. *Rba. sphaeroides* strains were grown in M22+ medium (Hunter and Turner, 1988). The liquid M22+ medium was supplemented with 0.1% casamino acids. *Rvi. gelatinosus* strains were grown in PYS medium (Nagashima *et al.*, 1996). *Rba. capsulatus* strains were grown in MPYE medium (Yen and Marrs, 1976) or on one occasion in PYS medium. If required, antibiotics were added at the following concentrations: kanamycin at 30 μg ml^{-1} for *Rba. sphaeroides*; kanamycin at 50 μg ml^{-1} and rifampicin at 40 μg ml^{-1} for *Rvi. gelatinosus*; kanamycin at 30 μg ml^{-1} and rifampicin at 20 μg ml^{-1} for *Rba. capsulatus*. Purple bacterial strains were stored at -70°C in 50% (v/v) glycerol in LB.

2.3.1 Growth conditions of purple bacteria

Semi-aerobic conditions were achieved by filling a 125 ml Erlenmeyer flask with 80 ml of medium and shaking at 150 rpm, which were applied for construction of mutants and purification of MgPME from a *Rvi. gelatinosus* $\Delta bchE\Delta acsF$ mutant (Section 4.3.6). High-oxygen conditions were achieved by filling a 250 ml Erlenmeyer flask with 20 ml of medium and shaking at 150 rpm, which were used to study the phenotypes of a *Rba. sphaeroides* $\Delta ccoP$ mutant (Section 3.3.3) and to analyse BChl production in *Rvi. gelatinosus* strains. Growth conditions with a gradient of oxygen tension were used and achieved by filling 250 ml Erlenmeyer flasks with 20, 40, 80 and 160 ml of medium and shaking at 150 rpm when analysing *Rba. sphaeroides* $\Delta bchE$ and $\Delta bchE\Delta ccoP$ strains (Section 3.3.4). *Rvi. gelatinosus* transposon mutants were grown in 10 ml of medium filled in 50-ml Falcon tubes with shaking at 150 rpm for phenotypic analysis (Sections 6.3.4 and 6.3.6). *Rba. capsulatus* strains were grown in 10 ml of medium filled in 50 ml Falcon tubes with shaking at 230 rpm for phenotypic analysis (Section 7.3.2).

2.3.2 Conjugal transfer of DNA to purple bacteria

Plasmids based on the pK18*mobsacB* (Schäfer *et al*, 1994) and pBBRBB-*Ppuf*$_{843-1200}$ (Tikh *et al.*, 2014) vectors were transferred to purple bacteria via conjugation. Transformation of plasmid into *E. coli* S17-1 strain was performed as described in Section 2.2.2. A single colony of purple bacterial strains was inoculated into 5 ml of growth medium in a 25 ml Universal tube and incubated for several days as starter. The starter was inoculated into 80 ml of growth

medium in a 125 ml Erlenmeyer flask and grown overnight. *E. coli* S17-1 strain harbouring the plasmid was grown for 24 hr before utilised for mating experiments. Purple bacteria cells from 30 ml of culture were resuspended in 100 μl of LB and mixed with *E. coli* cells from 30 μl (*Rba. sphaeroides* and *Rvi. gelatinosus* matings) or 3 ml (*Rba. capsulatus* mating) culture*.* The mating mixture was placed onto well-dried LB agar medium as drops and incubated at overnight 30°C. Transconjugants were selected on M22+ agar medium supplemented with 30 μg ml^{-1} of kanamycin for *Rba. sphaeroides*, PYS agar medium supplemented with 50 μg ml^{-1} of kanamycin and 40 μg ml^{-1} of rifampicin for *Rvi. gelatinosus*, and on MPYE agar medium supplemented with 30 μg ml^{-1} of kanamycin and 20 μg ml^{-1} of rifampicin for *Rba. capsulatus*.

2.3.3 Preparation of electrocompetent *Rvi. gelatinosus* cells

Rvi. gelatinosus strains were grown in 1.5 L of PYS medium in 2 L Erlenmeyer flasks until OD$_{680}$ reached ~0.6. The culture was cooled down in ice-water bath for 30 min with occasionally shaking. Cells were harvested by centrifugation at 5,000 *g* at 4°C for 30 min and then sequentially washed with 200 ml of ice-cold sterile ultrapure water, 100 ml and 50 ml of ice-cold sterile 10% (v/v) glycerol solution. Finally, the cell pellet was resuspended in 2 ml of ice-cold sterile 10% (v/v) glycerol solution and aliquoted in 50 μl. The prepared electrocompetent cells were either used immediately or flash frozen in liquid nitrogen and stored at -70°C.

2.3.4 Electroporation of *Rvi. gelatinosus*

A 50 μl aliquot of electrocompetent *Rvi. gelatinosus* cells was thawed on ice and then mixed with 4 μg of pK18*mobsacB* based plasmid DNA. The mixture was transferred to a pre-chilled electroporation cuvette (0.1 cm gap; Bio-Rad). Electroporation was performed using the MicroPulser (Bio-Rad) with the program Ec1 (voltage = 1.8 kV, pulse length = ~5 ms), followed by immediate addition of 1 ml of ice-cold PYS medium supplemented with 1% (w/v) glucose. The cell suspension in the cuvette was incubation on ice for 30 min, transferred to 10 ml of PYS medium in a 50 ml Falcon tube, and incubated at 30°C with shaking at 150 rpm. After 6 h incubation, cells were pelleted down and spread out onto PYS agar medium with 50 μg ml^{-1} of kanamycin for selection.

2.3.5 Construction of purple bacterial mutants

An allelic exchange suicide vector pK18*mobsacB* (Schäfer *et al*., 1994) was employed to construct markerless in-frame mutants of purple bacteria, of which the mechanism is shown in **Figure 3.2**. The gene knockout plasmid, pK18Δ*gene*, was constructed by cloning the upstream and downstream sequences of the indicated gene into the vector with an added

*Nde*I site between the two fragments. The gene insertion plasmid, pK18[*gene*], was built by cloning the indicated gene into the *Nde*I site of the pK18Δ*acsF* plasmid. The pK18*mobsacB*-based plasmid was transferred into a purple bacterium via either conjugation (*Rba. sphaeroides* and *Rba. capsulatus*, Section 2.3.2) or electroporation (*Rvi. gelatinosus*, Section 2.3.4). The selected kanamycin-resistant transformants containing the whole plasmid in the genome as a result of homologous recombination were inoculated into growth medium supplemented with kanamycin. The resulting culture was subjected to serial 10-fold dilutions and spread out onto agar medium with addition of 10% (w/v) sucrose, to select for a second homologous recombination event which excised the plasmid from the genome. The colonies showing up on the plate were transferred to two plates: one was agar medium supplemented with 10% (w/v) sucrose; and the other was agar medium supplemented with 10% (w/v) sucrose and kanamycin. The kanamycin-sensitive and sucrose-resistant colonies would either be the desired mutants or WT, which can be differentiated by colony PCR using primers flanking the upstream and downstream regions of the locus of interest.

2.4 *Synechocystis* strains

All *Synechocystis* strains used are listed in **Table 2.5**. All plasmids used for mutant construction were listed in **Table 2.3**. *Synechocystis* stains were grown at 30°C under constant illuminations in BG-11 medium (Rippka *et al.*, 1979) buffered with 10 mM TES (pH = 8.3, adjusted by potassium hydroxide). For mixotrophic growth conditions, glucose was added at the concentration of 5 mM. The following light conditions were utilised at different occasions: low (5 μE m^{-2} s^{-1}), low-moderate (15~20 μE m^{-2} s^{-1}) and moderate (30 μE m^{-2} s^{-1}). When constructing mutants, antibiotics were added at the following concentrations: kanamycin at 10~80 μg ml^{-1}, chloramphenicol at 5~80 μg ml^{-1} and zeocin at 2.5~10 μg ml^{-1}. *Synechocystis* strains were stored at -70°C in 10% (v/v) DMSO in BG-11.

2.4.1 Transformation of *Synechocystis*

Synechocystis is naturally transformable. *Synechocystis* strains were grown in liquid BG-11 medium to logarithmic phase. Cells from 5 ml of the resulting culture were harvested and resuspended in 50 μl of BG-11 medium. The cell suspension was mixed with 1 μl of plasmid DNA or purified PCR product. The mixture was incubated at 30°C under illumination for 30 min, followed by transferring onto BG-11 agar medium supplemented with 5 mM of glucose. After incubation at 30°C under constant illumination overnight, cells were collected from the plate and spread out onto BG-11 agar medium supplemented with 5 mM glucose and

appropriate antibiotic. Then the plate was incubated at 30°C under constant illumination for 7~14 days before the occurrence of tranformants.

2.4.2 Construction of *Synechocystis* strains

The pPD-FLAG vector was used to construct *Synechocystis* strains expressing genes under the promoter of a redundant gene *psbAII* (Hollingshead *et al.*, 2012). The pPD[*gene*] plasmid was constructed by cloning the indicated gene into the *Nde*I/*Bgl*II sites of the vector. To construct genetic knockout mutants, overlap extension PCR was conducted to generate a construct containing an antibiotic resistance gene or cassette flanked by the upstream and downstream sequences (~400 bp) of the gene to be deleted. The pPD[*gene*] plasmid or PCR construct were transformed into *Synechocystis* cells as described in Section 2.4.1. As *Synechocystis* contains multiple copies of its genome, the resulting transformants were subjected to a segregation process. The segregation level was checked by colony PCR using relevant primers. Antibiotic concentration was incrementally doubled until fully segregated mutants were achieved.

2.5 DNA manipulations

2.5.1 Isolation of plasmid DNA

E. coli overnight cultures were harvested by centrifugation and the cell pellets were used for isolation of plasmid DNA. Small-scale preparations (miniprep) were performed using the GenElute Plasmid Miniprep Kit (Sigma-Aldrich) following the manufacturer's instructions. The plasmid DNA was eluted with autoclaved ultrapure water.

2.5.2 Polymerase chain reactions (PCR)

PCR was performed in a TC-512 thermo cycler (Techne). All primers used are listed in **Table 2.6**. For molecular cloning, PCR reactions were performed using the ACCUZYME Mix (Bioline). The reaction was set up in 50 μl volume containing 25 μl of 2x ACCUZYME Mix, 0.4 μM of forward primer, 0.4 μM of reverse primer, 100 ng of template DNA and 2.5 μl of DMSO. The PCR program was as follows: 95°C for 3 min, 30 cycles of (1 min at 96°C, 45 s at 58°C and 1 min kb^{-1} at 72°C) and 72°C for 10 min. In some occasions, Q5 High-Fidelity Master Mix (NEB) was used. The reaction was set up in 50 μl volume containing 25 μl of 2x Q5 High-Fidelity Master Mix, 0.4 μM of forward primer, 0.4 μM of reverse primer and 100 ng of template DNA. The PCR program was as follows: 98°C for 1 min, 30 cycles of (20 s at 98°C, 20 s at 66°C and

20 s kb^{-1} at 72°C) and 72°C for 2 min. For screening colonies, PCR reactions were performed using the MyTaq HS Red Mix (Bioline). A bacterial colony was resuspended in 20 μl of autoclaved ultrapure water. The reaction was set up in 20 μl volume containing 10 μl of 2x MyTaq HS Red Mix, 0.4 μM of forward primer, 0.4 μM of reverse primer and 1 μl of colony suspension. The PCR program was as follows: 95°C for 2 min, 30 cycles of (20 s at 95°C, 20 s at 58°C and 1 min at 72°C) and 72°C for 2 min.

2.5.3 Restriction enzyme digestions

Restriction enzymes digestions were performed using enzymes from either Promega or NEB. A typical 50 μl reaction contained ~1 μg of DNA, 5 μl of 10x reaction buffer, and 10 units of each restriction enzyme. 100 μg ml^{-1} of acetylated bovine serum albumin was included in the reaction when Promega enzymes were used. The assembled reaction was incubated at 37°C for 1~4 hr. For digestion of plasmid vector, the reaction was incubated overnight. The digest was either directly purified or analysed by agarose gel electrophoresis.

2.5.4 Agarose gel electrophoresis of DNA

PCR products and restriction enzyme digests were analysed by electrophoresis using a 1% (w/v) agarose gel. The electrophoresis was conducted in TAE buffer (40 mM Tris, 40 mM acetic acid, 1 mM EDTA; Thermo Fisher Scientific) at a constant voltage of 80 V. If the DNA-containing gel slice was about to be used as template in overlap extension PCR, the gel was prepared from the TopVision Low Melting Point Agarose (Thermo Fisher Scientific) and the electrophoresis was conducted in modified TAE buffer (40 mM Tris, 40 mM acetic acid, 0.1 mM EDTA). The HyperLadder^{TM} 1kb (Bioline) was used as marker. DNA was stained with ethidium bromide in gel and visualised by exposure to UV light.

2.5.5 Purification of DNA fragments

The GenElute^{TM} PCR Clean-up kit (Sigma-Aldrich) was used to purify DNA fragments from solution according to manufacturer's instructions. The recovery of DNA fragments from agarose gel was performed using the GenElute^{TM} Gel Extraction kit (Sigma-Aldrich) following manufacturer's instructions. Purified DNA fragments were dissolved in autoclaved ultrapure water and stored at -20°C.

2.5.6 Ligation of DNA into vectors

Ligations were performed using the T4 DNA Ligase (NEB). A ligation reaction was set up in a 10 μl volume containing 1 μl of 10x reaction buffer, 1 μl of T4 DNA Ligase, cut vector DNA and

cut insert DNA. The molar ratio of vector to insert is variable between 1:1 and 1:10. The reaction was incubated either at room temperature for 2 hr or at 15°C overnight. 5 μl of the ligation reaction was used to transform 50 μl of chemically competent *E. coli* cells as described in Section 2.2.2.

2.5.7 Construction of plasmids using the 'Link and Lock' method

The 'Link and Lock' method, reported by McGoldrick *et al*. (2005), allows multiple genes to be consecutively cloned into a single vector by reusing the same restriction enzyme sites. The mechanism of the 'Link and Lock' method is shown in **Figure 7.6**. The pET3a vector (Novagen) was engineered to contain an added *Spe*I site immediately upstream of the native *BamH*I site. The resulting vector was utilised to perform the 'Link and Lock' cloning. Each individual gene was firstly cloned into the *Nde*I/*Spe*I sites of the pET3a vector, resulting in a few plasmids. The plasmid containing the first gene to be cloned was cut with *Spe*I/*Hind*III and the larger fragment was recovered, whereas the plasmid with the second gene to be cloned was cut with *Xba*I/*Hind*III and the gene-containing fragment was purified. The purified fragments were ligated to generate a plasmid containing the two genes in tandem. Using the same strategy, the remaining genes were sequentially added to get the desired construct.

2.5.8 DNA sequencing

Purified plasmids and DNA fragments were sent to GATC Biotech for the Sanger sequencing with corresponding primers.

2.5.8 Isolation of bacterial genomic DNA

Depending on the downstream application, bacterial genomic DNA was isolated in one of the three methods described here. Isolated genomic DNA was stored at -20°C before use.

Bacterial genomic DNA to serve as PCR template was isolated using a method based on phenol-chloroform extraction. Bacterial cells were suspended in 500 μl of TE buffer (10 mM Tris-HCl, pH = 8.0, 1 mM EDTA), followed by addition of 50 μl of 10% (w/v) SDS solution and incubation at 70°C for 15 min. Then 500 μl of phenol:chloroform:isoamyl alcohol (25:24:1, saturated with TE buffer; Sigma-Aldrich) was added and the sample was mixed thoroughly by vortex. After centrifugation at 14,000 *g* for 10 min, the upper phase was carefully transferred to a new Eppendorf tube, followed by addition of 350 μl of phenol:chloroform:isoamyl alcohol and thorough mixing by vortex. The sample was centrifuged at 14,000 *g* for 10 min and then the upper phase was transferred to a new Eppendorf tube. 25 μl of 3 M sodium

acetate (pH = 5.2, adjusted by glacial acetic acid) and 500 μl of pre-chilled ethanol were added to precipitate DNA. The sample was mixed by brief vortex and incubated at -20°C for 1 hr. DNA was pelleted by centrifugation at 14,000 g at 4°C for 10 min and washed once with 200 μl of pre-chilled 70% (v/v) ethanol solution. Then DNA pellet was air dried and dissolved in 100 μl of autoclaved ultrapure water.

Genomic DNA from the isolated *Rvi. gelatinosus* transposon mutants was purified using the MasterPure^{TM} DNA Purification Kit (Epicentre) according to manufacturer's instructions. The kit allows fast and parallel purification of many samples.

For next-generation sequencing, *Synechocystis* genomic DNA with high-integrity was isolated using a method developed from Williams (1988) and Wilson (2001). *Synechocystis* cells were collected from BG-11 agar plate and resuspended in saturated NaI solution by vortex. The suspension was incubated at 37°C for 20 min to remove extracellular polysaccharides. Then NaI was removed by addition of excessive ultrapure water and subsequent centrifugation at 5,000 g for 10 min. The cell pellet was resuspended in STE buffer (50 mM NaCl, 50 mM Tris-HCl, pH = 8.5, 5 mM EDTA) and sequentially treated with 10 mg ml^{-1} of lysozyme at 37°C for 45 min and 0.1 mg ml^{-1} of Proteinase K in the presence of 1% (w/v) SDS at 50°C overnight. The concentration of NaCl in the resulting cell lysate was adjusted to 0.7 M by adding 5 M NaCl solution. Then 0.1 volume of CTAB/NaCl solution (10% (w/v) CTAB in 0.7 M NaCl) was added to selectively precipitate cell wall debris, residual polysaccharides and proteins. The mixture was incubated at 65°C for 10 min. An equal volume of phenol:chloroform:isoamyl alcohol was added, followed by gently mixing by inverting the tube several times. After centrifugation at 5,000 g for 5 min, the upper phase was transferred to a new 50-ml Falcon tube. The phenol-chloroform extraction was repeated once. Then an equal volume of chloroform was added, followed by gently mixing by inverting the container several times. After centrifugation at 5,000 g for 5 min, the upper phase was transferred to a JA-25.50 centrifuge tube (Beckman Coulter) before 0.6 volume of isopropanol was added to precipitate DNA. DNA was pelleted by centrifugation at 20,000 g at 4°C for 5 min. The DNA pellet was washed once with 70% (v/v) ethanol solution and then dissolved in TE buffer. RNA contamination was eliminated by RNase treatment. Genomic DNA was recovered by phenol-chloroform extraction, isopropanol precipitation, wash and resuspension as described above. The purified genomic DNA was analysed by agarose gel electrophoresis and absorption spectroscopy before construction of library for sequencing.

2.6 RNA manipulations

2.6.1 Isolation of total bacterial RNA from *Rba. sphaeroides*

Rba. sphaeroides cultures were grown to mid-exponential phase and then one volume of bacterial culture with 0.5 OD_{680} units was immediately mixed with two volumes of the RNAprotect[TM] Bacterial Reagent (Qiagen). Cells were harvested and the pellets were stored at -70°C until use. Total RNA was isolated using the RNeasy Protect Bacteria Mini Kit (Qiagen) according to the manufacturer's instructions. The cell disruption was performed by treatment with 10 mg ml^{-1} lysozyme for 30 min at room temperature with constant shaking. RNA was eluted with 40 μl of RNase-free water. The TURBO DNA-free[TM] Kit (Ambion) was used to eliminate any potential genomic DNA contamination in the RNA. Before and after the DNase treatment, the concentration of RNA was determined by UV absorption spectroscopy using a FLUOstar Omega plate reader (BMG LABTECH) (1 Abs_{260} unit = 40 μg ml^{-1}). To check RNA integrity, 1 μg of RNA was separated on a 1% (w/v) agarose gel with the presence of β-mercaptoethanol and visualised by staining with ethidium bromide. The isolated RNA was either used immediately for cDNA synthesis or stored at -70°C.

2.6.2 Synthesis of cDNA

Reverse transcription was performed using the SensiFAST[TM] cDNA Synthesis Kit (Bioline) in a 20 μl reaction containing 4 μl of 5x TransAmp buffer, 1 μl of RTase and 1 μg of RNA. No-RT controls were included by omitting the reverse transcriptase in the reaction. The thermal cycling program was 10 min at 25°C, 30 min at 42°C and 5 min at 85°C. The cDNA was stored at -20°C.

2.6.3 Quantitative real time PCR (qPCR)

Primers for qPCR were designed using the NCBI Primer-BLAST (Ye *et al.*, 2012) with a melting temperature at around 60°C. To find out the appropriate dilution of cDNA for qPCR, PCR trials were performed using MyTaq[TM] HS Red Mix (Bioline) with serial dilutions of the synthesised cDNA (Section 2.6.2) as template. The qPCR assay was performed using SensiFAST[TM] SYBR Lo-ROX Kit (Bioline) with a Stratagene Mx3005P system (Agilent). Reactions were set up in triplicate with a 20 μl volume containing 10 μl of 2x SensiFAST[TM] SYBR Lo-ROX mix, 0.4 μM forward primers, 0.4 μM reverse primers and cDNA template. No-RT controls (using no-RT cDNA samples) and no-template controls (replacing cDNA with water) were also included. The *rpoZ* gene was used as an internal reference to normalise the expression level of target

genes (Gomelsky *et al.*, 2003). The primer efficiency was determined using 10-fold serial dilutions of genomic DNA from *Rba. sphaeroides* (Section 2.5.8). The thermal cycling conditions were as follows: 3 min at 95 °C, 40 cycles of 5 s at 95 °C and 30 s at 60 °C, and followed by melting curve analysis. The relative expression ratios of target genes were calculated and statistically analysed using the REST™ software (Pfaffl *et al.*, 2002) based on the Pfaffl method (Pfaffl, 2001).

2.7 Protein analysis by Western blot

2.7.1 Preparation of *Synechocystis* membranes

Synechocystis cells harvested from liquid culture with an OD_{750} of ~0.4 were used for membrane preparation under dim green light. Cells were resuspended in the thylakoid buffer (25 mM MES/NaOH, pH = 6.5, 5 mM $CaCl_2$, 10 mM $MgCl_2$, 20% (v/v) glycerol) and mixed with an equal volume of glass beads (0.1 mm diameter; BioSpec). Cell breakage was performed by 4 cycles of 1 min bead beating on a MiniBeadbeater™ (BioSpec) and 5 min incubation on ice. Cell lysate was collected from the upper layer of the mixture and the wash of the beads. A brief centrifugation at 3,000 *g* at 4°C was performed to remove the remaining beads in the cell lysate. Then membranes were pelleted by centrifugation at 36,000 *g* at 4°C for 20 min. The resulting supernatant was transferred to a new tube and the pellet was resuspended in the thylakoid buffer. The collected supernatant and the resuspended pellet were both centrifuged at 36,000 *g* at 4°C for 20 min. Pellets in both tubes were resuspended in the thylakoid buffer as the membrane fraction. The isolated *Synechocystis* membranes were either used immediately or flash frozen in liquid nitrogen and stored at -70°C.

2.7.2 SDS-polyacrylamide gel electrophoresis (SDS-PAGE)

Proteins were resolved by SDS-PAGE on a 12~20% linear gradient polyacrylamide gel containing 7 M urea using the PROTEAN™ II xi cell (Bio-Rad) (Komenda *et al.*, 2002). The isolated *Synechocystis* membranes, corresponding to 2 μg of Chl, were treated with 1% (w/v) SDS and 2% (w/v) DTT at room temperature for 30 min, followed by centrifugation at 15,000 *g* at 4°C for 10 min. Then the supernatant was loaded onto the gel. The gel was run at a constant current of 32 mA for 16 hr with controlled temperature at 23°C. After electrophoresis, the gel was stained with SYPRO Orange and then photographed using LAS 4000 (Fujifilm).

2.7.3 Transfer, blocking and antibody incubation

Resolved proteins were transferred from the SDS-PAGE gel to a Hybond-P PVDF membrane (GE Healthcare). Whatman™ 3MM filter paper was used in the transfer. The PVDF membrane was soaked in methanol for 10 s, rinsed twice in ultrapure water and equilibrated in carbonated buffer (3 mM Na_2CO_3, 10 mM $NaHCO_3$) for at least 10 min. The 'transfer sandwich' was assembled as the following order: blot pad-filter paper-gel-PVDF membrane-filter paper-blot pad. The assembled sandwich was placed in carbonated buffer with 10% (v/v) methanol. Transfer was performed at 4°C with a constant current of 0.85 A for 3 hr. After transfer, the membrane was blocked in TBS buffer (10 mM Tris/HCl, pH = 7.6, 150 mM NaCl) with 0.2% (v/v) Tween 20 for 1 hr on a gyro rocker. The membrane was probed with a primary antibody diluted in antibody buffer (TBS buffer, 0.05% (v/v) Tween 20) overnight at 4°C on a gyro rocker, followed by rinsing 3 times for 5 min in antibody buffer. The membrane was probed with a secondary antibody (conjugated with horseradish peroxidase) (Sigma-Aldrich) diluted in antibody buffer at room temperature for 1 hr on a gyro rocker. Then the membrane was washed 3 times for 5 min in antibody buffer before incubation with chemiluminescent reagent.

2.7.4 Detection of chemiluminescent signal

The resulting membrane from Section 2.7.3 was incubated with the Luminata Crescendo Western HRP substrate (Merck Millipore) for 5 min with occasional movements. Then the membrane was placed inside a folded clear plastic sheet and the chemiluminescent signal was detected using LAS 4000 (Fujifilm).

2.8 Pigment manipulations

2.8.1 Extraction of pigments

The OD of a liquid bacterial culture was measured on a Cary 60 UV-Vis spectrophotometer at 600 nm, 680 nm and 750 nm for *E. coli*, purple bacteria and *Synechocystis*, respectively. Cells were harvested from a liquid culture of known OD and washed once in HEPES buffer (25 mM, pH = 7.4). Pigments were extracted with an excess of 0.2% (v/v) ammonia in methanol by vigorous shaking using a MiniBeadbeater™ (BioSpec), followed by incubation on ice for 10 min. Then centrifugation was performed at 16,000 *g* for 5 min at 4°C. The resulting supernatant was transferred to a new Eppendorf tube as the pigment extract. In some cases, the extraction was repeated once to ensure completeness and the two extracts were pooled

together. Pigments extracts were either analysed immediately or dried in vacuum at 30°C using a Concentrator plus (Eppendorf) and stored at -20°C for future analysis.

2.8.2 Quantification of Chl *a* in *Synechocystis*

Chl *a* content was determined using three biological replicates of each strain. Chl was extracted from *Synechocystis* cells harvested from 4 ml of liquid culture at OD_{750} of 0.3~0.5 with 1 ml of methanol. The extraction was performed by vigorous shaking for 25 s using a MiniBeadbeater^{TM} (BioSpec) followed by incubation on ice for 10 min. The lysate was centrifuged at 16,000 *g* for 5 min at 4°C. The absorption spectrum of the resulting supernatant was measured on a Cary 60 UV-Vis spectrophotometer. Chl *a* content was calculated according to Porra *et al*. (1989) using the following formula:

Chl *a* content (mg L^{-1} OD_{750}^{-1}) = [16.29 × ($Abs_{665.2}$ −$Abs_{750.0}$) − 8.54 × ($Abs_{652.0}$ − $Abs_{750.0}$)]/ (4 × OD_{750})

2.8.3 Preparation of Zn-BChl *a*

Zn-BChl *a* was prepared from BChl *a* extracted from *Rba. sphaeroides* WT using a previously described method (Hartwich *et al*., 1998) with slight modifications. Briefly, one volume of BChl *a* methanol extract was mixed with an excess of anhydrous zinc acetate, 50 mM sodium ascorbate and 6 volumes of glacial acetic acid in a 1.5 ml Eppendorf tube. The tube with the mixture was incubated in boiling water for 2 hr with lid open. The supernatant was transferred to a new tube, clarified by centrifugation (16,000 *g* for 5 min at 4°C) and then dried in vacuum at 30°C using a Concentrator plus (Eppendorf). The dried pigments were reconstituted in 0.2% (v/v) ammonia in methanol and clarified by centrifugation (16,000 *g* for 5 min at 4°C) before analysed by HPLC.

2.8.4 Purification of MgPME

A Δ*bchE*Δ*acsF* mutant of *Rvi. gelatinosus* (described in Section 4.3.6) accumulates and excretes massive MgPME into the medium, which precipitates as granules due to its hydrophobic nature. The mutant was used for purification of MgPME. The mutant was grown in 80 ml of PYS medium in a 125 ml Erlenmeyer flask at 30°C for 2 days before purification. Cells were harvested and washed once in ultrapure water. The pigment granules were clearly visible on the top of the cell pellet. Then a small volume of methanol was added, followed by gentle shaking to facilitate the dissolution of MgPME into methanol. After centrifugation at 5,000 *g* at 4°C for 10 min, the red-coloured supernatant was collected. The resulting MgPME

solution was very pure with only tiny amount of contamination, as confirmed by HPLC. The concentration of MgPME in methanol was determined using the extinction coefficient at 589 nm of 18,000 M^{-1} cm^{-1} (Nasrulhaq-Boyce *et al.*, 1987). The MgPME solution was dried in vacuum at 30°C using a Concentrator plus (Eppendorf) and stored at -20°C for future use.

2.8.5 High performance liquid chromatography (HPLC)

Pigment solution either freshly extracted or reconstituted from dried sample was analysed on an Agilent 1200 HPLC system (Agilent) equipped with a diode array detector and a fluorescence detector.

For analysis of BChl species, pigment solution were separated on a Fortis UniverSil C18 reverse-phase column (5 μm particle size, 150 mm x 4.6 mm; Fortis) using a method modified from van Heukelem *et al.* (1994). Solvents A and B were methanol/500 mM ammonium acetate (80:20, v/v) and methanol/acetone (80:20, v/v), respectively. BChl species were eluted using a linear gradient of 92~93% solvent B over 10 min with a flow rate of 1 ml min^{-1} at 40°C. The elution of BChl species was monitored by absorbance at 770 nm and by the 788 nm fluorescence with 365 nm excitation.

For separation of Chl precursors, a method modified from Sobotka *et al.* (2011) was used. Pigment solution was separated using a Sigma-Aldrich Discovery C18 reverse-phase column (5 μm particle size, 250 mm x 4.6 mm; Sigma-Aldrich). Solvents A and B were methanol/500 mM ammonium acetate (30:70, v/v) and methanol, respectively. Chl precursors were eluted at 40°C at a flow rate of 1 ml min^{-1} with a linear gradient of 65~75% of solvent B over 35 min followed by column wash with 100% of solvent B for 10 min. The elution was monitored by absorbance at 400 nm, 416 nm, 433 nm, 440 nm, 632 nm, 665 nm and 770 nm. Additionally, the fluorescence detector was set to monitor fluorescence at 595 nm, 640 nm and 670 nm with excitation at 440 nm. Proto (Sigma-Aldrich), MgPME (purified from the *Rvi. gelatinosus* $\Delta bchE\Delta acsF$ mutant), a mixture of PChlide and Chlide (extracted from an *in vitro* enzyme assay of POR) were used as pigment standards.

2.9 Absorption spectroscopy

2.9.1 Measurement of whole-cell absorption

Cells were harvested from liquid culture and resuspended in 60% (w/v) sucrose solution to minimise the interference from light scattering. The whole-cell absorption spectrum was

recorded on a Cary 60 UV-Vis spectrophotometer. The obtained spectrum was normalised to cell number.

2.9.2 Measurement of pigment absorption

The absorption spectrum or the absorbance at a given wavelength of pigment solution was measured on a Cary 60 UV-Vis spectrophotometer.

2.10 Drop growth assays of *Synechocystis* strains

Drop growth assays on BG-11 agar medium were conducted to evaluate growth rates of *Synechocystis* strains under photoautotrophic and photomixotrophic conditions. The liquid culture of a *Synechocystis* strain was adjusted to OD_{750} of 0.4 and then subjected to several 10-fold dilutions. 4 μl of each diluted culture were dropped onto BG-11 agar medium either without or with the supplementation of 5 mM glucose. The plates were incubated at 30°C under low-moderate (15 μE m^{-2} s^{-1}) light conditions. Photographs of the plates were taken after 12-day incubation.

2.11 Transposon mutagenesis and mutant screening in *Rvi. gelatinosus*

2.11.1 Transposon mutagenesis in a *Rvi. gelatinosus* Δ*bchE* strain

Transposon mutagenesis was performed using the EZ-Tn5^{TM} <R6Kγ*ori*/KAN-2> Insertion Kit (Epicentre) in a *Rvi. gelatinosus* Δ*bchE* strain (Section 4.3.6), which is a markerless in-frame deletion mutant. The EZ-Tn5 transposome was prepared by assembling 2 μl of EZ-Tn5 Transposon DNA (100 μg ml^{-1}), 4 μl of EZ-Tn5 Transposase (1 unit μl^{-1}) and 2 μl of glycerol in an 8 μl reaction, followed by incubation at room temperature for 30 min. The resulting transposome was stored at -20°C before use. 1 μl of the transposome was mixed with 40 μl of electrocompetent Δ*bchE* cells (prepared as described in Section 2.3.3) and transferred to a pre-chilled electroporation cuvette (0.1 cm gap, Bio-Rad). Electroporation was performed as described in Section 2.3.4 except the incubation at 30°C with shaking at 150 rpm was 4 hr. After incubation, cells were plated out onto large square plates (22.5 cm x 22.5 cm) containing PYS agar medium supplemented with 50 μg ml^{-1} of kanamycin to select for transposon insertion mutants. The plates were incubated at 30°C for 3 days before screening.

2.11.2 First screening: fluorescence with 395 nm excitation

The first screening was performed by illuminating the colonies with a 395 nm LED flashlight. Colonies with apparent fluorescence judged by visual inspection were picked with sterile toothpicks and stabbed onto PYS agar medium supplemented with 50 μg ml^{-1} of kanamycin. Whenever there was an uncertainty during the screening, the mutant was provisionally considered to be positive. The isolated mutants were grown in liquid PYS medium supplemented with 50 μg ml^{-1} of kanamycin. The resulting cultures were used to make a stock of each mutant (Section 2.2).

2.11.3 Second screening: presence or absence of BChl a

The second screening was performed by analysing the production of BChl a in the isolated mutants from the first screening. The mutants were grown in 10 ml of PYS medium supplemented with 50 μg ml^{-1} of kanamycin in 50 ml Falcon tubes. Incubation was performed at 30°C with shaking at 250 rpm. Then pigments were extracted from cells harvested from overnight culture as described in Section 2.8.1. Absorption spectra of pigment extracts were measured between 350 nm and 850 nm on a Cary 60 UV-Vis spectrophotometer. The absence of a 770 nm peak in the absorption spectrum was considered to be positive. In the cases of difficult judgement for the 770 nm peak, the mutants were provisionally considered to be positive.

2.11.4 Random amplification of transposon ends (RATE) PCR

To identify the transposon insertion sites in the isolated mutants, RATE PCR was performed using a protocol based on Ducey and Dyer (2002) and communicated by Dr Fred Hyde (Illumina Technical Support, techsupport@illumina.com). The mechanism of RATE PCR was shown in **Figure 6.5**. The reaction was set up in a 25 μl volume containing 10 μl of MyTaq HS Red Mix (Bioline), 0.5 μM of the INV-2 primer (or the TN5SEQ R primer) and 1 μl of purified genomic DNA (Section 2.5.8). The thermal cycling program was as follows: 95°C for 3 min, 30 cycles of (15 s at 95°C, 15 s at 55°C and 60 s at 72°C), 30 cycles of (15 s at 95°C, 15 s at 30°C and 45 s at 72°C), 30 cycles of (15 s at 95°C, 15 s at 55°C and 45 s at 72°C) and 72°C for 2 min. The PCR products were either directly purified or run on an agarose gel followed by gel extraction (Sections 2.5.4 and 2.5.5). The purified DNA fragments were sent to sequence with the KAN-2 FP-1 primer (for RATE PCR using the INV-2 primer) or the R6KAN-2 RP-1 primer (for RATE PCR using the TN5SEQ R primer) (Section 2.5.8).

2.12 *In vivo E. coli* assays

In vivo assays were conducted using an *E. coli* C43(DE3) strain harbouring the pET14b-AcsF plasmid and a series of *E. coli* C43(DE3) strains overexpressing multiple Chl biosynthetic enzymes from a pET3a-based plasmid constructed using the 'Link and Lock' method (Section 2.5.7). Strains containing empty vector were also included as control. Strains were streaked out from glycerol stocks onto LB agar medium supplemented with 100 μg ml^{-1} of ampicillin. A single colony from the plate was inoculated into 10 ml of LB medium supplemented with 100 μg ml^{-1} of ampicillin in a 50 ml Falcon tube and grown overnight at 37°C with shaking at 230 rpm. The resulting culture was diluted 1/150 into 10 ml of LB medium supplemented with 100 μg ml^{-1} of ampicillin in a 50 ml Falcon tube and grown at 37°C with shaking at 230 rpm until OD$_{600}$ reached 0.6~0.8. The culture was cooled down at 30°C for 15 min. Then IPTG was added at a concentration of 0.5 mM. Meanwhile, purified MgPME (Section 2.8.4) was prepared in methanol solution and added to the cultures with pET14b-based plasmids. ALA and Mg^{2+} (MgSO$_4$:MgCl$_2$ = 1:1) were both added at a concentration of 10 mM to the cultures with pET3a-based plasmids. Incubation was performed in the dark at 30°C with shaking at 150 rpm for 24 hr. For activation of POR, the relevant cultures were incubated under 5 μE m^{-2} s^{-1} light conditions for the final 4 hr. Finally, cells were harvested from the culture and pigments were extracted as described in Section 2.8.1. Pigment extracts were analysed by HPLC with the method for separation of Chl precursors (Section 2.8.5).

Table 2.1 Growth media

Growth medium	Recipe for 1 L
LB	**LB** 25 g powdered LB medium (Formedium) Note: autoclave **LB agar** 40 g powdered LB agar medium (Formedium) Note: autoclave
SOC	**SOC stock solutions** 2 M magnesium stock: 203.3 g magnesium chloride (hexahydrate), 246.5 g magnesium sulfate (heptahydrate) 1 M glucose stock: 180 g glucose Note: sterilise by passing through a 0.2 μm filter **SOC** 20 g tryptone, 5 g yeast extract, 2 ml of 5 M sodium chloride, 2.5 ml of 1 M potassium chloride, 10 ml of 2 M magnesium stock, 20 ml of 1 M glucose stock. Note: autoclave, cool down to below 50°C, then add reagents in blue
M22+	**M22+ stock solutions** Solution C: 10 g nitrilotriacetic acid, 24 g magnesium chloride, 3.34 g calcium chloride, 0.125 g EDTA, 0.261 g zinc chloride, 0.25 g ferrous chloride, 0.09 g manganese chloride, 0.00925 g ammonium heptamolybdate, 0.00775 g cupric chloride, 0.0124 g cobaltous nitrate, 0.0057 g boric acid Note: adjust pH to 6.8, do not autoclave, store at -20°C 10x stock: 30.6 g potassium dihydrogen orthophosphate, 30 g dipotassium hydrogen orthophosphate, 25 g DL-lactic acid, 5 g ammonium sulfate, 5 g sodium chloride, 43.4 g sodium succinate, 2.7 g sodium L-glutamate, 0.4 g DL-aspartic acid, 200 ml Solution C Note: autoclave CAA stock: 20 g Casamino Acids Note: autoclave 10 000x vitamins: 10 g nicotimic acid, 5 g thiamine, 1 g 4-aminobenzoic acid (PABA), 0.1 g D-biotin Note: sterilise by passing through a 0.2 μm filter and store at 4°C **M22+ liquid** 100 ml 10x stock, 50 ml CAA stock, 0.1 ml 10 000x vitamins Note: autoclave, cool down to below 50°C, then add reagent in blue **M22+ agar** 100 ml 10x stock, 15 g Bacto™ Agar (BD Biosciences), Note: autoclave, cool down to below 50°C, then add reagent in blue

Growth medium	Recipe for 1 L
BG-11	**BG-11 stock solutions** Trace minerals: 2.86 g boric acid, 1.81 g manganese chloride, 0.22 g zinc sulfate, 0.39 g sodium molybdate, 0.079 g copper sulfate, 0.049 g cobaltous nitrate Note: pass through a 0.2 μm filter (using a vacuum filtration apparatus) 100x BG-11:149.6 g sodium nitrate, 7.49 g magnesium sulfate, 3.6 g calcium chloride, 0.6 g citric acid, 0.56 ml of 0.5 M EDTA (pH = 8.0, disodium salt), 100 ml trace minerals Note: pass through a 0.2 μm filter (using a vacuum filtration apparatus) 1000x iron stock: 6 g ferric ammonium citrate 1000x phosphate stock: 30.5 g dipotassium hydrophosphate 1000x carbonate stock: 20 g sodium carbonate 1 M glucose stock: 180 g glucose 1 M TES stock: 229.2 g TES, adjust to pH 8.2 (potassium hydroxide) Note: sterilise by passing through a 0.2 μm filter **BG-11** 10 ml 100x BG-11, 1 ml 1000x iron stock, 1 ml 1000x phosphate stock, 1 ml 1000x carbonate stock, 15 g Bacto^{TM} Agar (BD Biosciences) for agar medium, 10 ml 1 M TES stock, 5 ml 1 M glucose stock if desired Note: autoclave, cool down to below 50°C, then add reagents in blue
PYS	**PYS stock solutions** Trace elements solution: 11.16 g manganese sulfate, 2.88 g zinc sulfate, 2.92 g cobaltous nitrate, 2.52 g copper sulfate, 2.42 g sodium molybdate, 3.1 g boric acid, 41.2 g EDTA (trisodium salt) Note: pass through a 0.2 μm filter (using a vacuum filtration apparatus) Basal salt solution: 4.12 g EDTA (trisodium salt), 1.11 g ferrous sulfate, 24.65 g magnesium sulfate, 2.94 g calcium chloride, 23.4 g sodium chloride, 10 ml trace elements solution Note: pass through a 0.2 μm filter (using a vacuum filtration apparatus) **PYS** 5 g polypeptone (Bio Basic), 1 g yeast extract, 5 g sodium succinate, 10 ml basal salt solution, 15 g Bacto^{TM} Agar (BD Biosciences) for agar medium Note: autoclave
MPYE	3 g Bacto^{TM} Peptone (BD Biosciences), 3 g yeast extract, 1.6 ml of 1 M magnesium chloride, 1 ml of 1 M calcium chloride, 15 g Bacto^{TM} Agar (BD Biosciences) for agar medium Note: autoclave

Table 2.2 *E. coli* strains

Strain	Genotype	Source/Reference
JM109	*endA1, recA1, gyrA96, thi, hsdR17* (r_K^-, r_K^-), *relA1, supE44,* Δ(*lac-proAB*), [F' *traD36, proAB, laqI^{q}Z*Δm15]	Promega
S17-1	F$^-$, *recA, pro, thi, hsdR$^-$, hsdR$^+$*, RP4-2-Tc::Mu-Km::Tn7, λpir lysogen, Tp^R Sm^R	Simon *et al.*, 1983; de Lorenzo *et al.*, 1993
C43(DE3)	F$^-$, *ompT, hsdS$_B$*(r_B^-, m_B^-), *gal, dcm*, (DE3)	Miroux and Walker, 1996

Table 2.3 Plasmids

Plasmid	Characteristics	Source/Reference
pK18*mobsacB*	pK18-based allelic exchange suicide vector containing the RP4 origin of transfer, *sacB*, and the *lacZα* fragment, Km^R,	J. Armitage (University of Oxford, UK)
pK18Δ*bchE*^{Rs}	upstream-*Nde*I-downstrem of *Rba. sphaeroides bchE* cloned into the *Sma*I/*Hind*III sites of pK18*mobsacB*	This thesis
pK18Δ*acsF*^{Rs}	upstream-*Nde*I-downstrem of *Rba. sphaeroides acsF* cloned into the *Bam*HI/*Hind*III sites of pK18*mobsacB*	This thesis
pK18Δ*ccoP*^{Rs}	upstream-*Nde*I-downstrem of *Rba. sphaeroides ccoP* cloned into the *Xba*I/*Hind*III sites of pK18*mobsacB*	E. Martin
pK18Δ*bciE*^{Rs}	upstream-*Nde*I-downstrem of *Rba. sphaeroides bciE* cloned into the *Xba*I/*Hind*III sites of pK18*mobsacB*	D. Canniffe
pK18Δ*bchE*^{Rc}	upstream-*Nde*I-downstrem of *Rba. capsulatus bchE* cloned into the *Xba*I/*Hind*III sites of pK18*mobsacB*	This thesis
pK18Δ*ccoP*^{Rc}	upstream-*Nde*I-downstrem of *Rba. capsulatus ccoP* cloned into the *Xba*I/*Hind*III sites of pK18*mobsacB*	This thesis
pK18Δ*bchE*^{Rg}	upstream-*Nde*I-downstrem of *Rvi. gelatinosus bchE* cloned into the *Bam*HI/*Hind*III sites of pK18*mobsacB*	This thesis
pK18Δ*acsF*^{Rg}	upstream-*Nde*I-downstrem of *Rvi. gelatinosus acsF* cloned into the *Bam*HI/*Hind*III sites of pK18*mobsacB*	This thesis
pK18[*acsF*^{Rs}]	*Rba. sphaeroides acsF* cloned into the *Nde*I site of pK18Δ*acsF*^{Rg}	This thesis
pK18[*bciE-acsF*^{Rs}]	*Rba. sphaeroides bciE-acsF* cloned into the *Nde*I site of pK18Δ*acsF*^{Rg}	This thesis
pK18[*cycI*]	*Synechocystis cycI* cloned into the *Nde*I site of pK18Δ*acsF*^{Rg}	This thesis
pK18[*cycI-ycf54*]	*Synechocystis cycI* and *ycf54* with a RBS sequence placed between the two gens cloned into the *Nde*I site of pK18Δ*acsF*^{Rg}	This thesis
pK18[*cycI*^{SM}]	*Synechocystis cycI*^{SM}(D219G mutant of *cycI*) cloned into the *Nde*I site of pK18Δ*acsF*^{Rg}	This thesis
pPD-FLAG	pBluescript II KS (+)-based vector for replacing the *Synechocystis psbAII* gene with a cloned gene and Km^R cassette, with N-terminal 3xFLAG tag if the *Not*I/*Bgl*II sites are used, Amp^R, Km^R	P. Davison and D. Canniffe
pPD[*acsF*]	*Rvi. gelatinosus acsF* cloned into the *Nde*I/*Bgl*II sites of pPD-FLAG	This thesis
pPD[*cycI*]	*Synechocytis cycI* cloned into the *Nde*I/*Bgl*II sites of pPD-FLAG	This thesis
pPD[*cycI*^{SM}]	*Synechocytis cycI*^{SM} (D219G mutant of *cycI*) cloned into the *Nde*I/*Bgl*II sites of pPD-FLAG	This thesis
pACYC184	p15A-based expression vector, Tet^R, Cm^R	Fermentas

Plasmid	Characteristics	Source/Reference
pBBRBB-*Ppuf*$_{843-1200}$	pBBR1MCS-2-based expression vector containing the 843-1200 region of the *Rba. sphaeroides puf* promoter, with C-terminal 6x His tag if the *Bgl*II/*Not*I sites are used, Km^R	Tikh *et al.*, 2014
pBB[*bciE*]	*Rba. sphaeroides bciE* cloned into the *Bgl*II/*Not*I sites of pBBRBB-*Ppuf*$_{843-1200}$	A. Hitchcock
pBB[*bciE*$^{-Cys}$]	*Rba. sphaeroides bciE*$^{-Cys}$(C13G/C88G mutant of *bciE*) cloned into the *Bgl*II/*Not*I sites of pBBRBB-*Ppuf*$_{843-1200}$	A. Hitchcock
pBB[*acsF*]	*Rvi. gelatinosus acsF* cloned into the *Bgl*II/*Not*I sites of pBBRBB-*Ppuf*$_{843-1200}$	This thesis
pBB[*acsF*^{AD}]	*Rvi. gelatinosus acsF*^{AD} (A218D mutant of *acsF*) cloned into the *Bgl*II/*Not*I sites of pBBRBB-*Ppuf*$_{843-1200}$	This thesis
pBB[*acsF*^{AD}-*ycf54*]	*Rvi. gelatinosus acsF*^{AD} (A218D mutant of *acsF*) and *Synechocystis ycf54* with a RBS sequence placed between the two genes cloned into the *Bgl*II/*Not*I sites of pBBRBB-*Ppuf*$_{843-1200}$	This thesis
pET14b	pBR322-based expression vector containing T7 promoter and N-terminal 6xHis tag encoding sequence, Amp^R	Novagen
pET14b-AcsF	*Rvi. gelatinosus acsF* cloned into the *Nde*I/*BamH*I sites of pET-14b	This thesis
pET3a	pBR322-based expression vector containing T7 promoter, Amp^R	Novagen
pET3a(*Spe*I$^+$)	pET3a derivative with an added *Spe*I site immediately upstream of the *BamH*I site, Amp^R	A. Brindley
pET3a-IM	*Synechocystis chlI, chlD, chlH, gun4,* and *chlM* cloned into pET3a(*Spe*I$^+$) using the 'Link and Lock' method	A. Brindley and S. Hollingshead
pET3a-IA	*Rvi. gelatinosus acsF* cloned into pET3a-IM using the 'Link and Lock' method	This thesis
pET3a-ID	*Synechocystis por* and *dvr* (*bciB*) cloned into pET3a-IA using the 'Link and Lock' method	This thesis
pET3a-IG	*Synechocystis chlP* and *chlG* cloned into pET3a-IG using the 'Link and Lock' method	This thesis

Table 2.4 Purple bacteria strains

Strain	Characteristics	Source/Reference
Rba. sphaeroides		
2.4.1	WT	S. Kaplan (University of Texas Medical School at Houston, USA)
Δ*bchE*	unmarked deletion of *bchE* in WT	This thesis
Δ*acsF*	unmarked deletion of *acsF* in WT	This thesis
Δ*ccoP*	unmarked deletion of *ccoP* in WT	E. Martin
Δ*bchE*Δ*ccoP*	unmarked deletion of *bchE* and *ccoP* in WT	E. Martin
Δ*bchE*Δ*acsF*	unmarked deletion of *bchE* and *acsF* in WT	This thesis
Δ*bchE*Δ*acsF*Δ*ccoP*	unmarked deletion of *bchE*, *ccoP* and *acsF* in WT	E. Martin
Δ*bchE*Δ*ccoP*Δ*bciE*	unmarked deletion of *bchE*, *ccoP* and *bciE* in WT	D. Canniffe
Rvi. gelatinosus		
IL144	WT	S. Nagashima (Kanagawa University, Japan)
Δ*bchE*	unmarked deletion of *bchE* in WT	This thesis
Δ*acsF*	unmarked deletion of *acsF* in WT	This thesis
Δ*bchE*Δ*acsF*	unmarked deletion of *bchE* and *acsF* in WT	This thesis
Δ*bchE*Δ*acsF*::*acsF*^{Rs}	placement of *Rba. sphaeroides acsF* in-frame under the *acsF* promoter in Δ*bchE*Δ*acsF*	This thesis
Δ*bchE*Δ*acsF*::*bciE-acsF*^{Rs}	placement of *Rba. sphaeroides bciE-acsF* in-frame under the *acsF* promoter in Δ*bchE*Δ*acsF*	This thesis
Δ*bchE*Δ*acsF*::*cycI*	placement of *Synechocystis cycI* in-frame under the *acsF* promoter in Δ*bchE*Δ*acsF*	This thesis
Δ*bchE*Δ*acsF*::*cycI-ycf54*	placement of *Synechocystis cycI* and *ycf54* in-frame under the *acsF* promoter in Δ*bchE*Δ*acsF*	This thesis
Δ*bchE*Δ*acsF* Rif^{R}	spontaneous rifampicin resistant mutant isolated from Δ*bchE*Δ*acsF*	This thesis
Δ*bchE*Δ*acsF*::*cycI*^{SM}	placement of *cycI*^{SM}(D219G mutant of *cycI*) in-frame under the *acsF* promoter in Δ*bchE*Δ*acsF*	This thesis
Δ*bchE*Δ*acsF*::*cycI*^{SM}Rif^{R}	spontaneous rifampicin resistant mutant isolated from Δ*bchE*Δ*acsF*::*cycI*^{SM}	This thesis

Strain	Characteristics	Source/Reference
TN1~TN83	isolated transposon mutants (generated from Δ*bchE*) with strong fluorescence with 395 nm excitation	This thesis
TN2-1~TN2-32	isolated transposon mutants (generated from Δ*bchE*) with some fluorescence with 395 nm excitation	This thesis
B1~B45	isolated transposon mutants (generated from Δ*bchE*) with brown colouration with 395 nm excitation	This thesis
Rba. capsulatus		
SB1003	WT, rifampicin resistant	C. Bauer (Indiana University, USA)
Δ*bchE*	unmarked deletion of *bchE* in WT	This thesis
Δ*ccoP*	unmarked deletion of *ccoP* in WT	This thesis
Δ*ccoP*Δ*bchE*	unmarked deletion of *ccoP* and *bchE* in WT	This thesis

Table 2.5 *Synechocystis* strains

Strain	Characteristics	Source/Reference
sp. 6803	WT, glucose tolerant	R. Sobotka (Institute of Microbiology, Czech Republic; hereafter)
$\Delta ycf54$	Zeo^R replacement of central portion of *ycf54* in WT	Hollingshead *et al*., 2016
$acsF^{Rg+}$	$acsF^{Rg}$ (from *Rvi. gelatinosus*) and Km^R replacement of *psbAII* in WT	This thesis
$acsF^{Rg+}\Delta cycI$	Cm^R replacement of *cycI* in $acsF^{Rg+}$	This thesis
$acsF^{Rg+}\Delta cycI\Delta ycf54$	Zeo^R replacement of *ycf54* in $acsF^{Rg+}\Delta cycI$	This thesis
$acsF^{Rg+}\Delta cycI\Delta chlB$	Zeo^R replacement of *chlB* in $acsF^{Rg+}\Delta cycI$	This thesis
SM1	suppressor mutant 1 isolated from $\Delta ycf54$	R. Sobotka
SM4	suppressor mutant 4 isolated from $\Delta ycf54$	R. Sobotka
Δslr1916	Cm^R replacement of slr1916 in WT	This thesis
$\Delta ycf54\ cycI^+$	*cycI* and Km^R replacement of *psbAII* in $\Delta ycf54$	R. Sobotka
$\Delta ycf54\ cycI^{SM+}$	$cycI^{SM}$ (D219G mutant of *cycI*) and Km^R replacement of *psbAII* in $\Delta ycf54$	This thesis
$\Delta ycf54\Delta$::slr1916^{SM1}	SM1-level truncation of slr1916 by Cm^R insertion in $\Delta ycf54$	This thesis
$\Delta ycf54\Delta$::slr1916^{SM4}	SM4-level truncation of slr1916 by Cm^R insertion in $\Delta ycf54$	This thesis
$\Delta ycf54\Delta$slr1916	Cm^R replacement of slr1916 in $\Delta ycf54$	This thesis
$\Delta ycf54\Delta$::slr1916$^{SM1}cycI^{SM+}$	$cycI^{SM}$ and Km^R replacement of *psbAII* in $\Delta ycf54\Delta$::slr1916^{SM1}	This thesis
$\Delta ycf54\Delta$::slr1916$^{SM4}cycI^{SM+}$	$cycI^{SM}$ and Km^R replacement of *psbAII* in $\Delta ycf54\Delta$::slr1916^{SM4}	This thesis
$\Delta chlP$	Ery^R replacement of *chlP* in WT	Hitchcock *et al*., 2016

Table 2.6 Primers

Primer	Sequence (5'→3')
rsp-bchE KO UF(SmaI)	CTGCCCGGGCGACGGGCGTGATCGACGAGCCC
rsp-bchE KO UR(NdeI)	GGAATTCCATATGTGGACTCCCGCTGTGTCCATTTC
rsp-bchE KO DF(NdeI)	GGAATTCCATATGACCGCGCATGACCAGCGG
rsp-bchE KO DR(HindIII)	GCAAGCTTGGAATGTTTGGCGATGGCCGTGG
rsp-bchE KO screen F	GCAGATTGCCGCAGAGATCTCG
rsp-bchE KO screen R	GGTTCCGGGCAATCTCGAATGAC
rsp-acsF KO UF(BamHI)	CGCGGATCCCCTTCGAGCGGATGCTGTCC
rsp-acsF KO OE R	CCGGTGATCGTCAGAAGTCACATATGGTCACCTGCTCGGAGAAGGAG
rsp-acsF KO OE F	CTCCTTCTCCGAGCAGGTGACCATATGTGACTTCTGACGATCACCGG
rsp-acsF KO DR(HindIII)	CCCAAGCTTCCCGTGATGACGCCCGACAGG
rsp-acsF KO screen F	CCGAGCTCCAGGCATTCGGACC
rsp-acsF KO screen R	GCCCGCAGGAATCGCTCGG
rsp-bciE KO UF(XbaI)	GCTCTAGAGGAGCTGATCCCGCCCTTCC
rsp-bciE KO OE R	GGAGAGCCCTCCGGCCGGCGCGTTCATGGGGGTTCCCTTCTCTTGG
rsp-bciE KO OE F	CCAAGAGAAGGGAACCCCCATGAACGCGCCGGCCGGAGGGCTCTCC
rsp-bciE KO DR(HindIII)	GCAAGCTTCCCAGGTTCACCGCCACGCC
rsp-bciE KO screen F	GCCCCGGAGCGACAAGGAC
rsp-bciE KO screen R	GTATTTCTTGGCCTTGGTCAGG
rsp-ccoP KO UF(EcoRI)	CCGGAATTCGTTCCTCTCGCACACCGTGATC
rsp-ccoP KO OE R	GGATTACTCACTCATTTCCTCGCCTCCTCGG
rsp-ccoP KO OE F	GAAATGAGTGAGTAATCCAAGGAGCTGAAGCGG
rsp-ccoP KO DR(HindIII)	CCGCAAGCTTCAGATCGACGAGGATCGCCTG
rsp-ccoP KO screen F	CTACGTCTGTCACAGCCAGATGATC
rsp-ccoP KO screen R	GCTCGACGAGGATGAAGAGATCG
rsp-acsF F(BglII)	GAGTCTAGATCTGTGAACGCGCCGGCCGGAG
rsp-acsF R(NotI)	GAGTCTGCGGCCGCTCAATAGCTCGGCTCCAGTCGG
rsp-acsF remove BglII F	ATCGCGCGCCAGATATTCCCGGTCGAG
rsp-acsF remove BglII R	CTCGACCGGGAATATCTGGCGCGCGAT
rsp-acsF F(NdeI)	CCAGTACATATGTGAACGCGCCGGCCGGAGG
rsp-acsF R(NdeI)	CCAGTACATATGTCAATAGCTCGGCTCCAGTCGG
rsp-bciE F(NdeI)	GAGTCTCATATGGGTCTGTTCACGAAACAAGCG
rsp-acsF qPCR F	ATCGCTTCCACCCGATCTTC
rsp-acsF qPCR R	CGGATCGGTCTTCATCAGCA
rsp-rpoZ qPCR F	GACGGTTGAAGACTGCGTTG
rsp-rpoZ qPCR R	GTTCTTGTCATTGTCGCGGT
rge-acsF KO UF(BamHI)	GAGTCTGGATCCCTGCATGAGCGACAACGCGTC
rge-acsF KO UR(NdeI)	GAGTCTCATATGGAGGGTCTCCGTGGTGTGTCA
rge-acsF KO DF(NdeI)	GAGTCTCATATGAAGCGAGGACAGGATGCTGAGC

Primer	Sequence (5'→3')
rge-acsF KO DR(HindIII)	GAGTCTAAGCTTGGAACTCCTCGCTCAGGTTGCG
rge-acsF KO screen F	GAACGTTTGCCGGACACGGT
rge-acsF KO screen R	ACGAGGTACTTCAGGTGCTCC
rge-bchE KO UF(BamHI)	CTAGGTCAAGTAGGATCCTCATGCCGGCGGCGATCATG
rge-bchE KO UR(NdeI)	CTAGGTCAAGTACATATGGGAAACGGCTCCTCGCGATTC
rge-bchE KO DF(NdeI)	CTAGGTCAAGTACATATGCGACGGCTGGGTCACGATGC
rge-bchE KO DR(HindIII)	CTAGGTCAAGTAAAGCTTTGCCGGTGTAGAAGTCGCACGC
rge-bchE KO screen F	TAGCCGCCGACCATGCCGA
rge-bchE KO screen R	GCGGTGCACCAGCACCGTGA
rge-acsF F(NdeI)	GAGTCTCATATGCTCGCGACCCCGACGATCG
rge-acsF R(BamHI)	GAGTCTGGATCCTCACCATGCCGGGGCCATG
rge-acsF R(NotI)	GAGTCTGCGGCCGCTCACCATGCCGGGGCCATGC
rge-acsF F(BglII)	GAGTCTAGATCTATGCTCGCGACCCCGACGAT
rge-acsF remove BglII F	GATCACCAACGAGATATCCAAGCAGGT
rge-acsF remove BglII R	ACCTGCTTGGATATCTCGTTGGTGATC
rge-acsF A218D OE F	GCGAGTCGTTCGACCTGATCCTGCGTG
rge-acsF A218D OE R	CACGCAGGATCAGGTCGAACGACTCGC
acsF(A218D)-rbs-ycf54 OE F	GCCCCGGCATGGTGATATAGGAGCTTGGATTGTG
acsF(A218D)-rbs-ycf54 OE R	CACAATCCAAGCTCCTATATCACCATGCCGGGGC
rge-bchF TN F	ATGGGTCACAAGACCAACCTCGA
rge-bchF TN R	TCATGCGTAGGCTTCCGACTGG
rge-11930 TN F	GTGCGTGGCGGCCAGTTAATTA
rge-11930 TN R	TTAACTCCAGGCGGCGCCAG
rge-41380 TN F	ATGCTTGAAAAAACTCCGGTGTG
rge-41380 TN R	TCACCTTCCCAGGCGGCGTGT
rge-13740 TN F	ATGAGCTTCATTGACAAGCTCTG
rge-13740 TN R	TCACGTTCCGGCGCGGATG
rge-bchZ TN F	ATGTACGTGATCGACCACGACC
rge-bchZ TN R	TCATGCGGGCTCCTTCTGGCC
rge-bchL TN F	ATGAGCACGGCCACGATCTCC
rge-bchL TN R	TCAGTCGTAGCCCAGCAGGTC
rge-bchY TN F	ATGAGCGAGCAACACGTCTCCA
rge-bchY TN R	TCAGATCATCTCCTCGGCCTTG
rca-bchE KO UF (XbaI)	GAGTCTTCTAGACAGGACCGTTTCCACCTGCGTG
rca-bchE KO OE R	GCCGTCACTCCTTCTTATTCGCGCATGGCTGACCCTCC
rca-bchE KO OE F	GGAGGGTCAGCCATGCGCGAATAAGAAGGAGTGACGGC
rca-bchE KO DR(HindIII)	GAGTCTAAGCTTTCGACCCGGAACCGC
rca-bchE KO screen F	GGAATAGCCTTTTTCCGGTGC
rca-bchE KO screen R	GGTTGTCATCGATGCGGAAG

Primer	Sequence (5'→3')
rca-ccoP KO UF (XbaI)	GAGTCTTCTAGAGCTATCTGGCCAATGTGCCGC
rca-ccoP KO OE R	GATCCGTTTGGCTGTTACTGGCTCATCTCCACGCCTCCT
rca-ccoP KO OE F	AGGAGGCGTGGAGATGAGCCAGTAACAGCCAAACGGATC
rca-ccoP KO DR(HindIII)	GAGTCTAAGCTTGCCAGATCTCGAGCCCGAAGA
rca-ccoP KO screen F	GCAATCGGTGGTGCCGGAATC
rca-ccoP KO screen R	CCAAGCCCGGCCATGATCAGA
syn-cycI KO UF	GCCGATCCGGTTAACCTAGGCA
syn-cycI KO OE 5'F	ATATCCAGTGATTTTTTTCTCCATAGAGTTGTTTAAAATAGTTTCC
syn-cycI KO OE 5'R	GGAAACTATTTTAAACAACTCTATGGAGAAAAAAATCACTGGATAT
syn-cycI KO OE 3'R	GGTGATCCAGCGGAAGACAACCTTACGCCCCGCCCTGC
syn-cycI KO OE 3'F	GCAGGGCGGGGCGTAAGGTTGTCTTCCGCTGGATCACC
syn-cycI KO DR	TGGAGTTGTTGGGAGAGTTCGGTC
syn-cycI inside F	GGCCAAGGAAACCATCCTCA
syn-cycI inside R	TGGCAAAGACTGAGAGCAGG
syn-cycI F(NdeI)	GGAATTCCATATGGTTAATACCCTCGAAAAGCCCG
syn-cycI R(NdeI)	GGAATTCCATATGTTAGCGCACAGCTCCAGCCA
syn-cycI R(BglII)	GAGTCTAGATCTTTAGCGCACAGCTCCAGCCAA
syn-ycf54 R(NdeI)	GAGTCTCATATGCTAATCCAGGGATGCAAGGGG
syn-ycf54-ZeoR F	GTGGAAAGTTGGGCATTGACG
syn-ycf54-ZeoR R	CTAATCCAGGGATGCAAGGGG
syn-chlB KO UF	GCATCGCTTATTGTTCTCAACG
syn-chlB KO DR	CCTTCAAAGGCCATCACCC
syn-cycI F(BglII)	GAGTCTAGATCTATGGTTAATACCCTCGAAAAGCCC
syn-cycI R(NotI)	GAGTCTGCGGCCGCTTAGCGCACAGCTCCAGCCAAC
cycI-rbs-ycf54 OE F	GTTGGCTGGAGCTGTGCGCTAATATAGGAGCTTGGATTGTGGAAAGTT GGGCATTGACGA
cycI-rbs-ycf54 OE R	TCGTCAATGCCCAACTTTCCACAATCCAAGCTCCTATATTAGCGCACAGC TCCAGCCAAC
syn-ycf54 R(NotI)	GAGTCTGCGGCCGCCTAATCCAGGGATGCAAGGGGGT
syn-por F(NdeI)	TCTCATATGGAACAACCGATGAA
syn-por R(SpeI)	TCTACTAGTCTAAACCAGACCCACTAACTTTTC
syn-bciB F(NdeI)	TCTCATATGGACCGTTCCTGCCCCCCCAC
syn-bciB R(SpeI)	TCTACTAGTTTATTGCTGGGGAAGTTTATACTG
syn-psbAII UF	AAACGCCCTCTGTTTACCCA
syn-psbAII DR	TCAACCCGGTACAGAGCTTC
syn-slr1916 KO UF	GGTTACTGAACTGGGTTACATTTT
syn-slr1916 KO OE 5'R	ATATCCAGTGATTTTTTTCTCCATAGTTCTCGCAATTGCTACG
syn-slr1916 KO OE 5'F	CGTAGCAATTGCGAGAACTATGGAGAAAAAAATCACTGGATAT
syn-slr1916 KO OE 3'R	ACGGCCAACAATTGCCCCCATTTACGCCCCGCCCTGCCACT
syn-slr1916 KO OE 3'F	AGTGGCAGGGCGGGGCGTAAATGGGGGCAATTGTTGGCCGT

Primer	Sequence (5'→3')
syn-slr1916 KO DR	GGAGTAACCGCAGGGAACAGTTAA
syn-slr1916 SM UF	GGGTGGTGACTATGGAAAATTTG
syn-slr1916 SM1 OE 5'R	GCCCAGGGCTTCCCGGTATTACCCCCCCCCCAGCATTCACG
syn-slr1916 SM1 OE 5'F	CGTGAATGCTGGGGGGGGGGTAATACCGGGAAGCCCTGGGC
syn-slr1916 SM4 OE 5'R	GCCCAGGGCTTCCCGGTACTACCCCCCCTAAGGAATGGCCCA
syn-slr1916 SM4 OE 5'F	TGGGCCATTCCTTAGGGGGGTAGTACCGGGAAGCCCTGGGC
syn-slr1916 SM OE 3'R	CCCCAGCAGAGCGAAACTTTTTACGCCCCGCCCTGCCAC
syn-slr1916 SM OE 3'F	GTGGCAGGGCGGGGCGTAAAAAGTTTCGCTCTGCTGGGG
syn-slr1916 SM DR	CACCAAAGCCTAACAGATCAATG
syn-slr1916 seq F	TGTAAAACGACGGCCAGTATGCCCACCCTGGATCTTTTGG
syn-slr1916 seq R	CAGGAAACAGCTATGACCTCAGTGATCCGTAGCCAGGATT
syn-cycI seq F	TGTAAAACGACGGCCAGTATGGTTAATACCCTCGAAAAGCC
syn-cycI seq R	CAGGAAACAGCTATGACCTTAGCGCACAGCTCCAGCC
syn-slr2033 seq F	TGTAAAACGACGGCCAGTACCCCAGTCACAGTCTGGAC
syn-slr2033 seq R	CAGGAAACAGCTATGACCTCAACGAGTACAGCAAGGGCTC
R6KAN-2 RP-1	CTACCCTGTGGAACACCTACATCT
TN5SEQ R	TCGTTAAACATGAGAGCTTAGTACG
INV-2	GAACTTTTGCTGAGTTGAAGGATCA
KAN-2 FP-1	ACCTACAACAAAGCTCTCATCAACC
pK18 seq F	CGGGCCTCTTCGCTATT
pK18 seq R	TTAGCTCACTCATTAGG
pPD-FLAG seq F	CTCTCATTAATCCTTTAGAC
pPD-FLAG seq R	GCATTACGCTGACTTGACGG
pBBRBB seq F	GCAGGTCAGGTTGCGACA
pBBRBB seq R	CGCCGGTAGCACTTGGG
T7	TAATACGACTCACTATAGGG
pET-RP	CTAGTTATTGCTCAGCGG

Chapter 3

Absence of the *cbb₃* oxidase reveals an active aerobic cyclase involved in bacteriochlorophyll biosynthesis in *Rhodobacter sphaeroides*

3.1 Summary

This chapter reports the first experimental evidence that *Rba. sphaeroides* does possess a functional aerobic cyclase encoded by rsp_0294 catalysing the conversion of MgPME to PChlide. The activity of aerobic cyclase was assayed *in vivo* by measuring the yield of BChl from cells grown under varied conditions. Functional aerobic cyclase activity was demonstrated in the presence and absence of the cbb_3 oxidase. A much higher level of BChl was produced upon inactivation of the cbb_3 oxidase, which can be explained by the improved availability of the substrate O_2 as well as an approximately two-fold increase in the expression level of rsp_0294. Zn-BChl *a* was also detected together with Mg-BChl *a* in *bchE*-lacking strains under the tested aerobic conditions.

3.2 Introduction

There are two fundamentally different types of the MgPME cyclase. The anaerobic cyclase encoded by the *bchE* gene utilises an oxygen atom from water to form the isocyclic E ring, whereas the aerobic cyclase of which the first subunit is encoded by the *acsF* gene incorporates molecular oxygen into PChlide. Given *Rba. sphaeroides* belongs to anoxygenic phototrophs which typically perform photosynthesis in the absence of molecular oxygen, BchE is believed to play a dominant role in *Rba. sphaeroides* and other such phototrophs. Although some purple bacteria including *Rba. capsulatus*, *Rhodospirillum rubrum, Rhodospirillum photometricum*, *Phaeospirillum molischianum* and *Rhodomicrobium vannielii*, only contain the *bchE* gene, many other purple bacteria including *Rba. sphaeroides* and *Rvi.*

gelatinosus carry the *acsF* gene located inside their PGC (Boldareva-Nuianzina *et al.*, 2013). It has been demonstrated that the *Rvi. gelatinosus* AcsF is functional and is responsible for the biosynthesis of BChl under high-oxygenation conditions (Pinta *et al.*, 2002; Ouchane *et al.*, 2004). As the *Rba. sphaeroides* Rsp_0294 shares 51% amino acid identity with the *Rvi. gelatinosus* AcsF, it is rational to hypothesise that *Rba. sphaeroides* may also have a functional aerobic cyclase. Although *Rba. sphaeroides* is one of the most important model organisms for studying bacterial photosynthesis, there had been no literature regarding the aerobic cyclase in this organism when the project reported in this chapter was conceived.

The investigation of aerobic cyclase in *Rba. sphaeroides* was expected to be more difficult than that in *Rvi. gelatinosus*. The *Rvi. gelatinosus* Δ*bchE* was capable of synthesising a considerable amount of BChl via the AcsF route under both low-oxygenation (50 ml of medium in a 50 ml flask, shaken at 100 rpm) and high-oxygenation (20 ml of medium in a 250 ml flask, shaken at 100 rpm) conditions (Ouchane *et al.*, 2004). However, it is well known that PS assembly and BChl biosynthesis are repressed under high oxygen tension in *Rba. sphaeroides*. The cbb_3 terminal oxidase encoded by the *ccoNOQP* operon has been shown to be involved in the repression of photosynthesis gene expression under aerobic conditions (O'Gara and Kaplan, 1997). The flow of electrons through the cbb_3 oxidase generates a signal that inhibits the activity of the PrrB-PrrA two-component activation system (O'Gara *et al.*, 1998; Oh and Kaplan, 1999; Oh and Kaplan, 2000; Kim *et al.*, 2007). In addition, the cbb_3 oxidase exhibits a high affinity for oxygen with a K_m value in the order of 7~40 nM (Preisig *et al.*, 1996; Jackson *et al.*, 2007), which can be a strong competitor with aerobic cyclase for the substrate O_2. According to this background information, a *Rba. sphaeroides* strain lacking a functional cbb_3 oxidase may be helpful or even necessary for the revelation of aerobic cyclase activity in this organism.

3.3 Results

3.3.1 Construction of marker-free deletion mutants of *Rba. sphaeroides*

An allelic exchange suicide vector pK18*mobsacB* (Schäfer *et al*, 1994), depicted in **Figure 3.1**, was used to construct genetic deletion mutants to investigate the function of a gene in *Rba. sphaeroides*.
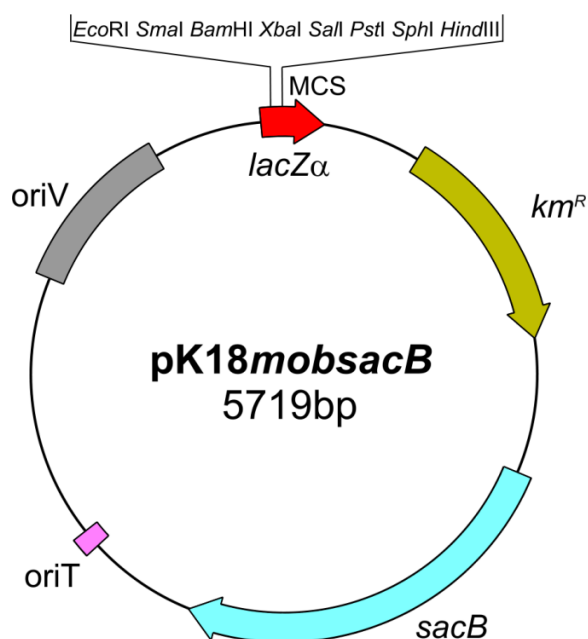
Figure 3.1 Map of the pK18*mobsacB* vector

The vector contains the pBR322 origin of replication (oriV), the RP4 origin of transfer (oriT), a kanamycin resistance gene (*km*^R), the levansucrase encoding gene (*sacB*) responsible for sucrose sensitivity and the *lacZα* fragment within which multiple cloning site (MCS) is located.

The mechanism of genetic knockout using pK18*mobsacB* is shown in **Figure 3.2**. The upstream and downstream of the gene of interest were amplified and cloned into the multiple cloning site of the vector. Confirmed by sequencing, the resulting construct was transformed into *E. coli* S17-1 strain, which was subsequently used to perform conjugation with *Rba. sphaeroides*. M22+ agar medium with kanamycin was used to select transconjugants in which the whole plasmid had integrated into the genome by homologous recombination. A second homologous recombination event which excises the plasmid from the genome was selected on M22+ agar medium with 10% (w/v) sucrose. Either the desired deletion mutant or the WT is generated by the second homologous recombination event. Colony PCR was performed to screen for the deletion mutant using forward primer and reverse primer, flanking the upstream and downstream region, respectively.
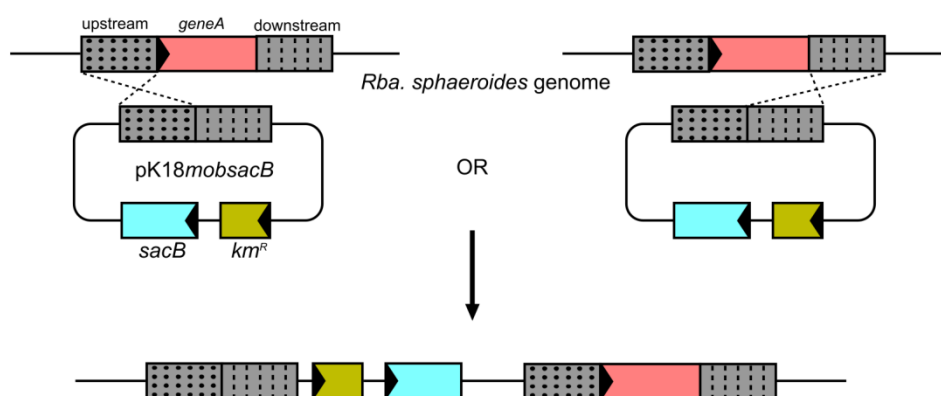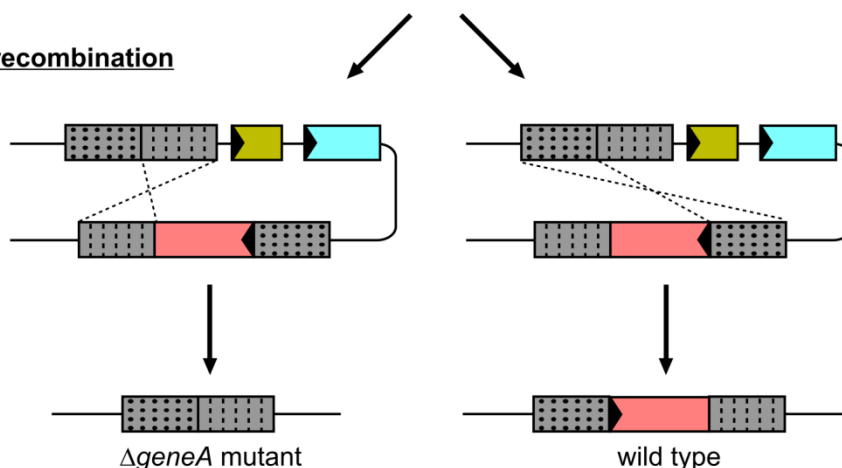
Figure 3.2 The mechanism of genetic knockout in *Rba. sphaeroides* using pK18*mobsacB*

The upstream and downstream regions of the gene of interest (*geneA*) were cloned into the multiple cloning site of the pK18*mobsacB* vector. Following conjugation into *Rba. sphaeroides*, the first homologous recombination event integrated the whole plasmid into the genome. The second homologous recombination event excised the plasmid from the genome, generating either Δ*geneA* mutant or wild type. The *sacB* and *km*^{R} genes confer sucrose sensitivity and kanamycin resistance, respectively.

Using the pK18*mobsacB*-based method, three deletion mutants of *Rba. sphaeroides* were constructed, which are Δ*bchE* (rsp_0281), Δrsp_0294 and Δ*ccoP* (rsp_0693). The arrangements of genes in the mutants and WT are shown in **Figure 3.3,** as well as the colony PCR gel images. As the deletion mutant generated by the method is marker-free, multiple in-frame changes can be introduced one after another. Thus, double deletion mutant Δ*bchE*Δ*ccoP* and triple deletion mutant Δ*bchE*Δ*ccoP*Δrsp_0294 were constructed.
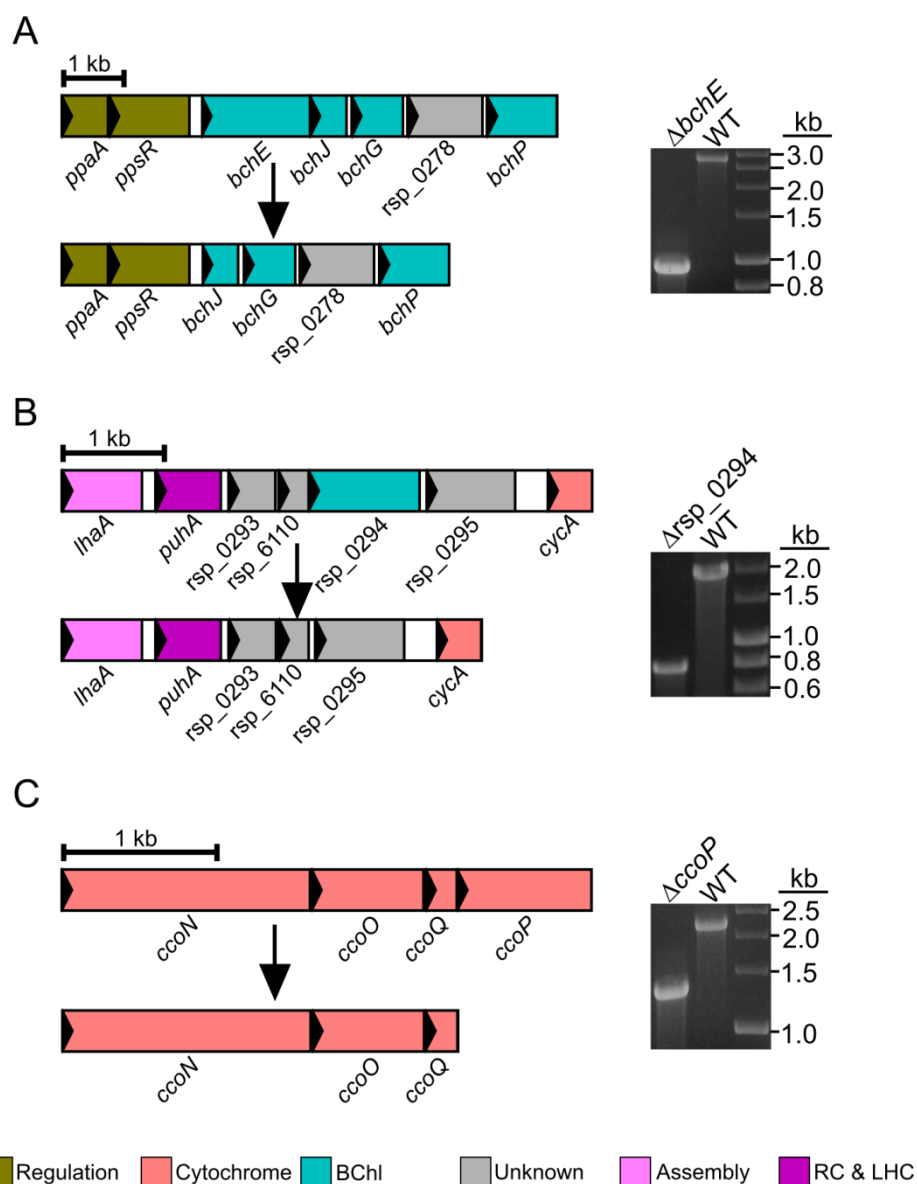
Figure 3.3 Deletion of the *bchE*, rsp_0294 and *ccoP* genes in *Rba. sphaeroides*

The genomic regions adjacent to the gene of interest from wild type and the deletion mutant are depicted in proportion to the scale bar. Genes are represented as colour filled rectangles within which the arrow head indicates the transcription direction. Colony PCR gel images are also presented. Abbreviations: BChl, bacteriochorophyll biosynthesis; RC&LHC, reaction centre and light-harvesting complexes. (**A**) Deletion of the *bchE* gene. Lengths of PCR products: wild type = 2798 bp; Δ*bchE* = 962 bp. (**B**) Deletion of the rsp_0294 gene**.** Lengths of PCR products: wild type = 1876 bp; Δrsp_0294 = 790 bp. (**C**) Deletion of the *ccoP* gene. Lengths of PCR products: wild type = 2230 bp; Δ*ccoP* = 1369 bp.

3.3.2 Phenotypic analysis of the Δ*bchE* and Δrsp_0294 mutants

The WT, Δ*bchE* and Δrsp_0294 strains of *Rba. sphaeroides* were streaked out onto M22+ agar medium and incubated at 30°C. Photographs of colonies were taken after 4-day incubation. A

single colony from the agar plate was inoculated into 5 ml of M22+ medium in a 25 ml Universal tube, as a starter culture, and incubated at 30°C with shaking at 200 rpm. The starter culture was subsequently inoculated to 40 ml of M22+ medium in a 125 ml Erlenmeyer flask and incubated at the same conditions as the starter culture. Photographs of the resulting cultures were taken. As shown in **Figure 3.4 A** and **B**, both the colony and liquid culture of Δrsp_0294 were red, indistinguishable from those of WT. However, the colony and liquid culture of Δ*bchE* looked orange, which was the colour of the endogenous carotenoids.
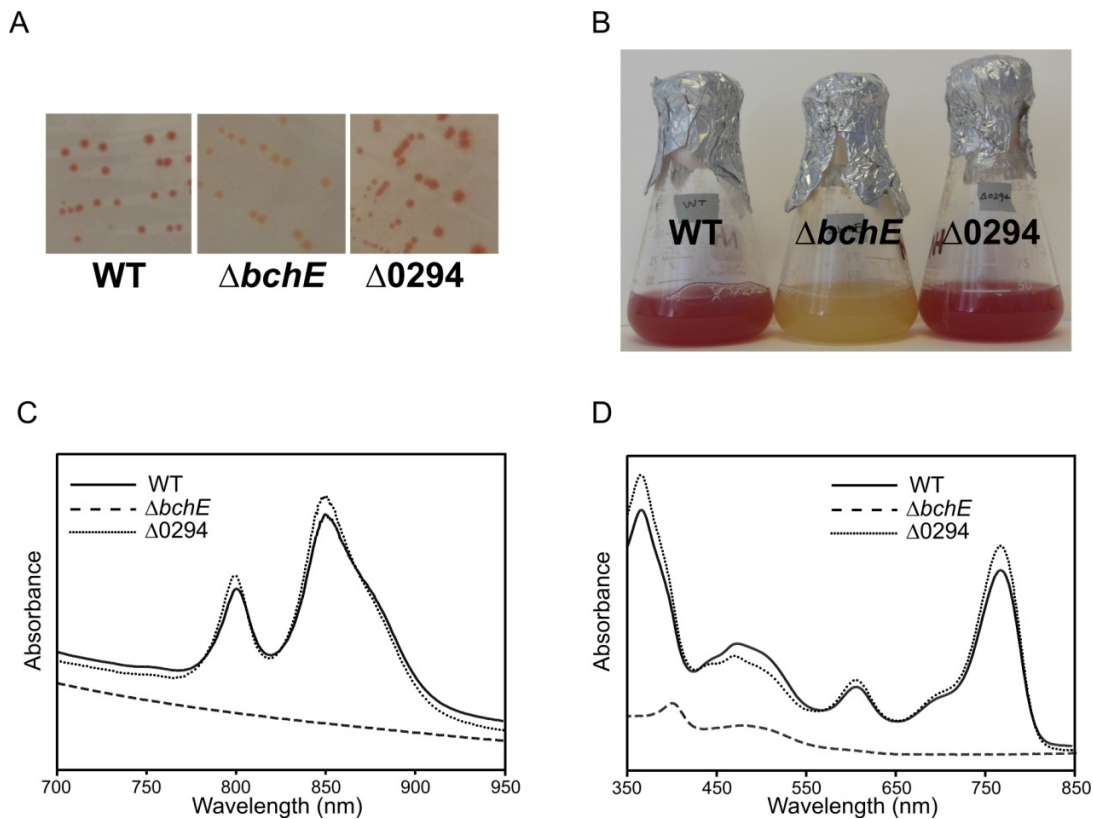
Figure 3.4 Phenotypic analyses of the Δ*bchE* and Δrsp_0294 mutants

(**A**) Photographs of colonies grown on M22+ agar medium. (**B**) Photograph of liquid culture of the wild type, Δ*bchE* and Δrsp_0294 strains. (**C**) Whole-cell absorption spectra of cells suspended in 60% (w/v) sucrose. (**D**) Absorption spectra of pigments extracted from cells standardised by OD_{680} using methanol.

1 ml of each culture standardised by OD_{680} was pelleted and resuspended in 60% (w/v) sucrose. The absorption spectra between 700 nm and 950 nm were recorded and are shown in **Figure 3.4 C**. Pigments were extracted from cells standardised by OD_{680} with an excess of methanol and the absorption spectra of 350~850 nm were recorded, as shown in **Figure 3.4 D**. No peak was present in the whole-cell absorption spectra of Δ*bchE*, whereas both WT and Δrsp_0294 had the absorption maxima typical of the light-harvesting complexes 1 and 2. A peak at 401 nm, instead of the BChl *a* characteristic peaks (365 nm and 770 nm in methanol),

was present in the absorption spectra of the pigments extracted from Δ*bchE*. The 401 nm peak indicates the accumulation of BChl precursors in Δ*bchE*.

3.3.3 Comparison of the Δ*ccoP* and wild type strains

The Δ*ccoP* strain looked almost identical to WT when streaked out onto an M22+ agar plate (**Figure 3.5 A**) or grown as liquid culture under low-oxygen conditions. In order to investigate the effect of *ccoP* deletion, both the Δ*ccoP* and WT strains were inoculated to 20 ml of M22+ medium in 250 ml Erlenmeyer flasks and grown at 30°C with shaking at 150 rpm, providing high-oxygen conditions. The Δ*ccoP* culture was apparently more pigmented than the WT culture (**Figure 3.5 B**). Whole-cell absorption spectra showed much more light-harvesting complexes present in Δ*ccoP* compared to WT (**Figure 3.5 C**). According to the absorption at 770 nm, the content of BChl in Δ*ccoP* was around 5 times more than that of WT under the high-oxygen conditions (**Figure 3.5 D**).
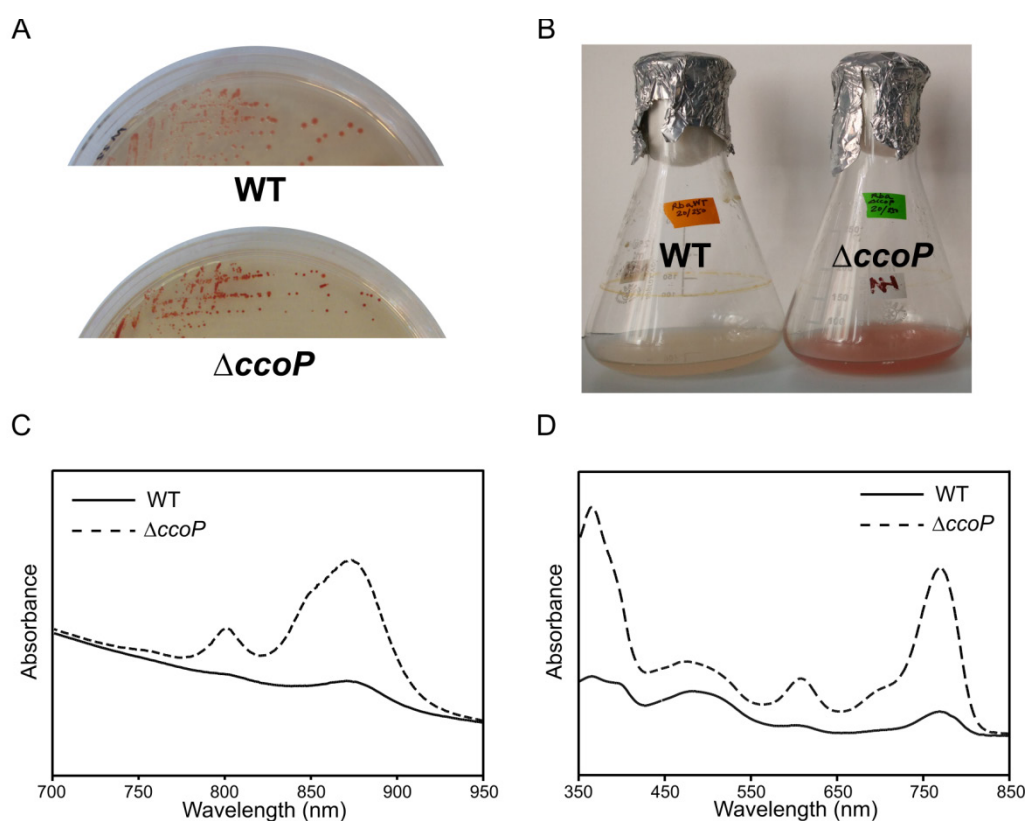
Figure 3.5 Comparison of the Δ*ccoP* and wild type strains

(**A**) Photographs of colonies grown on M22+ agar medium. (**B**) Photograph of liquid cultures of wild type and Δ*ccoP*. (**C**) Whole-cell absorption spectra of cells suspended in 60% (w/v) sucrose. (**D**) Absorption spectra of pigments extracted from cells standardised by OD_{680} using methanol.

3.3.4 HPLC analysis of pigments accumulated in Δ*bchE* and Δ*bchEΔccoP* grown under different aerations

Growth conditions with different aerations were achieved by filling 250 ml Erlenmeyer flasks with 20, 40, 80 and 160 ml of M22+ medium and were applied to grow the Δ*bchE* and Δ*bchEΔccoP* mutants. Pigments were extracted twice with an excess of 0.2% (v/v) ammonia in methanol from cells standardised by OD_{680}. The extracts were then dried in vacuum at 30°C. A small volume of 0.2% (v/v) ammonia in methanol was used to reconstitute the dried pigments before analysed by HPLC. BChl *a* species were separated on a Fortis UniverSil C18 reverse-phase column (5 μm particle size, 150 mm x 4.6 mm) using a method modified from van Heukelem *et al*. (1994). Solvents A and B were methanol/500 mM ammonium acetate (80:20, v/v) and methanol/acetone (80:20, v/v), respectively. The elution of pigments was performed using a linear gradient of 92~93% solvent B over 10 min with a flow rate of 1 ml min^{-1} at 40°C and monitored by absorbance at 770 nm. Pigments extracted from WT and Δ*bchEΔccoP*Δrsp_0294 were included as BChl *a* standard and the negative control, respectively.

The HPLC elution profiles were shown in **Figure 3.6**. The BChl *a* standard was represented as a peak at 8.0 min with this HPLC method and no peak was detected in the negative control. As shown in **Figure 3.6 A**, all the four Δ*bchE* cultures grown under different aerations apparently had no detectable BChl *a*. Nevertheless, BChl *a* was detected in the pigment extracts from the Δ*bchEΔccoP* cultures grown in flasks filled with 160, 80 and 40 ml of medium (traces 1, 2, 3, respectively), as shown in **Figure 3.6 B**. Only the Δ*bchEΔccoP* culture grown under the highest aeration (flask filled with 20 ml of medium) had almost no detectable BChl *a*.
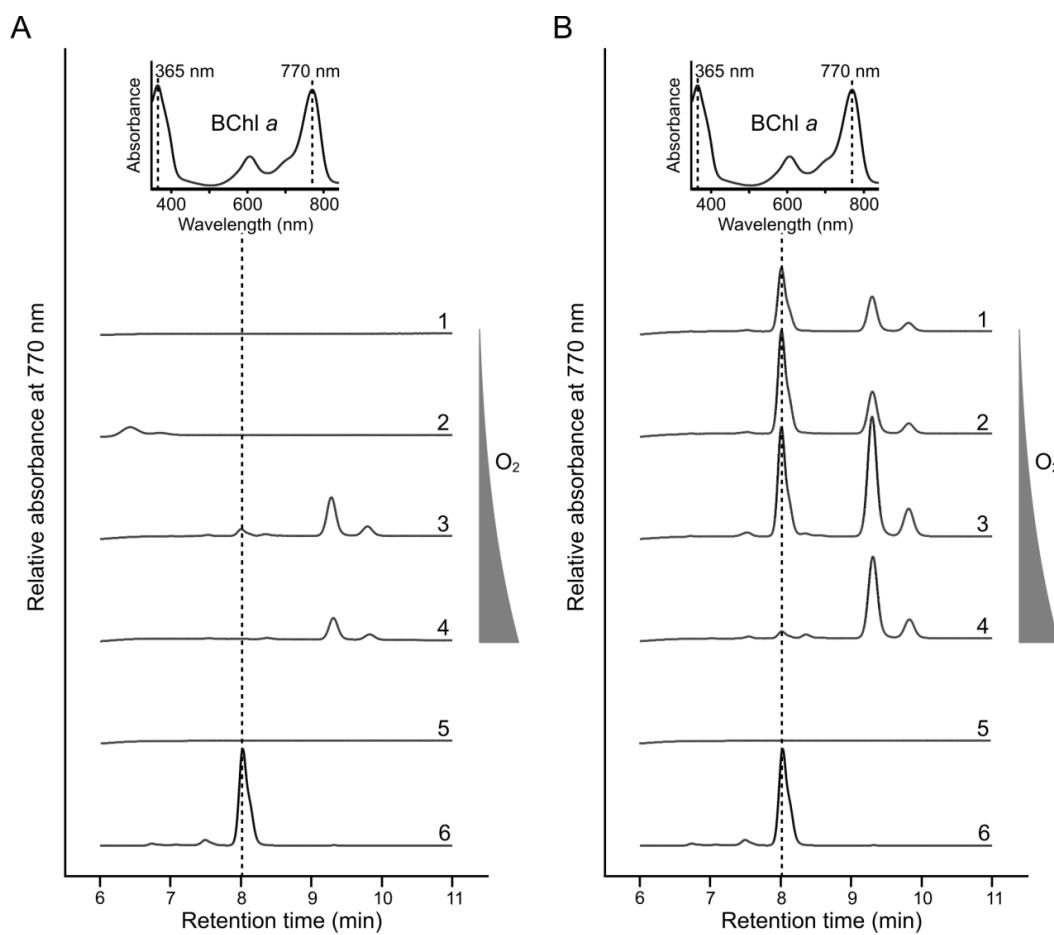
Figure 3.6 HPLC analysis of pigments extracted from the Δ*bchE* and Δ*bchE*Δ*ccoP* mutants grown under varied aerations

In both A and B, traces 1, 2, 3 and 4 represent pigments extracted from bacterial cultures grown in flasks filled with 160, 80, 40 and 20 ml of medium, respectively. Trace 5 is the pigment extract from the Δ*bchE*Δ*ccoP*Δrsp_0294 mutant. A BChl *a* standard is shown as trace 6. (**A**) HPLC elution profiles of pigments extracted from Δ*bchE* cultures. (**B**) HPLC elution profiles of pigments extracted from Δ*bchE*Δ*ccoP* cultures.

3.3.5 Assignment of the 9.3 min peak in the HPLC profiles

In addition to the 8.0 min peak which represented BChl *a*, another peak with a retention time of 9.3 min was clearly visible in the HPLC profiles of the pigments extracted from Δ*bchE*Δ*ccoP*. This 9.3 min peak represented a pigment which was more hydrophobic and had a blue-shifted absorption spectrum (Soret band = 356 nm, Q_y band = 762 nm, in methanol) compared to BChl *a*. It has been reported that a *bchD* mutant of *Rba. sphaeroides* contains zinc-bacteriochlorophyll (Zn-BChl) instead of normal BChl (Jaschke and Beatty, 2007). We hypothesised that the 9.3 min peak was Zn-BChl. In order to check this hypothesis, Zn-BChl was prepared from BChl *a* using a previously reported method (Hartwich *et al.*, 1998) with

slight modifications. One volume of BChl *a* methanol solution was mixed with an excess of anhydrous zinc acetate, 50 mM sodium ascorbate and six volumes of glacial acetic acid in a 1.5 ml Eppendorf tube. The tube containing the mixture was incubated at 100°C with the lid open. After 2 hr incubation, the upper solution was transferred to a new tube and clarified by centrifugation before analysed by HPLC. The prepared Zn-BChl behaved exactly the same as the 9.3 min pigment in HPLC analysis and also had the identical absorption spectrum as the 9.3 min pigment (**Figure 3.7**). This confirms that the Δ*bchE*Δ*ccoP* accumulated not only BChl but also Zn-BChl.
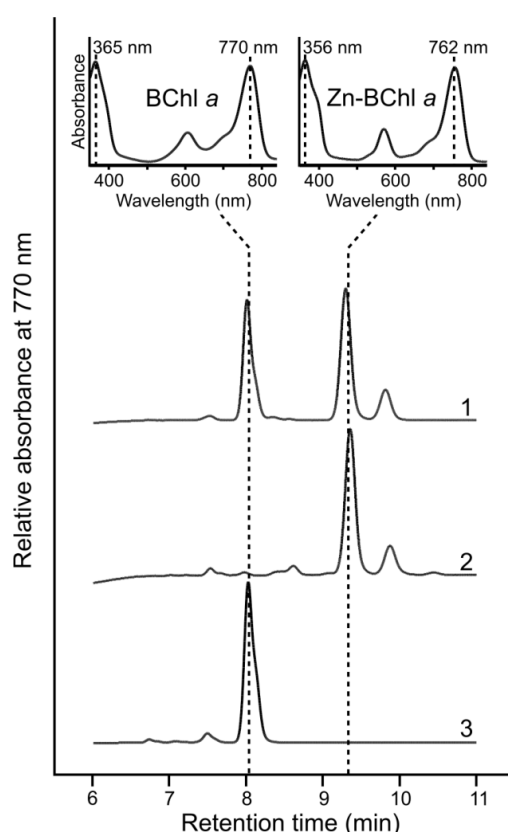
Figure 3.7 Assignment of the 9.3 min peak in the HPLC profiles

Trace 1 stands for pigments extracted from the Δ*bchE*Δ*ccoP* mutant (identical to the trace 3 in **Figure 3.6 B**). Trace 2 represents the prepared Zn-BChl. Trace 3 is the BChl *a* standard.

3.3.6 Analysis of the expression level of rsp_0294

The expression levels of rsp_0294 in WT, Δ*bchE* and Δ*bchE*Δ*ccoP* strains were analysed by qRT-PCR. Total RNA was isolated from cultures grown under the optimum conditions for BChl *a* production based on the HPLC results. Reactions were set up in triplicate to detect the rsp_0294 transcript level using the housekeeping gene *rpoZ* (encoding the ω-subunit of RNA polymerase) as an internal reference (Gomelsky *et al*., 2003). The primer efficiency was

deducted from a standard curve generated by using *Rba. sphaeroids* genomic DNA as a template in a series of 10-fold dilutions. The primer efficiencies for rsp_0294 and *rpoZ* were 99.09% and 97.35%, respectively. Based on melting curve analysis, the absence of primer dimers and specific amplifications were confirmed for both rsp_0294 and *rpoZ* PCR reactions. The REST^{TM} software based on the Pfaffl method (Pfaffl, 2001; Pfaffl *et al*., 2002) was applied to analyse the qRT-PCR data and to perform a statistical test. The threshold cycle deviation between a mutant strain and WT was normalised according to the internal reference with primer efficiency correction. The resulting value was used to calculate the relative expression level of rsp_0294 in mutant strain compared to WT. As shown in **Table 3.1**, the expression level of rsp_0294 was not significantly different from that of WT (P-value = 0.1), whereas rsp_0294 was significantly up-regulated in Δ*bchE*Δ*ccoP* by a factor of 2.3 relative to WT (P-value < 0.05).

Table 3.1 Expression levels of rsp_0294 in described strains determined by qRT-PCR

Strain	Expression level	95% C.I.	P(H1)
WT	1	N/A	N/A
Δ*bchE*	1.2	1.00 - 1.47	0.1
Δ*bchE*Δ*ccoP*	2.3	1.84 - 3.25	0.017

C.I. is abbreviated for confidence interval. P(H1) represents the probability of the alternative hypothesis that the difference between a mutant and WT is due only to chance. N/A, not applicable.

3.4 Discussion

3.4.1 A functional aerobic cyclase is revealed in *Rba. sphaeroides*

In order to test whether *Rba. sphaeroides* has a functional aerobic cyclase, Δ*bchE* and Δrsp_0294 mutants were constructed and compared with WT. At first, the strains were grown in 125 ml flasks filled with 40 ml of medium and the shaking was performed at 220 rpm. Under these conditions, Δ*bchE* was completely deprived of BChl whereas deletion of rsp_0294 had no effect on the biosynthesis of BChl, as revealed by absorption spectra of whole cell suspension and extracted pigments (**Figure 3.4**). Δrsp_0294 had comparable levels of light-harvesting complexes together with BChl content relative to WT.

Rba. sphaeroides, as a facultatively phototrophic bacterium, is capable of utilising energy from various metabolic pathways including photosynthesis, aerobic respiration, anaerobic respiration and fermentation. It is highly regulated which metabolic pathway is active,

depending on the environmental factors. Oxygen tension is a key factor that determines the expression of photosynthesis genes via two levels of regulation, the aerobic repression and the anaerobic induction circuits (Bauer and Bird, 1996; Gregor and Klug, 1999; Zeilstra-Ryalls and Kaplan, 2004). PpsR represses the expression of all photosynthesis genes under aerobic conditions. In response to the drop of oxygen tension, photosynthesis genes are derepressed by the formation of an AppA-PpsR complex and induced by FnrL and the two-component signal transduction system PrrB-PrrA. Considering the inhibitory effect of oxygen on photosynthesis genes and the requirement of oxygen for aerobic cyclase, a particular set-up of growth conditions is required to test whether a functional aerobic cyclase is present in *Rba. sphaeroides*. In addition, a sensitive detection method is also required as the activity of the aerobic cyclase in this organism will be very low at best.

To achieve this goal, the $\Delta bchE$ strain was incubated under a series of growth conditions with a gradient of oxygen tension and pigments were extracted twice with excessive solvent to guarantee completeness (described in **3.3.4**). Pigment extract from a culture that was equal to 14 OD_{680} units was injected for HPLC analysis. No apparent BChl *a* peak was present in the HPLC elution profiles (**Figure 3.6 A**). It is noteworthy that a tiny peak in trace 3 as shown in **Figure 3.6 A** had a retention time of 8.0 min same as BChl *a*. In addition, a peak with a longer retention time (9.3 min) compared to BChl *a* was present in two of the HPLC elution profiles (**Figure 3.6 A**, traces 3 and 4). This peak was speculated to represent Zn-BChl *a* based on the hydrophobicity and previous report that a *bchD* mutant of *Rba. sphaeroides* synthesises Zn-BChl *a* (Jaschke and Beatty, 2007). Due to the low abundance of the pigments represented by the 8.0 min and 9.3 min peaks, it was not possible to acquire a clean and reliable absorption spectrum of the pigment during HPLC analysis. Referring to the report that *Rba. sphaeroides* mutants lacking a functional cbb_3 oxidase have elevated photosynthesis gene expression under aerobic conditions (O'Gara and Kaplan, 1997), it was decided to knockout the *ccoP* gene (encoding a component of the cbb_3 oxidase) for the purpose of increasing the yield of pigments for further analysis. As expected, the comparison of WT and $\Delta ccoP$ clearly shows that more PS and BChl were produced when the *ccoP* gene was inactivated (**Figure 3.5**). Thus, a $\Delta bchE\Delta ccoP$ double knockout strain would provide an ideal background for demonstrating the activity of aerobic cyclase in *Rba. sphaeroides*.

As shown in **Figure 3.6 B**, pigment extracts from $\Delta bchE\Delta ccoP$ grown under three (traces 1, 2, 3) of the four tested conditions had a pronounced 8.0 min peak with a typical BChl *a* absorption spectrum. Trace 3 represented the best aeration for BChl *a* production which was

achieved by filling a 250 ml Erlenmeyer flask with 40 ml of medium. The abundance of the pigment represented by the 9.3 min peak in Δ*bchE*Δ*ccoP* (**Figure 3.6 B**) was increased in all the four tested conditions compared to that in Δ*bchE* grown under the corresponding conditions (**Figure 3.6 A**). A clean absorption spectrum of the 9.3 min peak was acquired and indicated a 356 nm Soret band and a 762 nm Q_y band (in methanol). The 9.3 min peak was eventually assigned as Zn-BChl *a* by comparing with the standard (**Figure 3.7**). Therefore, Δ*bchE* accumulated some level of Zn-BChl *a* (**Figure 3.6 A**, traces 3 and 4). Both BChl *a* (Mg) and Zn-BChl have a mature bacteriochlorin which requires MgPME cyclase for biosynthesis. No BChl species was detected when rsp_0294 was removed (**Figure 3.6**). Thus, without doubt, *Rba. sphaeroides* has a functional aerobic cyclase in the presence and absence of the cbb_3 oxidase. The activity of this functional aerbic cyclase is more easily detected in the absence of cbb_3 oxidase.

The boosting effect of inactivation of cbb_3 oxidase on the activity of aerobic cyclase in *Rba. sphaeroides* can be explained from two perspectives. Given the aerobic cyclase encoding gene, rsp_0294, is one of the photosynthesis genes and located in the PGC, a *Rba. sphaeroides* mutant lacking a functional cbb_3 oxidase may have an increased expression level of rsp_0294. On the other hand, considering that aerobic cyclase utilises O_2 as a substrate, an increase in cellular O_2 level through the removal of the cbb_3 oxidase, which is a high-affinity oxygen scavenger, may be sufficient to stimulate the activity of aerobic cyclase without the requirement of a higher level of rsp_0294. The expression level of rsp_0294, determined by qRT-PCR, was moderately enhanced upon the removal of the cbb_3 oxidase (**Table 3.1**). However, an approximate two-fold enhancement in the expression level of rsp_0294, on its own, cannot account for the large difference between Δ*bchE* and Δ*bchE*Δ*ccoP* with respect to the BChl production. Therefore, the contribution of the increased availability of cellular O_2 for aerobic cyclase must be also included.

3.4.2 *Rba. sphaeoides* potentially benefits from the possession of a functional aerobic cyclase

Since *Rba. sphaeroides* performs photosynthesis only under anaerobic conditions, the retention of a functional aerobic cyclase through evolution seems unnecessary at first glance. To understand the physiological role played by the aerobic cyclase in *Rba. sphaeroides*, it is important to explain the strategy adopted by purple anoxygenic phototrophs. It is well-known that purple anoxygenic phototrophs form photosynthetic machinery even under oxygen-limited conditions in the dark when photosynthesis is not ongoing. The large energy

input required for PS assembly can be met by aerobic respiration, which generates much more energy than anaerobic respiration and fermentation. However, an assembly system that only operates via the anaerobic cyclase might not permit BChl biosynthesis, whereas rsp_0294 can make an important contribution to the onset of PS assembly while there is still some oxygen available, by catalysing the formation of some PChlide.

Although the expression of the anaerobic cyclase encoding gene *bchE* is not repressed under aerobic conditions, the catalytic activity of BchE is oxygen-sensitive due to the presence of iron-sulfur cluster (Ouchane *et al.*, 2004). In *Rba. sphaeroides*, the overall contribution of aerobic cyclase to the BChl biosynthesis is small and thus, it does not make any difference when BchE is active. Nevertheless, it is reasonable to suggest that BchE is not functional under some conditions with certain oxygen tensions. In those occasions, BChl synthesised via the aerobic cyclase route, although in a tiny amount, slightly eases the transition from aerobic respiration to photosynthesis, which provides a competitive advantage for *Rba. sphaeroides.*

3.4.3 Presence of zinc-bacteriochlorophyll in *Rba. sphaeroides* has been documented

Zn-BChl *a* was detected in both the Δ*bchE* and Δ*bchE*Δ*ccoP* mutants (**Figure 3.6**), which is not a complete surprise. Natural photosynthesis using Zn-BChl *a* was discovered in an aerobic bacterium *Acidiphilium rubrum* (Wakao *et al.*, 1996). It was subsequently elucidated that in *Acidiphilium rubrum* Mg^{2+} is initially inserted into Proto by Mg-chelatase and Zn-BChl *a* is formed in a later step of BChl biosynthesis by a substitution of Zn^{2+} for Mg^{2+} (Masuda *et al.*, 1999). The presence of Zn-BChl *a* was also reported in a *bchD* (encoding the D subunit of Mg-chelatase) mutant of *Rba. sphaeroides* (Jaschke and Beatty, 2007). The biosynthetic route of Zn-BChl *a* in the *Rba. sphaeroides bchD* mutant must be different from the route in *Acidiphilium rubrum* which relies on a functional Mg-chelatase. It was demonstrated that in the *bchD* mutant the biosynthesis of Zn-BChl *a* begins with the formation of Zn-protoporphyrin catalysed by the ferrochelatase (Jaschke *et al.*, 2011). As the Mg-chelatase in the Δ*bchE* and Δ*bchE*Δ*ccoP* mutants is unaffected, the Zn-BChl *a* biosynthesis mechanism in the *bchD* mutant is unlikely to be applicable in this case. Instead, the Zn^{2+} insertion may occur after de-chelation of Mg^{2+} as in *Acidiphilium rubrum*. Growth conditions with high oxygenation prevent the assembly of the photosynthetic apparatus. Therefore, unbound BChl *a* synthesised via the aerobic cyclase route may be vulnerable to de-chelation by an as-yet unknown mechanism.

Chapter 4

Identification of three classes of aerobic cyclase involved in (bacterio)chlorophyll biosynthesis

4.1 Summary

This chapter reports the identification of three classes of aerobic cyclase catalysing the oxygen-dependent conversion of MgPME to PChlide across all known photosynthetic organisms. In addition to the first subunit AcsF, an ORF, rsp_6110, was identified that encodes a second subunit of the aerobic cyclase in *Rba. sphaeroides*, designated as the *bciE* gene. The *Rvi. gelatinosus acsF* gene was demonstrated to complement the loss of the *cycl* gene, an *acsF* homologue in *Synechocystis*. Deletion of the *ycf54* gene, a potential subunit of aerobic cyclase in *Synechocystis*, did not affect the complementation. The *acsF* and *bciE* genes from *Rba. sphaeroides*, and the *cycl* and *ycf54* genes from *Synechocystis*, were tested for their ability to complement the loss of the *acsF* gene in *Rvi. gelatinosus* which does not contain either the *bciE* or *ycf54* homologue. The complementation profiles identify three types of aerobic cyclase: AcsF (*Rba. sphaeroides*) + BciE ≡ AcsF (*Rvi. gelatinosus*) ≡ CycI + Ycf54. The presence or absence of BciE and Ycf54 homologues across phototrophs reveals the existence of three classes of aerobic cyclase regarding subunit composition: the Class I enzyme requires BciE and is possessed only by phototrophic *Alphaproteobacteria* such as *Rba. sphaeroides*; the Class II enzyme requires neither BciE nor Ycf54 and is present in anoxygenic phototrophs (*Rvi. gelatinosus*) excluding *Alphaproteobacteria*; and the Class III enzyme requires Ycf54 and is ubiquitous in all oxygenic phototrophs, including cyanobacteria, algae and higher plants. The evolutionary history of aerobic cyclase is discussed based on the phylogenetic analysis of AcsF proteins and the distribution of three classes of aerobic cyclase.

4.2 Introduction

The first subunit of aerobic cyclase, AcsF (aerobic cyclisation system Fe-containing subunit), was identified by Pinta *et al.* (2002) in *Rvi. gelatinosus*. Since then, homologues of AcsF have been found in all eukaryotic phototrophs and many prokaryotic phototrophs. Here only the homologues that have been confirmed by experiments to be aerobic cyclase encoding subunits are mentioned. These are Crd1 and Cth1 from *C. reinhardtii* (Moseley *et al.*, 2000; Moseley *et al.*, 2002), CHL27 from *Arabidopsis* (Tottey *et al.*, 2003), Xantha-l from barley (*Hordeum vulgare* L.) (Rzeznicka *et al.*, 2005), CycI and CycII from *Synechocystis* (Minamizaki *et al.*, 2008; Peter *et al.*, 2009), and AcsF (Rsp_0294) from *Rba. sphaeroides* (Chen *et al.*, 2016a; see Chapter 3). All these demonstrations were conducted on the native organism from which the AcsF homologue originates. Considering the high similarity shared by AcsF homologues, it is reasonable to hypothesise that AcsF proteins may function in a heterologous system that utilises aerobic cyclase, and that some new perspectives on aerobic cyclase could arise during testing this hypothesis.

It is noteworthy that AcsF exists as two isoforms, namely Crd1 and Cth1, in *C. reinhardtii*. Crd1 and Cth1 were shown to be differentially expressed as responses to environmental conditions regarding copper nutrition and oxygen tension (Allen *et al.*, 2008). Crd1 is indispensable as it was expressed under all tested conditions and its function could not be completely replaced by Cth1 (Moseley *et al.*, 2002). Likewise, *Synechocystis* also possesses two *acsF*-like genes, *cycI* and *cycII*. CycI contributes to the aerobic cyclase step of Chl biosynthesis under both aerobic and micro-oxic conditions, while CycII is additionally required under micro-oxic conditions (Minamizaki *et al.*, 2008; Peter *et al.*, 2009). Despite the presence of three *bchE*-like genes in *Synechocystis* genome, none of them appear to be involved in the conversion of MgPME to PChlide (Minamizaki *et al.*, 2008). Minamizaki *et al.* (2008) managed to achieve a fully segregated *Synechocystis* Δ*cycI* strain under micro-oxic conditions, whereas another research groups attempted but failed to fully knock out the *cycI* gene in *Synechocystis* (Peter *et al.*, 2009). Similarly, attempts to completely knock out the *cycI* gene in *Synechocytis* under various oxygen tensions also failed (data not shown). However, the discrepancy of *cycI* knockout results between different laboratories does not weaken the conclusion that the *cycI* gene is essential in *Synechocystis* under physiological conditions (aerobic and illuminated).

Unlike *Synechocystis*, it is not lethal to knock out the aerobic cyclase encoding genes in *Rvi. gelatinosus* which is metabolically versatile and can live without photosynthesis. Compared to *Rba. sphaeroides*, *Rvi. gelatinosus* has a more pronounced activity of aerobic cyclase and disruption of aerobic cyclase in this organism has obvious effects. DNA transfer methods via conjugation and electroporation have been developed in *Rvi. gelatinosus*, making mutant construction possible (Nagashima *et al*., 1996; Ouchane *et al*., 1996). Thus, *Rvi. gelatinosus* is considered to be an ideal system to study aerobic cyclase. In fact, it was in *Rvi. gelatinosus* that the first aerobic cyclase encoding gene, *acsF*, was identified (Pinta *et al*., 2002). Since the complete genomic sequence of *Rvi. gelatinosus* IL144 has been available since 2012 (Nagashima *et al*., 2012), this WT strain was obtained as a kind gift from Dr. Sakiko Nagashima (Kanagawa University, Japan) and used as a model organism to investigate aerobic cyclase.

Aerobic cyclase from plants as well as *Synechocystis* was resolved into membrane-bound and soluble components, and both components were required to reconstitute the activity of aerobic cyclase (Wong *et al*., 1984; Walker *et al*., 1991; Bollivar and Beale, 1996). The *acsF* gene was shown to encode a membrane-bound subunit of aerobic cyclase (Tottey *et al*., 2003). On the other hand, more than one genetic locus of barley were found to be involved in the aerobic cyclase reaction, namely *Xantha-l* and *Viridis-k* (Gough, 1972); thus, it is believed that aerobic cyclase is a multi-subunit enzyme. *Xantha-l* was demonstrated to be the *acsF* homologue in barley, whereas *Viridis-k* is likely to encode another unknown membrane-bound component of aerobic cyclase (Rzeznicka *et al*., 2005). Ycf54 and LCAA, the counterpart of Ycf54 in tobacco, were subsequently identified to be potential subunits of the aerobic cyclase and required for the stability of AcsF homologues in oxygenic phototrophs (Hollingshead *et al*., 2012; Albus *et al*., 2012; Hollingshead *et al*., 2016). Both the coding sequence and protein level of the Ycf54 homologue were shown to be unaffected in all the *viridis-k* mutants of barley (Bollivar *et al*., 2014). Together with the experimental results indicating that Ycf54 may be a membrane-bound subunit, it was proposed that apart from AcsF and Ycf54, there are at least two subunits of aerobic cyclase that remain to be identified (Bollivar *et al*., 2014).

4.3 Results

4.3.1 Sequence alignments of known AcsF homologues

As a member of the diiron carboxylate protein family, AcsF contains a coupled binuclear iron centre which is coordinated by four glutamate and two histidine residues (Berthold and Stenmark, 2003). Five known AcsF proteins with experimental evidence, *Rvi. gelatinosus* AcsF, *Synechocystis* CycI, *C. reinhardtii* CRD1, *Arabidopsis* CHL27 and *Rba. sphaeroides* Rsp_0294, were aligned using T-coffee (**Figure 4.1**). The signature diiron binding domain is completely conserved in all the five AcsF proteins. Regarding the species investigated in this thesis, *Rba. sphaeroides* Rsp_0294 shares 51% identity with *Rvi. gelatinosus*, while *Synechocystis* CycI is 42% identical to *Rvi. gelatinosus* AcsF.
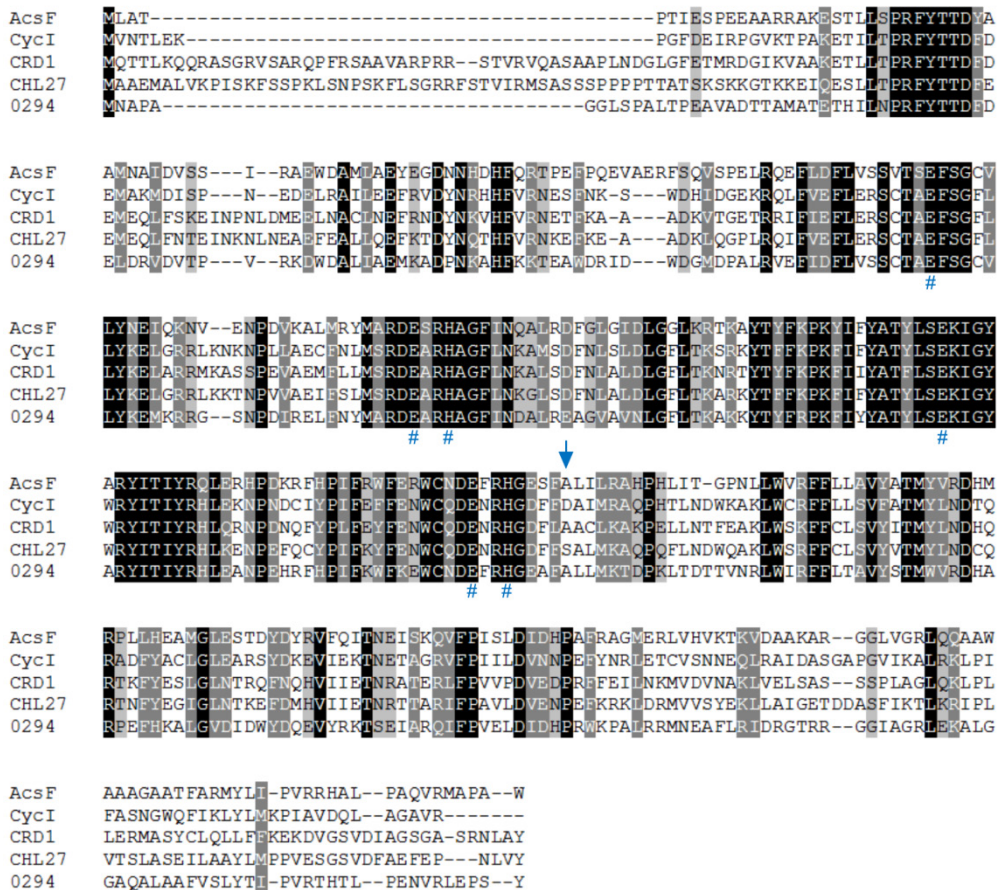
Figure 4.1 Amino acid sequence alignments of described AcsF proteins

The alignments were generated using T-coffee. Sequences are those from *Rvi. gelatinosus* (AcsF), *Synechocystis* (CycI), *C. reinhardtii* (CRD1), *Arabidopsis* (CHL27) and *Rba. sphaeroides* (Rsp_0294, abbreviated as 0294 in the figure). Conserved, highly similar and similar residues are highlighted in black, dark grey and light grey, respectively. The putative diiron-binding residues are marked by a blue hash (#). The amino acid residue marked by a blue arrow will be discussed in Chapter 5.

4.3.2 Construction of *Synechocytis* strain expressing *Rvi. gelatinosus acsF*

The pPD-FLAG vector was used in our group to construct *Synechocystis* strains expressing genes under the promoter of a redundant gene *psbAII* (one of the three genes encoding the PS D1 protein) (Hollingshead *et al.*, 2012). As shown in **Figure 4.2 A**, the pPD-FLAG vector contains the *psbAII* promoter and flanking sequences for homologous recombination allowing replacing the *psbAII* gene with the gene of interest in the *Synechocystis* genome. An N-terminal 3x FLAG tag is also available when the *Not*I site is used for cloning.
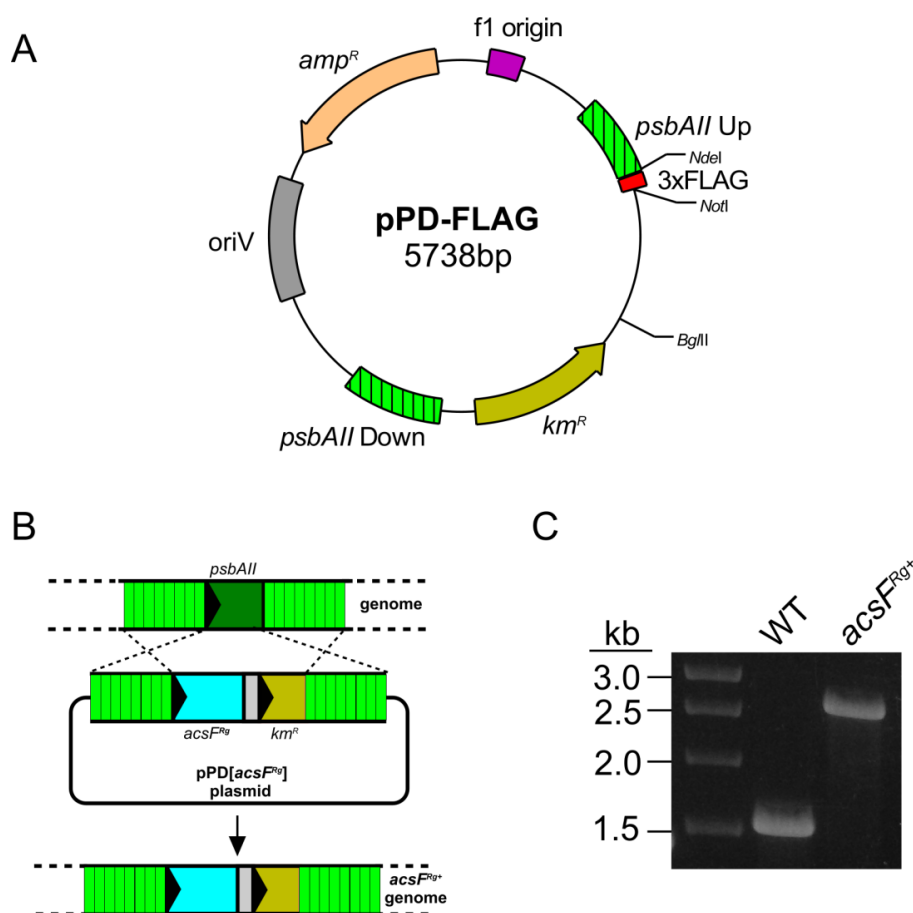
Figure 4.2 Construction of a *Synechocystis* strain expressing the *acsF^{Rg}* gene

(**A**) Map of the pPD-FLAG vector. The vector contains a pUC origin of replication (oriV), an f1 origin of single-strand DNA replication (f1 origin), a kanamycin resistance gene (*km*^R), an ampicillin resistance gene (*amp*^R), the upstream and downstream regions of the *psbAII* gene and a sequence encoding an N-terminal 3x FLAG tag. (**B**) Diagram depicting the replacement of the *psbAII* gene with *acsF^{Rg}* using the pPD[*acsF^{Rg}*] construct. (**C**) Construction of fully segregated strain was confirmed by colony PCR using primers flanking the *psbAII* gene. Lengths of PCR products: WT = 1551 bp, *acsF^{Rg+}* = 2643 bp.

Synechocystis contains multiple copies of its genome and GT-W, the WT strain used in this thesis, has been determined recently to contain 7~11 chromosome copies per cell (Tichy *et*

al., 2016). Thus, the construction of *Synechocystis* mutants requires a segregation process. The *acsF* gene was amplified from *Rvi. gelatinosus* WT genomic DNA and cloned into the *Nde*I/*Bgl*II sites of pPD-FLAG. The resulting construct pPD[*acsF*^Rg] was confirmed by sequencing, then transformed into *Synechocystis* WT. Transformants were selected on BG-11 agar medium supplemented with 10 μg ml^{-1} kanamycin and were subjected to segregation by successively doubling the concentration of kanamycin up to 80 μg ml^{-1}. The fully segregated mutant *acsF*^Rg+ was confirmed by colony PCR using primers syn-psbAII UF and syn-psbAII DR (**Figure 4.2 C**).

4.3.3 Deletion of the *cycI* and *ycf54* genes in the *acsF*-expressing strain of *Synechocystis*

As the *cycI* gene is indispensable to *Synechocystis*, it is impossible to achieve the fully segregated Δ*cycI* mutant in the WT background. To check whether the *Rvi. gelatinosus acsF* gene can complement the loss of *cycI* gene in *Synechocystis*, attempts to knock out *cycI* gene in the *acsF*^Rg+ mutant were made. The upstream and downstream regions (~400 bp) of the *cycI* gene were amplified from *Synechocystis* WT genomic DNA, separately. The chloramphenicol resistance gene was amplified from the pACYC184 vector (Fermentas). Then overlap extension PCR was performed to fuse the three PCR products to get the final Δ*cycI* construct in which the chloramphenicol resistance gene was flanked by the upstream and downstream sequence of the *cycI* gene (**Figure 4.3 A**). The Δ*cycI* construct was transformed into the *acsF*^Rg+ mutant and segregation was conducted using concentrations of chloramphenicol from 5 μg ml^{-1} to 80 μg ml^{-1}. Colony PCR using primers flanking the *cycI* gene showed that full segregation was achieved (**Figure 4.3 B**). However, as the PCR product of Δ*cycI* is shorter than that of WT, the WT amplicon may be produced less efficiently than for Δ*cycI*. Accordingly, primers within the *cycI* gene were designed and used for a second colony PCR. No PCR product was detected in Δ*cycI*, whereas a PCR amplicon with the expected size was produced for the WT (**Figure 4.3 B**). Thus, it is certain that the *cycI* gene was completely deleted. The deletion of *cycI* was repeated and fully segregated Δ*cycI* mutant was achieved again.
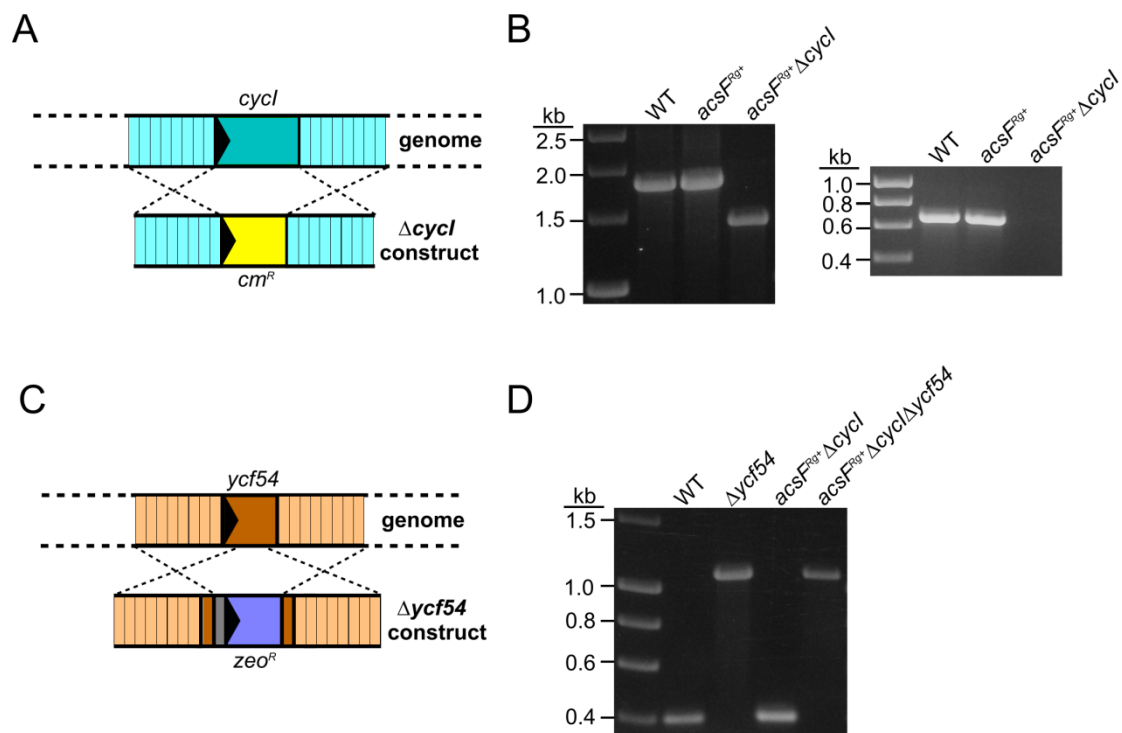
Figure 4.3 Inactivation of the *cycI* and *ycf54* genes in *Synechocystis*

(**A**) Diagram depicting the inactivation of the *cycI* gene by replacing it with a chloramphenicol resistance gene (*cm*^R). (**B**) Construction of fully segregated strain was confirmed by colony PCR using primers either flanking (left) or inside (right) the *cycI* gene. Length of PCR products: for flanking primers, WT = 1855 bp, Δ*cycI* = 1438 bp; for inside primers, WT = 683 bp, no product for Δ*cycI*. (**C**) Diagram depicting the inactivation of the *ycf54* gene by replacing it with a zeocin resistance cassette (*zeo*^R). (**D**) Construction of fully segregated strain was confirmed by colony PCR using primers flanking the *ycf54* gene. Lengths of PCR products: WT = 402 bp, Δ*ycf54* = ~1 kb.

The knockout of the *ycf54* gene in *Synechocystis* by replacing the central portion of *ycf54* with a zeocin resistance cassette has been recently reported (Hollingshead *et al.*, 2016). The Δ*ycf54* knockout construct was retrieved using the Δ*ycf54* genomic DNA as a template with primers syn-ycf54-ZeoR F and syn-ycf54-ZeoR R (**Figure 4.3 C**). The PCR product was used to transform the *acsF*^Rg+Δ*cycI* strain and segregation was conducted by sequentially doubling the concentration of zeocin from 2.5 μg ml^{-1} to 10 μg ml^{-1}. Colony PCR demonstrated that the fully segregated *acsF*^Rg+Δ*cycI*Δ*ycf54* was achieved (**Figure 4.3 D**).

4.3.4 Phenotypic analyses of the constructed *Synechocystis* strains

The phenotypes of the constructed *Synechocystis* mutants were analysed in respect of the whole-cell absorption spectrum, Chl content, and growth rate under various conditions. For mixotrophic growth, the medium was supplemented with 5 mM glucose. The light intensities for low, low-moderate and moderate light conditions were 5, 15 and 30 μE m^{-2} s^{-1},

respectively. *Synechocystis* strains were grown mixotrophically in liquid medium under low light conditions; when the OD_{750} reached 0.3~0.6 cells were harvested and resuspended in 60% (w/v) sucrose to minimise light scattering. The absorption spectrum of the suspension between 350~750 nm was recorded and standardised by OD_{750}. As shown in **Figure 4.4 A**, significant levels of Chl-containing complexes formed in the *acsF^{Rg+}ΔcycI* and *acsF^{Rg+}ΔcycIΔycf54* mutants, although they were somewhat lower than for the WT, whereas almost no Chl-containing complexes were detected in the *Δycf54* mutant. The phycobiliproteins represented by the 625 nm peak were not affected in all the three mutants.

As the *Δycf54* strain is unable to survive autotrophic growth or under intense light conditions, the mutant was grown mixotrophically in liquid medium under low light conditions. The WT, *acsF^{Rg+}ΔcycI* and *acsF^{Rg+}ΔcycIΔycf54* strains were grown autotrophically in liquid medium under moderate light conditions. Three biological replicates of each strain were used for Chl content determination; Chl was extracted from 4 ml of culture at OD_{750} of 0.3~0.5 using 1 ml of methanol. The absorbance spectrum of the extract was recorded and Chl concentration was calculated using a formula reported in Porra *et al.* (1989). The Chl concentration was then divided by the value of OD_{750} to get the Chl content expressed in mg L^{-1} OD_{750}^{-1}. Under the tested conditions, the *acsF^{Rg+}ΔcycI* and *acsF^{Rg+}ΔcycIΔycf54* mutants contained the same amount of Chl, which was 96% of that of WT (**Figure 4.4 B**). The *Δycf54* mutant had only 7.5% of Chl compared with WT (**Figure 4.4 B**).
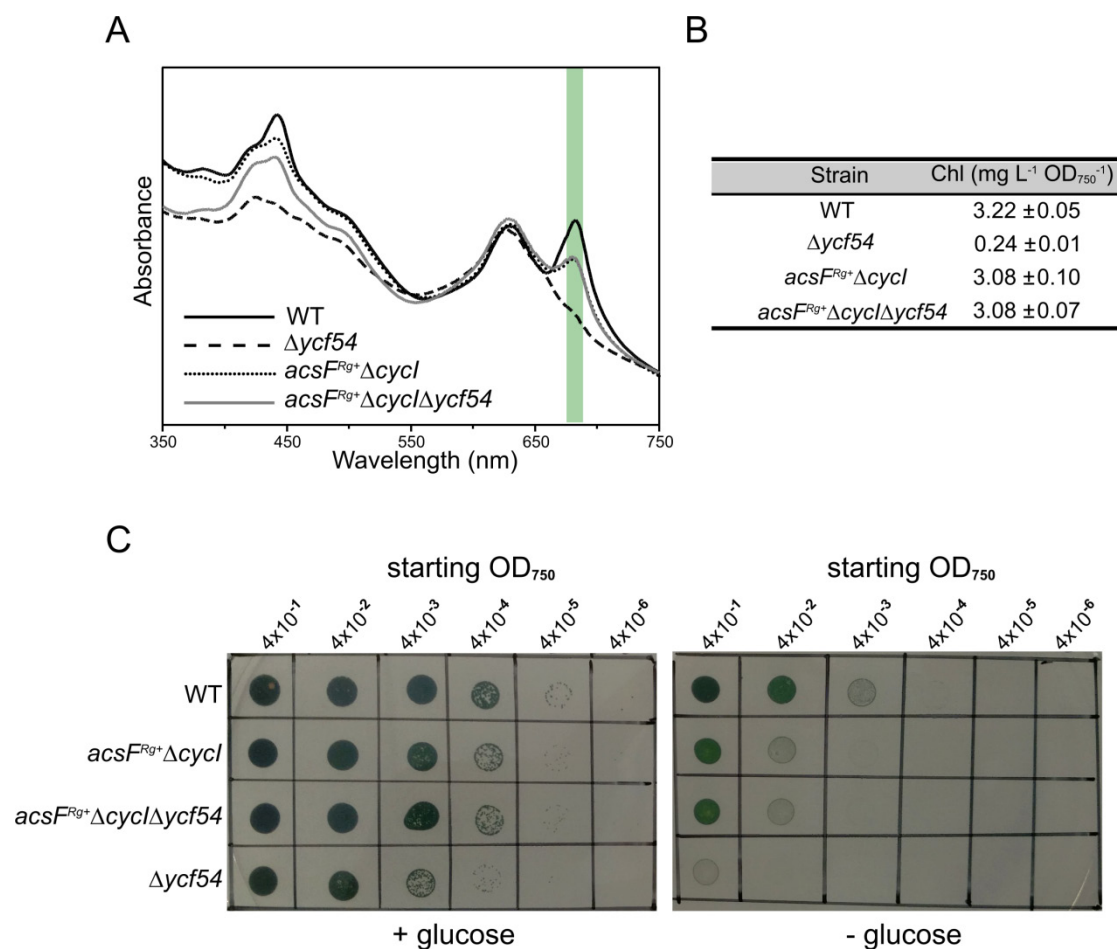
Figure 4.4 Phenotypic analyses of described *Synechocystis* strains

Glucose was supplemented at 5 mM for mixotrophic growth. The light intensities for low, low-moderate and moderate light conditions were 5, 15 and 30 μE m$^{-2}\cdot$s^{-1}, respectively. (**A**) Whole-cell absorption spectra of *Synechocystis* strains grown mixotrophically under low light conditions. Cell pellets were suspended in 60% (w/v) sucrose and absorption spectra were recorded. The peaks for Chl-containing complexes are marked by a green line. (**B**) The Chl contents of *Synechocystis* strains were determined spectroscopically from three biological replicates. Except the $\Delta ycf54$ strain which was grown mixotrophically under low light conditions, strains were grown autotrophically under moderate light conditions. (**C**) Drop growth assays of *Synechocystis* strains on BG-11 agar medium with or without glucose. Under the conditions described in (B), liquid cultures were grown until OD$_{750}$ reached 0.4~0.5, then cultures were adjusted to OD$_{750}$ of 0.4 and subjected to serial 10-fold dilutions. 5 μl of each dilution was spotted on agar medium. Photographs were taken after 12-day incubation at 30°C under low-moderate light conditions.

The growth rates of *Synechocystis* strains under various conditions were assessed by drop growth assays. Except the $\Delta ycf54$ strain was grown mixotrophically under low light conditions, other strains were grown autotrophically under moderate light conditions. Cultures were grown until OD$_{750}$ reached 0.4~0.5 and then cultures were adjusted to OD$_{750}$ of 0.4 and subjected to serial 10-fold dilutions. 5 μl of each dilution were spotted both on BG-11 agar

medium with and without 5 mM glucose. Plates were incubated at 30°C under low-moderate light conditions for 12 days before photographs were taken (**Figure 4.4 C**). Generally speaking, *Synechocystis* strains grew slower without supplementation of glucose. The growth rates of the *acsF*$^{Rg+}$*ΔcycI* and *acsF*$^{Rg+}$*ΔcycIΔycf54* mutants were similar to each other, and lower than that of WT with a rough difference of one 10-fold dilution, but higher than that of the *Δycf54* with a rough difference of one 10-fold dilution.

4.3.5 Distribution of rsp_6110 homologues among *Alphaproteobacteria*

Rba. sphaeroides, a model anoxygenic phototroph, has most of the genes encoding photosynthesis-related proteins organised in a 40.7 kb region of its genome, which is termed as PGC (Naylor *et al.*, 1999). Most of the genes encoding the enzymes for BChl biosynthesis, including *acsF*, *bchM*, *bchL*, *bchH*, *bchB*, *bchN*, *bchF*, *bchE*, *bchJ*, *bchG*, *bchP*, *bchD*, *bchI*, *bchC*, *bchX*, *bchY* and *bchZ*, are located in the PGC of *Rba. sphaeroides*. It has been demonstrated in Chapter 3 that *Rba. sphaeroides* possesses a functional aerobic cyclase of which rsp_0294 (designated as *acsF*) encodes one subunit. Literature suggests aerobic cyclase is a multi-subunit enzyme. In a search for gene(s) encoding the unknown subunit(s) of aerobic cyclase, rsp_6110, an ORF with no function assigned yet, drew our attention. Encoding a 98 AA protein, this ORF is located immediately upstream of the *acsF* gene and even shares four nucleotide base pairs with the *acsF* gene.

Before conducting experiments, the conservation of Rsp_6110 protein in phototrophic bacteria was checked. The amino acid sequence of Rsp_6110 was used as a BLAST query against the species studied in a paper discussing the distribution and origin of anaerobic and aerobic cyclase among phototrophic *Proteobacteria* (Boldareva-Nuianzina *et al.*, 2013). The protein BLAST results are listed in **Table 4.1**, exhibiting a pattern in which Rsp_6110 coexists with AcsF in the listed *Alphaproteobacteria*. Furthermore, no homologue of Rsp_6110 can be found in phototrophic *Alphaproteobacteria* that do not possess the *acsF* gene. Taken all together, Rsp_6110 is a highly likely candidate for involvement in the aerobic cyclase.

Table 4.1 Presence of AcsF and Rsp_6110 homologues in phototrophic *Proteobacteria*[a]

Species	Accession	Group[b]	AcsF	6110[c]
Acidiphilium multivorum AIU301	NC_015186	α1, AAP	✓	✓[d]
Phaeospirillum molischianum DSM 120	NZ_CAHP01000014	α1, PNB	✗	✗
Rhodospirillum centenum SW	NC_011420	α1, PNB	✓	✓
Rhodospirillum rubrum ATCC 11170	NC_007643	α1, PNB	✗	✗
Rhodospirillum photometricum DSM 122	NC_017059	α1, PNB	✗	✗
Ahrensia sp. strain R2A130	NZ_AEEB01000017	α2, AAP	✓	✓
Agrobacterium albertimagni AOL15	NZ_ALJF00000000	α2, AAP	✓	✓
Hoeflea phototrophica DFL43	NZ_CM002917	α2, AAP	✓	✓
Labrenzia alexandrii DFL11	NZ_EQ973121	α2, AAP	✓	✓
Methylobacterium sp. 4-46	NC_010511	α2, AAP	✓	✓
Methylobacterium radiotolerans JCM 2831	NC_010505	α2, AAP	✓	✓
Methylobacterium populi BJ001	NC_010725	α2, AAP	✓	✓
Methylobacterium extorquens AM1	NC_012808	α2, AAP	✓	✓
Methylocella silvestris BL2	NC_011666	α2, AAP	✓	✓
Bradyrhizobium sp. BTAi1	NC_009485	α2, PNB	✓	✓
Bradyrhizobium sp. ORS278	NC_009445	α2, PNB	✓	✓
Rhodomicrobium vannielii ATCC 17100	NC_014664	α2, PNB	✗	✗
Rhodopseudomonas palustris	Multiple[e]	α2, PNB	✓	✓
Dinoroseobacter shibae DFL12	NC_009952	α3, AAP	✓	✓
Jannaschia sp. CCS1	NC_007802	α3, AAP	✓	✓
Loktanella vestfoldensis SKA53	CH672414	α3, AAP	✓	✓
Roseobacter denitrificans Och 114	NC_008209	α3, AAP	✓	✓
Roseobacter litoralis Och 149	NC_015730	α3, AAP	✓	✓
Roseobacter sp. AzwK-3b	ABCR01000004	α3, AAP	✓	✓
Roseobacter sp. CCS2	AAYB01000001	α3, AAP	✓	✓
Roseovarius sp. TM1035	ABCL01000003	α3, AAP	✓	✓
Roseovarius sp. 217	CH902584	α3, AAP	✓	✓
Rhodobacter capsulatus SB 1003	NC_014034	α3, PNB	✗	✗
Rhodobacter sphaeroides	Multiple[f]	α3, PNB	✓	✓
Rhodobacter sp. SW2	ACYY01000004	α3, PNB	✓	✓
Erythrobacter sp. NAP1	CH672390	α4, AAP	✓	✓
Citromicrobium bathyomarinum JL354	NZ_ADAE01000008	α4, AAP	✓	✓
Sphingomonas spp.	Multiple[g]	α4, AAP	✓	✓
Brevundimonas subvibrioides ATCC 15264	NC_014375	α4, AAP	✓	✓
Rubrivivax gelatinosus IL114	NC_017075	β, PNB	✓	✗
Rubrivivax benzoatilyticus JA2	AEWG01000076	β, PNB	✓	✗
Methyloversatilis universalis FAM5	AFHG01000059	β, PNB	✓	✗
Limnohabitans sp. Rim28	NZ_ALKN01000024	β, PNB	✓	✗
Limnohabitans sp. Rim47	NZ_ALKO01000003	β, PNB	✓	✗
Allochromatium vinosum DSM 180	NC_013851	γ, PSB	✗	✗
Ectothiorhodospira sp. PHS-1	NZ_CP011994	γ, PSB	✗	✗
Halorhodospira halophila SL1	NC_008789	γ, PSB	✗	✗
Marichromatium purpuratum 984	NZ_CP007031	γ, PSB	✗	✗
Thiocapsa marina 5811	NZ_AFWV01000000	γ, PSB	✗	✗
Thiocystis violascens DSM198	NC_018012	γ, PSB	✗	✗
Thioflavicoccus mobilis 8321	NC_019940	γ, PSB	✗	✗
Thiorhodococcus drewsii AZ1	NZ_AFWT00000000	γ, PSB	✗	✗
Thiorhodospira sibirica ATCC 700588	NZ_AGFD00000000	γ, PSB	✗	✗
Congregibacter litoralis KT71	NZ_CM002299	γ, AAP	✓	✗
gamma proteobacterium NOR5-3	DS999405	γ, AAP	✓	✗
Luminiphilus syltensis NOR5-1B	DS999411	γ, AAP	✓	✗
marine gamma proteobacterium HTCC2080	NZ_AAVV01000005	γ, AAP	✓	✗
gamma proteobacterium HIMB55	NZ_AGIF02000001	γ, AAP	✓	✗

[a] Modified from Table 2 of Boldareva-Nuianzina *et al.*, 2013. Accession numbers were retrieved between 31st May and 1st June 2016.
[b] Abbreviations: α1-4, subgroups 1-4 of *Alphaproteobacteria*; β, *Betaproteobacteria*; γ, *Gammaproteobacteria*; AAP, aerobic anoxygenic phototrophs; PNB, purple non-sulfur bacteria; PSB, purple sulfur bacteria.
[c] Represents the homologues of Rsp_6110.
[d] Assigned if the organism possesses a protein with over 35% identity to Rsp_6110.
[e] Represents the following strains of *Rhodopseudomonas palustris*: TIE-1 (NC_011004), BisA53 (NC_008435), BisB18 (NC_007925), BisB5 (NC_007958), CGA009 (NC_005296), HaA2 (NC_007778), and DX-1 (NC_014834).
[f] Represents the following strains of *Rhodobacter sphaeroides*: 2.4.1 (NC_007493), KD131 (NC_011963), WS8N (NZ_CM001161), ATCC 17029 (NC_009049), and ATCC 17025 (NC_009428).[g] Represents the following strains of *Sphingomonas* strains: *Sphingomonas echinoides* ATCC 14820 (NZ_JH584235) and *Sphingomonas* sp. strains PAMC 26605 (NZ_JH584241), PAMC 26617 (NZ_JH594425), and PAMC 26621 (NZ_AIDW01000027).

4.3.6 Investigation of the role played by Rsp_6110 in *Rba. sphaeroides*

The analysis in **Table 4.1** suggested that it would be worthwhile to knock out rsp_6110 in a previously constructed *Rba. sphaeroides* Δ*bchE*Δ*ccoP* mutant in order to find out whether Rsp_6110 plays a role in aerobic cyclase activity. The Δ*bchE*Δ*ccoP*Δrsp_6110 mutant was made using the same procedures explained in Section 3.3.1 and was confirmed by colony PCR (**Figure 4.5 A**). The Δ*bchE*Δ*ccoP* and Δ*bchE*Δ*ccoP*Δrsp_6110 mutants were grown in 250 ml Erlenmeyer flasks containing 40 ml of M22+ medium with shaking at 150 rpm. Pigments were extracted and analysed by HPLC as described in Section 3.3.4. The elution profiles of pigments extracted from Δ*bchE*Δ*ccoP* and Δ*bchE*Δ*ccoP*Δrsp_6110 were shown as traces 4 and 3, respectively (**Figure 4.5 B**). Deletion of rsp_6110 resulted in complete loss of aerobic cyclase activity as no BChl species was detected in Δ*bchE*Δ*ccoP*Δrsp_6110.

Tikh *et al.* (2014) have reported the pBBRBB-*Ppuf*$_{843-1200}$ vector, which contains the 3' end of the *Rba. sphaeroides puf* promoter (1200 bp in total), allowing protein expression in *Rba. sphaeroides* even under high-oxygenation conditions (**Figure 4.5 C**). This vector was employed to test whether expression of Rsp_6110 from a plasmid can restore the activity of aerobic cyclase in the Δ*bchE*Δ*ccoP*Δrsp_6110 mutant. Besides, two cysteine residues (Cys13 and Cys88) in Rsp_6110 seem to be conserved in several analysed species. Thus, the expression of a mutant of Rsp_6110 with the two cysteines replaced with glycines in the Δ*bchE*Δ*ccoP*Δrsp_6110 mutant was also conducted to check whether the two cysteines are essential. The rsp_6110 gene was amplified from *Rba. sphaeroides* WT genomic DNA, whilst the mutated rsp_6110 gene was synthesised using gBlock®(IDT). The gene fragments were cloned into the *Bgl*II/*Not*I sites of the pBBRBB-*Ppuf*$_{843-1200}$ vector. Confirmed by sequencing, the resulting pBB[rsp_6110] and pBB[rsp_6110^{-Cys}] constructs were conjugated into the Δ*bchE*Δ*ccoP*Δrsp_6110 mutant of *Rba. sphaeroides* via *E. coli* S17-1, separately. Pigment analysis showed that the strain harbouring the pBB[rsp_6110] plasmid apparently had a functional aerobic cyclase (**Figure 4.5 B**). However, the mutated Rsp_6110 was incapable of restoring aerobic cyclase activity (**Figure 4.5 B**).
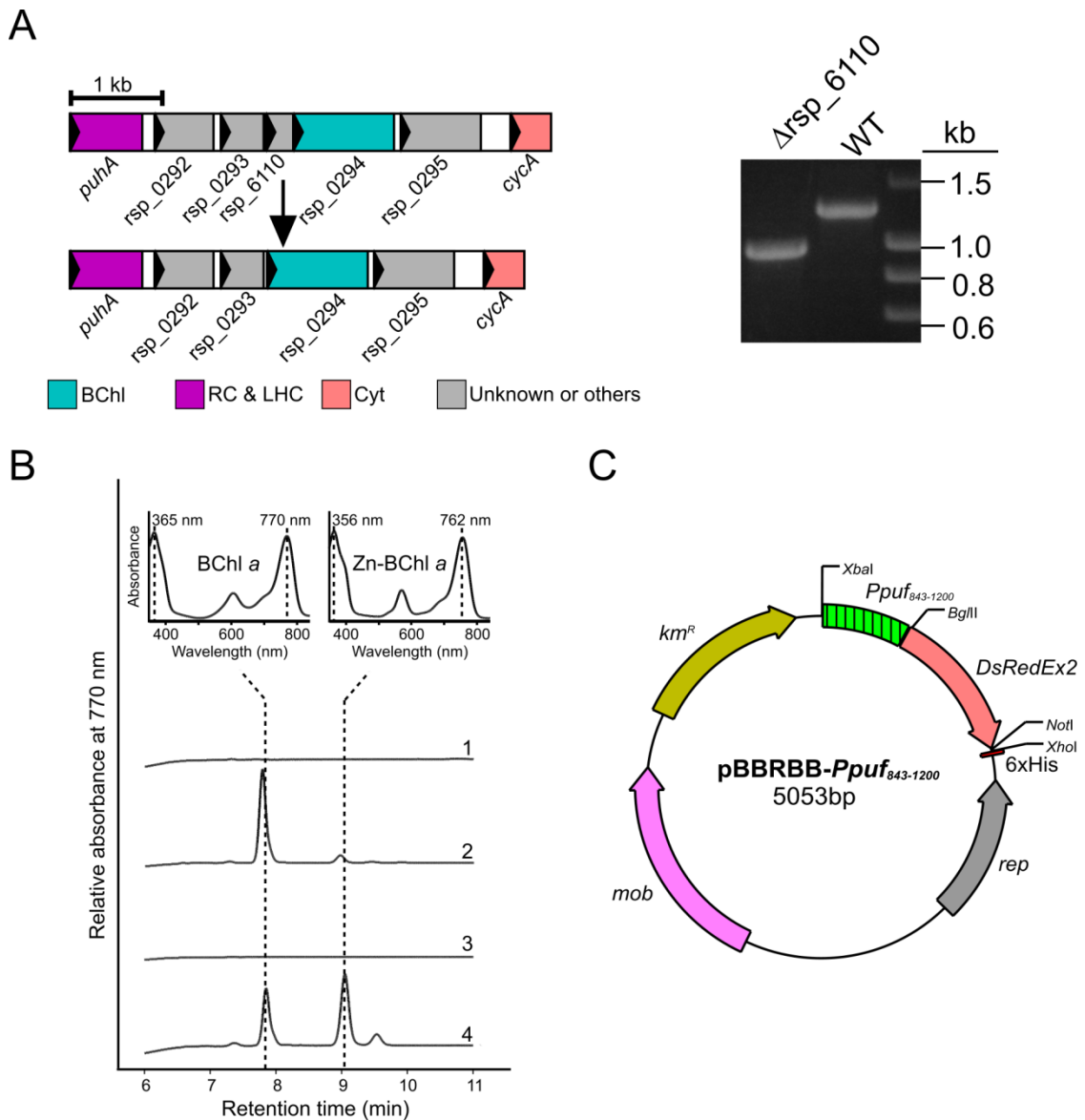
Figure 4.5 Deletion of the rsp_6110 gene in *Rba. sphaeroides* and complementation of the mutant with a plasmid harbouring the rsp_6110 gene

(**A**) The genomic regions adjacent to the rsp_6110 gene from WT and Δrsp_6110 are depicted in proportion to the scale bar. Genes are represented as colour filled rectangles within which the arrow indicates the transcription direction. Abbreviations: BChl, bacteriochlorophyll biosynthesis; RC&LHC, reaction centre and light-harvesting complexes; Cyt, cytochrome. Colony PCR gel is shown on the right and products of WT and Δrsp_6110 are 1251 bp and 958 bp, respectively. (**B**) HPLC analysis of pigments extracted from the constructed *Rba. sphaeroides* strains. Trace 1, *ΔbchEΔccoP*Δrsp_6110/pBB[rsp_6110^{-Cys}]; trace 2, *ΔbchEΔccoP*Δrsp_6110/pBB[rsp_6110]; trace 3, *ΔbchEΔccoP*Δrsp_6110; trace 4, *ΔbchEΔccoP*. (**C**) Map of the pBBRBB-*Ppuf$_{843-1200}$* vector. The vector contains the *rep* gene required for plasmid replication, the *mob* gene required for plasmid mobilisation, a kanamycin resistance gene (*km^R*), a partial sequence (843~1200) of the *puf* promoter and a sequence encoding a C-terminal 6x His tag. For cloning, the *DsRedEx2* gene was replaced with the gene of interest.

4.3.7 Construction of *Rvi. gelatinosus* strains expressing foreign genes under the *acsF* promoter

Although mutants of *Rvi. gelatinosus* have been reported by a number of papers, all of the gene disruptions were constructed by placing an antibiotic resistance cassette into the gene of interest, which may cause polar effects. In order to generate markerless in-frame mutants of *Rvi. gelatinosus*, the pK18*mobsacB*-based method employed in *Rba. sphaeroides* (Section 3.3.1) was attempted and finally succeeded. The gene deletion plasmid pK18Δ*gene* was constructed by cloning the upstream and downstream regions of the target gene into pK18*mobsacB* with an added *Nde*I site between the two fragments. It was proved to be impractical to conjugate pK18*mobsacB*-based plasmids to *Rvi. gelatinosus* via *E. coli* S17-1 as the selection of transconjugants of *Rvi. gelatinosus* was problematic with the two media tested. The PYS medium which was used to grow *Rvi. gelatinosus* was rich enough to support *E. coli* growth. Thus, large number of colonies of *E. coli* S17-1 were formed when selection was applied on PYS agar medium with kanamycin. On the other hand, the more minimal M22+ agar medium used for *Rba. sphaeroides* was not applicable either as *Rvi. gelatinosus* could not grow on this medium.

Instead, electroporation was utilised to construct *Rvi. gelatinosus* mutants according to Nagashima *et al*. (1996) with some modifications. Electrocompetent cells were prepared from *Rvi. gelatinosus* culture grown to logarithmic phase by stepwise washing the cells once with ice-cold sterile ultrapure water and twice with ice-cold sterile 10% (v/v) glycerol solution. 50 μl of the prepared electrocompetent cells were mixed with 4 μg of pK18*mobsacB* based plasmid DNA and transferred to a chilled electroporation cuvette (0.1 cm gap, Bio-Rad). Electroporation was performed using the MicroPulser (Bio-Rad) with the program Ec1 (Voltage = 1.8 kV, pulse length = ~5 ms), followed by immediate addition of 1 ml of chilled PYS medium supplemented with 1% (w/v) glucose and incubation on ice for 30 min. Then the cell suspension was transferred to 10 ml of PYS medium in a 50 ml falcon tube and incubated at 30°C with shaking at 150 rpm. After a 6 hr incubation, cells were pelleted down and spread out onto PYS agar medium with 50 μg ml^{-1} of kanamycin for selection. The following procedures were identical to the ones used for *Rba. sphaeroides* (Section 3.3.1). Finally, the in-frame modified mutants were differentiated from WT by colony PCR.
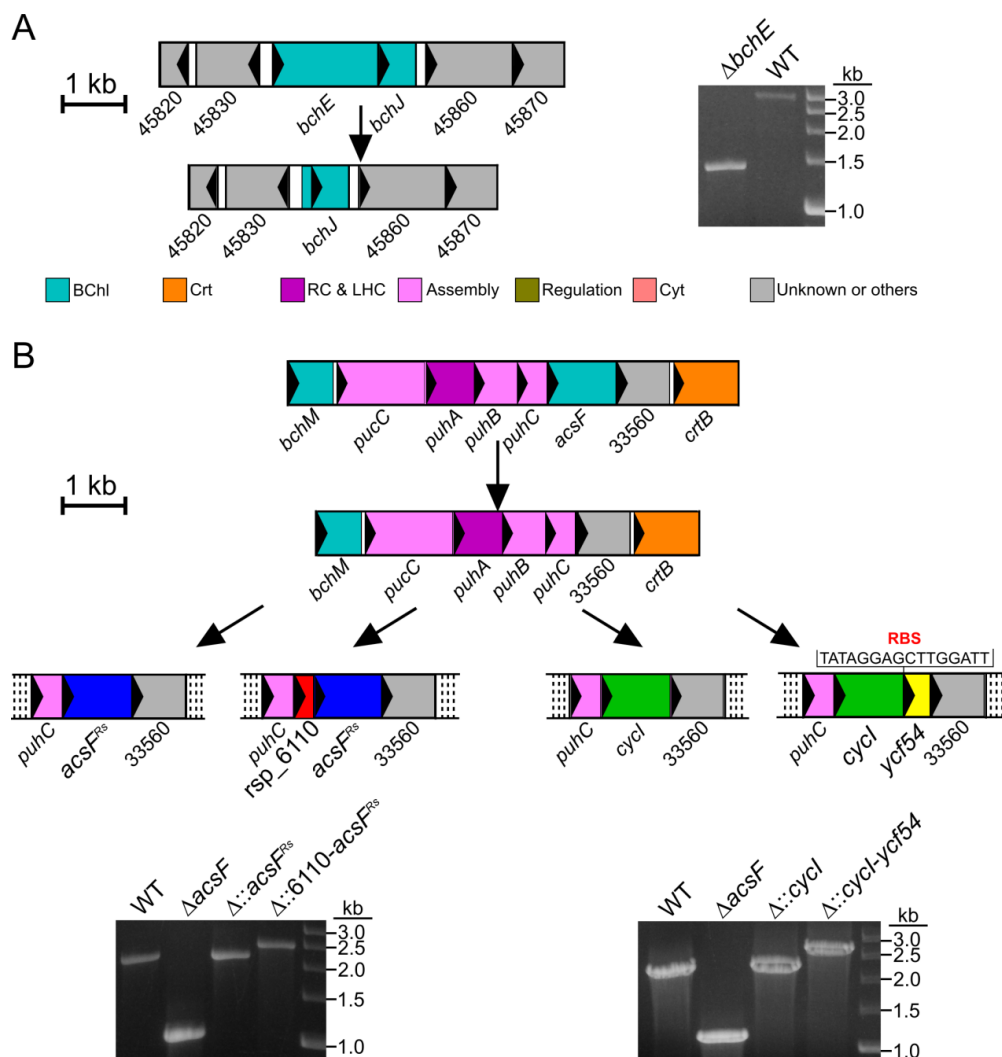
Figure 4.6 Genetic knockouts and replacements in *Rvi. gelatinosus*

The genomic regions subjected to genetic manipulations are depicted in proportion to the scale bar. Genes are represented as colour filled rectangles within which the arrow indicates the transcription direction. Abbreviations: BChl, bacteriochorophyll biosynthesis; Crt, carotenoid biosynthesis; RC&LHC, reaction centre and light-harvesting complexes; Cyt, cytochrome. Colony PCR gel are also presented. (**A**) Deletion of the *bchE* gene. Lengths of PCR products: WT = 2862 bp; Δ*bchE* = 1357 bp. (**B**) Deletion of the *acsF* gene and subsequent introduction of foreign genes under the *acsF* promoter. Lengths of PCR products: WT = 2137 bp; Δ*acsF* = 1066 bp; Δ*acsF*::*acsF*^Rs = 2164 bp; Δ*acsF*::rsp_6110-*acsF*^Rs = 2454 bp; Δ*acsF*::*cycI* =2146 bp; Δ*acsF*::*cycI-ycf54* = 2564 bp.

As both the aerobic and anaerobic cyclases are functional in *Rvi. gelatinosus*, the anaerobic cyclase encoding gene *bchE* was removed using the pK18Δ*bchE* construct as described above (**Figure 4.6 A**). Then a BChl-deficient mutant Δ*bchE*Δ*acsF* was subsequently created using the pK18Δ*acsF* construct (**Figure 4.6 B**), which served as the background strain for testing aerobic cyclases from other species. A series of pK18[*gene*] plasmids was generated by cloning the indicated gene into the *Nde*I site of the pK18Δ*acsF* plasmid. For the construction of

pK18[rsp_6110-*acsF*^{Rs}], rsp_6110 and *acsF*^{Rs} genes were amplified as a single fragment from *Rba. sphaeroides* genomic DNA using the forward primer of rsp_6110 and the reverse primer of *acsF*^{Rs} as the two genes share 4 base pairs. In the case of pK18[*cycI-ycf54*], a 16 bp sequence immediately upstream of the *pufA* gene of *Rvi. gelatinosus* was placed between the *cycI* and *ycf54* genes to provide a ribosome binding site for the *ycf54* mRNA. These pK18[*gene*] constructs were used to make the *Rvi. gelatinosus* mutants in which the *Rba. sphaeroides* *acsF*^{Rs} and *Synechocystis cycI* were placed in-frame under the native *acsF* promoter either alone or together with their associated genes, rsp_6110 or *ycf54*, respectively (**Figure 4.6 B**).

4.3.8 HPLC analysis of pigments accumulated in the constructed *Rvi. gelatinosus* strains

The constructed *Rvi. gelatinosus* strains were grown aerobically in 250 ml Erlenmeyer flasks filled with 20 ml of PYS medium with shaking at 150 rpm. Cultures standardised by OD$_{680}$ were used for pigment extraction with an excess of 0.2% (v/v) ammonia in methanol. This was repeated once to ensure complete extraction. The resulting extracts were dried in vacuum at 30°C and finally reconstituted in a small volume of the same solvent for HPLC analysis. Pigments were resolved on a Fortis UniverSil C18 reverse-phase column using exactly the same program as described in Section 3.3.4. The elution of BChl species was monitored by absorbance at 770 nm. As the Δ*bchE* strain produced a much higher level of BChl compared to any other strains, a diluted sample was loaded on HPLC to serve as positive control for BChl (trace 6 in **Figure 4.7**). No peak was detected in the BChl-deficient strain Δ*bchE*Δ*acsF* (trace 5 in **Figure 4.7**). CycI alone was not able to complement the loss of *acsF* since no BChl was produced in the Δ*bchE*Δ*acsF*::*cycI* strain (trace 4 in **Figure 4.7**). When Ycf54 was co-expressed with CycI in the Δ*bchE*Δ*acsF*::*cycI-ycf54* strain , BChl was produced at a considerable level (trace 3 in **Figure 4.7**). A tiny peak for BChl *a* was present in the elution profile of Δ*bchE*Δ*acsF*::*acsF*^{Rs} (**Figure 4.7**). Thus, it is safe to say that AcsF^{Rs} alone showed minimal, if any, aerobic cyclase activity, which was greatly enhanced by the addition of Rsp_6110 (traces 1 and 2 in **Figure 4.7**).
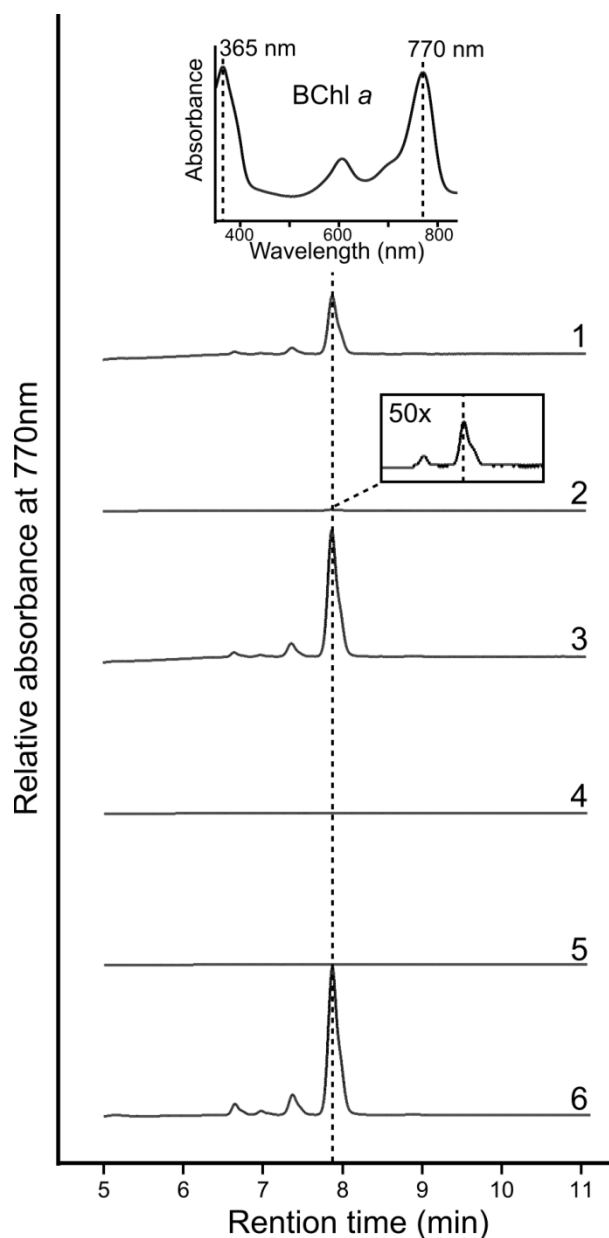
Figure 4.7 HPLC analysis of pigments extracted from *Rvi. gelatinosus* strains

Pigments were extracted from cells standardised by OD$_{680}$ except for the $\Delta bchE$ strain which contained much more BChl than any other strains. Trace 1, $\Delta bchE\Delta acsF$::rsp_6110-*acsF*^{Rs}; trace 2, $\Delta bchE\Delta acsF$::*acsF*^{Rs}; trace 3, $\Delta bchE\Delta acsF$::*cycI-ycf54*; trace 4, $\Delta bchE\Delta acsF$::*cycI*; trace 5, $\Delta bchE\Delta acsF$; and trace 6, $\Delta bchE$. Additionally, the tiny peak present in trace 2 is displayed in 50 times higher for easy inspection.

4.3.9 Whole-cell absorption spectra of constructed *Rvi. gelatinosus* strains

The constructed *Rvi. gelatinosus* strains were grown aerobically in 250 ml Erlenmeyer flasks filled with 20 ml of PYS medium with shaking at 150 rpm. Cells were harvested and resuspended in 60% (w/v) sucrose solution. Whole-cell absorption spectra were recorded and normalised to the absorbance at 750 nm. As shown in **Figure 4.8**, the $\Delta bchE\Delta acsF$ $\Delta bchE\Delta acsF$::*cycI* and $\Delta bchE\Delta acsF$::*acsF*^{Rs} strains were unable to produce light-harvesting

complexes due to lack of BChl *a*, whereas the presence of light-harvesting complexes in the Δ*bchE*Δ*acsF*::*cycI-ycf54* and Δ*bchE*Δ*acsF*::rsp_6110-*acsF*^{Rs} strains are clearly visable in the absorption spectra.
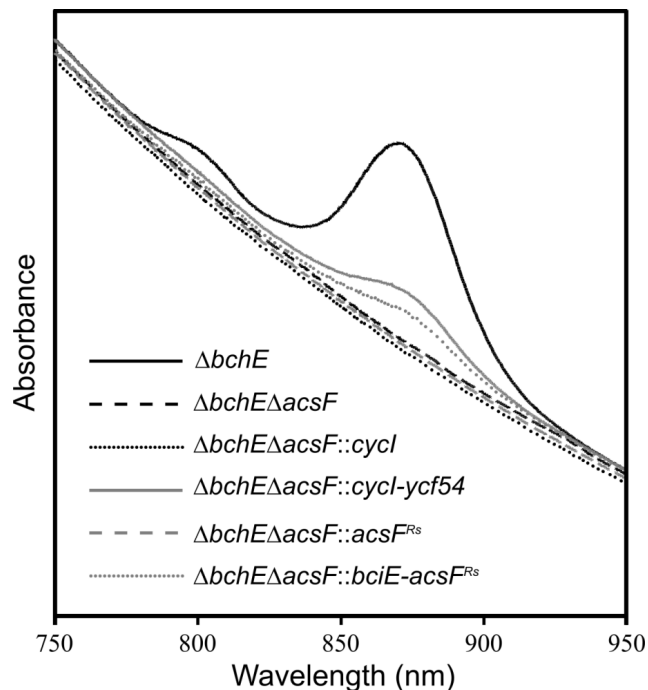
Figure 4.8 Whole-cell absorption spectra of *Rvi. gelatinosus* strains
Cell pellets were suspended in 60% (w/v) sucrose and absorption spectra were recorded. Spectra were normalised to the absorbance at 750 nm.

4.3.10 Phylogenetic analysis of AcsF homologues

To investigate the evolutionary history of AcsF homologues, phylogenetic analysis was conducted using the program MEGA6 (Tamura *et al.*, 2013). A DELTA-BLAST (Boratyn *et al.*, 2012) search was performed using *Rvi. gelatinosus* AcsF (WP_014429555) as a query against 69 phototrophs including 24 *Alphaproteobacteria*, 5 *Betaproteobacteria*, 5 *Gammaproteobacteria*, 13 cyanobacteria, 1 *Acidobacterium*, 4 *Chloroflexi*, 8 algae and 9 plants. The retrieved protein sequences were listed in **Table 4.2** and aligned using the ClustalW algorithm (Thompson *et al.*, 1994) built in the MEGA6 program. For the phylogeny construction, positions containing gaps or missing data in the alignment were removed automatically by the program, resulting in a total of 313 positions for analysis. The initial trees for the heuristic search were generated by applying the Neighbor-Joining method to a matrix of pairwise distances estimated using the Jones-Taylor-Thornton (JTT) AA substitution model (Jones *et al.*, 1992). The evolutionary history was inferred by using the Maximum

Likelihood method with the JTT model and was statistically tested by the bootstrap method with 1000 replicates.

The phylogenetic tree with the highest log likelihood (-17513.1099) was adopted and visualised using the online tool iTOL (http://itol2.embl.de/) (Letunic and Bork, 2011). The final processed tree is shown in **Figure 4.9**. AcsF proteins from species belonging to the same group are clustered in the same clade and the topology of the tree corresponds relatively well with the evolutionary relationships between the species being analysed (**Figure 4.9**). Additionally, the presence or absence of Rsp_6110 and Ycf54 homologues in the studied 69 species was checked by performing DELTA-BLAST searches using either *Rba. sphaeroides* Rsp_6110 (WP_002720458) or *Synechocystis* Ycf54 (P72777) as a query. As displayed in **Figure 4.9**, the distribution patterns of Rsp_6110 and Ycf54 homologues are apparently related with the phylogeny of AcsF proteins.

Table 4.2 Sequences used for phylogenetic analysis of AcsF Proteins

Species	AcsF Accession	Group
Acidiphilium multivorum AIU301	BAJ81253	*α-proteobacteria*
Agrobacterium albertimagni AOL15	WP_006724830	*α-proteobacteria*
Ahrensia sp. R2A130	WP_009758343	*α-proteobacteria*
Bradyrhizobium sp. BTAi1	WP_012046258	*α-proteobacteria*
Bradyrhizobium sp. ORS278	WP_011924755	*α-proteobacteria*
Brevundimonas subvibrioides ATCC 15264	ADL02380	*α-proteobacteria*
Citromicrobium bathyomarinum	WP_010236034	*α-proteobacteria*
Dinoroseobacter shibae DFL 12	WP_012180200	*α-proteobacteria*
Erythrobacter sp. NAP1	WP_007165012	*α-proteobacteria*
Hoeflea phototrophica DFL-43	WP_007196602	*α-proteobacteria*
Jannaschia sp. CCS1	WP_011453277	*α-proteobacteria*
Labrenzia alexandrii DFL-11	WP_008190570	*α-proteobacteria*
Loktanella vestfoldensis SKA53	WP_007206357	*α-proteobacteria*
Methylobacterium populi BJ001	WP_012457039	*α-proteobacteria*
Methylobacterium radiotolerans JCM 2831	WP_012318819	*α-proteobacteria*
Methylobacterium sp. 4-46	WP_012333507	*α-proteobacteria*
Methylocella silvestris BL2	WP_012591042	*α-proteobacteria*
Rhodobacter sphaeroides 2.4.1	WP_011338129	*α-proteobacteria*
Rhodobacter sp. SW2	EEW26208	*α-proteobacteria*
Rhodopseudomonas palustris CGA009	WP_011157111	*α-proteobacteria*
Rhodospirillum centenum SW	ACI99494	*α-proteobacteria*
Roseobacter denitrificans OCh 114	ABG29864	*α-proteobacteria*
Roseobacter litoralis OCh 149	WP_013984635	*α-proteobacteria*
Sphingomonas echinoides	WP_010405227	*α-proteobacteria*
Limnohabitans sp. Rim28	WP_019425982	*β-proteobacteria*
Limnohabitans sp. Rim47	WP_019429114	*β-proteobacteria*
Methyloversatilis universalis FAM5	WP_008064773	*β-proteobacteria*
Rubrivivax benzoatilyticus JA2	WP_009857119	*β-proteobacteria*
Rubrivivax gelatinosus IL144	WP_014429555	*β-proteobacteria*
Congregibacter litoralis KT71	WP_008296305	*γ-proteobacteria*
gamma proteobacterium HIMB55	WP_009470378	*γ-proteobacteria*
gamma proteobacterium NOR5-3	EED32399	*γ-proteobacteria*
Luminiphilus syltensis NOR5-1B	WP_009019082	*γ-proteobacteria*
marine gamma proteobacterium HTCC2080	EAW41193	*γ-proteobacteria*
Chloracidobacterium thermophilum B	WP_014099867	*Acidobacteria*

Species	AcsF Accession	Group
Chloroflexus aurantiacus J-10-fl	WP_012258449	*Chloroflexi*
Chloroflexus sp. MS-G	WP_035419164	*Chloroflexi*
Roseiflexus castenholzii DSM 13941	WP_012120062	*Chloroflexi*
Roseiflexus sp. RS-1	WP_011956640	*Chloroflexi*
Acaryochloris marina MBIC11017	WP_012162779	Cyanobacteria
cyanobacterium PCC 7702	WP_017306724	Cyanobacteria
Cyanothece sp. PCC 7425	WP_012629697	Cyanobacteria
Fischerella sp. PCC 9605	WP_026733301	Cyanobacteria
Myxosarcina sp. GI1	WP_036481222	Cyanobacteria
Nostoc sp. PCC 7120	WP_010997451	Cyanobacteria
Nostoc sp. PCC 7524	WP_015137252	Cyanobacteria
Oscillatoriales cyanobacterium JSC-12	WP_009555072	Cyanobacteria
Spirulina subsalsa	WP_017306724	Cyanobacteria
Synechococcus sp. PCC 7002	WP_012306336	Cyanobacteria
Synechocystis sp. PCC 6803	WP_010871211	Cyanobacteria
Synechocystis sp. PCC 7509	WP_009632883	Cyanobacteria
Thermosynechococcus elongatus BP-1	WP_011057266	Cyanobacteria
Bathycoccus prasinos	XP_007511675	Green algae
Chlamydomonas reinhardtii	XP_001692557	Green algae
Coccomyxa subellipsoidea C-169	XP_005650693	Green algae
Ostreococcus tauri	CEG01862	Green algae
Bangia fuscopurpurea	AKE98877	Red algae
Porphyra purpurea	NP_053887	Red algae
Porphyra umbilicalis	AFC39946	Red algae
Pyropia haitanensis	YP_007947806	Red algae
Arabidopsis thaliana	NP_191253	Plants
Cucumis sativus	XP_004144646	Plants
Hordeum vulgare	AAW80518	Plants
Ipomoea nil	AAB19120	Plants
Marchantia polymorpha	BAP05434	Plants
Nicotiana tabacum	AAO89565	Plants
Oryza sativa Japonica Group	NP_001042745	Plants
Triticum aestivum	CDM82987	Plants
Zea mays	XP_008655474	Plants
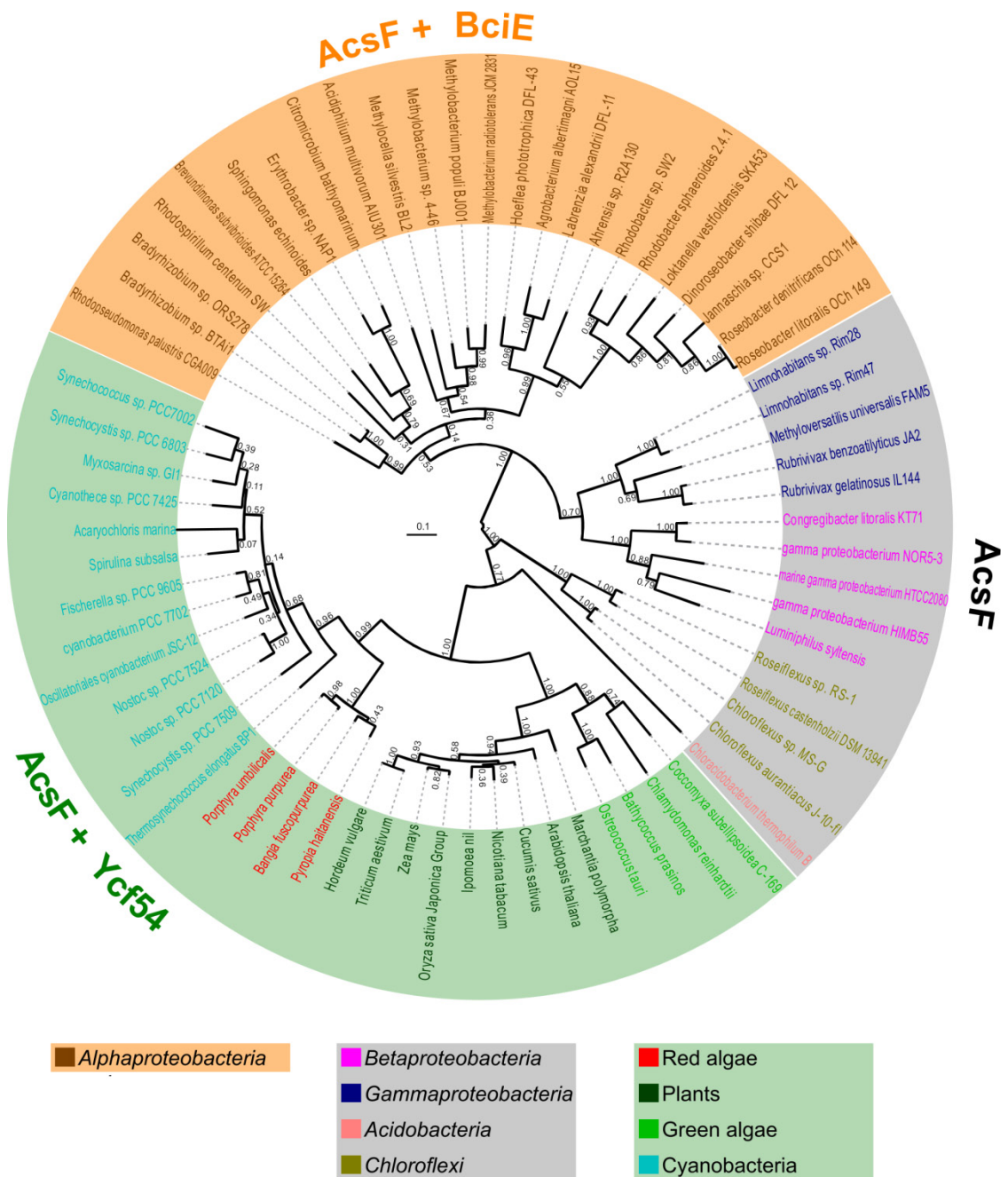
Figure 4.9 Phylogenetic tree of AcsF proteins

The evolutionary analysis was conducted in MEGA6 by using the Maximum Likelihood method based on the JTT matrix-based model. The analysis involved 69 protein sequences. The tree with the highest log likelihood (-17513.1099) is shown. Numbers next to each node indicate bootstrap values (1000 replicates) as percentages. Phyla are distinguished by the colours of species' names. The length of each branch represents the number of amino acid substitutions per site in proportion to the scale bar which is drawn at the centre of the tree. The presence/absence of BciE and Ycf54 are indicated by the colour of shadow over the species' names: grey shadow = no BciE or Ycf54; orange shadow = BciE only; and green shadow = Ycf54 only.

4.4 Discussion

4.4.1 *Rvi. gelatinosus acsF* can complement the loss of *cycI* in *Synechocystis*

To date, several cases have been reported in which a Chl biosynthesis enzyme was shown to be functional when heterologously expressed in an anoxygenic phototroph and these enzymes include POR (Suzuki and Bauer, 1995b), the GG reductase (ChlP) (Addlesee *et al*., 1996; Hitchcock *et al*., 2016) and the Chl synthase (ChlG) (Hitchcock *et al*., 2016). In the opposite direction, there has only been one report in which the DVR (BciA) from *Rba. sphaeroides* was demonstrated to be able to catalyse the 8-vinyl reduction in a *Synechocystis* Δ*bciB* mutant (Canniffe *et al*., 2013). Despite a high degree of sequence identity (42%) shared by the *Synechocystis* CycI and the *Rvi. gelatinosus* AcsF, no experimental evidence had been reported that the *Synechocystis* CycI can function in *Rvi. gelatinosus* or vice versa when this project was started. As is essential in *Synechocystis*, the *cycI* gene cannot be fully deleted. If a *cycI* homologue can function in *Synechocystis*, a full deletion of the *cycI* gene should be achieved in a *Synechocystis* strain expressing the *cycI* homologue of interest. This strategy was applied to *Rvi. gelatinosus acsF* and a fully segregated *acsF*$^{Rg+}$Δ*cycI* strain of *Synechocystis* was accomplished (**Figure 4.3 B**). The successful construction of the strain alone provided strong evidence to support that the *Rvi. gelatinosus acsF* can complement the loss of *cycI* in *Synechocystis.* Further phenotypic analyses of constructed *Synechocystis* strains revealed that the complemented strain produces a comparable level of Chl to that of WT and is competent for autotrophic growth (**Figure 4.4**). To our knowledge, this is the first successful replacement of a Chl biosynthetic enzyme in an oxygenic phototroph with the homologous enzyme from a BChl-producing organism.

(B)Chl biosynthesis is a complex process involving a number of enzymes, which from Proto are 7 enzymes and 10 enzymes for synthesising Chl *a* and BChl *a*, respectively. As porphyrin molecules, the intermediates of (B)Chl biosynthesis are both hydrophobic and phototoxic. A sophisticated mechanism is required to protect cell from the aggregation and photooxidative damage of (B)Chl precursors. It has been proposed that the (B)Chl intermediates could be channelled from one enzyme to the other without being released until the mature (B)Chl molecules are assembled into PS (Eckhardt *et al*., 2004; Hollingshead, 2014). This substrate channelling idea is appealing and relies on extensive protein-protein interactions between (B)Chl biosynthetic enzymes. It has been partially supported by the mutual dependence between ChlH (the H subunit of the Mg-chelatase) and ChlM (MgP methyltransferase)

(Hinchigeri *et al.*, 1997; Shepherd *et al.*, 2005; Alawady *et al.*, 2005). In *Arabidopsis*, a chloroplast membrane complex has been identified containing FLU (a negative regulator of Chl biosynthesis), CHL27 (AcsF homologue), PORB, PORC and ChlP (Kauss *et al.*, 2012). Additionally, a protein-protein interaction network for Chl biosynthetic enzymes has been established based on a series of *in vivo* FLAG pulldown experiments conducted in *Synechocystis* (Hollingshead, 2014). Inside the network, CycI has been found to physically interact with POR, DVR and ChlP (Hollingshead *et al.*, 2016).

The phenotype of the *acsF*$^{Rg+}$*ΔcycI* strain of *Synechocystis* (**Figure 4.4**) indicates that *Rvi. gelatinosus* AcsF is able to incorporate into the Chl biosynthesis pathway in *Synechocystis*. In the pathway, the aerobic cyclase step is followed by the reduction of PChlide (Canniffe *et al.*, 2014), which can be catalysed by POR or DPOR in *Synechocystis*. Considering *Rvi. gelatinosus* only possesses DPOR, it seems reasonable to speculate that the *Rvi. gelatinosus* AcsF would solely interact with DPOR in the hybrid *acsF*$^{Rg+}$*ΔcycI* strain of *Synechocystis*. Kopecna *et al.* (2013) reported a *Synechocystis* strain lacking POR which contained only 20% of the WT Chl level when grown photoautotrophically under moderate light conditions (30 μE m^{-2} s^{-1}). Under exactly the same conditions, the *Synechocystis acsF*$^{Rg+}$*ΔcycI* strain contained 96% of WT Chl level (**Figure 4.4 B**). This suggests that the *Rvi. gelatinosus* AcsF can cooperate with POR in *Synechocystis* in a similar way as the native CycI. To confirm this idea, it was decided to construct a strain that lacks DPOR in the *acsF*$^{Rg+}$*ΔcycI* background by replacing the *chlB* gene (slr0772, encoding one subunit of DPOR) with a zeocin resistance cassette (Canniffe *et al.*, 2014). A fully segregated *acsF*$^{Rg+}$*ΔcycIΔchlB* strain was easily achieved, which did not differ from *acsF*$^{Rg+}$*ΔcycI* when grown under constant illumination (data not shown). Likewise, the *Rvi. gelatinosus* AcsF may also interact with the DVR and ChlP of *Synechocystis* in order to ensure effective production of Chl in the *acsF*$^{Rg+}$*ΔcycI* strain. In the future, the interaction profile between *Rvi. gelatinosus* AcsF and the *Synechocystis* Chl biosynthetic enzymes can be established by conducting *in vivo* pulldown experiments using FLAG-tagged AcsF as a bait in *Synechocystis.*

4.4.2 *Rvi. gelatinosus* AcsF does not require Ycf54 for complementing the loss of CycI in *Synechocystis*

Despite the broad distribution of Ycf54 among oxygenic phototrophs including cyanobacteria, algae and plants, no Ycf54 homologue can be found in any anoxygenic phototroph containing functional aerobic cyclase. The fact that some aerobic cyclases can function without Ycf54 homologues is consistent with the conclusion that Ycf54 is not essential for aerobic cyclase

activity (Hollingshead *et al.*, 2016). However, removal of Ycf54 decreases the levels of CycI and ChlP, and also significantly disrupts the interactions between CycI, POR, DVR and ChlP, resulting in a dramatic decrease in Chl biosynthesis in *Synechocystis* (Hollingshead *et al.*, 2016). Although the exact role played by Ycf54 is not known, it is conceivable that the role must be highly relevant to aerobic cyclase since Ycf54 was discovered by *in vivo* pulldown experiments using FLAG-tagged CycI and CycII (Hollingshead *et al.*, 2012). As the interaction between Ycf54 and the Chl biosynthetic enzymes other than aerobic cyclase could not be identified by *in vivo* FLAG pulldown experiments (Hollingshead, 2014), it is less likely that Ycf54 is a mediator or a scaffold protein to facilitate the interactions between aerobic cyclase and other Chl biosynthetic enzymes. Instead, Ycf54 may play an important role to stabilise the CycI protein, which could explain the significantly reduced interactions between CycI, POR, DVR and ChlP upon removal of Ycf54. Nevertheless, the possibility that Ycf54 enhances the catalytic activity of CycI cannot be ruled out at this stage.

Is *Rvi. gelatinosus* AcsF vulnerable to an as-yet unidentified mechanism that destabilises CycI in *Synechocystis*? To answer this question, deletion of *ycf54* was conducted in the *acsF*$^{Rg+}$Δ*cycI* strain and a fully segregated *acsF*$^{Rg+}$Δ*cycI*Δ*ycf54* strain was achieved without any problem. With respect to the analysed phenotypic characteristics, no difference can be spotted between the *acsF*$^{Rg+}$Δ*cycI* and *acsF*$^{Rg+}$Δ*cycI*Δ*ycf54* strains (**Figure 4.4**). Additionally, the *Synechocystis* Δ*ycf54* mutant described in Section 4.3.3 can be greatly improved by simply expressing the *Rvi. gelatinosus acsF* in this strain (data not shown). It is apparent that *Rvi. gelatinosus* AcsF does not require Ycf54 to complement the loss of CycI in *Synechocystis*. The sequence difference between *Rvi. gelatinosus* AcsF and CycI may keep AcsF from being recognised by the mechanism responsible for the destabilisation of CycI, and make AcsF a more active enzyme than CycI in the absence of Ycf54.

4.4.3 Rsp_6110 is a new subunit of the aerobic cyclase in *Rba. sphaeroides*

The ORF, rsp_6110, is located immediately upstream of the *acsF* gene (rsp_0294) in the PGC of *Rba. sphaeroides*. The homologues of Rsp_6110 can be identified in all the AcsF-containing *Alphaproteobacteria* listed in Boldareva-Nuianzina *et al.* (2013) (**Table 4.1**). The function of rsp_6110 was investigated by knocking it out in a *Rba. sphaeroides* Δ*bchE*Δ*ccoP* strain of which the activity of aerobic cyclase has been demonstrated in Chapter 3. The resulting Δ*bchE*Δ*ccoP*Δrsp_6110 strain was unable to synthesise BChl due to lack of a functional aerobic cyclase (**Figure 4.5 B**). The activity of the aerobic cyclase was restored when rsp_6110 was expressed from a plasmid construct (**Figure 4.5 B**). This *in trans* complementation

eliminates the possibility that the effect of deletion of rsp_6110 is from the disruption of cotranscription between rsp_6110 and *acsF* (rsp_0294). Thus, it is rational to propose that rsp_6110 encodes a new subunit of aerobic cyclase in *Rba. sphaeroides*. According to the nomenclature for bacterial genetics suggested by Demerec *et al*. (1966), rsp_6110 was assigned as the *bciE* gene.

```
2.4.1     ----------M-GLFTKQAEEVPCTVEVSHQFESLHAHVRFDNGAIVHPGDEVLVHGAPVLAAFGEVVVEERTATI
OCh_114   ----------M-GLLTKDFERAPCTVEISHKFESLHAHVRFNNGAVIYPGDEVQVHGGEIMAPFGEVISEDREATI
DFL_12    ----------M-GFFTKTRETAPCTVSISHRFEELSAHVKFNNGAVVYPGDEVLVQGAEIMAPYGEVVSEDRIAVI
CCS1      ----------M-GLLTRDFEMAPCEVEVSHCFDSLHAHVKFLNGATINPGDEVQVKGPPVMAPYGEVVREERMARI
AOL15     ----------M-----RRRETVDCTVEINNTFEALGAHIRFDNGVVVHPGDEVLVHGAPVQIPYGSCQNFRRKATI
SKA53     ----------M-GLFLRETETAPCTVTISHRFEELSAHVRLDNGAIIYPGDTVQVQGPEIMAAFGELIEEKRTAVI
CGA009    ----------MFGLGKRTSFDVPCTVEIEQTSETLHAHVVLDGDIEIGPGDEVLVHDAPTHVDFGERLVVRRTATV
BJ001     MAAANIRGADM-AWIGKTIVEVPCTVEIEQTPESLHAHVTLDAGFEIEPGDEVQVHDAPTEIPYGERLTVRRTATV
                                    #

2.4.1     TRASGLERLWTRLTGDLGAMELCEFSFSEQVTL
OCh_114   IRASKLERLWTRLTGDFEVMELCEFSFSEEVKL
DFL_12    TRASGLERLWTRMTGDLEFIELCEFSFSEEVTL
CCS1      TRASKLEQLWTRMTGDFEFMELCEFSFSEEVSV
AOL15     TRAGFLERAWTRATGDLDMMELCEFSFTERALS
SKA53     TRASKLEQLWTRATGDFEFMELCEFSFSDEVLS
CGA009    VRAGLLDKIRARFEGYRELTELYEVSFSTGRVQ
BJ001     TRAGRLERAWTKLIAHLELTELYEVSFSERRKL
```

Figure 4.10 Amino acid sequence alignments of BciE proteins

The alignments were generated using T-coffee. Sequences are those from *Rba. sphaeroides* 2.4.1 (2.4.1), *Roseobacter denitrificans* Och 114 (Och144), *Dinoroseobacter shibae* DFL12 (DFL12), *Jannaschia* sp. strain CCS1 (CCS1), *Agrobacterium albertimagni* AOL15 (AOL15), *Loktanella vestfoldensis* SKA53 (SKA53), *Rhodopseudomonas palustris* CGA009 (CGA009) and *Methylobacterium populi* BJ001 (BJ001). Conserved, highly similar and similar residues are highlighted in black, dark grey and light grey, respectively. The conserved cysteine residue is marked by a blue hash (#).

Two conserved cysteine residues (Cys13 and Cys88, numbering in *Rba. sphaeroides*) are revealed by the sequence alignments of BciE proteins from *Rba. sphaeroides*, *Roseobacter denitrificans* Och 114, *Dinoroseobacter shibae* DFL12, *Jannaschia* sp. strain CCS1, *Agrobacterium albertimagni* AOL15 and *Loktanella vestfoldensis* SKA53 (**Figure 4.10**). When these two cysteine residues were mutated to glycines, the mutant BciE lost its activity (**Figure 4.5 B**). Surprisingly, if the sequence alignments include two more BciE proteins from *Rhodopseudomonas palustris* CGA009 and *Methylobacterium populi* BJ001, only the Cys13 is conserved (**Figure 4.10**). Thus, a mutant BciE that only has the Cys13 mutated needs to be tested before drawing a conclusion regarding the conserved cysteine residue. No conserved domain can be identified in BciE based on the NCBI Conserved Domain Database (Marchler-Bauer and Bryant, 2004; Marchler-Bauer *et al*., 2015). BciE may represent a novel protein family with unique folding which can be disclosed by structural determination in the future.

4.4.4 There are at least three classes of aerobic cyclase existing in nature

The pK18*mobsacB*-based method, used for generation of markerless in-frame mutants in *Rba. sphaeroides*, has been proved to be also applicable in *Rvi. gelatinosus*, facilitating the test of aerobic cyclases from *Rba. sphaeroides* and *Synechocystis* in the *Rvi. gelatinosus* platform. As the foreign aerobic cyclase encoding genes were placed under the native *acsF* promoter in *Rvi. gelatinosus* (**Figure 4.6 B**), the transcription levels of the introduced genes should be considered similar to that of *acsF* in the Δ*bchE* strain. HPLC analysis revealed that in *Rvi. gelatinosus* the *Synechocystis* CycI was only functional when co-expressed with Ycf54 (**Figure 4.7**). A residual activity of aerobic cyclase may be displayed by the *Rba. sphaeroides* AcsF alone, which was dramatically boosted by the inclusion of *Rba. sphaeroides* BciE (**Figure 4.7**). Furthermore, the BChl biosynthesis was restored to a substantial level that allowed assembly of the light-harvesting complexes in the Δ*bchE*Δ*acsF*::*cycI-ycf54* and Δ*bchE*Δ*acsF*::*bciE-acsF*^{Rs} strains (**Figure 4.8**). Taken together these findings with the obvious effects of Δ*ycf54* in *Synechocystis* and Δ*bciE* in *Rba. sphaeroides*, it is rational to conclude that both the Ycf54 and BciE are authentic subunits of the aerobic cyclase.

Synechocystis does not possess a BciE homologue and no homologue of Ycf54 can be found in *Rba. sphaeroides*. In the case of *Rvi. gelatinosus,* neither the BciE nor the Ycf54 homologue is present. Clearly, the subunit composition of aerobic cyclase varies among these three investigated species. It is of great interest to elucidate whether the variation is widespread across phototrophs or just limited within several particular species. Therefore, the distribution of BciE and Ycf54 homologues among different groups of phototrophs was surveyed (**Figure 4.9**). The evolutionary history of the AcsF protein, the common catalytic subunit of aerobic cyclase, was investigated based on 69 AcsF protein sequences representing photosynthetic organisms from *Proteobacteria*, cyanobacteria, *Acidobacteria*, *Chloroflexi*, algae and plants (**Figure 4.9**). Without doubt, the difference in subunit composition of aerobic cyclase is a general phenomenon, calling for a reclassification of aerobic cyclases. According to the distribution patterns of BciE and Ycf54 homologues, we propose that there are at least three classes of aerobic cyclase utilised by phototrophs. The Class I aerobic cyclase possessed by phototrophic *Alphaproteobacteria* requires BciE for activity. All anoxygenic phototrophs excluding the ones from *Alphaproteobacteria* employ the Class II aerobic cyclase, of which the only known subunit so far is AcsF. The Class III aerobic cyclase requires Ycf54 for function and is present in all oxygenic phototrophs including cyanobacteria, algae and plants. The requirement of a facilitating subunit, BciE or Ycf54, is closely related with the phylogeny of

AcsF proteins. Based on the complementation tests conducted in *Rvi. gelatinosus* (**Figure 4.7**), the relationships between the known subunits of aerobic cyclase can be summarised as shown in **Figure 4.11.** At this stage, there is no clue regarding possibly existent missing subunit(s), which will be addressed in the remaining chapters.
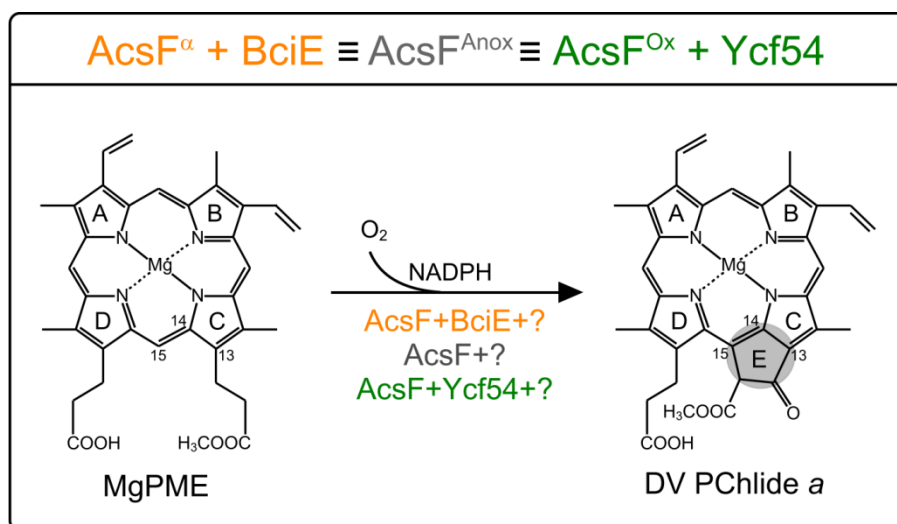
Figure 4.11 Updated knowledge of the aerobic cyclase

The aerobic cyclase converts MgPME to DV PChlide *a* via the formation of the isocyclic E ring using molecular oxygen. NADPH is believed to be a cofactor for aerobic cyclase. The subunit composition of aerobic cyclase varies across phototrophs, as summarised by the equation shown in this figure. In this equation, $AcsF^{\alpha}$, $AcsF^{Anox}$ and $AcsF^{Ox}$ represent AcsF proteins from phototrophic *Alphaproteobacteria*, anoxygenic phototrophs and oxygenic phototrophs, respectively.

4.4.5 The evolution of aerobic cyclase in prokaryotic phototrophs

The phylogeny of AcsF proteins and the variety of aerobic cyclase together with published evolutionary relationships between prokaryotic phototrophs provides an excellent opportunity to probe the origin and evolution of aerobic cyclase. As cyanobacteria are generally considered to be the progenitors of chloroplasts in eukaryotic phototrophs, it is plausible that eukaryotic phototrophs may have inherited the aerobic cyclase encoding genes directly from cyanobacteria. This would be consistent with the fact that plants, algae and cyanobacteria all contain the Class III aerobic cyclase and they are clustered well in a clade of the phylogenetic tree of AcsF proteins (**Figure 4.9**). Thus, the following discussion only concerns prokaryotic phototrophs for simplicity. Six major distinct groups of bacteria have been found to be capable of photosynthesis (Blankenship, 2014). Five groups are anoxygenic phototrophs, which are purple bacteria (members of *Proteobacteria*), green sulfur bacteria

(members of *Chlorobi*), filamentous anoxygenic phototrophs (also known as green non-sulfur bacteria, members of *Chloroflexi*), *Heliobacteria* (members of *Firmicutes*) and *Chloroacidobacteria* (members of *Acidobacteria*). Only the cyanobacterial group performs oxygenic photosynthesis. Recently, *Gemmatimonadetes* has been documented to be the seventh bacterial phylum that contains phototrophic species (Zeng *et al.*, 2014). As *Gemmatimonadetes* was suggested to have acquired a PGC through horizontal transfer from purple bacteria (Zeng *et al.*, 2014), it is not included for discussion. As strict anaerobes, green sulfur bacteria and *Heliobacteria* do not contain aerobic cyclase, and thus are not included either.

AcsF is the key subunit of aerobic cyclase and is shared by all the three classes of aerobic cyclase. Therefore, the phylogeny of AcsF is informative for illuminating the evolution of aerobic cyclase. AcsF is highly conserved among all the four groups being investigated here, suggesting a common ancestor for AcsF. In addition, it is difficult to believe that the *acsF* gene could have evolved in anoxygenic phototrophs since they originated from anaerobes. Considering oxygenic cyanobacteria were naturally exposed to oxygen, it is likely that the *acsF* gene came first in cyanobacteria (Boldareva-Nuianzina *et al.*, 2013). We hypothesise that anoxygenic phototrophs may have adopted the *acsF* gene from cyanobacteria via horizontal gene transfer. The *Proteobacteria* clade of the tree shown in **Figure 4.9** corresponds well with the 16S rRNA-based phylogeny of *Proteobacteria* species presented in the supplemental material of Boldareva-Nuianzina *et al.* (2013). This implies that phototrophic *Proteobacteria* may have acquired the *acsF* gene in a single event which occurred before the diversification of *Alpha-*, *Beta-*, and *Gamma-proteobacteria*.

The cases of *Acidobacteria* and *Chloroflexi* seem more complicated. For clarity, the tree shown in **Figure 4.9** is simplified to only display the relative positions of the four phyla of phototrophic bacteria with all the eukaryotic clades being omitted and subtrees being compressed (**Figure 4.12 A**). The evolutionary relationships between cyanobacteria, *Chloroflexi*, *Acidobacteria* and *Proteobacteria* are displayed in **Figure 4.12 B**, which is based on the three phylogenetic models reviewed in Cardona (**2015**). Cyanobacteria are closer to *Chloroflexi* and *Acidobacteria* closer to *Proteobacteria* (**Figure 4.12 B**). However, cyanobacterial AcsF proteins are closer to those from *Acidobacteria*, whilst there is more homology between AcsF proteins from *Chloroflexi* and *Proteobacteria* (**Figure 4.12 A**). The obvious discrepancy in the overall topology between the relationships depicted in **Figure 4.12 A** and **Figure 4.12 B** implies the possibility of horizontal transfer of the *acsF* gene. It is likely

that the *acsF* gene was transferred from cyanobacteria to the common ancestor of *Acidobacteria* and *Proteobacteria*, followed by a sequential transfer from *Proteobacteria* to *Chloroflexi* (**Figure 4.12 B**).
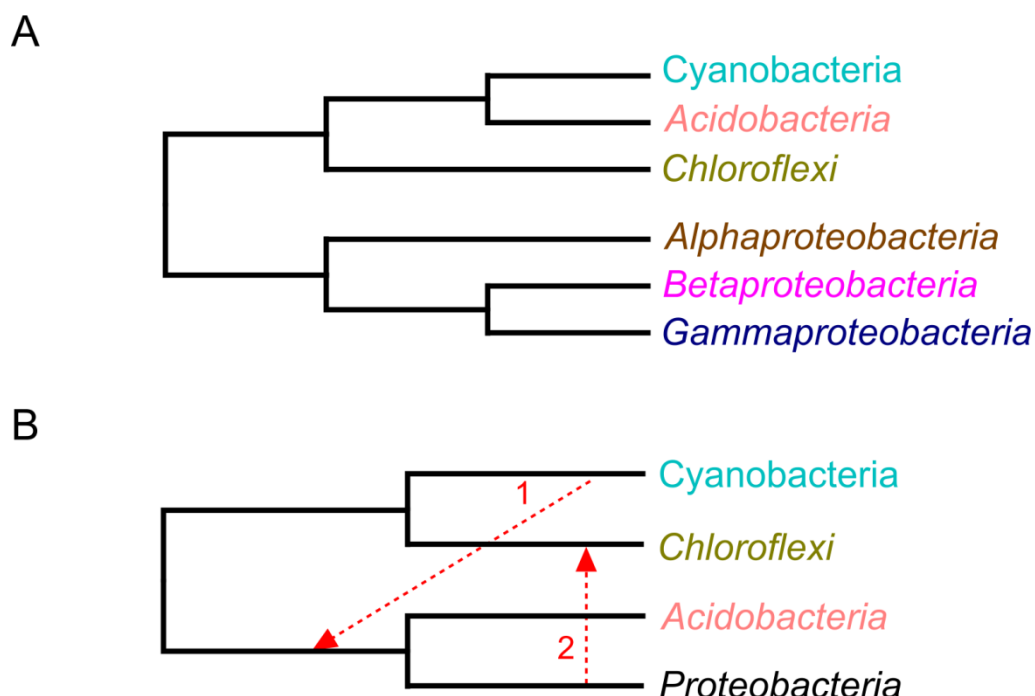
Figure 4.12 Proposed horizontal transfers of the *acsF* gene

(**A**) Schematic phylogenetic tree of AcsF proteins. The tree was simplified from the original tree shown in **Figure 4.8**. Only the topology of the prokaryotic phyla is shown. (**B**) Evolutionary relationships of the four prokaryotic AcsF-containing phyla with arrows indicating the proposed horizontal transfers of the *acsF* gene.

Given that *ycf54* is only present in cyanobacteria, it may not have been transferred together with the *acsF* gene as these two genes are usually not adjacent to each other in the cyanobacterial genome. Alternatively, *ycf54* may have emerged in cyanobacteria after the horizontal gene transfer. After the acquisition of the *acsF* gene from cyanobacteria, anoxygenic phototrophs may have accumulated mutations in the *acsF* gene, which freed AcsF from the dependence on Ycf54. The evolution of Ycf54-independent AcsF can even be imitated under laboratory conditions, which will be demonstrated in Chapter 5. By applying selection pressures on the *Synechocystis* Δ*ycf54* mutant, four suppressor mutants were isolated and genomic sequencing of these mutants revealed two of them both harbour an *acsF* gene encoding a D219G alteration. This mutated AcsF was subsequently confirmed to be functional in the absence of Ycf54. Regarding the *bciE* gene, it is rational to suggest that this gene appeared after the divergence of *Alphaproteobacteria* from other subgroups of

Proteobacteria. The emergence of the *bciE* gene may be beneficial or even necessary for AcsF to function in the particular cellular conditions of *Alphaproteobacteria.*

Nevertheless, the proposals here regarding the origin and evolution of aerobic cyclase are still hypothetical. Phylogenetic analysis of AcsF using much larger dataset should be conducted in the future. Phylogenetic analysis of Ycf54 and BciE will be informative. The evolutionary analysis of the (B)Chl biosynthesis pathway and phototrophy will help to position the evolution of aerobic cyclase within a bigger picture. On the other hand, it is possible to induce microevolution of aerobic cyclase under carefully designed laboratory conditions, which can serve as a test for certain theories.

Chapter 5

Microevolution towards photosynthetically competent Δ*ycf54* strain of *Synechocystis* sp. PCC6803

5.1 Summary

This chapter reports the identification of two spontaneous suppressor mutations arising in a Δ*ycf54* mutant of *Synechocystis*. Four suppressor mutants were isolated with significantly improved Chl biosynthesis and photoautotrophic growth, designated as SM1 to SM4, among which SM1 and SM4 exhibit near-WT phenotypes. Ultra-deep genomic sequencing revealed both SM1 and SM4 harbour a D219G mutation in the *cycI* gene. Additionally, the slr1916 gene was found to be substantially mutated after 129 WT residues in SM1 and after 104 WT residues in SM4 from a total of 283. The identified suppressor mutations were introduced into the Δ*ycf54* mutant, resulting in 'artificial' suppressor mutants. According to whole-cell absorption spectroscopy and drop growth assays, the suppressor effects present in SM1 and SM4 are reproduced in the 'artificial' suppressor mutants. The D219G mutation was shown to be able to free the dependence of CycI on Ycf54. Inactivation of the slr1916 gene was observed to cause suppression of photomixotrophic growth. Further study is required to uncover the mechanisms behind the suppressor mutations identified in the *cycI* and slr1916 genes.

5.2 Introduction

In addition to CycI and Ycf54, it was proposed that the aerobic cyclase contains at least two unknown subunits (Bollivar *et al.*, 2014). *In vivo* FLAG pulldown experiments combined with mass spectrometry has been demonstrated to be useful in the identification of Ycf54 (Hollingshead *et al.*, 2012). A series of comprehensive FLAG pulldown experiments were reported by Hollingshead (2014). Even though N-terminal and C-terminal FLAG-tagged CycI, CycII and Ycf54 were all used as bait, these pulldown experiments did not disclose any new candidate for the subunit of aerobic cyclase. It is likely that the procedures used for FLAG pulldown experiments with *Synechocystis* are not gentle enough to maintain protein-protein interaction between known and unknown subunits of the aerobic cyclase. Thus, other methods are required in order to search for any unknown subunits.

Synechocystis contains multiple copies of its genome, which makes it easier to tolerate mutations than organisms containing a single copy of their genome. As a result, *Synechocystis* is prone to accumulate mutations during cultivation. The generation of substrains from the same original strain in different laboratories is very common. Several of such substrains have been sequenced, revealing lots of mutations in the Kazusa strain which is the first *Synechocystis* strain to be sequenced (Kaneko *et al.*, 1996; Tajima *et al.*, 2011; Traumann *et al.*, 2012; Ding *et al.*, 2015; Tichy *et al.*, 2016). Spontaneous suppressor mutations can occur easily in *Synechocystis* mutants subjected to selection pressures. The isolation of suppressor mutants have been widely used and shown to be powerful for identification of new genes or new mutations associated with a certain function or phenotype (Huang *et al.*, 2001; Yu *et al.*, 2003; Chandler *et al.*, 2003; Kobayashi *et al.*, 2005; Nishijima *et al.*, 2015). In this chapter, the *Synechocystis* Δ*ycf54* strain, as reported in Hollingshead *et al.* (2016) and described in Section 4.3.3, is employed to isolate suppressor mutants with the intention of identifying new genes related with the aerobic cyclase.

5.3 Results

5.3.1 Isolation and characterisation of suppressor mutants derived from a Δ*ycf54* strain of *Synechocystis*

The Δ*ycf54* strain of *Synechocystis* is viable only when incubated mixotrophically under low light (5 μE m^{-2} s^{-1}) conditions. Dr Roman Sobotka isolated four spontaneous suppressor mutants by growing the Δ*ycf54* strain under autotrophic growth conditions with moderate light (40 μE m^{-2} s^{-1}). These suppressor mutants exhibit enhanced Chl biosynthesis and photosynthetic growth, and accumulate much less MgPME compared with the parental Δ*ycf54* strain. They were designated as SM1 to SM4. As the phenotypic improvements in SM1 and SM4 are much stronger than those in SM2 and SM3, further characterisation and investigation were mainly conducted in SM1 and SM4.
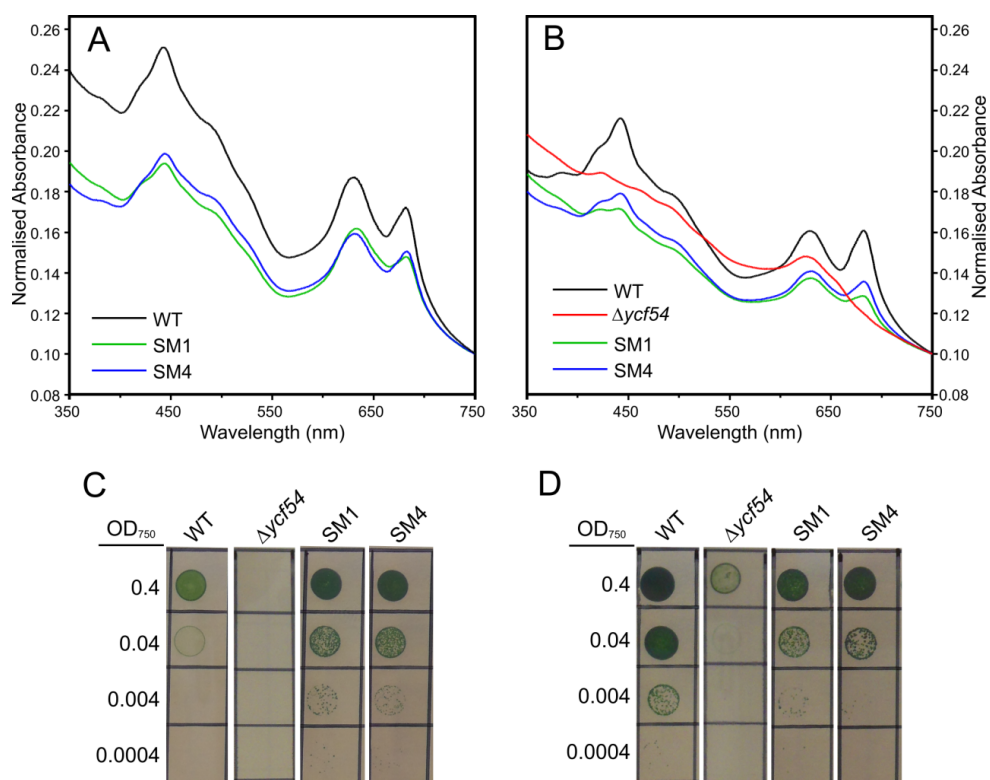
Figure 5.1 Whole-cell absorption spectra and drop growth assays of SM1 and SM4

Whole-cell absorption spectra of cultures either grown autotrophically under low-moderate (15~20 μE m^{-2} s^{-1}) light conditions (**A**) or mixotrophically under low (5 μE m^{-2} s^{-1}) light conditions (**B**) were recorded in 60% (w/v) sucrose solution. Absorbance was normalised to the absorbance at 750 nm. The Δ*ycf54* strain could not grow autotrophically under low-moderate light conditions. For drop growth assays, liquid cultures of *Synechocystis* strains grown mixotrophically under low light conditions were adjusted to OD$_{750}$ of 0.4 and subjected to serial 10-fold dilutions. 4 μl of each dilution was spotted on BG-11 agar medium without (**C**) or with (**D**) glucose. Photographs were taken after 12-day incubation under low-moderate (15 μE m^{-2} s^{-1}) light conditions.

SM1 and SM4 as well as the WT strains were grown in liquid BG-11 medium photoautotrophically under low-moderate (15~20 μE m^{-2} s^{-1}) light conditions. Cells harvested from liquid cultures were resuspendend in 60% (w/v) sucrose to minimise light scattering, and absorption spectra between 350 and 750 nm were recorded on a Cary 60 UV-Vis spectrophotometer. The acquired spectra were normalised to light scattering of 0.1 at 750 nm, as shown in **Figure 5.1 A**. To compare SM1 and SM4 with the $\Delta ycf54$ mutant which is unable to conduct autotrophic growth, *Synechocystis* strains were grown in liquid BG-11 medium supplemented with 5 mM glucose under low (5 μE m^{-2} s^{-1}) light conditions. The whole-cell absorption spectra were acquired, processed and shown in **Figure 5.1 B**. The overall spectra of SM1 and SM4 are very similar to each other and seem to shift to a lower absorption level in relation to the spectra of the WT and $\Delta ycf54$ strains. The content of Chl per optical density at 750 nm indicated by the 682 nm peak is apparently restored to a reasonable level in SM1 and SM4.

The growth rates of SM1 and SM4 under autotrophic and mixotrophic conditions were evaluated using drop growth assays on BG-11 agar medium. *Synechocystis* strains were grown photomixotrophically in liquid BG-11 medium under low (5 μE m^{-2} s^{-1}) light conditions. The liquid cultures were adjusted to OD$_{750}$ of 0.4 and subjected to 10-fold dilutions. 4 μl of each dilution were dropped on BG-11 agar medium either without or with supplementation of 5 mM glucose. The plates were incubated at 30°C under low-moderate (15 μE m^{-2} s^{-1}) light conditions for 12 days. Then photographs of the plates were taken and shown in **Figure 5.1 C** and **D**. As expected, the $\Delta ycf54$ mutant could not grow under autotrophic conditions and grew markedly slowly under mixotrophic conditions. SM1 and SM4 again exhibited similar behaviours in drop growth assays. Both SM1 and SM4 grew faster than WT under autotrophic conditions but slower than the WT in the presence of 5 mM glucose.

The content and synthesis of PS in SM1 were compared to those of the WT and $\Delta ycf54$ strains, which were reported in Hollingshead *et al.* (2016). The experiment was conducted by Dr Roman Sobotka using the same methods as described in Hollingshead *et al.* (2016). *Synechocystis* SM1 cells were radiolabelled with [^{35}S]Met/Cys mixture (Trans-label; MP Biochemicals) using a 30 min pulse. Isolated membrane proteins were separated by clear-native (CN) PAGE on a 4~14% linear gradient gel, followed by 12~20% SDS-PAGE for the second dimension. The loading for SM1 was comparable with that for WT in Hollingshead *et al.* (2016). The white-light and Chl fluorescence images of the CN-PAGE gel were recorded using LAS 4000 (Fujifilm). The two-dimensional (2D) gel was stained with Coomassie Blue and

photographed using the same imager. Then the stained gel was dried and exposed to a photophorimager plate (GE Healthcare), which was scanned by Storm (GE Healthcare).
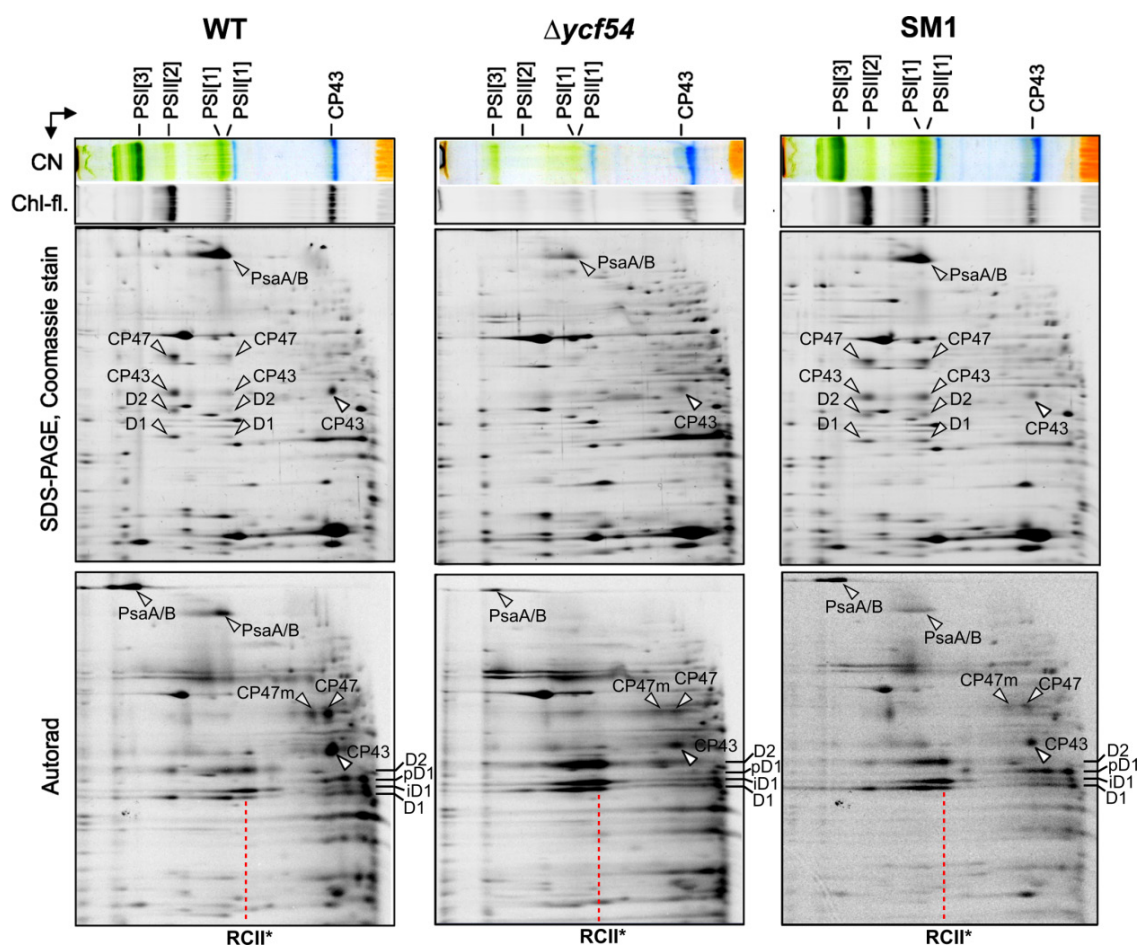
Figure 5.2 Synthesis of PSI and PSII subunits in the *Synechocystis* WT, *Δycf54* and SM1 strains

Isolated membrane proteins from *Synechocystis* cells that had been radiolabelled with [35S]Met/Cys mixture were separated by CN-PAGE on a 4~14 % linear gradient gel, followed by 12~20 % SDS-PAGE for the second dimension. Regarding the cell number, the loading for the *Δycf54* sample was 4 times as much as for the WT and SM1 samples to allow detection of weakly labelled proteins (PsaA/B) in the *Δycf54* sample. CN-PAGE gels were photographed (CN). Excited by blue light, Chl fluorescence of CN-PAGE gels was detected (Chl-fl.). 2D gels were stained with Coomassie Blue and photographed (SDS-PAGE, Coomassie stain). Then gels were dried and exposed to a phosphorimager plate to visualise labelled proteins (Autorad). Complexes and proteins were assigned according to Hollingshead *et al*. (2016). Designations: PS[3] and PS[1], trimeric and monomeric PSI; PS[2] and PS[1], dimeric and monomeric PSII; CP47m, CP47 assembly module; pD1, precursor of D1; iD1, incompletely processed D1; RCII*, the larger one of the two PSII assembly intermediates (reaction core). Shown for the WT and *Δycf54* strains were modified from Hollingshead *et al*. (2016). Shown for SM1 was kindly provided by Dr Roman Sobotka.

All the obtained images for SM1 are shown in **Figure 5.2** together with the images for the WT and Δ*ycf54* strains, which were modified from Hollingshead *et al*. (2016). It needs to be stressed that the loading for the Δ*ycf54* sample was 4 times as much as for WT and SM1 samples in order to make weakly labelled proteins (PsaA/B) detectable. Shown by the CN-PAGE images, both the PSI and PSII in SM1 are apparently restored to a WT-level. 2D electrophoresis with Coomassie Blue staining revealed that the PSI core subunits PsaA/B in SM1 were of much higher level than those in the Δ*ycf54* strain and similar to those in WT. The synthesis of both PSI trimers and monomers in SM1 during the 30 min radiolabelling was slightly lower than that of WT. In contrast, only a modest level of PSI trimer was synthesised in the Δ*ycf54* strain. The dots representing the large Chl binding subunits (D1, D2, CP47 and CP43) from both dimeric and monomeric PSII differ in intensity between WT and SM1, but were almost invisible in the 2D gel of the Δ*ycf54* strain. Considering 3 times more proteins were loaded for the Δ*ycf54* strain, the synthesis of CP43 and CP47 in SM1 was greatly improved.

The CycI levels in the four suppressor mutants were analysed by Western blot. Membrane fractions prepared from *Synechocystis* strains, corresponding to 2 μg of Chl, were separated by 12~20% SDS-PAGE. Loading of sample was checked by staining the gel with Sypro Orange. Then proteins were blotted from the SDS-PAGE gel to a polyvinylidene fluoride (PVDF) membrane. After blocking, the membrane was probed with a primary antibody raised against CHL27 (the CycI homologue in *Arabidopsis*) (Agrisera), followed by probing with a secondary antibody conjugated with horseradish peroxidase (Sigma-Aldrich). Finally, the membrane was incubated with Luminata Crescendo Western HRP substrate (Merck Millipore) before chemiluminescent signal was detected by LAS 4000 (Fujifilm). The Sypro Orange staining and Western blot are shown in **Figure 5.3 A**. In addition, the significantly reduced CycI level in the Δ*ycf54* strain as reported in Hollingshead *et al.* (**2016**) is also shown for reference (**Figure 5.3 B**). As revealed by Sypro Orange staining (**Figure 5.3 A**), the loading in **Figure 5.3 A** was not ideal, with SM1 and SM3 loaded clearly more than WT. Even so, the scale of sample overloading for suppressor mutants does not catch the scale of reduction of CycI (less than one fourth of that in WT) in the Δ*ycf54* strain. Therefore, Western blot analysis indicates increased levels of CycI in the suppressor mutants relative to the Δ*ycf54* strain.
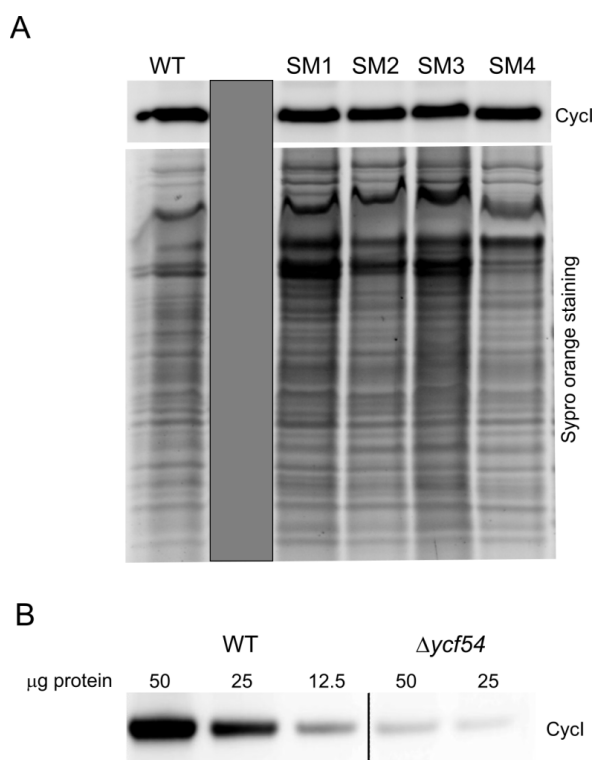
Figure 5.3 Analysis of the CycI protein levels in *Synechocystis* strains by Western blot

Membrane fractions prepared from *Synechocystis* strains were separated by SDS-PAGE and then blotted onto a PVDF membrane. CycI protein was detected by probing the membrane with antibody raised against CHL27 (CycI homologue in *Arabidopsis thaliana*) (Agrisera). (**A**) Membrane proteins corresponding to 2 μg Chl from indicated strains were separated by 12~20 % SDS-PAGE. The gel was stained with Sypro Orange before Western blot to check the loading. (**B**) The data shown was modified from Hollingshead *et al*. (2016). Membrane proteins of indicated amounts from the WT and Δ*ycf54* strains were separated by 12% NuPAGE^TM Bis-Tris precast gel (Thermo Fischer Scientific), followed by Western blot.

5.3.2 Genomic sequencing and identification of genomic variations between suppressor mutants and the Δ*ycf54* strain

In order to identify the suppressor mutations, it was decided to sequence the genomes of SM1, SM2, SM3 and SM4. Differences in genomic sequences between various *Synechocystis* substrains have been reported by several research groups (Tajima *et al*., 2011; Kanesaki *et al*., 2012; Trautmann *et al*., 2012; Ding *et al*., 2015; Tichy *et al*., 2016). Furthermore, new substrains can be generated during cultivation. Thus, to be cautious, the WT strain and the background Δ*ycf54* strain used in the present study were also included for genomic sequencing.

It is crucial to use genomic DNA with high purity and integrity for reliable next-generation sequencing. *Synechocystis* cells are known to be difficult to break due to the presence of copious extracellular polysaccharides. Vigorous physical breakage is not applicable in this case since high-quality genomic DNA is required. A method for extraction of genomic DNA from *Synechocystis* was developed based on Williams (1988) and Wilson (2001). Genomic DNA of each strain was isolated from *Synechocystis* cells collected from BG-11 agar plate as described in Section 2.5.8 and analysed by agarose gel electrophoresis and absorption spectroscopy.

Genomic DNA was fragmented by nebulisation using nitrogen gas. DNA library for paired-end sequencing were constructed from the fragmented genomic DNA using Nextera^{TM} DNA Library Preparation Kit (Illumina) with a median insert size of ~300 bp. The constructed library was subjected to 100-bp paired-end sequencing on an Illumina HiSeq 2000 platform according to the manufacturer's instructions. 9.92, 11.21, 7.03, 5.61, 5.51 and 6.64 million reads were obtained for WT, $\Delta ycf54$, SM1, SM2, SM3 and SM4, respectively. Considering the *Synechocystis* genome has a size of 3.6 Mb, these sequencing data corresponds to 502-, 567-, 178-, 284-, 279- and 168-fold coverage of the WT, $\Delta ycf54$, SM1, SM2, SM3 and SM4 genomes, respectively.

Variants were called using mapping based method. The GT-S strain was chosen as the reference strain, which is closest to the WT strain we used. The chromosomal sequence of the GT-S strain (NC_017277) (Tajima *et al*., 2011), as well as the sequences of the four large plasmids (pSYSM, NC_005229; pSYSA, NC_005230; pSYSG, NC_005231; pSYSX, NC_005232) (Kaneko *et al*., 2003) and the three small plasmids (pCA2.4, NC_020289; pCB2.4, NC_020298; pCC5.2, NC_020290) (Trautmann *et al*., 2012), was used as reference. Each read was mapped to the references using BWA (Li and Durbin, 2010) version 0.7.12 with default options. Duplicates were removed using Picard (http://broadinstitute.github.io/picard/) version 1.139 and indel intervals were locally realigned with GATK (McKenna *et al*., 2010; DePristo *et al*., 2010) version 3.5. Then single-nucleotide polymorphism (SNP) and indel variants were called using the HaplotypeCaller tool from GATK with the parameter ploidy set as 1. To further reduce false-positive errors, variants were filtered according to the following criteria: mapping quality > 0, quality score > 30, approximate read depth > 20, quality by depth > 2, genotype quality > 60 and read support > 50%. The effects of putative genetic variants were predicted using SnpEff (Cingolani *et al*., 2012) version 4.2. The variants found in the suppressor mutants but not in the $\Delta ycf54$ strain are identified as putative suppressor

mutations. In addition, variants are also found in the Δ*ycf54* strain when compared with our WT strain. The final sets of SNPs and indels found in the Δ*ycf54* strain and the suppressor mutants are listed in **Table 5.1**. More variants were found in SM1 and SM4 than in SM2 and SM3. The identified variants are not shared by different suppressor mutants except for the D219G mutation found in the *cycI* gene, which is present in both SM1 and SM4. The location within the gene encoding the catalytic subunit of aerobic cyclase and occurrence in two separate suppressor mutants highlight this D219G mutation. On the other hand, the gene slr1916, which probably encodes an esterase with 283 AAs according to CyanoBase (http://genome.microbedb.jp/cyanobase/), was found to be truncated in both SM1 and SM4. Both truncations are due to frameshift caused by a G insertion, but were at various levels with 129 AAs and 104 AAs left intact in SM1 and SM4, respectively. Truncation usually causes a huge effect on the function of a protein, especially when the truncation level is high. As it is truncated in two separate suppressor mutants, the slr1916 gene is of great interest. The two variants regarding the slr1916 gene, as well as the variant within the *cycI* gene, were validated by PCR and the Sanger sequencing. It was also confirmed that the WT, Δ*ycf54*, SM2 and SM3 strains do not contain any of these variants. Although other variants listed in **Table 5.1** may also be involved in the suppressor effects, it is rational to prioritise the examination of the D219G mutation in the *cycI* gene and truncations in the slr1916 gene.

Table 5.1 Locations and effects of SNPs and indels found in the Δ*ycf54* strain and suppressor mutants

No.	Type	Start	End	Size	NT change	AA change	Result	Gene ID	Annotation	Gene product
Δ*ycf54*										
1	S	132171	132171	1	G→A	A74T	missense	slr0742	-	hypothetical protein
2	S	446122	446122	1	T→C	-	-	trnR-CCU	-	tRNA-Arg(CCT)
3	I	3550296	3550297	6	-	-	2 additional His	sll0567	*fur*	ferric uptake regulation protein
SM1										
1	S	3613	3613	1	T→C	D219G	missense	sll1214	*cycI*	oxygen-dependent MgPME cyclase
2	D	45844	45844	1	T→*	F301L	frameshift	slr1494	-	ABC transporter
3	I	619995	619996	1	*→G	I130N	frameshift	slr1916	-	probable esterase
4	S	759568	759568	1	T→C	V247A	missense	slr2018	-	hypothetical protein
5	I	1065632	1065633	1	*→A	-	-	IGR ssr2406-sll1360	-	-
6	S	2873102	2873102	1	T→C	V41A	missense	slr0076	-	hypothetical protein
7	I	2994522	2994523	1	*→A	I510N	frameshift	slr0114	-	putative PP2C-type protein phosphatase
8	S	3255694	3255694	1	C→A	A749D	missense	slr0554	-	hypothetical protein
9	I	3364585	3364586	1	*→C	A10G	frameshift	sll1496	-	mannose-1-phosphate guanyltransferase
SM4										
1	S	3613	3613	1	T→C	D219G	missense	sll1214	*cycI*	oxygen-dependent MgPME cyclase
2	I	619923	619924	1	*→G	S105G	frameshift	slr1916	-	probable esterase
3	D	1802607	1802607	1	C→*	G118A	frameshift	sll1876	*hemN*	oxygen-independent Copro'gen oxidase
4	S	1921416	1921416	1	T→C	I159T	missense	slr1160	-	periplasmic protein with unknown function
5	S	2320583	2320583	1	T→C	Y957C	missense	sll0163	-	WD repeat protein
6	D	2595137	2595137	1	C→*	A83R	frameshift	sll0055	-	processing protease
7	S	3190324	3190324	1	T→C	V247A	missense	slr0531	*ggtD*	glucosylglycerol transport system permease protein
8	S	3425395	3425395	1	A→G	I3V	missense	ssr1256	-	hypothetical protein
SM2										
1	S	304379	304379	1	C→T	A147A	silent	slr1301	-	hypothetical protein
2	S	1507627	1507627	1	T→C	Y320C	missense	sll0252	-	protein with unknown function
3	S	1782556	1782556	1	T→C	-	-	IGR ssl3549-slr1972	-	-
4	S	2604365	2604365	1	T→C	D116G	missense	sll0462	-	hypothetical protein
5	I	2869735	2869736	1	*→A	M143I	frameshift	sll0088	-	hypothetical protein
SM3										
1	S	134878	134878	1	A→C	T148P	missense	slr0744	*infB*	translation initiation factor IF-2
2	I	143094	143095	1	*→C	L41P	frameshift	slr0241	-	hypothetical protein
3	S	1215117	1215117	1	T→C	I7T	missense	slr1871	-	transcriptional regulator
4	I	2509313	2509314	1	*→C	I267D	frameshift	sll0209	-	hypothetical protein
5	S	3265260	3265260	1	C→G	H719D	missense	slr0557	*valS*	valyl-tRNA synthetase

Only chromosomal variants are shown in this table. Nucleotide position is referred to the GT-S sequence (NC_017277). Gene ID is referred to CyanoBase (http://genome.microbedb.jp/cyanobase/). For the Δ*ycf54* strain, shown are the variants compared to WT. As large indels cannot be called accurately using short-read sequencing method, the deletion of the *ycf54* gene was not identified. For the suppressor mutants, shown are the variants compared to the Δ*ycf54* strain. The variant shared by SM1 and SM4 is marked in blue. Abbreviations: S, single-nucleotide polymorphism; D, deletion; I, insertion; IGR, intergenic region; ABC, ATP-binding cassette; PP2C, protein phosphatase 2C family; WD, Trp-Asp.

5.3.3 Introduction of suppressor mutations into the Δ*ycf54* strain

In order to check whether the mutations identified in the *cycI* and slr1916 genes play an important role in the suppressor effects, 'artificial' suppressor strains were created through introduction of the mutations into the Δ*ycf54* strain (**Table 5.2**).

Table 5.2 List of the *Synechocystis* strains described in this chapter

Strain	Characteristics	Source/Reference
WT	sp. PCC6803	R. Sobotka[a]
Δ*ycf54*	*Zeo*[R] replacement of central portion of *ycf54* in WT	S. Hollingshead[b]
SM1	Suppressor mutant 1 isolated from Δ*ycf54*	R. Sobotka
SM4	Suppressor mutant 4 isolated from Δ*ycf54*	R. Sobotka
Δslr1916	*Cm*[R] replacement of slr1916 in WT	This study
Δ*ycf54 cycI*[+]	*cycI* and *Km*[R] replacement of *psbAII* in Δ*ycf54*	R. Sobotka
Δ*ycf54 cycI*[SM+]	*cycI*[SM] and *Km*[R] replacement of *psbAII* in Δ*ycf54*	This study
Δ*ycf54*Δ::slr1916[SM1]	SM1-level (129/283)[c] truncation of slr1916 by *Cm*[R] insertion in Δ*ycf54*	This study
Δ*ycf54*Δ::slr1916[SM4]	SM4-level (104/283)[d] truncation of slr1916 by *Cm*[R] insertion in Δ*ycf54*	This study
Δ*ycf54*Δslr1916	*Cm*[R] replacement of slr1916 in Δ*ycf54*	This study
Δ*ycf54*Δ::slr1916[SM1] *cycI*[SM+]	*cycI*[SM] and *Km*[R] replacement of *psbAII* in Δ*ycf54*Δ::slr1916[SM1]	This study
Δ*ycf54*Δ::slr1916[SM4] *cycI*[SM+]	*cycI*[SM] and *Km*[R] replacement of *psbAII* in Δ*ycf54*Δ::slr1916[SM4]	This study

[a] Institute of Microbiology, Department of Phototrophic Microorganisms, Opatovicky mlyn, 379 81 Trebon, Czech Republic.
[b] This strain was reported in Hollingshead *et al*. (2016) and was described in Chapter 4.
[c] The truncated Slr1916 protein (283 AAs) in SM1 consists of the N-terminal 129 AAs.
[d] The truncated Slr1916 protein (283 AAs) in SM4 consists of the N-terminal 104 AAs.

The D219G variant (*cycI*[SM]) of the *cycI* gene was directly amplified from the genomic DNA of SM1 and subsequently cloned into the *Nde*I/*Bgl*II sites of pPD-FLAG to get the pPD[*cycI*[SM]] construct. Confirmed by sequencing, the pPD[*cycI*[SM]] plasmid was used to make the Δ*ycf54 cycI*[SM+] strain in which the *psbAII* gene was replaced by the *cycI*[SM] gene and a kanamycin resistance cassette (**Figure5.4 A**), as described in Section 4.3.1. Meanwhile, a control strain, Δ*ycf54 cycI*[+], was also generated using the pPD[*cycI*] plasmid which was constructed by cloning the native *cycI* gene into the *Nde*I/*Bgl*II sites of pPD-FLAG. Complete segregation was achieved for both mutants as confirmed by colony PCR using primers syn-psbAII UF and syn-psbAII DR (**Figure 5.4 B**).
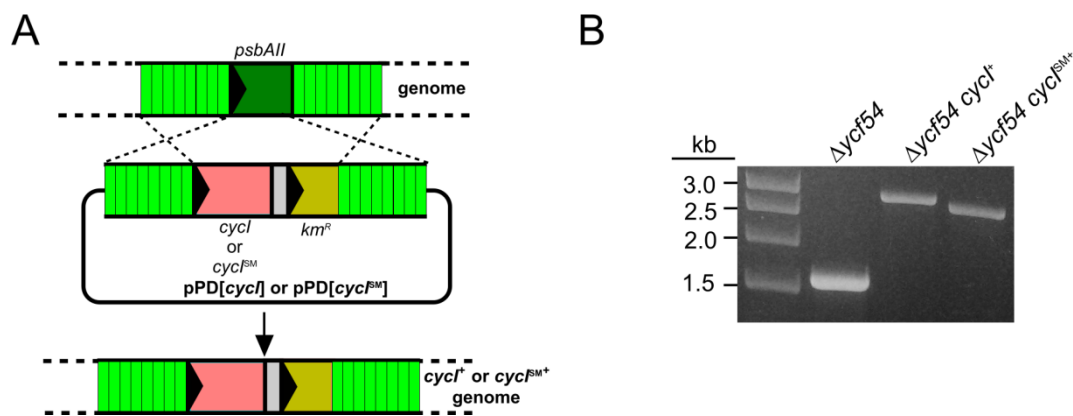
Figure 5.4 Construction of the *Synechocystis* strains expressing the *cycI* and *cycI*^SM^ genes
(**A**) Diagram displaying the replacement of the *psbAII* gene with the *cycI* gene or the *cycI*^SM^ gene in conjunction with a kanamycin resistance gene (*km*^R^). (**B**) Complete segregation was confirmed by colony PCR using primers flanking the *psbAII* gene. Lengths of PCR products: WT = 1551 bp, *cycI*⁺ = 2643 bp, *cycI*^SM+^ = 2643 bp.

As shown in **Figure 5.5 A**, the truncated Slr1916 protein in SM1 consists of 136 AAs (where there is a new stop codon) among which the C-terminal 7 AAs are not native residues. In SM4, the truncated Slr1916 protein is composed of 118 AAs with 14 non-native C-terminal AAs preceding the new stop codon at position 119. It is unlikely that these C-terminal AAs resulted from reading frame change could be important. Thus, it was decided to ignore these non-native C-terminal AAs during the construction of the 'artificial' suppressor strains. The strategy used to knockout the *cycI* gene as described in Section 4.3.2 was adopted with slight modification to create mutants with truncated variants of the slr1916 gene. Overlap extension PCR was performed to generate a construct containing a G (nucleotide), a stop codon and a chloramphenicol resistance cassette (amplified from the pACYC184 vector, Fermentas) which were flanked by the upstream and downstream sequences with reference to the location of G insertion (**Figure 5.5 B**). The resulting SM1-version and SM4-version constructs were used to make the Δ*ycf54*Δ::slr1916^SM1^ and Δ*ycf54*Δ::slr1916^SM4^ strains, respectively. Colony PCR using primers syn-slr1916 SM UF and syn-slr1916 SM DR showed both strains are fully segregated (**Figure 5.5 C**). Additionally, deletion of the slr1916 gene was conducted in WT and the Δ*ycf54* strains by replacing the gene with a chloramphenicol resistance gene (as described in Section 4.3.2), resulting in the Δslr1916 and Δ*ycf54*Δslr1916 strains (**Figure 5.5 D**). Both strains were confirmed to be completely segregated by colony PCR using primers syn-slr1916 SM UF and syn-slr1916 SM DR (**Figure 5.5 E**).
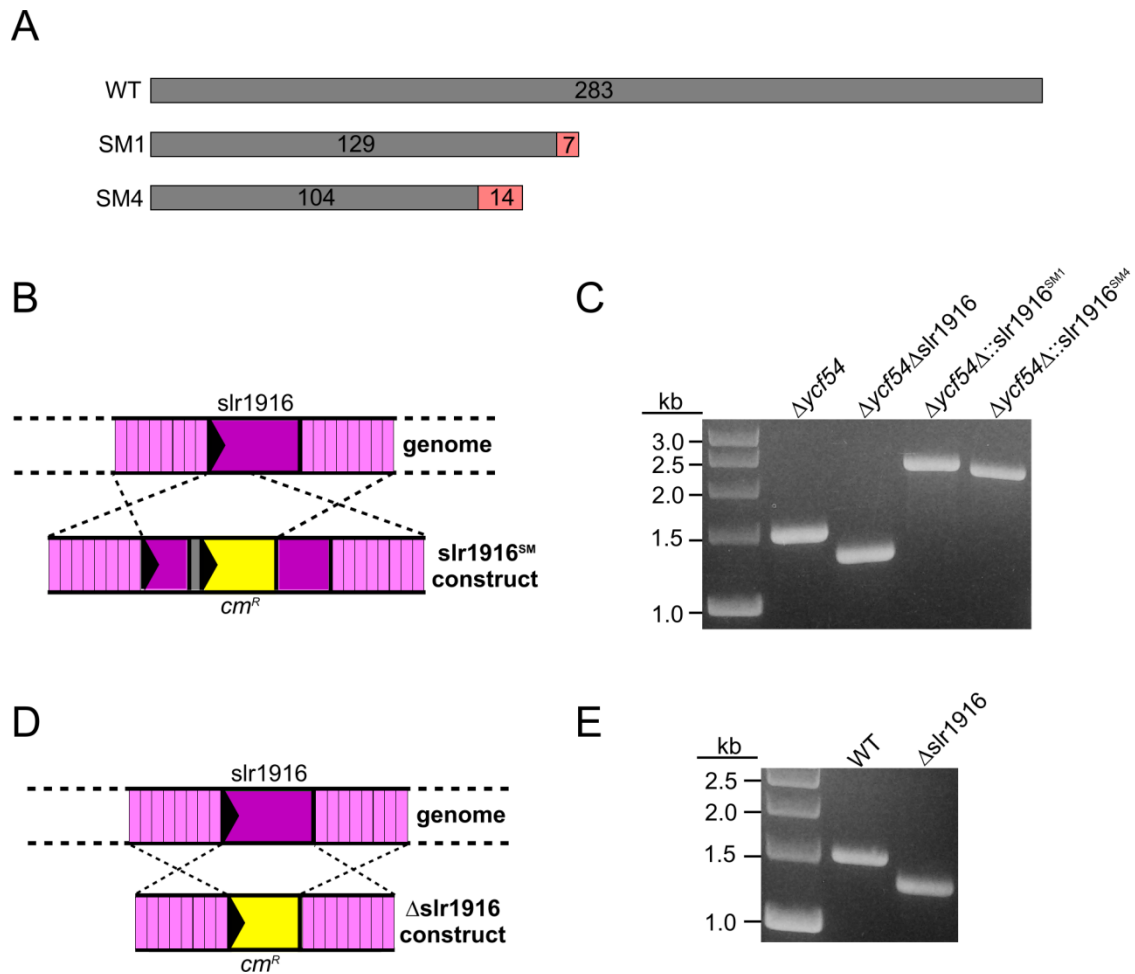
Figure 5.5 Truncations and deletion of the slr1916 gene in *Synechocystis*

(**A**) Diagram showing the levels of Slr1916 truncation in SM1 and SM4. Numbers of AAs are indicated. The C-terminal non-native AAs are marked in red. (**B**) Diagram displaying the truncations of the slr1916 gene by insertion a G (nucleotide), a stop codon and a chloramphenicol resistance cassette into the gene. (**C**) Complete segregation was confirmed by colony PCR using primers flanking the slr1916 gene. Lengths of PCR products: WT = 1491 bp, Δ::slr1916^{SM1} = 2276 bp, Δ::slr1916^{SM1} = 2201 bp. (**D**) Diagram showing the deletion of the slr1916 gene by replacing it with a chloramphenicol resistance gene. (**E**) Complete segregation was confirmed by colony PCR using primers flanking the slr1916 gene. Lengths of PCR products: WT = 1491 bp, Δslr1916 = 1299 bp.

In the attempt to reproduce the phenotypes of SM1 and SM4, the D219G mutation in the *cycI* gene was combined with the mutations in the slr1916 gene to generate the Δ*ycf54*Δ::slr1916^{SM1}*cycI*$^{SM+}$ and Δ*ycf54*Δ::slr1916^{SM4}*cycI*$^{SM+}$ strains. Both strains are resistant to zeocin (Δ*ycf54*), chloramphenicol (Δslr1916) and kanamycin (*cycI*$^{SM+}$).

5.3.4 Phenotypic analyses of the 'artificial' suppressor mutants

The 'artificial' suppressor mutants were compared with the WT, Δ*ycf54*, SM1 and SM4 strains regarding whole-cell absorption spectra and growth rates on BG-11 agar medium without or

with the addition of 5 mM gluocose. Experiments were performed exactly the same way as described in Section 5.3.1. The obtained data for *cycI*-related mutants, slr1916-related mutants and combined mutants were shown in **Figure 5.6, 5.7** and **5.8**, respectively.
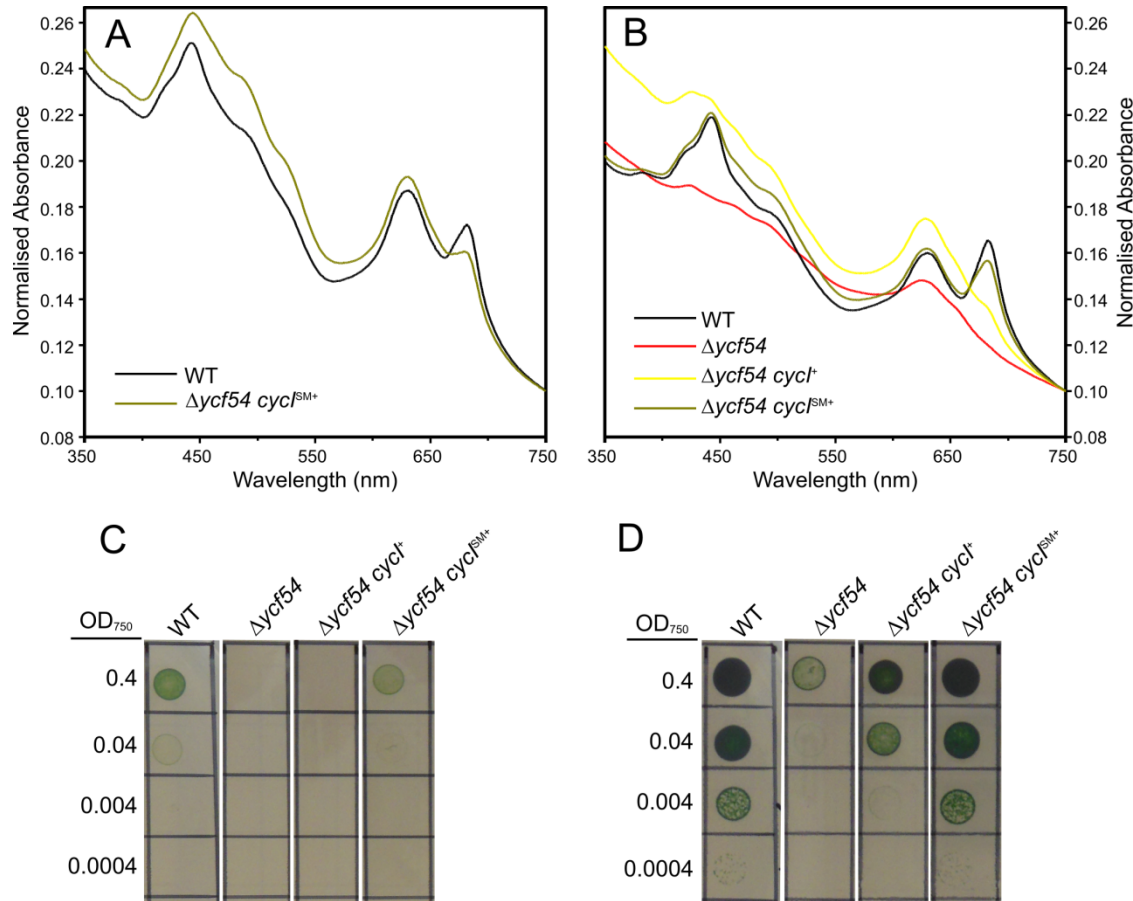
Figure 5.6 Whole-cell absorption spectra and drop growth assays of the constructed *cycI*-related *Synechocystis* mutants

See legend of **Figure 5.1** for experimental procedures.

When the D219G mutated *cycI* was introduced into the Δ*ycf54* strain under the *psbAII* promoter (Section 5.3.3), the native *cycI* gene was not removed. To check whether the phenotype observed in the constructed Δ*ycf54 cycI*^SM+ strain is from a dosage effect, a control strain, Δ*ycf54 cycI*^+, was constructed. The only difference between these two strains is the D219G point mutation. Some improvement was observed in the control strain, which synthesised a little more Chl (**Figure 5.6 B**) and grew faster (**Figure 5.6 D**) than the Δ*ycf54* strain under mixotrophic conditions. However, this control strain still could not grow under autotrophic conditions (**Figure 5.6 C**). Instead, the Δ*ycf54 cycI*^SM+ strain was capable of autotrophic growth and the level of Chl biosynthesis was slightly lower than that of WT under

these conditions (**Figure 5.6 A**). The difference in Chl content between the *Δycf54 cycI*^SM+ strain and WT cultivated with the addition of glucose was almost negligible (**Figure 5.6 B**). Additionally, the growth rates of the *Δycf54 cycI*^SM+ strain under both tested conditions were indistinguishable from those of WT (**Figure 5.6 C** and **D**). Clearly, the introduction of the D219G mutated *cycI* gene greatly improves the parental *Δycf54* strain especially under mixotrophic conditions and the dosage effect is not significant.
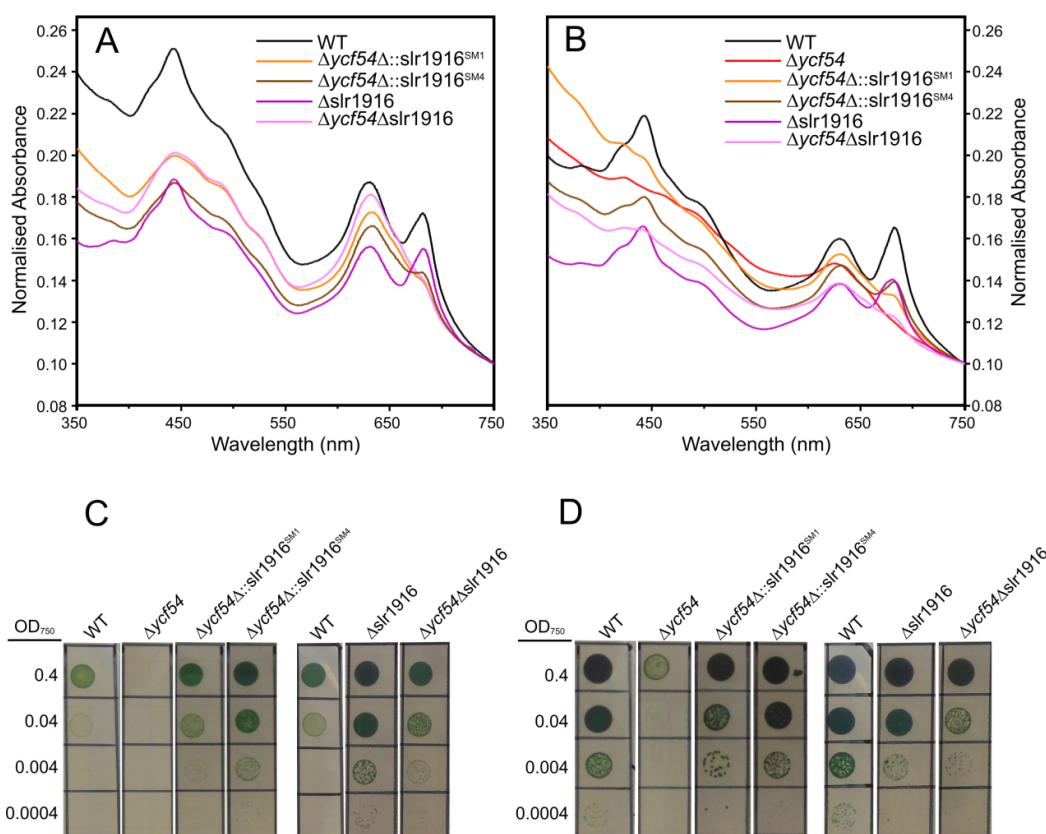
Figure 5.7 Whole-cell absorption spectra and drop growth assays of the constructed slr1916-related *Synechocystis* mutants
See legend of **Figure 5.1** for experimental procedures.

The slr1916 gene encodes 129 and 108 WT residues of the original 283 residues in SM1 and SM4, respectively, each of which are followed by a few frameshifted residues and then new stop codons. Considering less than half of the total AAs are intact, both truncations are severe. In addition, the Δslr1916 and *Δycf54*Δslr1916 strains were also constructed to check the effect of deletion of the slr1916 gene. The overall spectra of the slr1916-related mutants seemed to shift down similarly as observed in SM1 and SM4, especially for the spectra of the Δslr1916 strain under both autotrophic and mixotrophic conditions (**Figure 5.7 A** and **B**). Compared to the *Δycf54* strain, the *Δycf54*Δ::slr1916^SM1, *Δycf54*Δ::slr1916^SM4 and

$\Delta ycf54\Delta$slr1916 strains showed increased levels of Chl biosynthesis, of which the level in $\Delta ycf54\Delta$::slr1916^{SM4} was much more noticeable (**Figure 5.7 A** and **B**). The Δslr1916 strain grew much faster under autotrophic conditions but slightly slower under mixotrophic conditions compared with WT (**Figure 5.7 C** and **D**). The truncations and deletion of the slr1916 gene all greatly enhance the parental $\Delta ycf54$ strain regarding the ability of photoautrophic growth, resulting in an even higher growth rate than that of WT (**Figure 5.7 C**). Under mixotrophic conditions, the $\Delta ycf54\Delta$::slr1916^{SM1}, $\Delta ycf54\Delta$::slr1916^{SM4} and $\Delta ycf54\Delta$slr1916 strains grew at a similar or somewhat lower rate than WT, but still much faster than the $\Delta ycf54$ strain (**Figure 5.7 D**). According to whole-cell absorption spectroscopy and drop growth assays, the $\Delta ycf54\Delta$::slr1916^{SM1} and $\Delta ycf54\Delta$slr1916 strains are similar to each other, while the $\Delta ycf54\Delta$::slr1916^{SM4} strain shows the best improvement among the three strains.

The mutations in the *cycI* and slr1916 genes were combined by constructing the $\Delta ycf54\Delta$::slr1916^{SM1}*cycI*$^{SM+}$ and $\Delta ycf54\Delta$::slr1916^{SM4}*cycI*$^{SM+}$ strains. The whole-cell absorption spectra and drop growth assays of these strains were shown alongside those of SM1 and SM4 for comparison (**Figure 5.8**). The combination of the D219G mutation in the *cycI* gene and the truncation in the slr1916 gene seems to have an additive effect in which the increase in Chl content compared with the $\Delta ycf54$ mutant comes mainly from the *cycI* mutation, and the down shifted whole-cell absorption spectrum and faster growth under autotrophic conditions referring to WT correspond mainly to the slr1916 truncation (**Figure 5.8**). It is hard to tell which mutation plays a bigger role in the slightly faster growth under mixotrophic conditions compared with WT. The spectra of the $\Delta ycf54\Delta$::slr1916^{SM1}*cycI*$^{SM+}$ and $\Delta ycf54\Delta$::slr1916^{SM4}*cycI*$^{SM+}$ strains were almost identical to those of SM1 and SM4 (**Figure 5.8 A** and **B**). Furthermore, in the drop growth assay experiments, the $\Delta ycf54\Delta$::slr1916^{SM1}*cycI*$^{SM+}$ and $\Delta ycf54\Delta$::slr1916^{SM4}*cycI*$^{SM+}$ strains behaved just like SM1 and SM4 under autotrophic conditions (**Figure 5.8 C**) and grew faster than SM1 and SM4 under mixotrophic conditions.
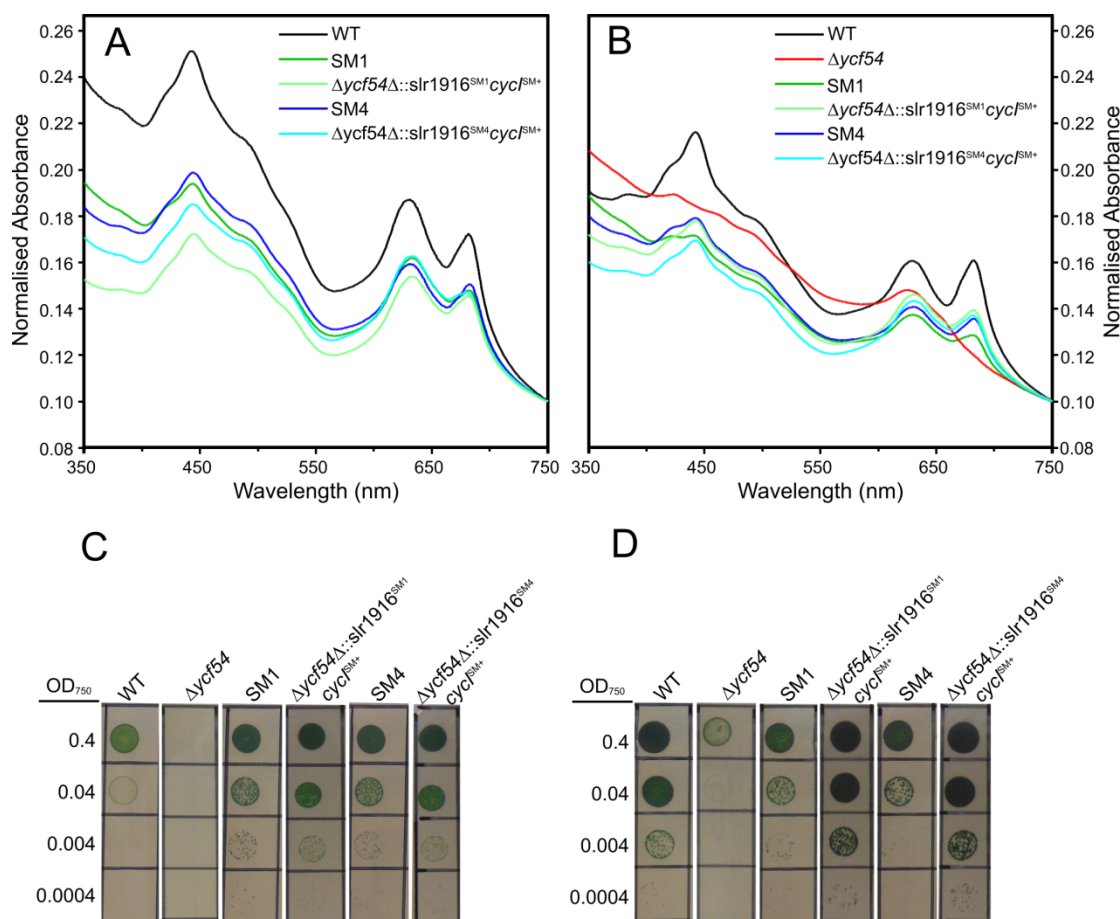
Figure 5.8 Whole-cell absorption spectra and drop growth assays of the constructed *Synechocystis* strains with both mutated *cycI* and slr1916

See legend of **Figure 5.1** for experimental procedures.

5.3.5 *In vivo* activities of the CycI D219G and the AcsF A218D mutants in *Rvi. gelatinosus*

The D219G point mutation frees the dependence of CycI on Ycf54, demonstrated by the great improvement observed in the Δ*ycf54 cycI*^SM+ strain. A classification of the aerobic cyclase is proposed In Chapter 4 (Section 4.4.4) with respect to subunit composition. This single point mutation is able to change the classification of the *Synechocystis* CycI from Class III (Ycf54 is required) to Class II (neither Ycf54 nor BciE is required). Amino acid sequence alignments of AcsF proteins showed the D219 position in CycI corresponds to an Ala in *Rvi. gelatinosus* AcsF, *C. reinhardtii* CRD1 and *Rba. sphaeroides* AcsF, and a Ser in *Arabidopsis* CHL27 (indicated by a blue arrow in **Figure 4.1**). A pattern regarding the AA identity at the D219 position was found by examining all the AcsF homologue sequences listed in **Table 4.2**. All the 13 cyanobacterial AcsF proteins uniformly possess an Asp at the position at which all the 9 plant AcsF proteins have a Ser. The AcsF proteins belonging to Class I (BciE is required) and Class II (neither Ycf54

nor BciE is required) of the aerobic cyclase contain an Ala or Ser at the position with the only exception being the AcsF from *Chloracidobacterium thermophilum* B in which a Gly is present. The 219 position (numbering referred to *Synechocystis* CycI) is conserved as an Asp in cyanobacteria. As an acidic AA, Asp is clearly distinct from Ala, Ser and Gly, making the cyanobacterial AcsFs divergent from other AcsF-containing organisms.

As demonstrated in Chapter 4, *Rvi. gelatinosus* is an ideal system to study the aerobic cyclase. The activity of an exogenous aerobic cyclase can be assayed *in vivo* in *Rvi. gelatinosus* by expressing the encoding gene(s) in a Δ*bchE*Δ*acsF* strain which is unable to produce BChl *a*. As shown in Section 4.3.7, the *Synechocystis* CycI is only functional in the presence of Ycf54. To analyse the activity of the CycI D219G mutant protein, a Δ*bchE*Δ*acsF*::*cycI*^{SM} strain of *Rvi. gelatinosus* was constructed using the same method as described in Section 4.3.6. In addition, it was also checked whether BciE (required by Class I aerobic cyclase) has any effect on the mutated CycI. By plating out cells of the constructed Δ*bchE*Δ*acsF*::*cycI*^{SM} strain onto PYS agar medium supplemented with 40 μg ml^{-1} of rifampicin, a spontaneous rifampicin mutant, named as Δ*bchE*Δ*acsF*::*cycI*^{SM} *Rif*^{R}, was isolated. The pBBRBB-*Ppuf*$_{843-1200}$ vector employed for protein expression in *Rba. sphaeroides* (Section 4.3.5) was shown to be also applicable in *Rvi. gelatinosus.* The pBB[*bciE*] (mentioned as pBB[rsp_6110] in Section 4.3.5) plasmid was conjugated into the Δ*bchE*Δ*acsF*::*cycI*^{SM} *Rif*^{R} strain via *E. coli* S17-1. The selection of transconjugants was performed on PYS agar medium supplemented with 50 μg ml^{-1} of kanamycin and 40 μg ml^{-1} of rifampicin, on which *E. coli* S17-1 could not survive.

On the other hand, an A218D (corresponding to the D219 in CycI) variant of the *Rvi. gelatinosus acsF* was generated using overlap extension PCR (Ho *et al*., 1989) and subsequently cloned into the *Bgl*II/*Not*I sites of the pBBRBB-*Ppuf*$_{843-1200}$ vector, resulting in a plasmid named as pBB[*acsF*^{AD}]. Besides, a pBB[*acsF*^{AD}-*ycf54*] plasmid was also constructed in which a ribosome binding site was placed between the *acsF*^{AD} and *ycf54* genes the same way as the pK18[*cycI*-*ycf54*] plasmid (Section 4.3.6). To serve as a positive control, a pBB[*acsF*] plasmid was built by cloning the native *acsF* gene into the *Bgl*II/*Not*I sites of the pBBRBB-*Ppuf*$_{843-1200}$ vector. After confirmation by sequencing, each plasmid was transferred into a Δ*bchE*Δ*acsF Rif*^{R} strain (a spontaneous rifampicin mutant isolated from the Δ*bchE*Δ*acsF* strain) via conjugation. All the *Rvi. gelatinosus* strains and pBBRBB-*Ppuf*$_{843-1200}$ based plasmids used in this chapter are listed in **Table 5.3**.

Table 5.3 List of *Rvi. gelatinosus* strains and pBB[*gene*] plasmids described in this chapter

Strain/plasmid	Characteristics	Source
Rvi. gelatinosus		
$\Delta bchE\Delta acsF$	Unmarked deletion mutant of *bchE* and *acsF* in WT	Chapter 4
$\Delta bchE\Delta acsF$ Rif^R	Spontaneous rifampicin resistant mutant isolated from $\Delta bchE\Delta acsF$	This study
$\Delta bchE\Delta acsF$::*cycI*^{SM}	*cycI*^{SM} replacement of *acsF* in $\Delta bchE$	Chapter 4
$\Delta bchE\Delta acsF$::*cycI*^{SM} Rif^R	Spontaneous rifampicin resistant mutant isolated from $\Delta bchE\Delta acsF$::*cycI*^{SM}	This study
Plasmid		
pBB[*bciE*]^a	*Rba. sphaeroides bciE* (rsp_6110) cloned into the *BglII/NotI* sites of pBBRBB-*Ppuf*$_{843-1200}$	Chapter 4
pBB[*acsF*]	*Rvi. gelatinosus acsF* cloned into the *BglII/NotI* sites of pBBRBB-*Ppuf*$_{843-1200}$	This study
pBB[*acsF*^{AD}]	A218D mutated *acsF* cloned into the *BglII/NotI* sites of pBBRBB-*Ppuf*$_{843-1200}$	This study
pBB[*acsF*^{AD}-*ycf54*]^b	*acsF*^{AD}-ycf54 cloned into the *BglII/NotI* sites of pBBRBB-*Ppuf*$_{843-1200}$	This study

^{a} This plasmid is first mentioned as pBB[rsp_6110] in Chapter 4.
^{b} A 16 bp sequence (immediately upstream of the *Rvi. gelatinosus pufA* gene) was placed between *acsF*^{AD} and *ycf54* to provide a ribosome binding site for the *ycf54* mRNA.

The constructed *Rvi. gelatinosus* strains were grown overnight in 20 ml of PYS medium filled in 250 ml Erlenmeyer flasks at 30°C with shaking at 150 rpm. Kanamycin was added at 50 μg ml^{-1} for the strains harbouring the pBBRBB-*Ppuf*$_{843-1200}$ based plasmids. Pigment extraction and HPLC analysis were conducted using the same method as described in Section 4.3.7. BChl species was monitored by the absorbance at 770 nm and by the 788 nm fluorescence excited at 365 nm as well. Except for the $\Delta bchE\Delta acsF$ Rif^R/pBB[*acsF*] strain in which BChl *a* is produced at a much higher level, the HPLC elution profiles of other strains shown in **Figure 5.9** are comparable since they represent the pigments extracted from cells standardised by OD$_{680}$. In contrast to the lack of activity detected in $\Delta bchE\Delta acsF$::*cycI* (trace 4), the activity of the CycI D219G mutant protein was demonstrated although in a small scale (traces 2 and 3). The presence of the *Rba. sphaeroides* BciE did not make any difference (trace 1). The A218D mutation was shown to have a dramatic inhibitory effect on AcsF as only residual activity was detected in $\Delta bchE\Delta acsF$ Rif^R/pBB[*acsF*^{AD}] (trace 6). Co-expression of the *Synechocystis* Ycf54 did not enhance the activity of the AcsF A218D mutant protein (trace 5).
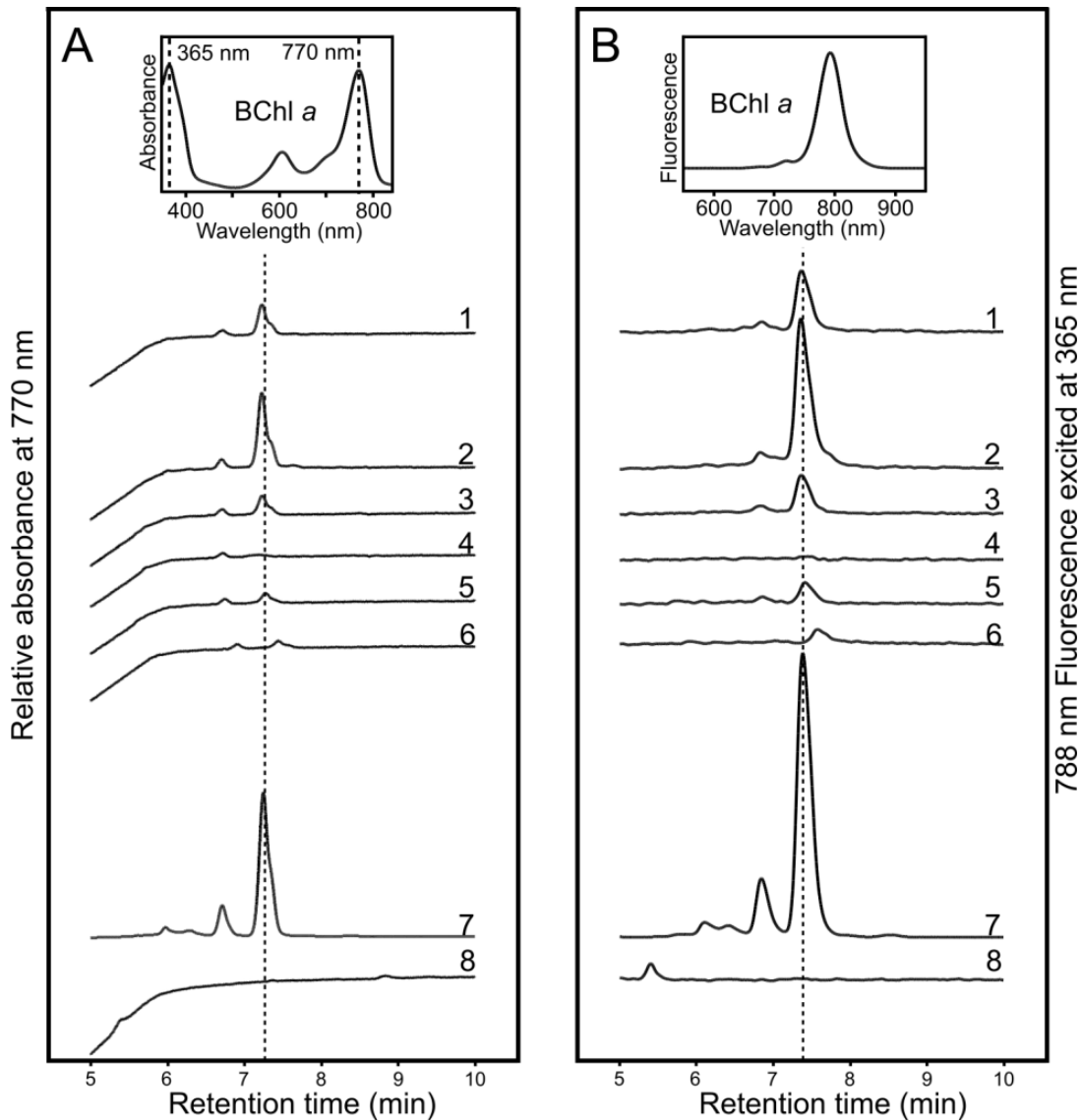
Figure 5.9 HPLC elution profiles of pigments extracted from *Rvi. gelatinosus* strains

Pigments were extracted from cells standardised by OD$_{680}$ except for the $\Delta bchE \Delta acsF\ Rif^R$/pBB[*acsF*] (trace 7) strain which contained much more BChl *a* than any other strains. Trace 1, $\Delta bchE \Delta acsF::cycI^{SM}Rif^R$/pBB[*bciE*]; trace 2, $\Delta bchE \Delta acsF::cycI^{SM}Rif^R$; trace 3, $\Delta bchE \Delta acsF::cycI^{SM}$; trace 4, $\Delta bchE \Delta acsF::cycI$; trace 5, $\Delta bchE \Delta acsF\ Rif^R$/pBB[*acsF*^{AD}-*ycf54*]; trace 6, $\Delta bchE \Delta acsF\ Rif^R$/pBB[*acsF*^{AD}]; trace 7, $\Delta bchE \Delta acsF\ Rif^R$/pBB[*acsF*]; and trace 8, $\Delta bchE \Delta acsF\ Rif^R$. Elution of BChl *a* was monitored by absorbance at 770 nm (**A**) and by fluorescence at 788 nm excited at 365 nm (**B**).

5.4 Discussion

5.4.1 Two mutations are confirmed to be mainly responsible for the suppressor effects in SM1 and SM4

As it suffers from Chl deficiency, the *Synechocystis* Δ*ycf54* strain is unable to conduct photoautotrophic growth and the growth rate is much lower than that of WT under photomixotrophic conditions (Hollingshead *et al.*, 2016; Section 4.3.3). Such a poor strain provides an excellent opportunity to perform a suppressor screen. Four suppressor mutants, which exhibit great improvement in Chl biosynthesis and photoautotrophic growth, were isolated. Two of the four suppressor mutants, SM1 and SM4, are highlighted by their near-WT phenotypes. These two mutants were then substantially characterised using a combination of whole-cell absorption spectroscopy, drop growth assays, 2D electrophoresis with radiolabelling and Western blot analysis. Together with the increased level of CycI (**Figure 5.3**), SM1 and SM4 show greatly improved Chl biosynthesis compared with the Δ*ycf54* strain (**Figure 5.1 A** and **B**). Accordingly, the biogenesis of PS in SM1 (presumably also in SM4) recovered from the lack of Chl and is restored to a WT-level (**Figure 5.2**). The increase in the synthesis of PSI subunits PsaA/B is especially obvious in SM1 (**Figure 5.2**), indicating PSI is highly sensitive to *de novo* Chl biosynthesis (Kopecna *et al.*, 2012). As a result, SM1 and SM4 exhibit significantly enhanced ability of photosynthesis as they can grow photoautotrophically at an even higher rate than WT (**Figure 5.1 C**). Supplementation of 5 mM glucose slightly inhibits the growth of SM1 and SM4 (**Figure 5.1 D**). In summary, suppressor mutations occurred in SM1 and SM4 evidently help the strains to overcome the loss of the *ycf54* gene.

The genomes of the suppressor mutants together with the WT and Δ*ycf54* strains were sequenced with more than 150-fold coverage. Variants were then called by mapping the reads to reference sequences from database and filtered using a set of relatively harsh criteria. Two *Synechocystis* strains designated as GT-W and GT-P have been recently sequenced and a tandem duplication of a 110 kb chromosomal region was found in GT-W (Tichy *et al.*, 2016). The special genetic background of the GT-W strain has been proposed to allow successful construction of the fully segregated Δ*ycf54* mutant (Hollingshead *et al.*, 2016), which seems impossible in GT-P and other *Synechocystis* substrains (Tichy *et al.*, 2016). Although the WT strain used in the present study originated from the GT-W strain, sequencing confirmed that the 110 kb duplication region is not present in any of the strains examined. The loss of the duplication region is likely to be caused by growth under

autotrophic growth conditions (Tichy *et al.*, 2016). On the other hand, 12 putative chromosomal variants were surprisingly found in the WT strain when compared to the GT-S strain (Tajima *et al.*, 2011) (data not shown). One of the 12 variants, a C insertion between the 569,312 and 569,313 positions (numbering referred to the GT-S genome, NC_017277) is particularly interesting, which causes a frameshift in the *rubA* gene (slr2033) with only 59 out of the native 115 AAs remaining unaffected. The *rubA* gene, encoding a membrane-associated rubredoxin, has been reported to be required for the normal accumulation of PSII in oxygenic photoautotrophs including *Synechocystis* (Calderon *et al.*, 2013). This frameshift mutation was verified in all the six sequenced strains by PCR and the Sanger sequencing but not present in the GT-P strain. The truncated *rubA* gene may help the strain to survive the deletion of the *ycf54* gene. Nevertheless, the involvement of other mutations found in the WT strain cannot be ruled out.

3 genomic variances are found in the Δ*ycf54* strain with respect to the WT strain, with one of them causing an in-frame insertion of 2 His in a ferric uptake regulation protein encoded by the *fur* gene (sll0567) (**Table 5.1**)**.** Putative suppressor mutations are identified based on the presence in suppressor mutants and absence in the Δ*ycf54* strain (**Table 5.1**). Considering the number of mutations (≥ 5) found in each suppressor mutant, it is impractical to test every single of them. Instead, the *cycI* and slr1916 genes, mutated in both SM1 and SM4, were given priority of investigation. After confirmation by PCR and the Sanger sequencing, these mutations were introduced alone or combined into the Δ*ycf54* strain to check whether the suppressor effects observed in SM1 and SM4 could be reproduced. Whole-cell absorption spectroscopy and drop growth assays were employed as primary phenotypic analyses. As SM1, SM4 and the constructed strains with mutations in the slr1916 gene show down shifted whole-cell absorption spectra compared with other strains, possibly due to altered light scattering, relative ratios of phycobiliproteins to Chl were estimated from whole-cell absorption data to facilitate the spectral comparison of different strains. The ratio was calculated as $(Abs_{630} - Abs_{750})/(Abs_{682} - Abs_{750})$ and then normalised to that of WT, as shown in **Table 5.4**. It is demonstrated that all these 'artificial' suppressor mutants are able to conduct Chl biosynthesis and photosynthetic growth better than the Δ*ycf54* mutant (**Figure 5.6**, **5.7**, and **5.8**). Remarkably, the behaviours of the constructed strains containing both mutations are almost indistinguishable from those of SM1 and SM4 based on the primary phenotypic analysis (**Figure 5.8**). The minute differences between 'artificial' and genuine suppressor mutants are likely to be caused by other identified mutations which were not tested here and the way that the mutated *cycI* gene was introduced (Section 5.3.3). It is

reasonable to conclude that the mutations found within the *cycI* and slr1916 genes are mainly responsible for the phenotypic improvements observed in SM1 and SM4.

Table 5.4 Relative ratios of phycobiliproteins to Chl estimated from whole-cell absorption spectra

	Relative phycobiliproteins:Chl ratio	
Strain	**Autotrophic, low-moderate light**	**Mixotrophic, low light**
WT	1	1
Δ*ycf54*	-	2.57
SM1	1.06	1.43
SM4	0.97	1.25
Δ*ycf54 cycI*[+]	-	2.25
Δ*ycf54 cycI*[SM+]	1.28	1.20
Δ*ycf54*Δ::slr1916[SM1]	1.52	1.76
Δ*ycf54*Δ::slr1916[SM4]	1.24	1.31
Δslr1916	0.84	1.04
Δ*ycf54*Δslr1916	1.65	1.88
Δ*ycf54*Δ::slr1916[SM1] *cycI*[SM+]	0.97	1.28
Δ*ycf54*Δ::slr1916[SM4] *cycI*[SM+]	1.10	1.27

The whole-cell absorption spectra shown in **Figures 5.1**, **5.6**, **5.7** and **5.8** were used to estimate the relative ratios of phycobiliproteins to Chl. Ratio (phycobiliproteins:Chl) = (Abs_{630} − Abs_{750})/(Abs_{682} − Abs_{750}). The calculated ratios were normalised to that of WT, resulting in the relative ratios. Light conditions: low light, 5 μE m^{-2} s^{-1}; low-moderate light, 15~20 μE m^{-2} s^{-1}. The Δ*ycf54* and Δ*ycf54 cycI*[+] strains could not grow autotrophically under low-moderate light conditions.

5.4.2 The D219 mutation has huge effects on CycI

Two independently isolated suppressor mutants both harbour the same D219G point mutation in the *cycI* gene. Such a mutation when introduced on its own to the Δ*ycf54* strain is good enough to convert a weak strain into a relatively normal (WT-like) strain (**Figure 5.6**), in which dosage effect only play little part. The better performance of the constructed Δ*ycf54 cycI*[SM+] strain in the presence of glucose may be explained by the redox control of the *psbA* promoter. It was reported that addition of glucose, which increases the reducing power in cells, induces the *psbA* transcription but destabilises the *psbA* transcript (Alfonso *et al.*, 2000). The enhanced transcription of the *cycI*[SM+] gene driven by the *psbAII* promoter is unlikely to be offset by the mechanism that destabilises the *psbA* transcript. Thus, the level of the *cycI*[SM+] mRNA is increased.

The D219 residue is important but not essential for the activity of CycI as the D219G substitution alters the character of the WT residue significantly. As expected, the D219 position is not conserved in the investigated AcsF-containing species and Ala, Ser or Gly as well as Asp can be found at this position. Nevertheless, the analysed cyanobacterial AcsFs, of which the activity depends on Ycf54, all contain an Asp at the position, whereas an Ala is present in most of the Ycf54-independent AcsFs (Classes I and II of the aerobic cyclase). It is amazing that the single-AA mutation D219G frees the dependence of CycI on Ycf54. This evokes the question regarding the role played by Ycf54 in the function of the Class III aerobic

cyclase. Although the function of Ycf54 is still a mystery (Hollingshead *et al*., 2016), it is possible to make several proposals as discussed in Section 4.4.2 based on experimental evidence. Together with the fact that the CycI D219G mutant is independent from Ycf54 and the experimental results from *in vivo* assays conducted in *Rvi. gelatinosus* (Section 5.3.5), the discussion can go a little further. The interaction between CycI and Ycf54 may stabilise and enhance the enzymatic activity of the aerobic cyclase. Despite the direct physical interaction between Ycf54 and other Chl biosynthetic enzymes including POR, DVR and ChlP could not be found by *in vivo* FLAG pulldown experiments (Hollingshead, 2014), it is still possible that Ycf54 can enhance the interactions between CycI and other Chl biosynthetic enzymes by inducing conformational change of CycI. In *Synechocystis,* the CycI D219G mutant does not require Ycf54 for function based on the phenotypic analysis. However, the CycI D219G mutant only showed slight activity when expressed in *Rvi. gelatinosus* (**Figure 5.9**), which is not comparable to the activity of CycI with Ycf54 (**Figure 4.7**). This may be caused by differences in the cellular context between *Synechocystis* and *Rvi. gelatinosus*. Alternatively, the CycI D219G mutant may interact poorly with DPOR of *Rvi. gelatinosus*, making the whole biosynthetic pathway ineffective. On the other hand, the A218D (corresponding to the D219 of CycI) mutation in AcsF lowers the activity of *Rvi. gelatinosus* AcsF to a trace level (**Figure 5.9**). From an evolutionary perspective as discussed in Section 4.4.5, the ancestor of *Rvi. gelatinosus* may have acquired the *cycI* gene from cyanobacteria without the *ycf54* gene. Under selection pressure, the acquired *cycI* gene gradually became functional as a result of accumulated mutations, which was nicely simulated in the process of isolating the suppressor mutants in the present work. It is not surprising that no enhancement was observed when the AcsF A218D mutant was co-expressed with Ycf54 since they may have lost the capability to interact with each other during evolution (**Figure 5.9**).

Moreover, primary analysis revealed that CycI is subjected to degradation in the dark, which is pronounced even with 1 hr darkness treatment (data not shown). In contrast, the $\Delta ycf54$ $cycI^{SM+}$ and $acsF^{Rg+}\Delta cycI$ strains did not show any sign of CycI degradation, indicating that the CycI D219G mutant and *Rvi. gelatinosus* AcsF are immune to the mechanism causing the degradation process. Further analysis with appropriate control strains is required to confirm this finding. It is well accepted that Chl biosynthesis is tightly controlled to achieve the fine coordination with the synthesis of apoproteins of PS. The synchronisation of Chl and Chl-binding proteins synthesis is vital since unbound Chl is phototoxic to cells (Sobotka, 2014; Wang and Grimm, 2015). To adapt to various environmental conditions and cellular states, it is conceivable that Chl biosynthesis is regulated at multiple levels and with various

checkpoints. The known checkpoints include the ALA formation, the Mg-chelatase step and the light-dependent POR reaction. The phenomenon that CycI protein is degraded during a period of darkness suggests that the aerobic cyclase reaction could be a new checkpoint for regulation of Chl biosynthesis. In their natural habitats, all phototrophs on Earth live a diurnal life cycle. Degradation of CycI protein triggered by darkness can provide the last safety measure to ensure the accumulation of PChlide at night is within a suitable level. Once solar irradiation begins the POR reaction, converting the accumulated PChlide to Chlide, will be unstoppable. If excess PChlide is synthesised, the scale of Chl biosynthesis will overload the biosynthesis and assembly of Chl-binding proteins, resulting in potentially catastrophic effects on the cell. Although exhibiting near-WT phenotypes under continuous illumination, the $\Delta ycf54\ cycI^{SM+}$ and $acsF^{Rg+}\Delta cycI$ strains may be constrained by light/dark cycles if the regulation via CycI degradation really operates.

5.4.3 The *Synechocystis* Slr1916 protein is involved in the control of photosystem stoichiometry

The slr1916 gene is also highly relevant to the suppressor effects as it is truncated in two independently isolated suppressor mutants at different levels. Chl biosynthesis and photosynthetic growth were shown to be significantly improved when the native slr1916 gene was replaced with the truncated gene or simply deleted in the $\Delta ycf54$ mutant (**Figure 5.7**). Deletion of the slr1916 gene in the WT background resulted in a strain which has a much higher photoautotrophic growth rate and slightly lower photomixotrophic growth rate than WT under low-moderate (15 μE m^{-2} s^{-1}) light conditions (**Figure 5.7**). Interestingly, the Δslr1916 strain always has a whole-cell absorption spectrum which is notably lower than that of WT, as do other constructed slr1916-related strains (**Figure 5.7 A** and **B**). This reflects an alteration in the light-scattering nature of cells, which may arise from changes in their size, morphology and contents. The Δslr1916 strain looks greener than WT both in liquid culture and on BG-11 agar medium. Additionally, it is noteworthy that the photomixophic growth of the Δslr1916 strain is severely suppressed on BG-11 agar medium supplemented with 5 mM glucose under higher (55 μE m^{-2} s^{-1}) light conditions. All these observations indicate the slr1916 gene is linked with photosynthesis. According to NCBI Conserved Domain Database (Marchler-Bauer *et al.*, 2015), Slr1916 belongs to the alpha/beta hydrolase superfamily, which is functionally diverse and contains proteases, lipases, peroxidases, esterases, epoxide hydrolases and dehydrogenases. It is provisionally annotated as an esterase in CyanoBase

without experimental evidence. Slr1916 is conserved in cyanobacteria, whereas no apparent homologue can be identified outside cyanobacteria.

Previously published papers have found that the slr1916 gene is upregulated in response to salt/hyperosmotic stress, UV-B light, acid stress and heat shock in *Synechocystis* (Kanesaki *et al.*, 2002; Shoumskaya *et al.*, 2005; Huang *et al.*, 2002; Ohta *et al.,* 2005; Singh *et al.*, 2006). It is unlikely that any of these reports are relevant to the effects from inactivation of the slr1916 gene. On the other hand, Ozaki *et al.* (2007) reported the identification of *Synechocystis* mutants defective in the adjustment of PS stoichiometry. One mutant group, including a slr1916-disrupted mutant, had higher levels of Chl and PSI compared with the WT especially under high (200 μE m^{-2} s^{-1}) light conditions. Moreover, suppression of photomixotrophic growth was observed in this group of mutants (Ozaki *et al.*, 2007). These findings are consistent with the present work and may provide a clue why the truncation of the slr1916 gene occurred in the suppressor mutants. The severely reduced PSI level in the $\Delta ycf54$ mutant is alleviated by the inactivation of the slr1916 gene, allowing more ATP and NADPH to be produced to support uptake of inorganic carbon and carbon fixation. Nonetheless, extra reducing power from glucose could cause redox imbalance in the electron transport chain in a slr1916-disrupted strain which is unable to downregulate PSI level. It is imaginable that high light conditions could worsen the overreduction problem. Besides, the degradation of CycI upon 1 hr darkness treatment was not detected in the Δslr1916 strain (data not shown). It seems that Slr1916 is involved in an unknown mechanism that is accountable for the degradation of CycI. Such an involvement could be related with the regulation of the level of PSI, which is the major destination for Chl from *de novo* biosynthesis (Kopecna *et al.*, 2012).

5.4.4 Future work

The approach of isolating suppressor mutants originated from the $\Delta ycf54$ mutant did not reveal any new subunit of the aerobic cyclase. Instead, the identification of suppressor mutations within the *cycI* and slr1916 genes provides an opportunity to study the regulation of Chl biosynthesis at the aerobic cyclase step as well as the control of PS stoichiometry. The primary analysis of the suppressor mutations in the present work identifies several directions for future work. The effects of the D219G mutation on CycI should be explored more thoroughly, which could reveal the exact role played by the Ycf54 subunit. The pulldown experiments described in Hollingshead *et al.* (2016) should be conducted using FLAG-tagged CycI D219G mutant protein as bait in order to check whether the protein-protein interactions

are affected by the mutation. It is necessary to construct two new strains to allow careful check for the degradation of CycI in the dark. The WT and D219G mutated *cycI* genes will be placed under the *psbAII* promoter as described in Section 5.3.3, followed by the deletion of the native *cycI* gene as described in Section 4.3.2. The resulting *cycI$^+$ΔcycI* and *cycI^{SM+}ΔcycI* strains, together with the WT and Δslr1916 strains, will be subjected to light/dark transitions and the protein levels of CycI and other Chl biosynthetic enzymes will be analysed by Western blot. Likewise, more information can be obtained regarding the regulation of the aerobic cyclase by applying other conditions or stresses to these four strains, for example, nitrogen depleted conditions and high light conditions. Once confirmed, the degradation of CycI will be considered as a new mechanism to modulate Chl biosynthesis in response to environmental changes.

If CycI is confirmed to be vulnerable to degradation in WT but remain stable in the Δslr1916 strain under the same conditions, it will be worthwhile to consider that Slr1916 is a protease targeting CycI. For initial analysis, both the slr1916 and *cycI* genes can be coexpressed in *E. coli* using a vector containing two multiple cloning sites, such as pCOLADuet™-1 (EMD Millipore). In a control strain, the *cycI* gene will be expressed alone using the same vector. The CycI levels in different *E. coli* strains can be checked by Western blot. For further analysis, both the CycI and Slr1916 proteins can be purified and then examined by *in vitro* protease assay. However, it will be challenging to purify the CycI protein and to pinpoint the proper conditions for the protease assay.

Chapter 6

Development of a transposon mutagenesis system for inactivating bacteriochlorophyll biosynthetic genes in *Rubrivivax gelatinosus*

6.1 Summary

This chapter reports the examination of the *Rvi. gelatinosus* genome to search for genes encoding potential subunit(s) of aerobic cyclase. A transposon mutagenesis library of more than 30,000 mutants was generated using the EZ-Tn5 Transposome, providing a seven-fold coverage of the genome. The first screening of the library was based on the fluorescence of MgPME, the substrate of the aerobic cyclase. Mutants that passed the first screening were subjected to a second screening during which absence of BChl *a* in the pigment extract was taken as positive. Detailed pigment profiles of the isolated mutants were revealed by HPLC analysis. The genomic region adjacent to the transposon in each isolated mutant was amplified using a specially designed PCR protocol called random amplification of transposon ends (RATE). The transposon insertion sites were then disclosed by sequencing the PCR products. Apart from the identification of four unique transposon insertions within the *acsF* gene, no additional gene was found to encode a subunit of aerobic cyclase in *Rvi. gelatinosus*. Transposon insertions were also found in genes encoding enzymes involved in later steps of BChl biosynthesis, including the *bchB*, *bchL*, *bchN*, *bchY*, *bchZ*, *bchF*, *bchC* and *bchG* genes.

6.2 Introduction

According to the literature, as summarised in Section 4.2, there should be at least two unknown subunits of the aerobic cyclase, of which one is a membrane-bound component (encoded by the *Viridis-k* locus in barley) (Rzeznicka *et al.*, 2005) and the other is a soluble subunit. Transposons have been widely used for random insertional mutagenesis in searches for genes associated with a particular phenotype. During the early studies of BChl biosynthesis pathway, many BChl-deficient mutants of *Rba. capsulatus* (Zsebo and Hearst, 1984), *Rba. sphaeroides* (Hunter and Coomber, 1988) and *Rhodospirillum centenum* (Yildiz *et al.*, 1991) were isolated through transposon mutagenesis, which greatly facilitated the identification of the *bch* genes. In order to search for the unknown subunits of aerobic

cyclase, it was decided to conduct a programme of transposon mutagenesis in *Rvi. gelatinosus*, the bacterium used to identify the AcsF component of this enzyme (Pinta *et al.*, 2002).

As mentioned in Section 4.2, *Rvi. gelatinosus* is considered to be an ideal system for studying aerobic cyclase. A *Rvi. gelatinosus* Δ*bchE* strain, described in Section 4.3.6, can only produce BChl via the aerobic cyclase route, making it an appropriate host strain for mutagenesis. Moreover, the EZ-Tn5™ system, as an optimised transposon mutagenesis tool, has been successfully applied to *Rvi. gelatinosus* strains CBS and S1 by different research groups (Vanzin *et al.*, 2010; Steunou *et al.*, 2013; Azzouzi *et al.*, 2013). In this chapter, the EZ-Tn5™ <R6Kγ*ori*/KAN-2> Insertion Kit (Epicentre) was used to create a mutagenesis library with the *Rvi. gelatinosus* Δ*bchE* strain as host. The library was screened subsequently by two strategies and the isolated mutants were characterised both genetically and phenotypically.

6.3 Results

6.3.1 Overview of the experimental design

The methodology of this chapter is diagrammed as a flowchart in **Figure 6.1**. *In vivo* Tn5 transposon mutagenesis was conducted in the *Rvi. gelatinosus* Δ*bchE* strain (described in Section 4.3.6) and cells were plated out onto medium supplemented with kanamycin to select for mutants with the Tn5 transposon inserted in the genome. Two strategies were applied to screen the mutagenesis library for mutants lacking functional aerobic cyclase. The first screening is based on the fluorescent nature of MgPME which serves as the substrate of aerobic cyclase. Mutants passed the first screening if they emitted fluorescence under the illumination of a 395 nm LED flashlight. Each mutant isolated from the first screening was inoculated into liquid PYS medium supplemented with kanamycin and incubated under aerobic conditions. Pigment extracts from the liquid cultures were checked for the presence of BChl *a* by absorption spectra. Mutants with no detectable BChl *a* passed the second screening. These mutants were of great interest and warranted a detailed analysis of their genotypes and phenotypes. Genomic DNA was isolated from each mutant and used as the template for a specially designed PCR called random amplification of transposon ends (RATE). The RATE PCR product which usually contains multiple amplicons was separated on an agarose gel. An abundant band was excised and DNA was recovered by gel extraction. The purified DNA was sequenced by the Sanger method. To identify the locations of transposon inserts, the sequencing results were used to conduct BLAST searches against the *Rvi.*

gelatinosus genome. On the other hand, the identities of the pigments accumulated in each mutant were disclosed by HPLC analysis. Comparing the insertion site with the corresponding pigment profile, there is a good chance that genes associated with aerobic cyclase can be identified.
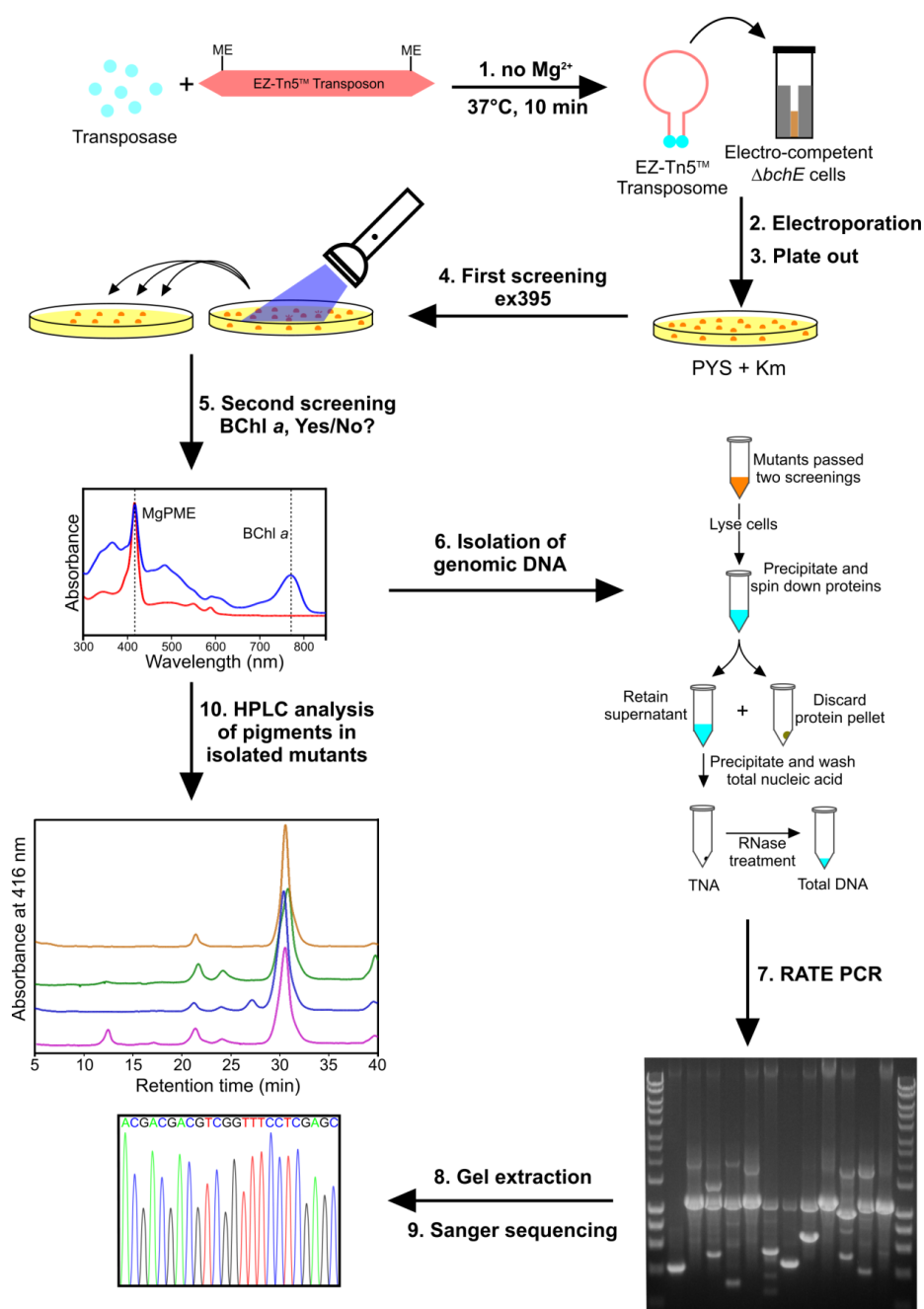
Figure 6.1 Overview of the methodology applied in Chapter 6

As depicted in the form of the flowchart, the experimental design of this chapter includes transposon mutagenesis (steps 1, 2 and 3), two types of screenings (steps 4 and 5), determination of the transposon sites (steps 6, 7, 8 and 9) and pigment analysis of isolated mutants (step 10). The steps 1, 2, 3, and 6 are based on figures from Epicentre website (www.epibio.com).

6.3.2 Transposon mutagenesis in *Rvi. gelatinosus* Δ*bchE* strain

The EZ-Tn5 Transposome was produced in the absence of Mg^{2+} using the reagents provided in the EZ-Tn5^{TM} <R6Kγ*ori*/KAN-2> Insertion Kit (Epicentre). As shown in **Figure 6.2**, the EZ-TN5 <R6Kγ*ori*/KAN-2> transposon contains an R6Kγ origin of replication, a kanamycin resistance gene and two 19 bp inverted repeat Mosaic End (ME) sequences that can be recognised by the transposase.
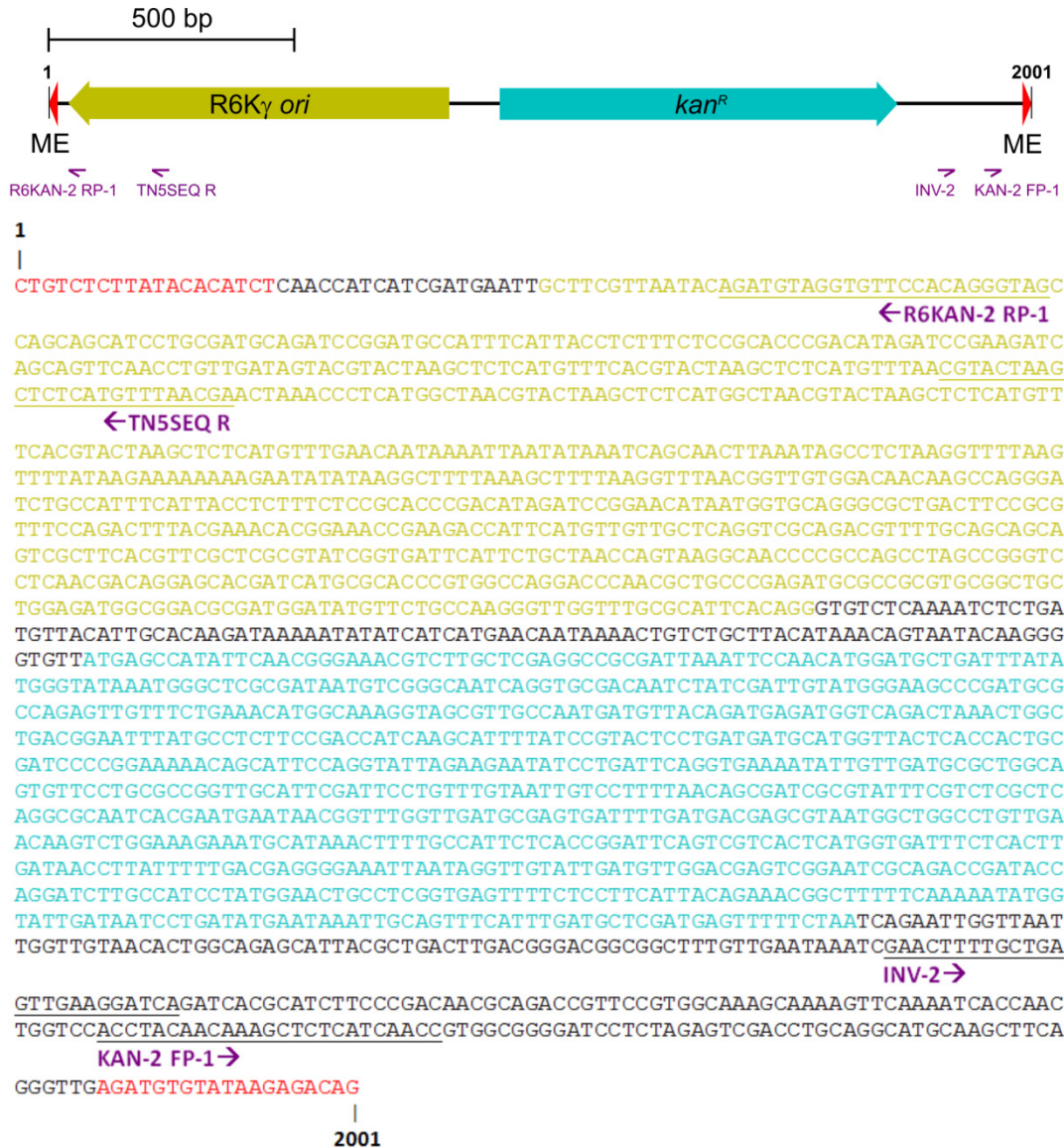
Figure 6.2 Map and sequence of the EZ-TN5 <R6Kγ*ori*/KAN-2> transposon

The EZ-TN5 <R6Kγ*ori*/KAN-2> transposon contains an R6Kγ origin of replication, a kanamycin resistance gene and two 19 bp inverted repeat Mosaic End (ME) sequences. The locations and sequences of the four primers used in this chapter are also shown. Primers INV-2 and TN5SEQ R were used for RATE PCR, separately. Primers KAN-2 FP-1 and R6KAN-2 RP-1 were used for Sanger sequencing.

This Δ*bchE* mutant described in Chapter 4 (Section 4.3.6) was used as the host strain for transposon mutagenesis. Electrocompetent cells of the Δ*bchE* strain were prepared as described in Section 2.3.3. Transposon mutagenesis in the Δ*bchE* strain was performed as described in Section 2.11.1 and cells were plated out onto PYS agar medium supplemented with 50 μg ml^{-1} of kanamycin to select for transposon insertion mutants.

To ensure a full coverage of the genome, a large number of mutants are required for the transposon library. Large square plates (22.5 cm x 22.5 cm) with a usable area of ~506 cm^2 were used for selection on agar medium. A total of 5 electroporations were conducted and subsequently plated out onto 11 large square plates, labelled 1 to 11. Plate 1 resulted from a single electroporation. Plate 2 was also from a single electroporation during which arcing happened. Thus, Plate 2 had far fewer colonies than Plate 1 (**Figure 6.3 B**). A single electroporation was spread equally onto Plates 3, 4 and 5 (**Figure 6.3 B**). Likewise, Plates 6, 7 and 8 were from a single electroporation, so are Plates 9, 10 and 11. Unfortunately, Plates 5 to 11 were not suitable for downstream screening due to accidentally elongated incubation. By sampling representative areas of the plates, the numbers of colonies on Plates 1 to 5 were estimated to be more than 18,000, 1,000, 4,500, 3,700 and 4,600, respectively. Thus, a total of more than 30,000 transposon mutants were contained in the library.
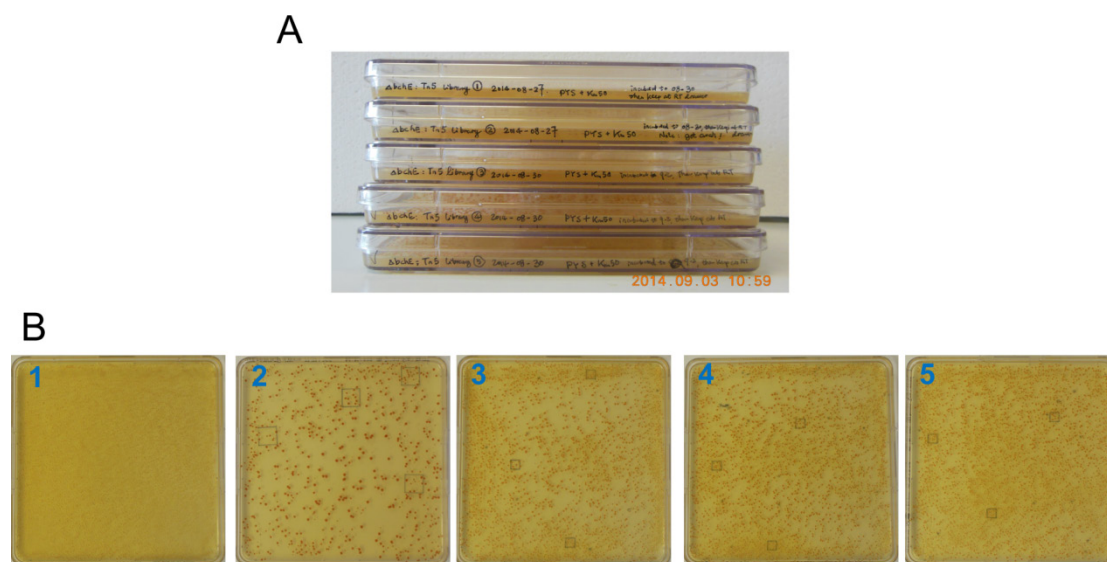
Figure 6.3 The transposon insertion mutant library

(**A**) The transposon insertion mutants were selected on PYS agar medium supplemented with kanamycin. Five large square plates (22.5 cm x 22.5 cm) were used and contained more than 30, 000 colonies. (**B**) Photographs of colonies on each plate. Electroporation was conducted using 40 μl of competent cells mixed with 1 μl of transposome. Plate 1 was from a single electroporation. Plate 2 was from a single electroporation during which arcing occurred. A third electroporation was spread equally onto three plates, namely Plates 3, 4 and 5.

6.3.3 First screening: fluorescence with 395 nm excitation

MgPME, the tetrapyrrole substrate of the aerobic and anaerobic cyclases, has a fluorescence excitation maximum at 416 nm (in methanol) and an emission maximum at 595 nm (in methanol). Disruption of any gene associated with the aerobic cyclase in the Δ*bchE* host strain will cause the accumulation of MgPME, resulting in fluorescent mutants. Colonies of the Δ*bchE*Δ*acsF* mutant (described in Section 4.3.6) could be easily discriminated from the colonies of the Δ*bchE* mutant, demonstrating the feasibility of a screening method based on the fluorescence nature of MgPME.
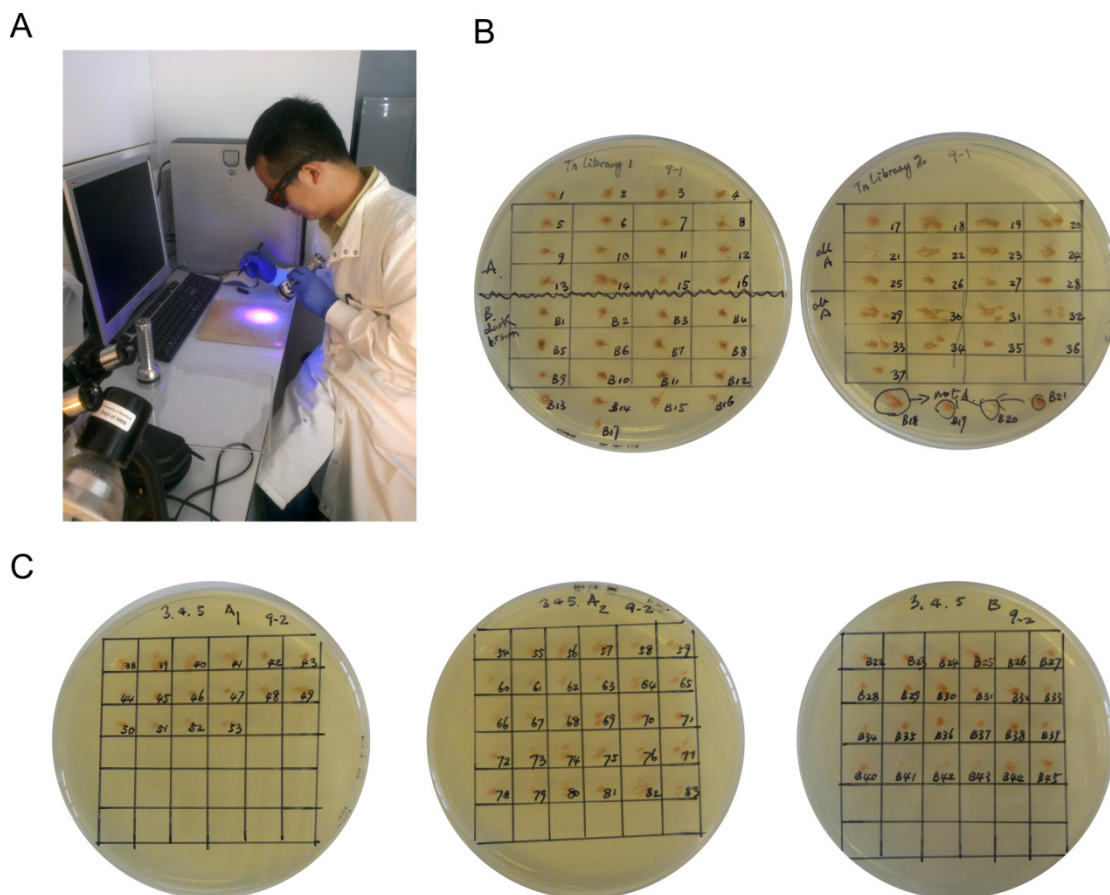
Figure 6.4 First screening based on fluorescence excited at 395 nm and the isolated mutants (**A**) Photograph of me performing the first screening with a 395 nm LED flashlight. Under the illumination of the flashlight, colonies with apparent fluorescence judged by visual inspection were transferred to PYS agar medium supplemented with kanamycin. (**B**) The isolated mutants from Plates 1 and 2. (**C**) The isolated mutants from Plates 3, 4 and 5.

The transposon mutagenesis library was subjected to the first screen using a 395 nm LED flashlight to illuminate the colonies **(Figure 6.4 A)**. Colonies with apparent fluorescence were picked with sterile toothpicks and stabbed onto PYS agar medium supplemented with

kanamycin. A total of 83 mutants was isolated from Plates 1 to 5 and they were designated as TN1 to TN83 (**Figure 6.4 B** and **C**). Despite overgrowth of the colonies on Plates 6 to 11, 32 mutants with generally less fluorescence compared with TN mutants, as assigned by visual inspection, were isolated in the same way and were named as TN2-1 to TN2-32. Another group of mutants had a brown colouration under the 395 nm light. These mutants, named as B1 to B45, were not related to the aerobic cyclase but could be useful for some other aspects of PS biogenesis (**Figure 6.4 B and C**).

6.3.4 Second screening: presence or absence of BChl *a*

Molecular oxygen is potentially limited for cells grown on agar medium, especially for the cells in the colony interior. This could cause false-positive errors with the first screening as aerobic cyclase utilises molecular oxygen as a substrate. Additionally, the chance of false-positive error might increase in the efforts to avoid false-negative error. Without a functional anaerobic cyclase, BChl *a* can only be synthesised via the aerobic cyclase route, so mutants isolated from the first screen were subjected to a second screen based on whether they could produce BChl *a*. Mutants were inoculated into 10 ml of PYS medium supplemented with 50 μg ml^{-1} of kanamycin in 50 ml Falcon tubes. Incubation was performed at 30°C with shaking at 250 rpm. Pigments were extracted from overnight cultures with 0.2% (v/v) ammonia in methanol. Absorption spectra of the pigment extracts were recorded on a Cary 60 UV-Vis spectrophotometer. If there was no 770 nm peak in the absorption spectrum, the mutant was considered positive in the second screening. In the cases where it was difficult to judge whether there was a 770 nm peak, the mutants were considered as positive in order to avoid any potential false-negative error. 32 out of the 83 TN mutants passed the second screening, whilst only 6 of the 32 TN2- mutants were found to be positive.

6.3.5 Identification of transposon insertion sites in isolated mutants

Genomic DNA was purified from isolated mutants using the MasterPure^{TM} DNA Purification Kit according to manufacturer's instructions (**Figure 6.1**, step 6). It was shown to be impossible to directly sequence the genomic DNA using the R6KAN-2 RP-1 or KAN-2 FP-1 primer (**Figure 6.2**) supplied in the EZ-Tn5^{TM} <R6Kγ*ori*/KAN-2> Insertion Kit (Epicentre) due to the complexity of genomic DNA. Although the transposon contains an R6Kγ origin of replication that allows 'rescue cloning' of the genomic regions adjacent to the transposon, it requires significant effort to perform this operation with all the 38 mutants. This problem was overcome using a RATE PCR protocol, which is based on the original report from Ducey and

Dyer (2002), and communicated by Dr Fred Hyde, Illumina Technical Support (techsupport@illumina.com). RATE PCR allows rapid and easy identification of the EZ-Tn5 transposon insertion sites in the host genome.
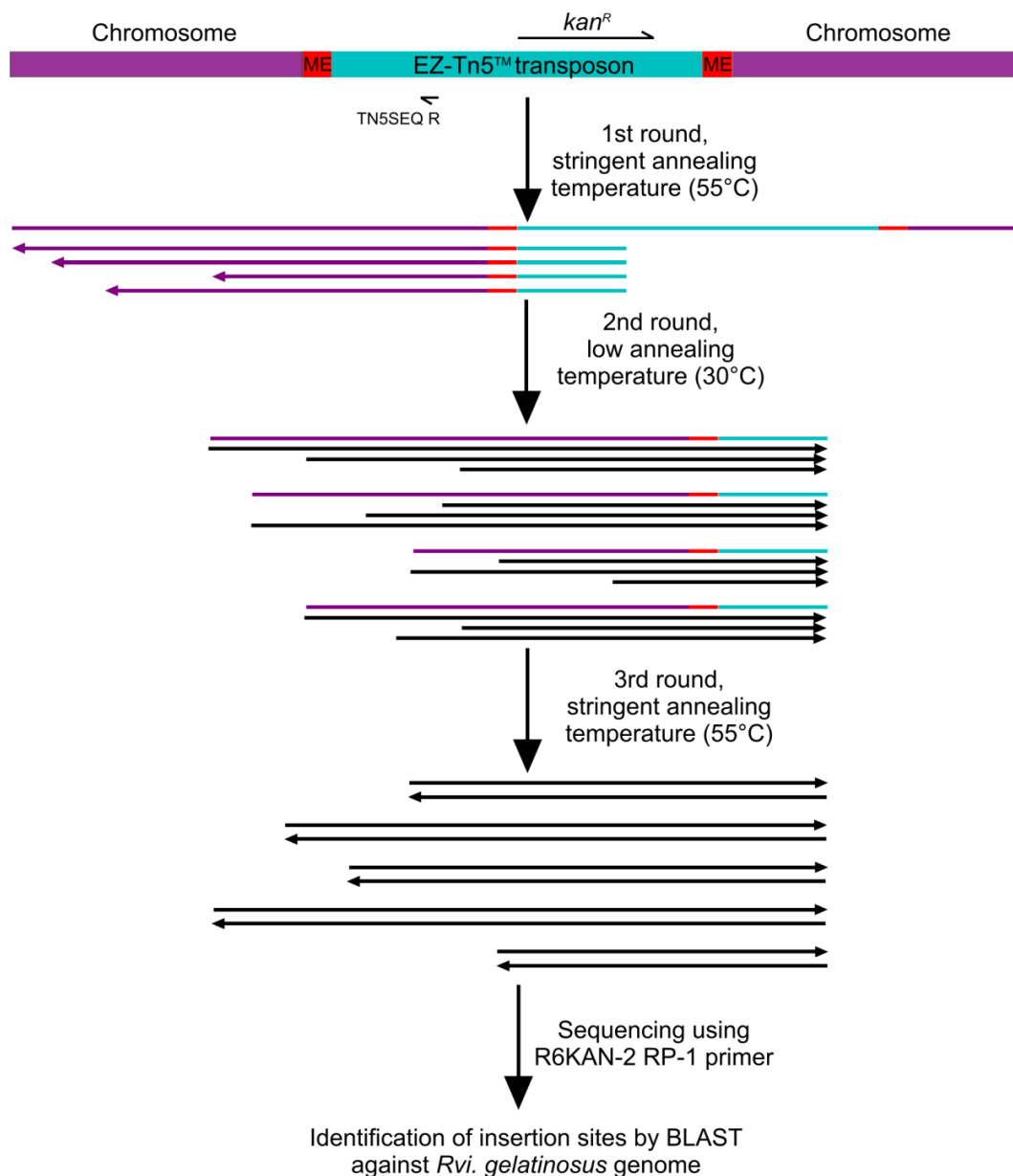
Figure 6.5 Mechanism of RATE PCR

RATE PCR is a single-primer PCR with three rounds of cycling conditions performed in the same reaction. A stringent annealing temperature (55°C) is used in the first round of cycling in which a series of single-strand products are generated by the unidirectional primer extension. In the second round of cycling, the low annealing temperature (30°C) allows non-specific amplification of the single strand products created in the first round. Finally, all the PCR products from the second round of cycling are amplified in the third round of cycling with a stringent annealing temperature (55°C). This figure is based on Ducey and Dyer (2002) and communication with Dr Fred Hyde (Illumina Technical Support).

As depicted in **Figure 6.5**, a single primer within the transposon is used in RATE PCR with three rounds of thermal cycling program all performed in the same reaction. Each round of the cycling program consists of 30 cycles of steps of denaturation, annealing and elongation. In the first round of cycling, a stringent annealing temperature (55°C for the TN5SEQ R primer) is used to generate a series of single-strand products from the unidirectional primer extension. The second round of cycling applies a low annealing temperature (30°C), which allows non-specific amplification of the single-strand products generated from the first round. As a result, a nested set of PCR products (same 5'-region, variable 3'-region) is produced. Finally, a stringent annealing temperature is used again in the third round of cycling. In this round, the nested products from the second round are amplified in a classic PCR manner. DNA purified from the RATE PCR products is directly sequenced using the Sanger method using a primer (R6KAN-2 RP-1 in the case of using TN5SEQ R primer for RATE PCR) located within the region of transposon that is amplified in RATE PCR.

At first, the INV-2 primer (**Figure 6.2**) was used in RATE PCR as described in Section 2.11.4. 5 μl of the RATE PCR products were resolved on a 1% agarose gel to check for successful amplification. The remaining reaction was purified using the GenElute^{TM} PCR Clean-up Kit (Sigma-Aldrich) according to the manufacturer's instructions. Then the purified DNA was sent for sequencing using the KAN-2 FP-1 primer (**Figure 6.2**). The transposon insertion sites were revealed by performing BLAST searches using the obtained sequences as a query against the *Rvi. gelatinosus* genome. Surprisingly, 18 out of the 38 isolated mutants appeared to contain the transposon inserted at exactly the same location within the *bchF* gene. This indicates an error in the procedure. So in order to check the accuracy of the identified transposon locations, confirmatory PCR was performed using a primer from the genomic region neighbouring the transposon and a primer within the transposon. This analysis showed that the insertion sites in 16 out of the 18 '*bchF*' mutants and 3 other ones are not at the proposed locations.
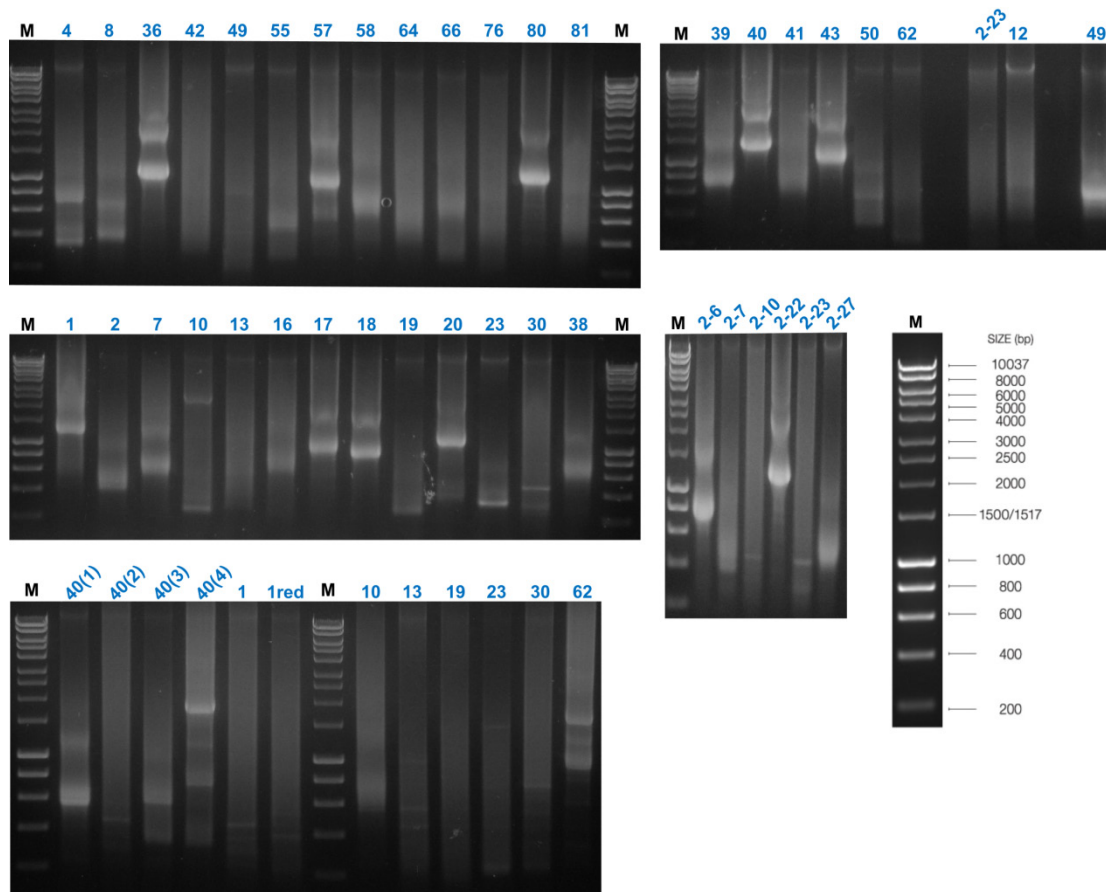
Figure 6.6 RATE PCR products resolved by agarose gels

RATE PCR products were resolved on 1% agarose gels and visualised by ethidium bromide staining. M stands for the HyperLadder™ 1kb (Bioline) DNA marker. The molecular weight of each band of the DNA marker is shown at the bottom right. Lanes are labelled by the designation numbers of mutants on the top. 40(1), (2), (3) and (4) are RATE PCR reactions using four individual colonies of TN40 mutant as a template.

RATE PCR and subsequent sequencing were repeated for the 19 mutants that could not be confirmed by PCR, as above. However, the results were the same. This unexpected outcome likely arises from a problem with RATE PCR with *Rvi. gelatinosus* genomic DNA, specifically the INV-2 primer. Accordingly a new primer, TN5SEQ R (**Figure 6.2**), was designed for RATE PCR. Using the TN5SEQ R primer with the same reaction conditions and the same cycling program, RATE PCR was performed with all the 38 mutants. This time, the whole RATE PCR reaction was resolved on a 1% agarose gel as shown in **Figure 6.6**. Multiple and smeared bands are normal for RATE PCR products according to the mechanism explained in **Figure 6.5.** An abundant band was excised from which DNA was purified using the GenElute™ Gel Extraction Kit (Sigma-Aldrich) following the manufacturer's instructions. Purified DNA was sequenced using the R6KAN-2 RP-1 primer (**Figure 6.2**). The identified transposon insertion

sites are listed in **Table 6.1**. All 19 mutants with transposon locations previously confirmed by PCR were correctly located by RATE PCR with the TN5SEQ R primer. The remaining 19 mutants were revealed to contain unique transposon insertions by RATE PCR with the TN5SEQ R primer. TN38, 39 and 43 share the same transposon insertion site, so do TN41 and TN42. On these two occasions, the mutants may have originated from a common parental mutant. It is also worth mentioning that the originally isolated 'TN1' mutant was subsequently found to be a mixture of two mutants. The designation TN1 was given to the mutant with the *bchC* gene inactivated by transposon insertion. The other mutant was named as TN1red, which is able to synthesise BChl. The transposon loci identified via the second RATE PCR correspond well with the phenotypes of the mutants, including the colouration of the colony, whole-cell absorption spectrum and conclusively, the pigment profile revealed by HPLC. The transposon locations in the isolated BChl-deficient mutants were mapped to the PGC of *Rvi. gelatinosus* genome as shown in **Figure 6.7**.

Table 6.1 Transposon locations and genes affected in isolated mutants

Mutant	Insertion site[a]	Locus tag	Gene	Gene product	Gene location[b]
TN1[c]	3,599,428	RGE_33710	*bchC*	3-HE BChlide *a* dehydrogenase	3,598,761..3,599,714
TN2	3,596,084	RGE_33680	*bchZ*	Z subunit of Chlide *a* oxidoreductase	3,594,756..3,596,219
TN4	3,595,544	RGE_33680	*bchZ*	Same as above	Same as above
TN16	3,595,818	RGE_33680	*bchZ*	Same as above	Same as above
TN18	3,596,165	RGE_33680	*bchZ*	Same as above	Same as above
TN76	3,595,889	RGE_33680	*bchZ*	Same as above	Same as above
TN30	3,596,418	RGE_33690	*bchY*	Y subunit of Chlide *a* oxidoreductase	3,596,219..3,597,751
TN13	3,572,409	RGE_33450	*bchF*	3-V BChlide *a* hydratase	3,572,212..3,572,721
TN19	3,572,453	RGE_33450	*bchF*	Same as above	Same as above
TN8	3,575,074	RGE_33470	*bchB*	B subunit of dark-operative PChlide reductase	3,574,003..3,575,634
TN49	3,574,893	RGE_33470	*bchB*	Same as above	Same as above
TN2-23[d]	3,574,418	RGE_33470	*bchB*	Same as above	Same as above
TN7	3,579,661	RGE_33490	*bchL*	L subunit of dark-operative PChlide reductase	3,579,360..3,580,268
TN10	3,579,613	RGE_33450	*bchL*	Same as above	Same as above
TN20	3,579,966	RGE_33490	*bchL*	Same as above	Same as above
TN55	3,579,387	RGE_33490	*bchL*	Same as above	Same as above
TN80	3,580,251	RGE_33490	*bchL*	Same as above	Same as above
TN2-22	3,580,222	RGE_33490	*bchL*	Same as above	Same as above
TN23	3,573,407	RGE_33450	*bchN*	N subunit of dark-operative PChlide reductase	3,572,718..3,574,001
TN81	3,572,989	RGE_33460	*bchN*	Same as above	Same as above
TN17	3,585,140	RGE_33550	*acsF*	Oxygen-dependent MgPME cyclase	3,584,367..3,585,443
TN38	3,584,842	RGE_33550	*acsF*	Same as above	Same as above
TN39	3,584,842	RGE_33550	*acsF*	Same as above	Same as above
TN41	3,584,457	RGE_33550	*acsF*	Same as above	Same as above
TN42	3,584,457	RGE_33550	*acsF*	Same as above	Same as above
TN43	3,584,842	RGE_33550	*acsF*	Same as above	Same as above
TN50	3,584,408	RGE_33550	*acsF*	Same as above	Same as above
TN2-7	3,567,368	RGE_33410	*bchG*	BChl *a* synthase	3,567,056..3,567,940
TN2-10	3,567,909	RGE_33410	*bchG*	Same as above	
B37	3,579,066	RGE_33480	*bchH*	H subunit of Mg chelatase	3,575,606..3,579,316
TN1red[e]	1,242,174	RGE_11930	N/A	Hypothetical protein	1,242,167..1,242,313
TN36	2,488,567	RGE_23650	*aceE*	Pyruvate dehydrogenase E1 component	2,486,488..2,489,190
TN40	4,436,161	RGE_41330	*luxE*	Acyl-protein synthetase	4,436,022..4,437,110
TN57	3,496,809	RGE_32740	N/A	Putative methyltransferase	3,496,358..3,497,188
TN58	2,960,446	RGE_27920	*lon*	ATP-dependent protease La, Lon	2,958,826..2,961,249
TN62	1,408,573	RGE_13740	N/A	RfaE bifunctional protein, domain II	1,408,250..1,408,726
TN64	4,556,898	RGE_42470	*grxD*	Glutaredoxin-4	4,556,750..4,557,064
TN66	3,398,834	RGE_31860	*fnrL*	Anaerobic regulatory protein FnrL	3,398,594..3,399,337
TN2-6	4,398,614	RGE_40920	*rne*	Ribonuclease E	4,397,543..4,400,446
TN2-27	3,540,734	RGE_33180	*pstC*	Phosphate ABC transporter permease PstC	3,540,260..3,541,237

[a] Transposon was inserted after this base pair.

[b] The number in blue indicates where the transcription starts.

[c] Further analysis revealed the 'TN1' mutant isolated at the beginning was a mixture of two mutants. Here, TN1 represents one of the two mutants and is unable to synthesise BChl.

[d] TN2-x mutants were isolated from a second mutagenesis library as described in Section 6.3.3.

[e] Further analysis revealed the 'TN1' mutant isolated at the beginning was a mixture of two mutants. Here, TN1red represents one of the two mutants and has the ability to synthesise BChl.

[f] N/A, gene symbol is not available in the database.
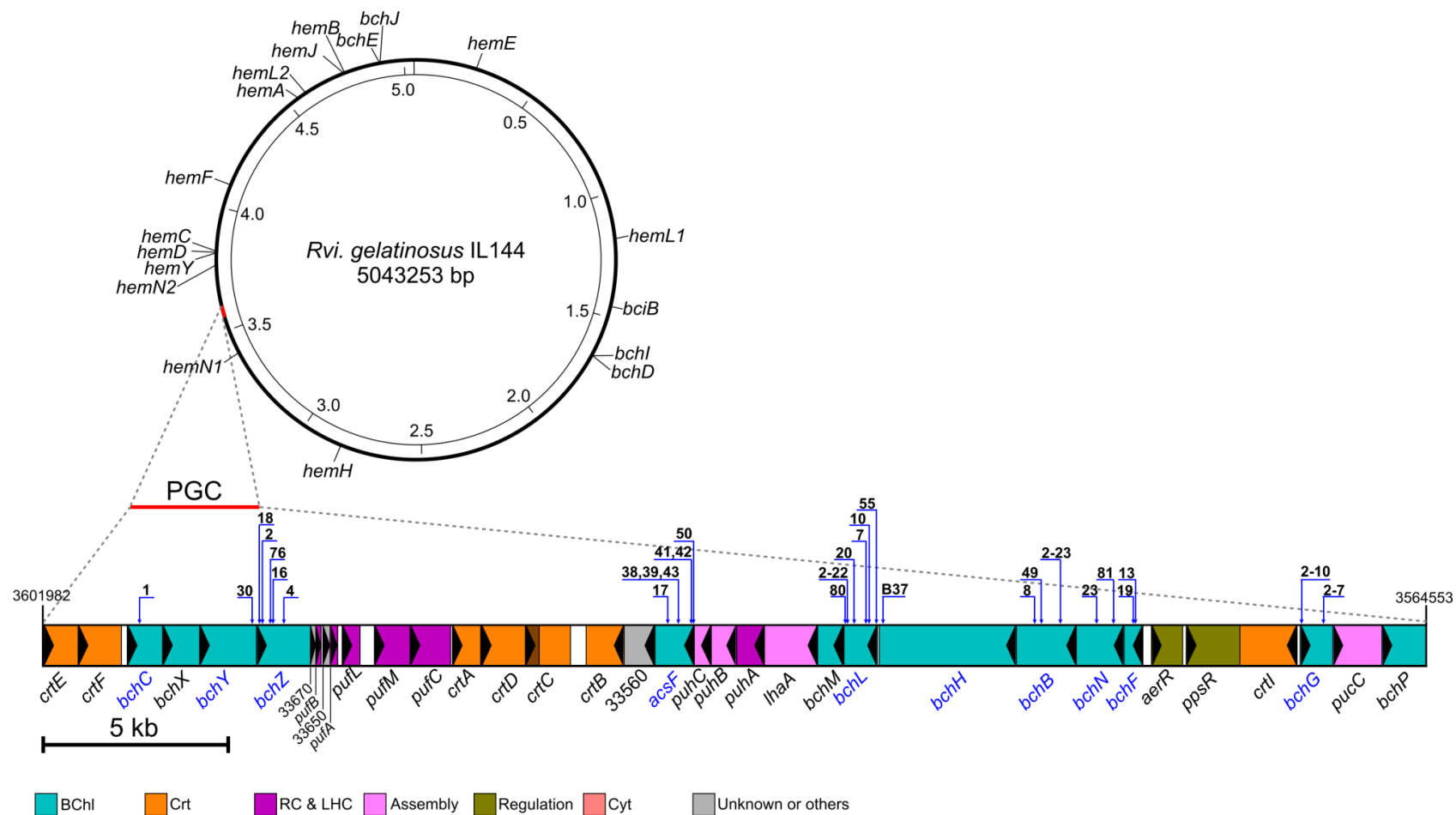
Figure 6.7 Locations of transposon inserts within the *Rvi. gelatinosus* genome

The transposon insertion sites in isolated mutants are mapped in the PGC of *Rvi. gelatinosus* genome. Genes in the PGC are represented as colour filled rectangles within which the arrow indicates the transcription direction. A locus tag is used with the omission of the RGE_ where a gene symbol is unavailable. Genes associated with BChl biosynthesis but located outside the PGC are also indicated in the genome. Abbreviations: PGC, photosynthetic gene cluster; BChl, bacteriochlorophyll biosynthesis; Crt, carotenoid biosynthesis; RC&LHC, reaction centre and light-harvesting complexes; Cyt, cytochrome.

6.3.6 HPLC analysis of pigments accumulated in isolated mutants

The isolated transposon mutants were directly inoculated from glycerol stocks into 10 ml of PYS medium supplemented with 50 μg ml^{-1} of kanamycin in a 50 ml Falcon tube. Incubation was performed at 30°C with shaking at 150 rpm for 3 days. Pigments were extracted from cells pelleted from the whole 10 ml culture as described in Section 2.8.1. The resulting extracts were analysed by HPLC using the program for separation of Chl precursors (Section 2.8.5).

Pigments accumulated in all the 39 mutants that passed the two screenings were analysed by HPLC as described above. The analysis of the B37 mutant was also included as this mutant will be employed and discussed in Chapter 7. The 10 mutants with transposon insertion at a gene that is not obviously involved in BChl biosynthesis were shown to produce BChl *a* by the HPLC analysis. These mutants are TN1red, TN36, TN40, TN57, TN58, TN62, TN64, TN66, TN2-6 and TN2-27, as listed in **Table 6.1**. Without doubt, no BChl was detected in the remaining 30 mutants. As mutants with the same gene inactivated by transposon insertion typically had a similar pigment profile, only one representative pigment profile of these mutants is shown for the sake of conciseness. As shown in **Figure 6.8**, the absorbance at an indicated wavelength was plotted against the retention time. The peaks were labelled by a lowercase letter. Peaks sharing both the absorption spectrum and the retention time were given the same label. The absorption spectra of peaks were shown at the top right (**Figure 6.8**).
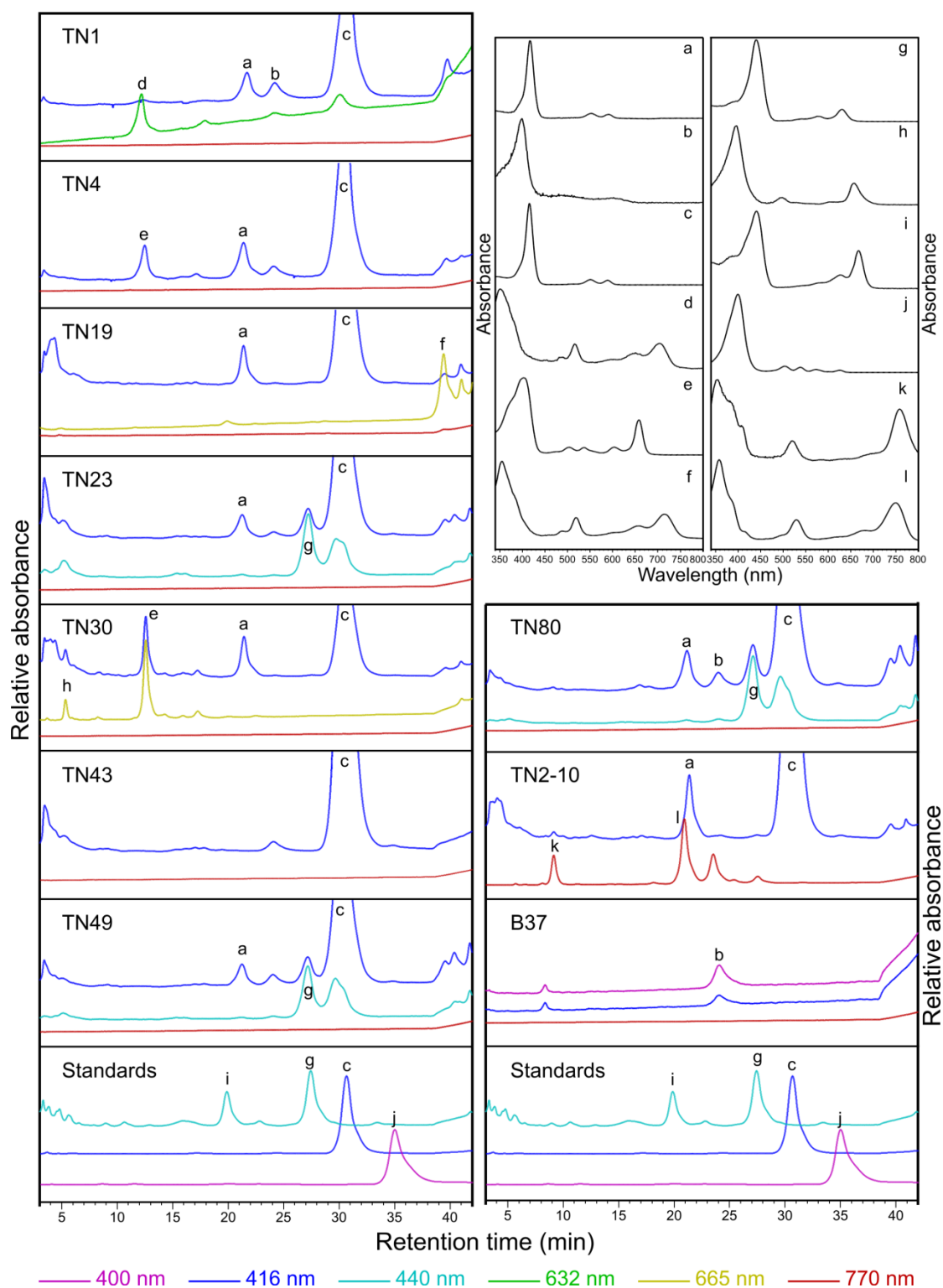
Figure 6.8 HPLC analysis of pigments accumulated in isolated mutants

Pigments extracted from aerobic cultures of the isolated mutants were analysed by HPLC. The relative absorbance at an indicated wavelength (colour coded) is plotted against retention time. Peaks are marked by lowercase letters. Absorption spectra of the peaks are shown at the top right. The identities of the peaks are described in Section 6.3.6.

The retention times and the absorption maxima of the peaks present in the HPLC elution profiles of the transposon mutants are listed in **Table 6.2**. Assignments of peaks were done or attempted by referring to the standards or published reports in respect of hydrophobicity and absorption spectra.

Table 6.2 Assignments of the peaks in HPLC elution profiles of transposon mutants

Peak	Retention time (min)	Soret (nm)	Q_x (nm)	Q_y (nm)	Assignment
a	21.41	416			MgP
b	23.99	400			Haem?
c	30.63	416			MgPME
d	12.20	350	515	703	3-HE BChlide *a*
e	12.47	405		659	3-HE Chlide *a*
f	39.42	354	519	714	3-V BChlide *a* with a tail?
g	27.44	440		631	DV PChlide *a*
h	5.32	398		657	?
i	19.88	442		668	DV Chlide *a*
j	34.96	401			Proto
k	9.13	355	522	760	Zn-Bpheid *a*
l	20.91	359	530	750	Bpheid *a*

As shown by the standards, Peaks c, g, i and j represented MgPME, DV PChlide *a*, DV Chlide *a* and Proto, respectively. Peak a was assigned as MgP as it was eluted between DV Chlide *a* and MgPME, as well as having a Soret maximum at 416 nm. Peak b (Soret band = 400 nm) with a retention time close to that of MgP but much shorter than that of Proto, is likely to be a haem or haem derivative species (Chu *et al.*, 1999). Peak d (Q_y band = 703 nm) was assigned as 3-HE BChlide *a* by comparing it with the pigment extracts from a *Rba. sphaeroides bchC* mutant (Hunter and Coomber, 1988) and a *Rba. capsulatus bchC* mutant (Wellington and Beatty, 1989). The order of the two steps catalysed by COR (encoded by the *bchX*, *bchY* and *bchZ* genes) and 3-V BChlide *a* hydratase (encoded by the *bchF* gene) is interchangeable (Pudek and Richards, 1975), which was considered when assigning Peaks e, f and g. Peak e (Q_y band = 659 nm) was assigned as 3-HE Chlide *a* based on the pigment analysis of a COR-deficient mutant of *Rba. sphaeroides* (Hunter and Coomber, 1988). Peak f (retention time = 39.42 min) had a much more hydrophobic nature compared with other intermediates of BChl biosynthesis, suggesting the presence of an isoprenoid moiety. The absorption spectrum of Peak f (Q_x band = 519 nm, Q_y band = 714 nm) was almost identical to that of 3-V BChlide *a*, a pigment shown to be accumulated in a *bchF* mutant of *Rba. capsulatus* (Burke *et al.*, 1993a). Thus, it is likely that Peak f represented a pigment resulted from the esterification of 3-V BChlide *a* with an isoprenoid alcohol. Although the identity of Peak h is not clear, it is certain

that Peak h represented a chlorin pigment since it had a Q_y band at 657 nm. Furthermore, Peak h (retention time = 5.32 min) could not be 3-acetyl Chlide *a* which would come out between 3-HE Chlide *a* and Chlide *a* (Lange *et al.*, 2015). The absorption spectra of Peaks k and l resembled that of BChlide *a*, and exhibited blue shifts of all the absorbance maxima. Referring to the absorbance maxima of metal-substituted BChls reported by Hartwich *et al.* 1998), Peaks k and l were assigned as Zn-bacteriopheophorbide (Zn-Bpheid) *a* and Bpheid *a*, respectively. The assignments of Peaks k and l are supported by the reports that Zn-BChl *a* was detected in a Δ*bchE* mutant of *Rba. sphaeroides* (described in Chapter 3, Chen *et al.*, 2016a) and that *Rba. sphaeroides bchG* mutants were shown to accumulate Bpheid *a* (Addlesee *et al.*, 2000).

6.4 Discussion

6.4.1 Evaluation of transposon mutagenesis and mutant screening

Transposon mutagenesis can be performed effectively using the EZ-Tn5 Transposome system with electrocompetent *Rvi. gelatinosus* Δ*bchE* cells. A single electroporation with 1 *μ*l of the transposome and 40 *μ*l of competent cells was able to generate 13,000~18,000 transposon containing mutants, which does not count the unviable mutants. A comprehensive library consisting of more than 30,000 mutants was created to search for gene(s) encoding hitherto unidentified subunit(s) of the aerobic cyclase. Unlike classic transposon mutagenesis, the mutants generated by the EZ-Tn5 Transposome are stable during further culturing since the EZ-Tn5 transposon does not contain a gene encoding transposase. This allows detailed characterisation of the isolated mutants without the risk of generating secondary transposon mutations.

Rvi. gelatinosus (strain IL144) has a genome of 5,043,253 bp, comprising 4,767 genes (Nagashima *et al.*, 2012). Very recently, the number of essential genes in *Rvi. gelatinosus* has been determined by Curtis (2016). In this report, transposon sequencing was used to identify essential genes in *Rvi. gelatinosus* grown in a rich medium under aerobic conditions. The author designated 388 genes as essential, 103 genes as unresolved and the remaining 4,276 genes as non-essential. Although emphasised by the author to be putative, the designation was based on experimental evidence and should be taken as the best currently available. The work in this chapter employed strain (IL144) of *Rvi. gelatinosus* as in Curtis (2016) and also used a rich medium and aerobic conditions to select for transposon mutants. Thus, the number of essential genes determined by Curtis (2016) can be safely applied to the present

study, which would be 388 if the 103 unsolved genes are hypothesised to be non-essential. Only non-essential genes can be represented by a mutagenesis library as it is lethal to inactivate essential genes. A mutagenesis library of more than 30,000 mutants can provide a 7-fold coverage of the *Rvi. gelatinosus* genome containing 4,379 non-essential genes. Such a high-level coverage laid a solid foundation for the project.
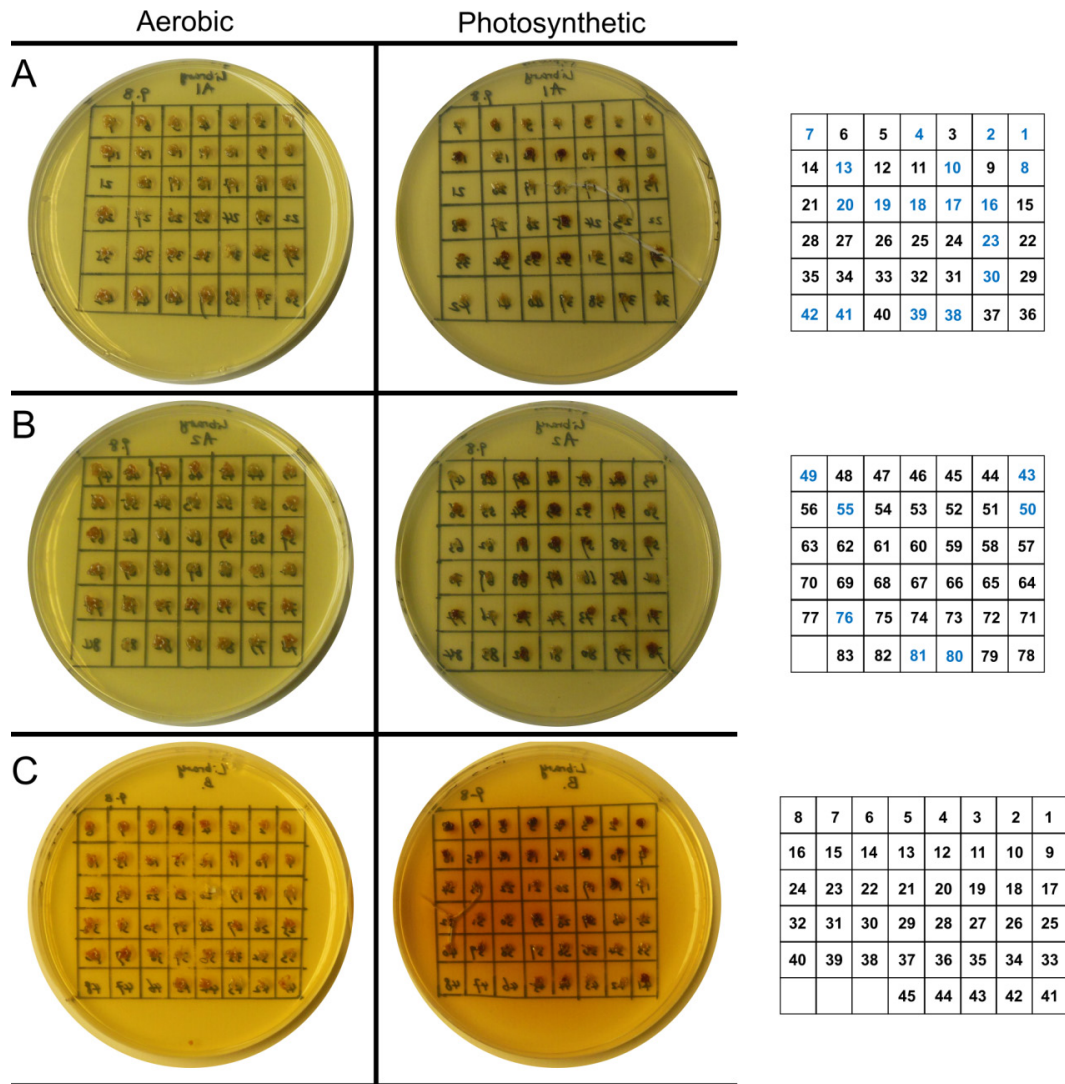
Figure 6.9 Comparison of aerobic growth and photosynthetic growth of the isolated mutants

Each mutant was stabbed onto two plates containing PYS agar medium supplemented with kanamycin. One plate was incubated under aerobic conditions (left) and the other plate was incubated under photosynthetic conditions (anaerobic and illuminated; right). The designation number of each mutant is indicated in the number box. (**A**)(**B**) Mutants isolated because of exhibiting apparent fluorescence excited at 395 nm. The numbers in blue represent mutants which are unable to synthesise BChl. (**C**) Mutants isolated due to displaying brown colour when illuminated by 395 nm light.

The first mutant screen was carried out simply with a 395 nm LED flashlight providing the excitation light source and visual inspection (protected by laser safety glasses) of colony fluorescence. The 30,000 colonies were narrowed down to 83 mutants, all of which displayed apparent fluorescence, demonstrating the power and efficiency of the first screen. It is worth mentioning that a 3-day incubation at 30°C (Plates 1 to 5) was shown to be ideal for the screening and extended incubation generally diminished fluorescence intensity (Plates 6 to 11), as described in Section 6.3.2. For the purpose of searching for the unknown gene(s), any false-negative error would jeopardise the whole project, whereas false-negative errors could be easily ruled out by a second screening. Thus, when there was an uncertainty during the screening, the mutant was considered to be positive. The comparison of aerobic growth and photosynthetic growth of isolated mutants including the 83 fluorescent mutants and the 45 B-type mutants was shown in **Figure 6.9**. A colour difference between colonies grown under aerobic and photosynthetic conditions usually indicates the ability to photosynthesise. As expected, many of the 83 mutants were shown to be false-positive since they were able to synthesise BChl, which is essential to photosynthesis (**Figure 6.9**).

An aerobic cyclase mutant with a $\Delta bchE$ background is unable to synthesise BChl. Thus, in the second screening, pigment extracts from liquid cultures of the isolated mutants were checked for the presence of BChl *a* by absorption spectra. When it was difficult to judge Bchl content from the absorption spectrum, the same rule was applied as the first screening to avoid any false-negative error; the 83 mutants were further narrowed down to 33. In addition, the 32 mutants isolated from Plates 6 to 11 were narrowed down to only 6. The number of mutants that passed the two screening strategies was in the practical range for a thorough analysis of the pigment profile of each mutant. HPLC analysis ruled out all the false-positive mutants, leaving 29 that are absolutely unable to produce BChl *a*. The HPLC elution profiles revealed high levels of MgPME, which were detected in all 29 mutants, even in those that apparently have a functional aerobic cyclase (**Figure 6.8**).This accumulation of MgPME might arise from inhibition of the aerobic cyclase by the build-up of the downstream intermediates of BChl. Alternatively, a fully active aerobic cyclase may require the presence of other BChl biosynthesis enzymes, as discussed in Section 4.4.1.

6.4.2 Evaluation of locating the transposon insertion sites

The transposon insertion sites in the 39 mutants isolated were successfully determined using a method based on RATE PCR, which was applied to amplify the genomic region flanking the transposon from the mutants that passed the two screens. DNA purified from the RATE PCR

reaction was directly sequenced by the Sanger method using a primer within the transposon. The traditional 'rescue cloning' method involves purification of genomic DNA, digestion, self-ligation, transformation, plasmid extraction and sequencing. In contrast, the method based on RATE PCR is straightforward, cost- and time-saving, and provides a significant advantage over the 'rescue cloning' method. Despite the use of purified genomic DNA as the template for RATE PCR in this chapter, there should be no problem to directly use mutant cells as the template, which would make the method even simpler. As a low annealing temperature is applied in the second round of cycling (Section 6.3.5), RATE PCR generates a mixture of many different amplicons (**Figure 6.6**). Although the RATE PCR reaction can be directly cleaned up for sequencing, agarose gel electrophoresis of the reaction and subsequent gel extraction are recommended in order to lower the complexity of the products and improve sequencing efficiency. The mechanism of RATE PCR (**Figure 6.5**) and the experiments performed indicate that the selection of a band in the gel does not affect the sequencing result as long as an adequate amount of DNA can be purified from the excised band.

Section 6.3.5 mentions some difficulties with RATE PCR and the INV-2 primer, since it failed to accurately identify transposon sites in half of the analysed mutants. The problem was solved when a newly designed primer, TN5SEQ R, was used for RATE PCR although the reason for this improvement is not easily explained. Trialling several primers for RATE PCR to find a good match with a certain organism is worthwhile. Confirmatory PCR should be performed using a primer located in the genomic region close to the disclosed transposon site and a primer within the transposon.

6.4.3 No additional subunit of aerobic cyclase is found in *Rvi. gelatinosus*

The locations of the transposon in the isolated mutants are listed in **Table 6.1** together with the genes affected by the insertion. 29 of the 39 mutants have transposon insertions within genes encoding enzymes involved in the BChl biosynthesis pathway. These insertions, including 4 insertions (all listed are unique) in *acsF*, 3 in *bchB*, 6 in *bchL*, 2 in *bchN*, 1 in *bchY*, 5 in *bchZ*, 2 in *bchF*, 1 in *bchC* and 2 in *bchG*, were mapped in the PGC of *Rvi. gelatinosus* genome (**Figure 6.7**). Pigment profiles of the mutants of *bchB*, *bchL*, *bchN*, *bchY*, *bchZ*, *bchF*, *bchC* and *bchG*, clearly eliminate the possibility that these 8 genes are involved in the aerobic cyclase reaction, and they also demonstrate the wide coverage of *bch* genes identified by the transposon insertion method used here. The remaining 10 mutants contain insertions in genes that are not directly associated with BChl biosynthesis. Given HPLC analysis revealed that all these 10 mutants can produce BChl *a*, it is unlikely the genes affected in these

mutants could encode a subunit of aerobic cyclase. In conclusion, no additional subunit of aerobic cyclase has been found in *Rvi. gelatinosus* through transposon mutagenesis.

Compared with positive data, negative results are more difficult to rationalise, and this search for another aerobic cyclase gene did not yield any candidates. Such a gene, or genes, could still await identification, and confidence in *acsF* being the only such gene is completely dependent on the quality assessment of the searching procedures. The EZ-Tn5 transposon mutagenesis has been demonstrated to be a reliable method for random mutatgenesis in previous studies (Vanzin *et al.*, 2010; Steunou *et al.*, 2013; Azzouzi *et al.*, 2013), and also by the identification of 26 *bch* insertions in the present work. The omission of a transposase-encoding gene in the transposon sequence ensures no secondary transposon mutation arises during downstream characterisation. A 7-fold coverage of the genome should guarantee all the non-essential genes of *Rvi. gelatinosus* were represented by mutants in the library. During the two screenings, false-negative errors were intentionally avoided in the cost of many false-positive errors. Above all, 4 unique insertions within the *acsF* gene were generated and identified, clearly demonstrating the excellent quality of the searching procedures. Therefore, this mutagenesis study leads to the tentative conclusion that no additional subunit is required by aerobic cyclase in *Rvi. gelatinosus*.

6.4.4 The isolated mutants are potentially useful for future study

As the by-products of the searching procedures, the isolated transposon mutants can serve as good resources for future studies. The identified BChl-deficient mutants can not only be utilised to prepare tetrapyrrole substrates for assays of enzymes in the BChl biosynthesis pathway but also be used as host strains to perform complementation test with a gene of interest. For example, a POR enzyme can be introduced into the mutants with disrupted DPOR (*bchB*, *bchL* and *bchN* mutants) to check whether it can be functional in *Rvi. gelatinosus*. As a good example, TN43 (*acsF* mutant) and B37 (*bchH* mutant) will be employed to demonstrate the entry of MgPME into cells in Chapter 7. The 10 mutants which are not defective in BChl biosynthesis can potentially facilitate studies in other fields, such as TN36 (*aceE* mutant) which can be used to study carbon metabolism, TN66 (*fnrL* mutant) which can be a useful strain for exploring the anaerobic regulation of photosynthetic genes, TN2-27 (*pstC* mutant) which can help with the study of phosphate transport, and so on. Although the remaining mutants including the ones isolated from the first screening but failed to pass the second screening and the B mutants are not of the concern in this chapter, they exhibit lots of interesting phenotypes, such as a yellow-green colour for liquid cultures, and an orange-

red colour in some growth media and anomalous peaks for light-harvesting complexes in the whole-cell absorption spectra. These mutants are worthy of more detailed investigations in the future.

Chapter 7

Introduction of the aerobic cyclase into *Rhodobacter capsulatus* and construction of the core pathway of chlorophyll biosynthesis in *E. coli*

7.1 Summary

This chapter reports the first experimental evidence that AcsF is the only subunit required for activity of the aerobic cyclase in *Rvi. gelatinosus.* Another purple bacterium, *Rba. capsulatus*, which does not contain *acsF*, was shown to be able to synthesise BChl *a* via the aerobic cyclase route upon expression of the *Rvi. gelatinosus acsF* gene. More conclusively, the aerobic cyclase activity was demonstrated *in vivo* with an *E. coli* strain expressing the *Rvi. gelatinosus acsF* gene from a plasmid. A pET3a-based plasmid harbouring 8 Chl biosynthetic genes cloned from *Synechocystis* and *Rvi. gelatinosus* was built and shown to endow *E. coli* with the capability to synthesise Chlide. The construction of the core pathway of Chl biosynthesis in *E. coli* has laid the foundation for engineering *E. coli* into a phototrophic organism.

7.2 Introduction

One of the major themes of this thesis is the endeavour to identify the unknown subunits of the aerobic cyclase, the existence of which having been suggested by several previous studies. So far, considerable efforts have been spent to serve this purpose. As reported in Chapter 5, the Δ*ycf54* mutant of *Synechocystis,* which exhibits compromised activity of the aerobic cyclase, was subjected to a suppressor screen. Four suppressor mutants were isolated and subsequently analysed by genomic sequencing, which did not reveal any candidate for the unknown subunits of the aerobic cyclase. The result of the suppressor screen is, far from conclusive, but might be interpreted as weak support of an alternative hypothesis regarding the subunit composition of this enzyme. On the other hand, as presented in Chapter 6, the *Rvi. gelatinosus* genome was surveyed by transposon mutagenesis with 7-fold coverage. The identification of 4 unique insertions in the *acsF* gene clearly validates the coverage of the mutagenesis and reliability of the screening method. Even so, no additional subunit of the

aerobic cyclase was found. The result of the transposon mutagenesis provides a strong argument against the existence of unknown subunits of the aerobic cyclase.

The approach to study the genetic identity of an enzyme by mutagenesis in the native system is informative but not always conclusive. The ultimate proof of enzyme composition is usually obtained by testing the enzymatic activity of heterologously expressed gene products. Since the suppressor screen and transposon mutagenesis failed to uncover any new subunit of the aerobic cyclase, it is worthwhile to test whether the known subunits are able to catalyse the cyclase reaction. As shown in Chapter 4, three classes of the aerobic cyclase were identified by complementation experiments conducted in *Rvi. gelatinosus*, among which the Class II enzyme is the simplest. Thus, the only known subunit of the Class II enzyme, AcsF, was selected to be investigated first. The results of Chapter 3 demonstrate that a functional aerobic cyclase is present in *Rba. sphaeroides*, the activity of which is greatly stimulated upon the removal of the cbb_3 terminal oxidase. Another purple bacterium, *Rba. capsulatus*, is a well-studied phototrophic organism and exhibits a high degree of similarity with *Rba. sphaeroides*. Unlike *Rba. sphaeroides*, genome sequence data confirm that *Rba. capsulatus* does not possess *acsF*, and thus lack the aerobic cyclase (Strnad *et al*., 2010). The close relation with a bacterium displaying aerobic cyclase activity, together with confirmed absence of the genes encoding an aerobic cyclase, makes *Rba. capsulatus* an ideal expression host for *acsF* at the initial stage. The sequenced *Rba. capsulatus* SB1003 strain was obtained as a kind gift from Professor Carl Bauer (Indiana University, USA) and employed in this chapter to assay the activity of AcsF from *Rvi. gelatinosus*. Following this, it is essential to conduct the test in an *E. coli* system in order to determine whether *Rba. capsulatus* contains some facilitating factors that are required for cyclase activity.

7.3 Results

7.3.1 Mutant construction and expression of the *Rvi. gelatinosus acsF* gene in *Rba. capsulatus*

The *Rba. capsulatus* strain (SB1003) used in this study confers resistance to rifampicin (Yen and Marrs, 1976) and was grown in MPYE medium (Koch *et al*., 1998). The pK18*mobsacB* vector has been applied to generate markerless, in-frame mutants in *Rba. capsulatus* (Pekgöz *et al*., 2011). Thus, the method described in Section 3.3.1 was trialled and shown to be employable in *Rba. capsulatus* if slight modifications were applied. The first modification was the addition of 20 μg ml^{-1} of rifampicin to counter-select against *E. coli* during the selection

for *Rba. capsulatus* transconjugants, as MPYE medium contains 0.3% (w/v) peptone and 0.3% (w/v) yeast extract, which support the growth of *E. coli*. The second modification was an extra culturing procedure. The obtained kanamycin-resistant *Rba. capsulatus* transconjugants were sub-cultured three times in non-selective medium to permit a second homologous recombination. Other procedures were conducted as the same as described in Section 3.3.1.
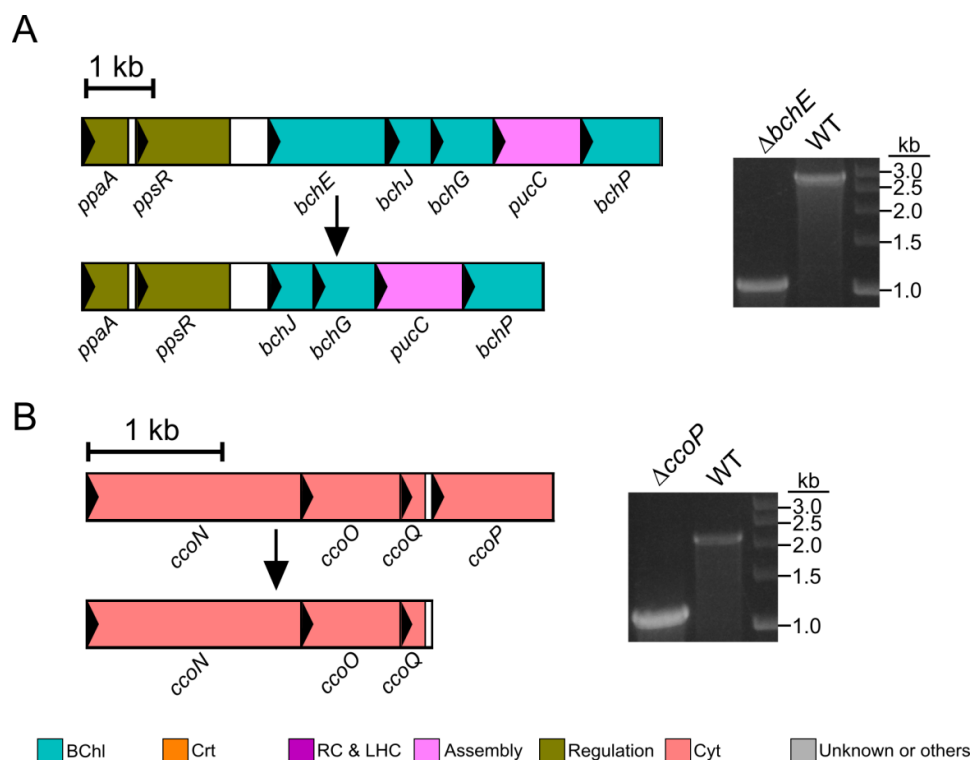
Figure 7.1 Deletion of the *bchE* and *ccoP* genes in *Rba. capsulatus*

The genomic regions adjacent to the gene of interest from wild type and the deletion mutant are depicted in proportion to the scale bar. Genes are represented as colour filled rectangles within which the arrow head indicates the transcription direction. Colony PCR gel are also presented. Abbreviations: BChl, bacteriochorophyll biosynthesis; Crt, carotenoid biosynthesis; RC & LHC, reaction centre and light-harvesting complexes; Cyt, cytochrome. (**A**) Deletion of the *bchE* gene. Lengths of PCR products: wild type = 2762 bp; Δ*bchE* = 1046 bp. (**B**) Deletion of the *ccoP* gene. Lengths of PCR products: wild type = 2046 bp; Δ*ccoP* = 1164 bp.

The anaerobic cyclase encoding gene *bchE* was deleted using the method described above, resulting in a Δ*bchE* mutant (**Figure 7.1 A**). As shown in Chapter 3 and reported in Chen *et al*. (2016a), inactivation of the cbb_3 terminal oxidase is beneficial for detection of aerobic cyclase activity in *Rba. sphaeroides*. Considering *Rba. capsulatus* is a close relative to *Rba. sphaeroides*, inactivation of the cbb_3 oxidase in *Rba. capsulatus* by deleting one of its encoding genes, the *ccoP* gene, was also carried out (**Figure 7.1 B**). By combining the two deletions, a Δ*ccoP*Δ*bchE* mutant was constructed and employed as the background strain to

test the activity of the aerobic cyclase. The *Rvi. gelatinosus acsF* gene was introduced into the ΔccoPΔbchE mutant through the pBB[*acsF*] plasmid (Section 5.3.5) by conjugation, resulting in the ΔccoPΔbchE pBB[*acsF*] strain.

7.3.2 Phenotypic analyses of the constructed *Rba. capsulatus* mutants

The WT, Δ*ccoP*, Δ*bchE*, Δ*ccoP*Δ*bchE* and Δ*ccoP*Δ*bchE* pBB[*acsF*] mutants were streaked out onto MPYE agar medium (supplemented with 30 μg ml^{-1} of kanamycin for Δ*ccoP*Δ*bchE* pBB[*acsF*]) and incubated at 30°C. Colonies of each strain were photographed after 6 days (**Figure 7.2**, top). Only the WT and Δ*ccoP* strains were red-coloured. The Δ*bchE* and Δ*ccoP*Δ*bchE* pBB[*acsF*] strains were orange-coloured and the Δ*ccoP*Δ*bchE* strain looked pale (**Figure 7.2**, top). It appeared that the expression of the *Rvi. gelatinosus acsF* gene did not enable the parental Δ*ccoP*Δ*bchE* strain to synthesise BChl based on the colours of colonies. Molecular oxygen, a substrate of the aerobic cycalse, is potentially limited for cells grown on agar medium. To ensure the ready availability of oxygen, growth conditions with high aeration were achieved by culturing the strains in 10 ml of medium in 50 ml Falcon tubes with shaking at 230 rpm. These cells were harvested and the cell pellets were photographed (**Figure 7.2**, bottom). Unlike the orange-coloured Δ*bchE* and Δ*ccoP*Δ*bchE* strains, the Δ*ccoP*Δ*bchE* pBB[*acsF*] strain was red-coloured, indistinguishable from the WT and Δ*ccoP* strains (**Figure 7.2**, bottom).
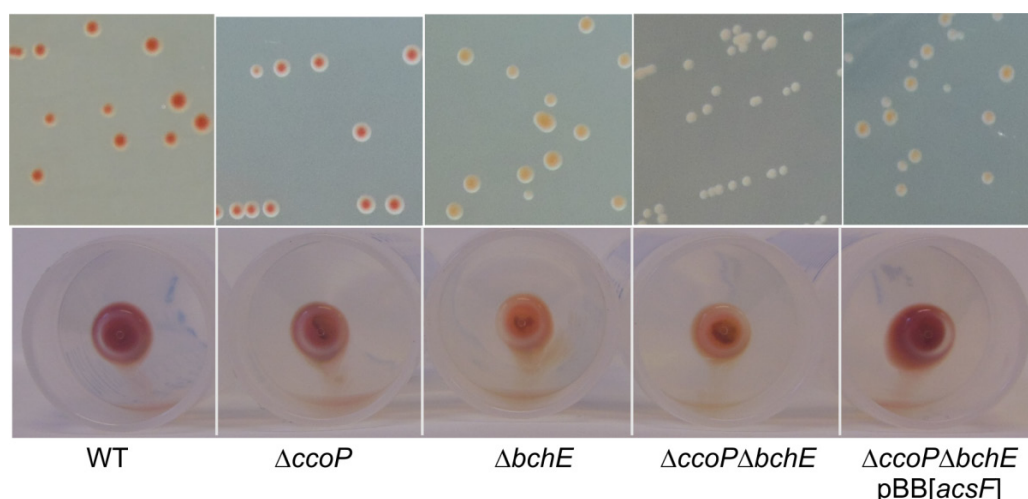
Figure 7.2 Colour phenotypes of *Rba. capsulatus* strains

Photographs of colonies (top) grown on MPYE agar medium and cell pellets (bottom) from liquid cultures.
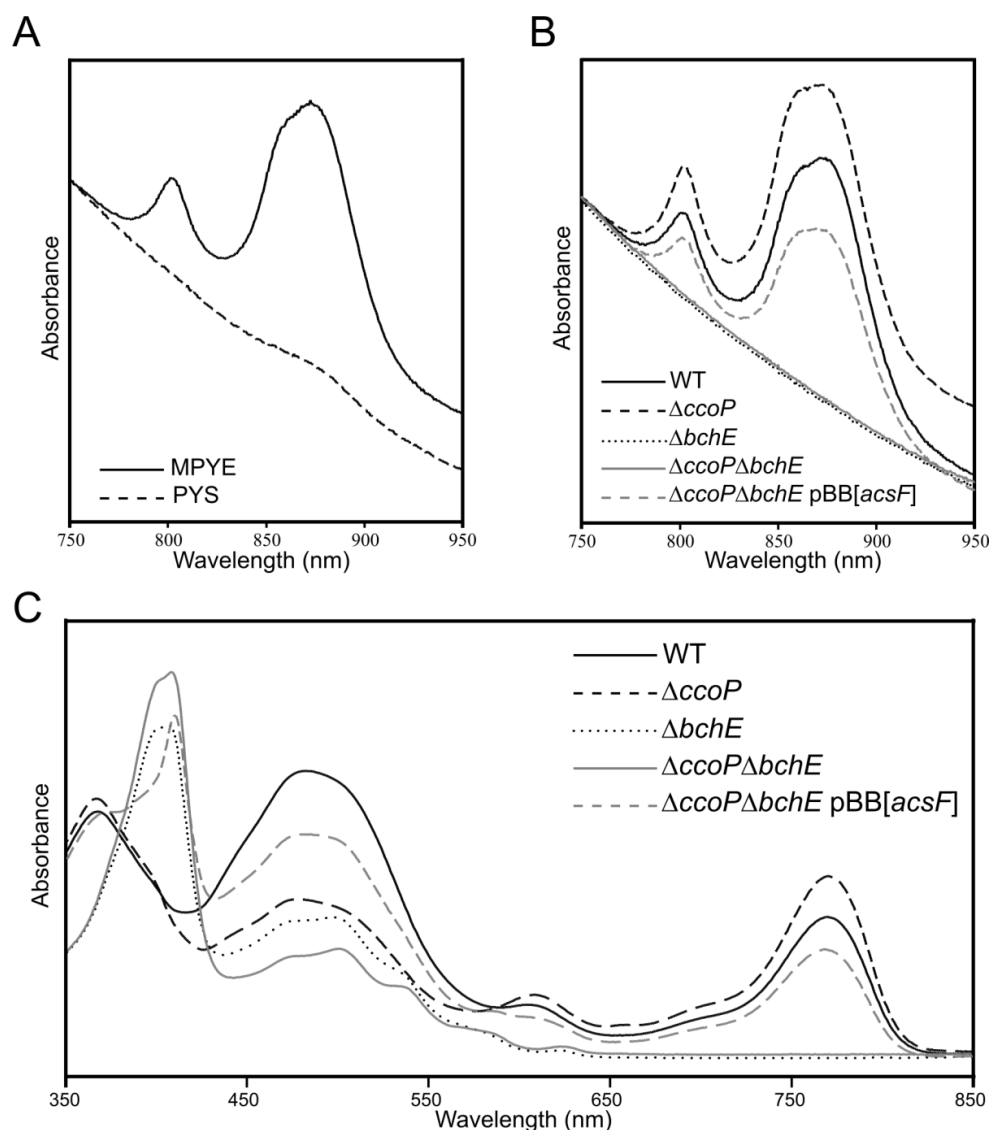
Figure 7.3 Absorption spectra of cells and pigment extracts of *Rba. capsulatus* strains
(**A**) Whole-cell absorption spectra of the Δ*ccoP*Δ*bchE* pBB[*acsF*] strain grown in MPYE and PYS media. Spectra were recorded with cells suspended in 60% (w/v) sucrose. (**B**) Whole-cell absorption spectra of described strains grown in MPYE medium. Spectra were recorded with cells suspended in 60% (w/v) sucrose. (**C**) Absorption spectra of pigments extracted from cells standardised by OD_{680}.

As *Rba. capsulatus* was found to grow slowly in MPYE medium, PYS medium, used to grow *Rvi. gelatinosus* (Chapter 4), was also tried. Under the same growth conditions, *Rba. capsulatus* grew much faster in PYS medium but contained significantly decreased levels of light-harvesting complexes and BChl than when grown in MPYE medium (**Figure 7.3 A**), which may be explained by the higher concentration of $CaCl_2$ present in MPYE medium (recipes for media are shown in **Table 2.1**). Given BChl biosynthesis was under investigation it was decided to continue with MPYE medium. The *Rba. capsulatus* strains were further analysed to compare whole-cell absorption spectra and pigment contents. Cells harvested from liquid

culture were resuspended in 60% (w/v) sucrose solution before absorption spectra were recorded. Spectra were normalised to light scattering of 0.1 at 750 nm (**Figure 7.3 B**). The $\Delta ccoP\Delta bchE$ pBB[*acsF*] strain showed comparable peaks of light-harvesting complexes as the WT and $\Delta ccoP$ strains; these data explicate the colour of cell pellets of these strains (**Figure 7.2**, bottom). Pigments were extracted from cells standardised by OD_{680} using methanol. The absorption spectra of the pigment extracts were recorded between 300 and 850 nm (**Figure 7.3 C**). The representative 770 nm peak for BChl *a* was present in the spectra of pigment extracts from the WT, $\Delta ccoP$ and $\Delta ccoP\Delta bchE$ pBB[*acsF*] strains (**Figure 7.3 C**). As expected, the $\Delta ccoP\Delta bchE$ pBB[*acsF*] strain still accumulated a high level of Chl precursors represented by the peak at around 410 nm, which was dominant in the spectra of the pigment extracts from the $\Delta bchE$ and $\Delta ccoP\Delta bchE$ strains (**Figure 7.3 C**).

7.3.3 Experiments with *Rvi. gelatinosus* transposon mutants TN43 and B37

Two *Rvi. gelatinosus* transposon mutants isolated in Chapter 6 were utilised in this section to investigate whether MgPME is able to enter bacterial cells. The transposon mutants were generated from the $\Delta bchE$ strain (Section 6.3.2). The *bchH* gene was disrupted in B37, whilst TN43 contains transposon within the *acsF* gene (**Table 6.1**). Both B37 and TN43 are unable to synthesise BChl and therefore light-harvesting complexes cannot form in these mutants. The first experiment was conducted by growing B37 and TN43 together as a single co-culture in 10 ml PYS medium supplemented with 50 μg ml^{-1} of kanamycin in a 50 ml Falcon tube. B37 and TN43 were also grown as separate cultures under the same conditions to serve as controls. Then cells were harvested and resuspended in 60% (w/v) sucrose solution. The absorption spectra were recorded and normalised to the absorbance at 750 nm, as shown in **Figure 7.4 A**. According to the acquired spectra, the co-culture of B37 and TN43 produced light-harvesting complexes, which did not exist in the B37 or TN43 culture. As both the anaerobic and aerobic cyclases are disabled in TN43, the mutant accumulates and excretes the cyclase substrate, MgPME. On the other hand, although B37 possesses the aerobic cyclase, the mutant lacks MgPME since the pathway is interrupted at the Mg-chelatase step. The restored BChl biosynthesis in the co-culture of B37 and TN43 indicates the excreted MgPME from TN43 was able to enter the B37 cells and to be utilised as substrate for the aerobic cyclase.
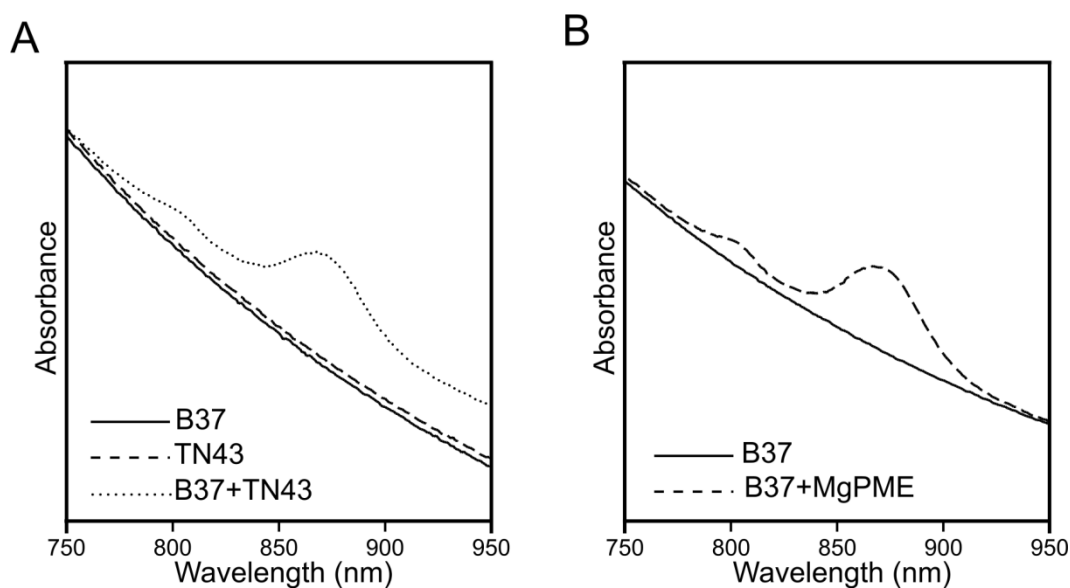
Figure 7.4 Whole-cell absorption spectra of the *Rvi. gelatinosus* B37 and TN43 mutants

Whole-cell absorption spectra were recorded with cells suspended in 60% (w/v) sucrose solution and normalised to absorbance at 750 nm. (**A**) Spectra of cells from the cultures of B37, TN43, and the co-culture of B37 and TN43. (**B**) Spectra of cells from the culture of B37, with and without MgPME feeding.

To check whether the uptake of MgPME is dependent on the contact or interaction between bacterial cells, the B37 culture was fed with purified MgPME (dissolved in methanol) and then incubated for two more days. Then whole-cell absorption spectrum was recorded and shown in **Figure 7.4 B**. The presence of light-harvesting complexes upon feeding with MgPME clearly demonstrates that MgPME in the medium was able to enter the B37 cells.

7.3.4 *In vivo* cyclase assay with an *E. coli* strain expressing the *Rvi. gelatinosus acsF* gene

Although *Rba. capsulatus* was shown to have aerobic cyclase activity when expressing the *Rvi. gelatinosus acsF* gene, the requirement of an additional subunit for this reaction had not been determined conclusively at this stage. *Rba. capsulatus* may contain a protein that is essential to the activity of the *Rvi. gelatinosus* AcsF. The test of the activity of AcsF in *E. coli*, a non-photosynthetic organism, is therefore necessary. The determination that MgPME is able to enter bacterial cells via exogenous delivery permits *in vivo* cyclase assays in *E. coli* via substrate feeding.

The *Rvi. gelatinosus acsF* gene was amplified and cloned into the *Nde*I/*BamH*I sites of the pET14b (Novagen) vector, resulting in the pET14b-AcsF plasmid. The AcsF protein produced from this plasmid contains an N-terminal 6x His tag, which was thought unlikely to interfere

with the activity of AcsF. The overexpression of AcsF, a membrane-associated protein, is highly toxic and causes the formation of inclusion bodies in *E. coli*. Since isolated by Miroux and Walker (1996), the *E.coli* C43(DE3) strain has been successfully applied to express many toxic proteins. Thus, it was decided to use the C43(DE3) strain as the host for expression of the *Rvi. gelatinosus acsF* gene. The *in vivo* cyclase assay was conducted using the C43(DE3) strain harbouring either empty pET14b or the pET14b-AcsF plasmid. The detailed procedures of the *in vivo* cyclase assays are described in Section 2.12. The *E. coli* strains were grown at 37°C with shaking at 230 rpm in 10 ml LB medium supplemented with 100 μg ml^{-1} of ampicillin in 50 ml Falcon tubes. When OD_{600} reached 0.6~0.8, 0.5 mM IPTG and purified MgPME (dissolved in methanol) were added and further incubation was performed at 30°C with shaking at 150 rpm. Cells were harvested from the 10 ml cultures and subjected to pigment extraction as described in Section 3.3.4. Pigments were analysed by HPLC using the method for separation of Chl precursors (Section 6.3.6). Elution of pigment species was monitored by absorbance at 416 nm for MgPME and at 440 nm for PChlide.
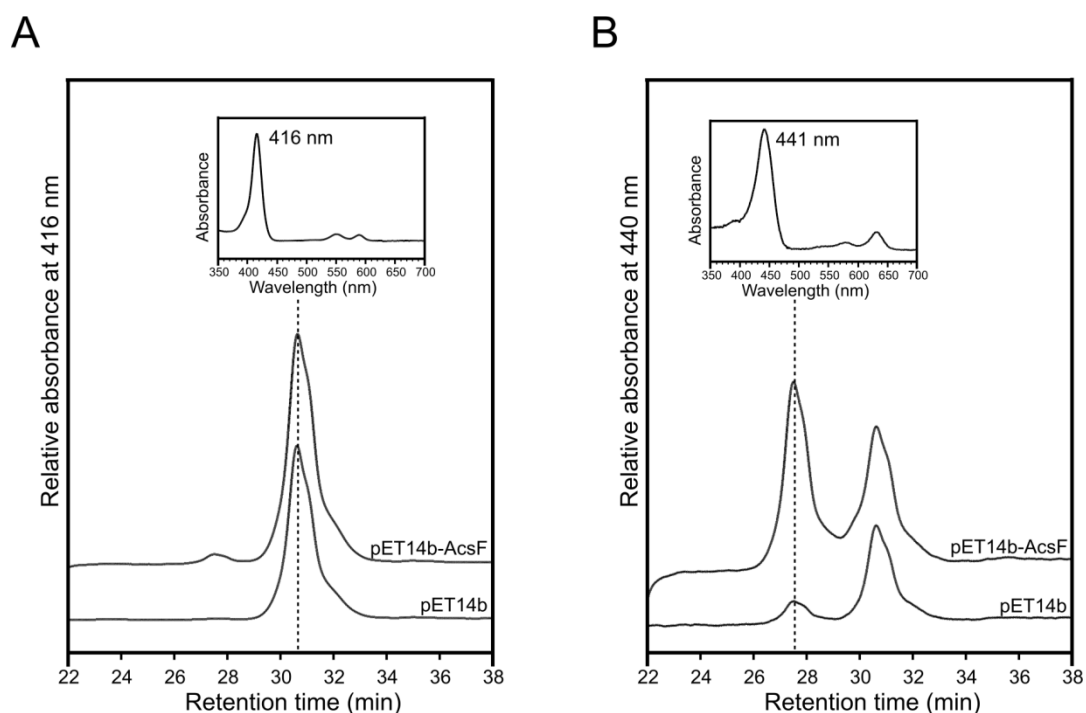
Figure 7.5 HPLC analysis of pigments extracted from *in vivo* cyclase assays

In vivo cyclase assays were performed with the *E. coli* C43(DE3) strain containing either the pET14b or pET14b-AcsF plasmid. IPTG was added to a final concentration of 0.5 mM when cultures reached OD_{600} of 0.6~0.8. MgPME dissolved in methanol was also added directly to *E. coli* cultures. Pigment extracts were analysed by HPLC. (**A**) Elution profiles monitored by absorbance at 416 nm. (**B**) Elution profiles monitored by absorbance at 440 nm.

The obtained elution profiles are shown in **Figure 7.5**. The 30.7 min peak with maximum absorbance at 416 nm represents MgPME and was detected in both strains at a similar level (**Figure 7.5 A**), a result of MgPME feeding. DV PChlide *a* was apparently detected in the pET14b-AcsF sample, represented by the 27.5 min peak in the 440 nm elution profile (**Figure 7.5 B**). The 27.5 min peak was also present in the pET14b sample but at a much lower level, which was obviously incomparable to the one detected in the pET14b-AcsF sample. The tiny peak probably resulted from a contamination of PChlide in the HPLC system, which is routinely used for purification of PChlide. However, it does not weaken the conclusion that the *E. coli* strain expressing the *Rvi. gelatinosus* AcsF was able to convert MgPME into DV PChlide *a*. Therefore, AcsF alone is the aerobic cyclase in *Rvi. gelatinosus*, requiring no additional subunit for activity.

7.3.5 Consecutive cloning of Chl biosynthetic genes into a pET3a vector using the 'Link and Lock' method

The demonstration of the activity using recombinant proteins is a milestone in the study of an enzyme. *E. coli* is the most commonly utilised system for heterologous expression. In the Chl biosynthetic pathway, there are 7 enzymatic steps from the branch point with haem biosynthesis, Proto, to Chl *a*. 6 out of the 7 steps have been successfully validated using recombinant enzymes produced in *E. coli* thanks to many researchers' efforts. These studies are summarised and listed in **Table 7.1.** The only step that has not been demonstrated using recombinant enzyme is the formation of the isocyclic E ring. Although the step catalysed by the aerobic cyclase has been assayed *in vitro* by various researchers, all the assays were performed with enzyme-containing fractions prepared from the native organism. It is generally believed that the aerobic cyclase consists of unknown subunit(s). However, the classical belief is completely reversed by the finding that *Rvi. gelatinosus* AcsF alone is able to catalyse the aerobic cyclase reaction (Section 7.3.4). It has finally become conceivable that the whole Chl biosynthetic pathway could be engineered in *E. coli*.

Table 7.1 Demonstrations of Chl biosynthetic steps using proteins heterologously expressed in *E. coli*

Step	Organism	Genes	References
Mg chelation	*Rba. sphaeroides*	*bchH, bchI, bchD*	Gibson *et al.*, 1995
	Synechocystis	*chlH, chlI, chlD*	Jensen *et al.*, 1996
	Chlorobium vibrioforme	*bchH, bchI, bchD*	Petersen *et al.*, 1998
	Rba. capsulatus	*bchH, bchI, bchD*	Willows and Beale, 1998
	Synechocystis	*gun4*	Davison *et al.*, 2005; Verdicia *et al.*, 2005
MgP methylation	*Synechocystis*	*chlM*	Shepherd *et al.*, 2003
	Nicotiana tobacum	*CHLM*	Alawady *et al.*, 2005
8-vinyl reduction	*Arabidopsis thaliana*	*DVR*	Nagata *et al.*, 2005
	Chlorobium tepidum	*bciA*	Chew and Bryant, 2007a
	Oryza sativa	*DVR*	Wang *et al.*, 2010
	Zea mays	*DVR*	Wang *et al.*, 2013
	Cucumis sativus	*DVR*	Wang *et al.*, 2013
	Chloroherpeton thalassium	*bciB*	Saunders *et al.*, 2013
PChlide reduction	*Hordeum vulgare* L.	*POR*	Schulz *et al.*, 1989
	Pisum sativum L.	*POR*	Martin *et al.*, 1997
	Synechocystis	*por*	Townley *et al.*, 1998
	Thermosynechococcus elongatus BP-1	*por*	Heyes and Hunter, 2004
	Chlorobium tepidum	*bchN, bchB, bchL*	Bröcker *et al.*, 2008
Chlide esterification	*Synechocystis*	*chlG*	Oster *et al.*, 1997
	Arabidopsis thaliana	*CHLG*	Oster and Rüdiger, 1997
	Avena sativa	*CHLG*	Schmid *et al.*, 2001
GG reduction	*Arabidopsis thaliana*	*CHLP*	Keller *et al.*, 1998
	Rba. sphaeroides	*bchP*	Addlesee and Hunter, 1999

Only the first demonstration with genes from the indicated organism is listed.

It was decided to employ the Chl biosynthetic genes from *Synechocystis* to this aim, except for the aerobic cyclase encoding gene *acsF*, which was from *Rvi. gelatinosus*. Thus, 10 genes in total were required to be expressed in *E. coli* to construct the Chl biosynthetic pathway. It is impractical to use the conventional expression strategy, with genes harboured on separate plasmids. Instead, the 'Link and Lock' method reported by McGoldrick *et al.* (2005) was adopted. Such a method allows cloning of multiple genes into a single vector by repetitively using the same set of restriction enzymes, where two of these share compatible cohesive ends, which do not yield a restriction site after ligation. The method is depicted in **Figure 7.6** with the cloning of 3 genes as an example. Furthermore, the transcription of multiple genes in tandem from a single promoter seems feasible as demonstrated by McGoldrick *et al.* (2005) with a construct containing 10 genes.
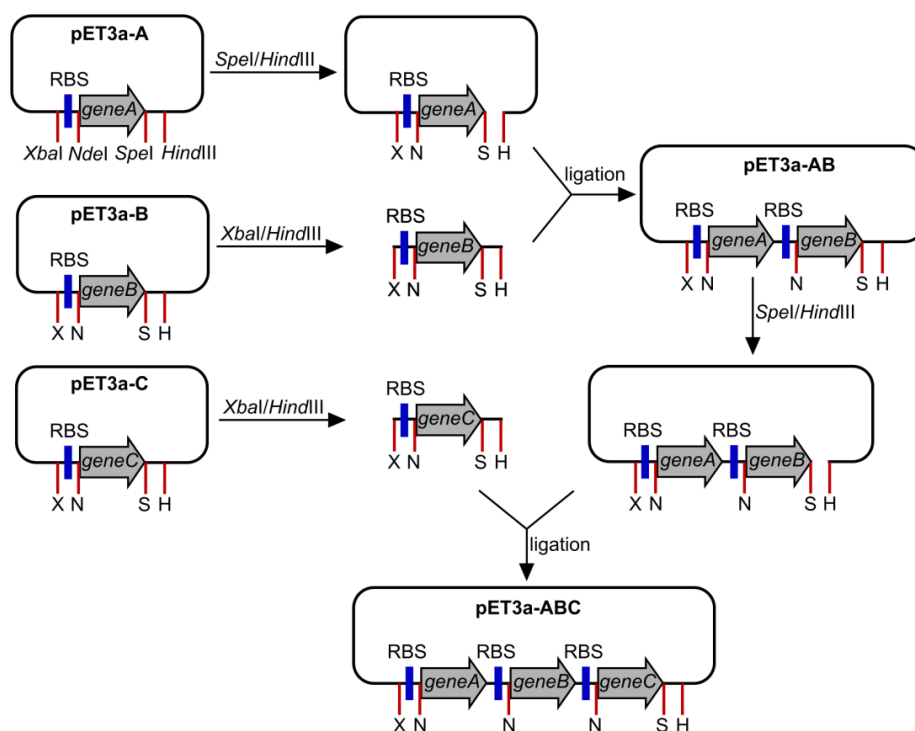
Figure 7.6 Mechanism of the 'Link and Lock' method

The 'Link and Lock' cloning was conducted using an engineered pET3a vector, which contains an added *Spe*I site. Construction of a plasmid containing 3 genes is depicted as an example. More genes can be added using the same methodology. Genes to be cloned were first cloned into the *Nde*I/*Spe*I sites of the vector, resulting in the pET3a-A, pET3a-B and pET3a-C plasmids. The pET3a-A plasmid serving as the master vector is cut with *Spe*I/*Hind*III and the *geneB* fragment serving as the insert is cut out from the pET3a-B plasmid with *Xba*I/*Hind*III. As the *Spe*I and *Xba*I sites on one end of the fragments are eliminated after ligation, the resulting pET3a-AB contains only one *Spe*I site. For the construction of the pET3a-ABC plasmid, the pET3a-AB plasmid serves as the subsequent master vector and the *geneC* fragment serves as the insert. RBS, ribosome binding site.

To apply the 'Link and Lock' method, the pET3a (Novagen) vector was engineered to contain an added *Spe*I site immediately upstream of the *BamH*I site. The 10 genes including *chlI*, *chlD*, *chlH*, *gun4*, *chlM*, *acsF*, *por*, *dvr* (*bciB*), *chlP* and *chlG*, were cloned into the vector consecutively, in the order described (as detailed in Section 2.5.7), resulting in a series of constructs. The transcription of all the genes is driven by a single T7 promoter located upstream of the *chlI* gene. A ribosome binding site is placed upstream of each gene to facilitate the translation (**Figure 7.6**). The construct containing the first 5 genes from *chlI* to *chlM* was designated as pET3a-IM. Accordingly, the constructs containing genes from *chlI* to *acsF*, to *dvr* and to *chlG*, were designated as pET3a-IA, pET3a-ID and pET3a-IG, respectively. The map of pET3a-IG is shown in **Figure 7.7** together with the Chl biosynthetic steps catalysed by the gene products.
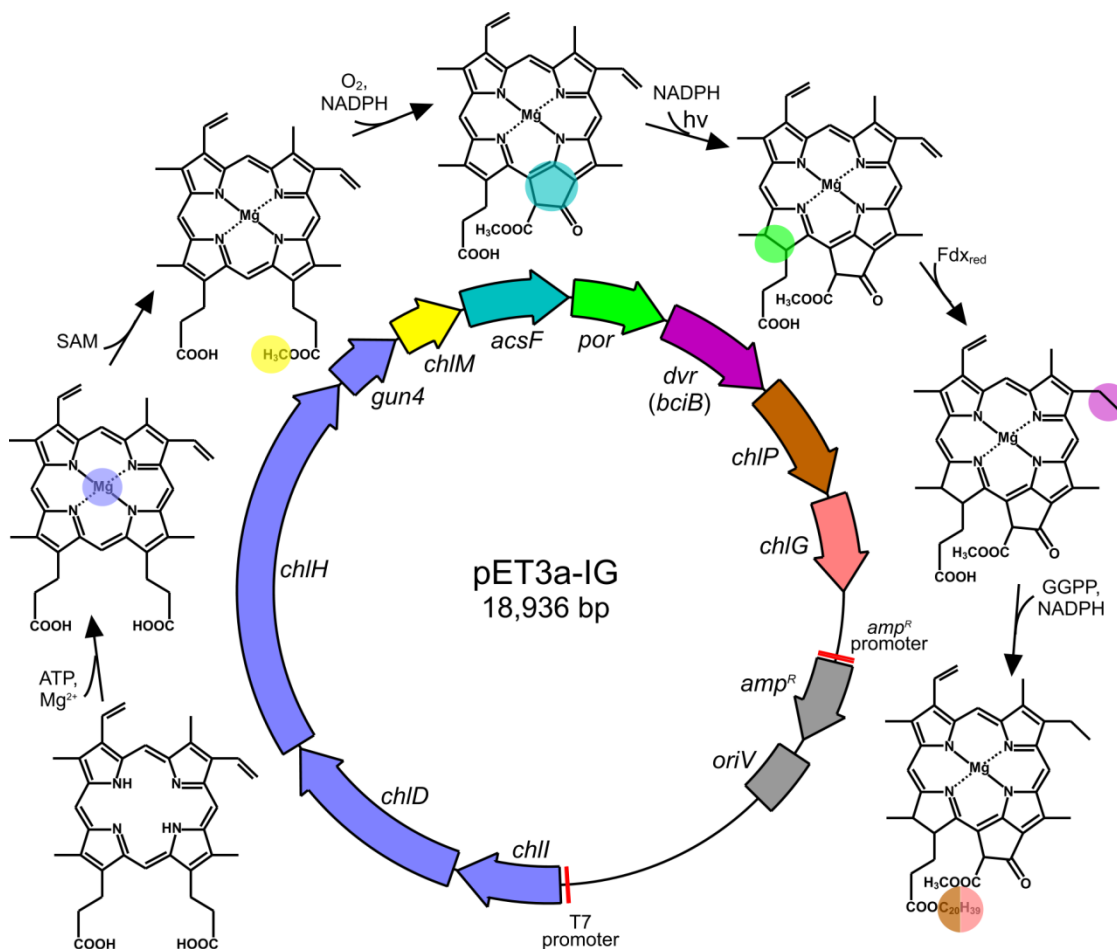
Figure 7.7 Introduction of the Chl biosynthetic pathway into *E. coli* via the pET3a-IG plasmid
The pET3a-IG plasmid was constructed using the 'Link and Lock' method and contains 10 Chl biosynthetic genes including the *chlI*, *chlD*, *chlH*, *gun4*, *chlM*, *acsF*, *por*, *dvr*, *chlP* and *chlG* genes. The Chl biosynthetic steps catalysed by the products of the 10 genes are also displayed. Abbreviations: *amp*[R], ampicillin resistance gene; *oriV*, the pBR322 origin of replication; SAM, *S*-Adenosyl methionine; Fdx_{red}, reduced ferredoxin; hv, light; GGPP, geranylgeranyl pyrophosphate.

7.3.6 HPLC analysis of pigments accumulated in *E. coli* strains expressing multiple Chl biosynthetic genes

The pET3a, pET3a-IM, pET3a-IA, pET3a-ID and pET3a-IG plasmids were separately transformed into the *E. coli* C43(DE3) strain. The resulting strains were assayed for their capability to produce Chl intermediates. Given the recombinant Mg-chelatase shares the substrate with the native ferrochelatase, Proto, addition of ALA, the precursor of all tetrapyrroles, was used in order to enhance synthesis of MgP. Additionally, Mg^{2+}, another substrate of Mg-chelatase, could be limiting in *E. coli* cytosol. The production of MgP in an *E. coli* strain overexpressing the *Synechocystis* Mg-chelatase from a pET9a-based plasmid was analysed with supplementation of ALA and Mg^{2+} at a range of concentrations (Canniffe, 2010).

It was found that the highest level of MgP was accumulated when ALA and Mg^{2+} were added both at 10 mM (Canniffe, 2010). Thus, the *in vivo E. coli* assays in the present study were conducted with the addition of ALA and Mg^{2+} at this concentration. The *E. coli* strains were grown at 37°C with shaking at 230 rpm in 10 ml of LB medium with 100 μg ml^{-1} of ampicilin in 50 ml Falcon tubes to OD$_{600}$ of 0.6~0.8. Gene expression was induced by addition of IPTG at a concentration of 0.5 mM. At the same time ALA and Mg^{2+} were also added. Further incubation was performed in the dark at 30°C with shaking at 150 rpm for 24 hr. Activation of POR was conducted by illumination at 5 μE m^{-2} s^{-1} for the final 4 hr. Cells were harvested and pigments were extracted as described in Section 3.3.4. Pigments were analysed by HPLC using the method for separation of Chl precursors (Section 6.3.6). Pigments extracted from an *in vitro* enzyme assay of POR with DV PChlide *a* as a substrate were used as standards for both DV Chlide *a* and DV PChlide *a*. Chl standards were also included, which were Chl *a* extracted from *Synechocystis* WT and GG-Chl *a* extracted from a *Synechocystis* Δ*chlP* mutant (Hitchcock *et al.*, 2016). Elution of pigment species were monitored by absorbance at 416 nm, 440 nm and 665 nm.

As shown in **Figure 7.8**, none of the Chl intermediates were detected in the control strain, which contains the empty pET3a vector. MgPME was produced in the pET3a-IM sample as indicated by the 30.5 min peak with maximum absorbance at 416 nm (**Figure 7.8 A**). The detection of DV PChlide *a* (retention time = 27.3 min, Soret band = 441 nm) in the pET3a-IA sample further confirms that the *Rvi. gelatinosus* AcsF is capable of catalysing the aerobic cyclase reaction on its own (**Figure 7.8 B**). Two peaks with retention times corresponding to those of the DV Chlide *a* and DV PChlide *a* were present in the elution profiles of the pET3a-ID sample (**Figure 7.8 C**). The 20.2 min peak was assigned as MV Chlide *a* based on its blue-shifted Soret band compared to that of DV Chlide *a*. Likewise, the 27.2 min peak was assigned as MV PChlide *a*. With activation by 4 hr illumination, the content of MV Chlide *a* increased remarkably in accordance with a substantial decrease in the level of MV PChlide *a* (**Figure 7.8 C**). The reaction catalysed by POR is evidently the cause of this change. The modest level of MV Chlide *a* in the sample without light activation was likely to be a result of unavoidable exposure to light during the experimental procedures. Despite the fact BciB prefers to use DV Chlide *a* as substrate in native systems (Canniffe *et al.*, 2014), the accumulation of DV PChlide *a* without being reduced by POR in the dark led to BciB-catalysed reduction of the 8-vinyl group of DV PChlide *a*, yielding MV PChlide *a*.
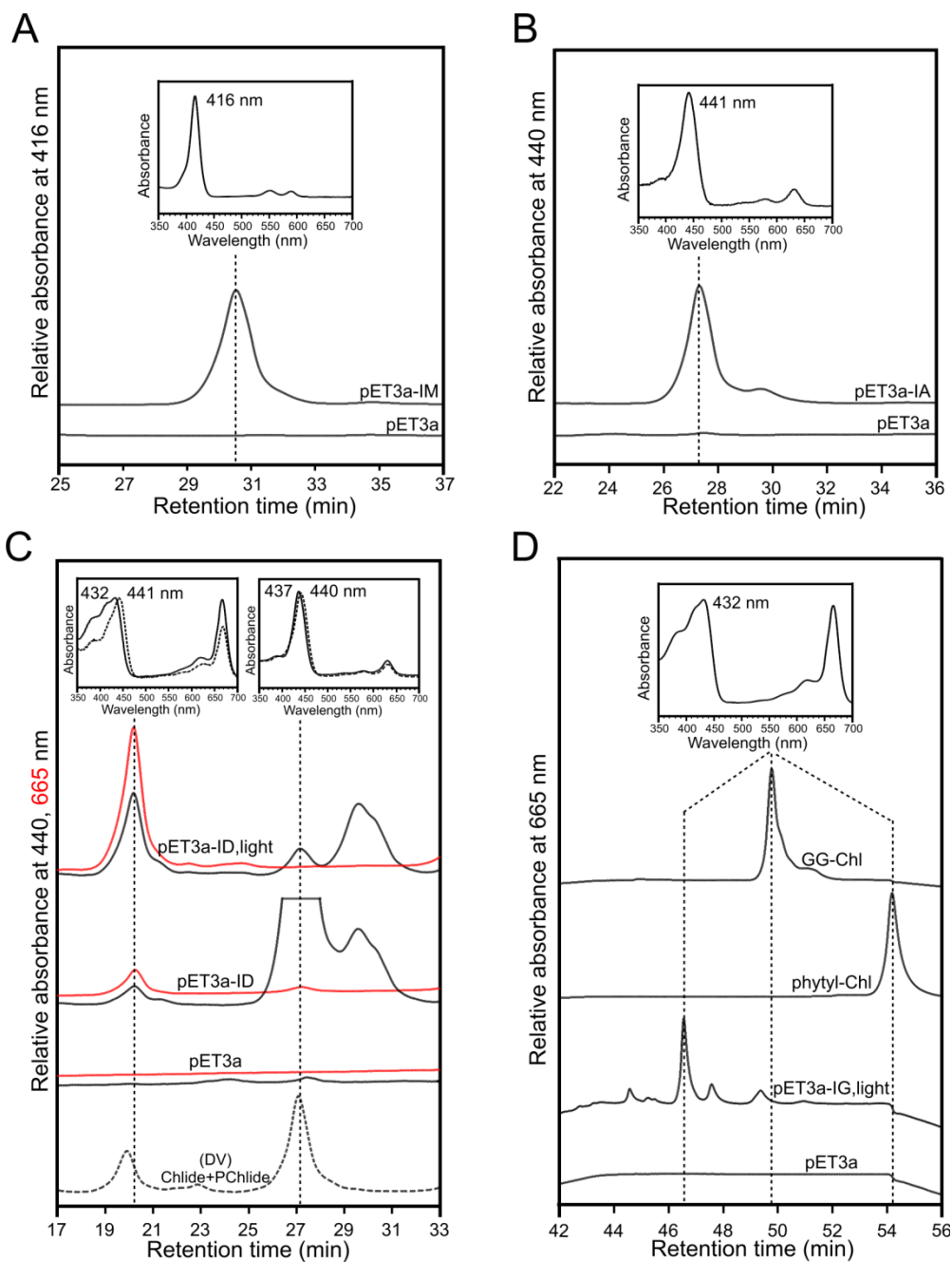
Figure 7.8 HPLC analysis of pigments accumulated in *E. coli* strains expressing Chl biosynthetic genes

E. coli strains harbouring Chl biosynthetic genes were grown to OD_{600} of 0.6~0.8 before addition of 0.5 mM IPTG, 10 mM ALA and 10 mM Mg^{2+} ($MgSO_4$:$MgCl_2$ = 1:1). Then after 24 hr incubation, pigments were extracted and analyzed by HPLC. POR was activated by exposure to 5 μE m^{-2} s^{-1} light for the final 4 hr of the incubation. (**A**) Elution profiles monitored by absorbance at 416 nm. (**B**) Elution profiles monitored by absorbance at 440 nm. (**C**) Elution profiles monitored by absorbance at 440 and 665 nm. (DV)Chlide+PChlide, mixture of DV Chlide *a* and DV PChlide *a*, was extracted from an *in vitro* enzyme assay of POR and used as standards for both pigments. The elution profile and absorption spectra of DV pigments are shown in dashed lines. (**D**) Elution profiles monitored by absorbance at 665 nm.

Since *E. coli* does not possess a GGPP synthase, it is unlikely that the strain containing pET3a-IG could synthesise Chl. Surprisingly, the elution profile of the pET3a-IG sample showed a mysterious peak with an identical absorption spectrum to that of MV Chlide *a* and a retention time of 46.6 min (**Figure 7.8 D**), which is much longer than the 20.2 min of MV Chlide *a* (**Figure 7.8 C**). The pigment represented by the mysterious peak is less hydrophobic than GG-Chl *a* and phytyl-Chl *a* as it was eluted earlier (**Figure 7.8 D**). According to the absorption spectrum and hydrophobicity, this pigment is likely to be a Chl species esterified with an isoprenoid alcohol that is shorter than phytol (C_{20}). It was reported that Chl synthase in etioplast membranes could utilise farnesyl (C_{15}) PP as the alcohol substrate (Rüdiger *et al*., 1980). As the immediate precursor of GGPP, farnesyl PP can be synthesised by *E. coli*. Taken together it is rational to suggest that the mysterious pigment could be farnesyl-Chl *a*, which can be tested by mass spectrometry in the future.

7.4 Discussion

7.4.1 AcsF is the only subunit of the aerobic cyclase in *Rvi. gelatinosus*

The subunit composition of the aerobic cyclase has perplexed researchers for many years. Based on biochemical fractionation and study with barley mutants accumulating MgPME, it has generally been believed that the aerobic cyclase consists of multiple subunits including both soluble and membrane-bound components. AcsF, as the first identified subunit of the aerobic cyclase, is a membrane-bound component (Pinta *et al*., 2002; Tottey *et al*., 2003). The barley mutants at the *Xantha-l* and *Viridis-k* loci were demonstrated to be defective in different membrane-bound components of the aerobic cyclase (Rzeznicka *et al*., 2005). Although *Xantha-l* was confirmed to encode the AcsF homologue in barley, the identity of *Viridis-k* is unknown (Rzeznicka *et al*., 2005). Ycf54 was identified to be the second subunit of aerobic cyclase in cyanobacteria and plants (Hollingshead *et al*., 2012; Albus *et al*., 2012; Hollingshead *et al*., 2016). The barley Ycf54 was subsequently found to be membrane associated and not encoded by *Viridis-k* (Bollivar *et al*., 2014). According to these published results, the aerobic cyclase in oxygenic phototrophs was proposed to contain at least four subunits including AcsF, Ycf54 and two unknown subunits (Bollivar *et al*., 2014). With respect to the classification of aerobic cyclase proposed in Chapter 4, the *Rvi. gelatinosus* AcsF (Class II) is equivalent to the combination of AcsF (Class III) and Ycf54 from oxygenic phototrophs. Thus, it would be reasonable to expect that the aerobic cyclase in *Rvi. gelatinosus* contains AcsF and at least two unknown subunits.

Nevertheless, the results of the *in vivo E. coli* assays (Sections 7.3.4 and 7.3.6) unquestionably demonstrated that AcsF is the only subunit of the aerobic cyclase in *Rvi. gelatinosus*. This indicates the complete subunits of the aerobic cyclase in oxygenic phototrophs have already been identified as well, namely AcsF and Ycf54. These findings are obviously contradictory to the claims found in literature, which makes it necessary to reconsider the previous work regarding the subunit composition of the aerobic cyclase.

Although in oxygenic phototrophs the aerobic cyclase was resolved into soluble and membrane-bound fractions, neither of the fractions was purified to homogeneity. It is certain that the membrane-bound fraction contains the AcsF subunit. However, it is clueless that whether the soluble fraction contains a protein component of the aerobic cyclase. Non-protein factors in the soluble fraction may be the reason why the soluble fraction was required to reconstitute the enzyme activity. Although the barley mutants at the *Viridis-k* locus accumulate MgPME upon ALA feeding, the mutations are not necessarily within the genes encoding the aerobic cyclase. Since Chl biosynthesis is not only a complicated process but also tightly regulated, it is possible that mutation in genes that do not encode a subunit of the aerobic cyclase could cause the accumulation of MgPME. Recently, Steccanella *et al.* (2015) have linked the aerobic cyclase reaction with the plastoquinone pool in plants and found that both the two barley *Viridis-k* mutants have a more reduced plastoquinone pool, which may cause an inhibitory effect on the aerobic cyclase.

On the other hand, it appears that NADPH is involved in the aerobic cyclase reaction since the dependence on NADPH was observed in the enzyme systems from various oxygenic phototrophs (Chereskin *et al.*, 1982b; Wong and Castelfranco, 1984; Whyte and Castelfranco, 1993; Nasrulhaq-Boyce *et al.*, 1987; Bollivar and Beale, 1995; Bollivar and Beale 1996). NADPH could serve as the electron donor, which is required for the reduction of the diiron centre of aerobic cyclase during the catalytic cycle (Berthold and Stenmark, 2003; Steccanella *et al.* 2015). However, no NADPH-binding domain can be identified in AcsF or Ycf54 according to the AA sequence, indicating NADPH may not directly involved in the cyclase reaction. The aerobic cyclase reaction is known to generate reactive oxygen species which can inactivate the enzyme. Therefore, a mechanism that scavenges reactive oxygen species is required to protect the enzyme. The addition of catalase and ascorbate was demonstrated to significantly stimulate the *in vitro* cyclase activity (Bollivar and Beale, 1996). A H_2O_2-scavenging system consisting of NTRC and 2-Cys peroxiredoxins, was found to protect the aerobic cyclase from peroxide at the expense of NADPH, especially in the dark (Stenbaek *et al.*, 2008). Considering

all the reported cyclase assays were conducted with fractions containing numerous kinds of proteins in addition to the aerobic cyclase, it is conceivable that some NADPH-dependenet H_2O_2-scavenging systems were present in the assay, responsible for the protection of the aerobic cyclase. Furthermore, if the link between the plastoquinone pool and the cyclase reaction exists, the addition of NADPH would play a role in maintaining the appropriate redox state of the plastoquinone pool, which is likely to be more oxidised under the assay conditions (Steccanella *et al.* 2015). Although the subunits have now been identified, the precise electron donor has not – efforts will be made to test the PQ theory with purified recombinant proteins.

7.4.2 The core pathway of Chl biosynthesis has been constructed in *E. coli*

As the 'pigments of life', modified tetrapyrrole molecules are indispensible for many fundamental biochemical processes. Among the naturally occurring tetrapyrroles including (B)Chls, haems, vitamin B_{12}, sirohaem, cofactor F_{430} and bilins, *E. coli* can synthesise sirohaem and haems. One of the intermediates, Uro'gen, is the direct precursor of sirohaem, vitamin B_{12} and cofactor F_{430}. By expressing the first 10 genes dedicated for vitamin B_{12} biosynthesis, part of the biosynthetic pathway was successfully constructed in *E. coli*, which produces hydrogenobyrinic acid from Uro'gen (McGoldrick *et al.*, 2005). Another intermediate, Proto, is the branch point for haem and (B)Chl biosynthesis. Expression of the Chl biosynthetic genes via the pET3a-ID plasmid enabled *E. coli* to synthesise Chlide *a* from Proto (Section 7.3.6). Given Chlide *a* is the universal precursor of all Chls and BChls, the synthesis of Chlide *a* from Proto was named as the core pathway of Chl biosynthesis (Chew and Bryant, 2007b). The achieved construction of the core pathway in *E. coli* has great significance to the studies of Chl biosynthesis and photosynthesis in at least three perspectives. Firstly, this provides solid evidence to further support previous findings regarding the identities of the enzymes involved in the core pathway, especially for the puzzling step of the aerobic cyclase. Secondly, the *E. coli* strain with the recombinant core pathway can serve as a valuable platform for investigating the latter biosynthetic steps for various types of Chls and BChls. Thirdly, this is the first step on a challenging journey towards engineering *E. coli* to harvest solar energy.

7.4.3 Future work

Many research directions can be proposed since the subunit composition of the aerobic cyclase has been established by the present work. The activity of the Classes I and III aerobic cyclase will also be assayed *in vivo* in *E. coli* C43(DE3) strains, following the same procedures

as for the *Rvi. gelatinosus* AcsF (Section 7.3.4). The results from these assays will provide further experimental evidence to support the classification of aerobic cyclase proposed in Chapter 4. A series of mutated pET14b-AcsF plasmids can be generated easily by site-directed mutagenesis and subsequently employed to identify the important residues of AcsF through *in vivo* cyclase assays. Intensive efforts will be required to set up *in vitro* cyclase assays with recombinant proteins, which is apparently challenging. The purification and structural determination of Ycf54 from cyanobacteria have been completed (Hollingshead, 2014). Nonetheless, the overexpression and purification of the catalytic subunit AcsF have proved to be problematic and requires extensive optimisation of the process. A few strategies can be considered including changes in expression host, affinity tag, induction conditions and source of the AcsF-encoding gene.

As listed in **Table 7.1**, the final two steps of Chl *a* biosynthesis have been demonstrated using recombinant enzymes produced in *E. coli*, indicating the entire pathway from Proto to Chl *a* could be constructed in *E. coli*. GGPP serves as the isoprenoid alcohol substrate for the esterfication of Chlide, this pathway must be introduced into our *E. coli* system. *E. coli* is known to utilise the non-mevalonate pathway to produce isopentenyl (C_5) PP, the common building block for iosprenoid biosynthesis (Hunter, 2007), and also contain the enzymes catalysing the formation of geranyl (C_{10}) PP and farnesyl (C_{15}) PP through successive addition of the isoprene unit. The GGPP synthase, encoded by the *crtE* gene, catalyses the synthesis of GGPP through the addition of one isoprene unit to farnesyl PP and is not present in *E. coli*. It has been extensively reported that overexpression of an exogenous *crtE* gene enabled *E. coli* to produce GGPP at a level that could be utilised by an engineered metabolic pathway. On the other hand, the first step of the non-mevalonate pathway is the formation of 1-deoxy-D-xylulose 5-phosphate from glyceraldehyde-3-phosphate and pyruvate, which is catalysed by the *dxs* gene product. This step was shown to be one of the rate-limiting steps in the pathway and increase of the Dxs protein level by overexpressing either the native or an exogenous gene enhanced metabolic flux to the synthesis of isopentenyl PP (Harker and Bramley, 1999; Estévez *et al*., 2001; Kim and Keasling, 2001; Kim *et al*., 2006; Zhao *et al*., 2011). In the future, the *crtE* gene from *Rvi. gelatinosus* and the *dxs* gene from *E. coli* will be cloned together into a dual-expression vector such as the pCOLADuet-1 (Novagen) vector. The resulting construct will be transformed into the *E. coli* C43(DE3) strain harbouring the pET3a-IG plasmid. Hopefully, the complete pathway for Chl *a* biosynthesis will be established with these efforts. Additionally, the fine tuning of the expression level of each Chl biosynthetic enzyme will be necessary in order to optimise Chl production in *E. coli*.

Chapter 8

Concluding remarks

In this thesis, the aerobic magnesium-protoporphyrin IX monomethyl ester cyclases (the aerobic cyclases) from *Rba. sphaeroides*, *Rvi. gelatinosus* and *Synechocystis*, have been extensively investigated in their native and heterologous systems using multiple approaches including molecular cloning, genetic engineering, pigment profiling, spectroscopy, suppressor screening, transposon mutagenesis and *in vivo* enzymatic assays. The outcome of these investigations has significantly increased our knowledge of the aerobic cyclase to a new level. The key achievements reported in this thesis are the identification of three classes of aerobic cyclase in various phototrophs and the demonstration of the complete subunit composition of the aerobic cyclase.

Chapter 3 shows the first experimental evidence that a functional aerobic cyclase is present in *Rba. sphaeroides*, which was previously believed to synthesise BChl only via the anaerobic cyclase route. Chapter 4 reports the first demonstration that the deletion of the *cycl* gene in *Synechocystis* can be complemented by the *Rvi. gelatinosus acsF* gene. A previously unknown ORF, rsp_6110, has been discovered, which encodes a subunit of the aerobic cyclase in *Rba. sphaeroides* and is designated as the *bciE* gene. Complementation experiments conducted in *Rvi. gelatinosus* led to the identification of three classes of aerobic cyclase regarding subunit composition, which corresponds well to the phylogenetic analysis of the catalytic subunit, AcsF. Chapters 5 and 6 report the attempts to identify the unknown subunits of the aerobic cyclase suggested by previous studies; these efforts failed to discover any additional gene. Nevertheless, the suppressor screen reported in Chapter 5 has highlighted a D219G mutation in the *cycl* gene and a previously unknown gene slr1916, which may provide insights into the regulation of the cyanobacterial aerobic cyclase. The transposon mutagenesis study reported in Chapter 6 has generated a number of BChl-deficient mutants in *Rvi. gelatinosus*, which will serve as a valuable resource for future studies in BChl biosynthesis and PS biogenesis.

Chapter 7 puts an end to the pursuit of the unknown subunits of aerobic cyclase by demonstrating the capability of the *Rvi. gelatinosus* AcsF to act solely as a functional aerobic cyclase in heterologous systems known to lack an aerobic cyclase. This demonstration was first accomplished in a purple phototrophic bacterium, *Rba. capsulatus*, and then in *E. coli*. Based on the equivalence of subunits from various aerobic cyclases, the complete subunits of

all the three classes of aerobic cyclase have been identified. Removal of this last impediment to the assembly of sections of the Chl biosynthesis pathway allowed the core set of (B)Chl biosynthetic enzymes to be engineered into *E. coli*, which enables the host to produce Chlide *a*, the universal precursor for all Chls and BChls.

Chapter 4 shows the *Rvi. gelatinosus ∆bchE∆acsF* mutant to be an invaluable system to test the aerobic cyclase activity from heterologously expressed protein(s). Chapter 7 demonstrates the *E. coli* C43 strain with MgPME feeding can be used to study *in vivo* cyclase activity. Both these two systems can be applied to investigate the aerobic cyclase activity of a gene in its native form or mutated forms if appropriate negative and positive controls are included. Combinations of different genes can also be tested to dissect the subunit composition of particular aerobic cyclases. (B)Chl biosynthesis is known to be subject to tight regulation in which the aerobic cyclase step can be a checkpoint. The *Synechocystis* system developed in this thesis can be applied to study regulatory mechanisms, which can be initiated by studying the D219G mutation in CycI and the protein Slr1916. The advantage of using *Synechocystis* is that anything learnt will be highly relevant to eukaryotic photosynthetic organisms. All these studies will lead to greatly enhanced knowledge in aerobic cyclases from various phototrophs.

The finding that all the subunits required for the aerobic cyclase have been identified is of great significance. This will refocus our attention to reconstitute the cyclase reaction *in vitro* with recombinant proteins. Systematic trials are necessary in order to find out the right conditions in which the aerobic cyclase activity can be assayed *in vitro*. Only after that can the kinetics of aerobic cyclase be studied. On the other hand, structural determination of aerobic cyclase is of equal importance. The thermophile, *Chloracidobacterium thermophilum* B, possesses a Class II aerobic cyclase which only requires AcsF for function. The *acsF* gene from this organism will be a good candidate for recombinant expression, purification and structural work. As it is a membrane-associated protein, AcsF may be difficult to crystallise. Recent developments in cryo-electron microscopy could be used as an alternative method for structural studies if the purified AcsF protein forms a sufficiently large oligomer. The enzymatic and structural characterisation of the aerobic cyclase will provide the experimental basis for understanding the catalytic mechanism of the enzyme.

The artificial core pathway of (B)Chl biosynthesis which has been constructed in *E. coli* can serve as a 'Chlide module', into which enzymes at latter steps can be integrated to give *E. coli* the ability to synthesise a full spectrum of Chls and BChls. The resulting '(B)Chl modules' can

then be combined with modules synthesising other cofactors required for photosynthesis, such as 'carotenoid modules'. Genes encoding the apoproteins of light harvesting complexes and reaction centres as well as their assembly factors will be co-expressed with the cofactor biosynthesis modules using compatible vectors. All these efforts are aimed at creation of an artificial PS to enable *E. coli* to harvest and utilise light energy for ATP production. Admittedly, this is extremely challenging as it will be a definitive test for our understanding of molecular mechanism of PS assembly. However, this will also be hugely rewarding once achieved as a phototrophic *E. coli* will serve as a prototype for synthetic biology in light-driven metabolic engineering.

References

Adams NB, Reid JD (2012) Nonequilibrium isotope exchange reveals a catalytically significant enzyme-phosphate complex in the ATP hydrolysis pathway of the AAA(+) ATPase magnesium chelatase. *Biochemistry* **51:** 2029-2031

Adams NB, Reid JD (2013) The allosteric role of the AAA+ domain of ChlD protein from the magnesium chelatase of synechocystis species PCC 6803. *J Biol Chem* **288:** 28727-28732

Addlesee HA, Fiedor L, Hunter CN (2000) Physical mapping of bchG, orf427, and orf177 in the photosynthesis gene cluster of Rhodobacter sphaeroides: functional assignment of the bacteriochlorophyll synthetase gene. *J Bacteriol* **182:** 3175-3182

Addlesee HA, Gibson LC, Jensen PE, Hunter CN (1996) Cloning, sequencing and functional assignment of the chlorophyll biosynthesis gene, chlP, of Synechocystis sp. PCC 6803. *FEBS Lett* **389:** 126-130

Addlesee HA, Hunter CN (1999) Physical mapping and functional assignment of the geranylgeranyl-bacteriochlorophyll reductase gene, bchP, of Rhodobacter sphaeroides. *J Bacteriol* **181:** 7248-7255

Alawady A, Reski R, Yaronskaya E, Grimm B (2005) Cloning and expression of the tobacco CHLM sequence encoding Mg protoporphyrin IX methyltransferase and its interaction with Mg chelatase. *Plant Mol Biol* **57:** 679-691

Alawady AE, Grimm B (2005) Tobacco Mg protoporphyrin IX methyltransferase is involved in inverse activation of Mg porphyrin and protoheme synthesis. *Plant J* **41:** 282-290

Albus CA, Salinas A, Czarnecki O, Kahlau S, Rothbart M, Thiele W, Lein W, Bock R, Grimm B, Schottler MA (2012) LCAA, a novel factor required for magnesium protoporphyrin monomethylester cyclase accumulation and feedback control of aminolevulinic acid biosynthesis in tobacco. *Plant Physiol* **160:** 1923-1939

Alexander FW, Sandmeier E, Mehta PK, Christen P (1994) Evolutionary relationships among pyridoxal-5'-phosphate-dependent enzymes. Regio-specific alpha, beta and gamma families. *Eur J Biochem* **219:** 953-960

Alfonso M, Perewoska I, Kirilovsky D (2000) Redox control of psbA gene expression in the cyanobacterium Synechocystis PCC 6803. Involvement of the cytochrome b(6)/f complex. *Plant Physiol* **122:** 505-516

Allen MD, Kropat J, Merchant SS (2008) Regulation and localization of isoforms of the aerobic oxidative cyclase in Chlamydomonas reinhardtii. *Photochem Photobiol* **84:** 1336-1342

Alwan AF, Mgbeje BI, Jordan PM (1989) Purification and properties of uroporphyrinogen III synthase (co-synthase) from an overproducing recombinant strain of Escherichia coli K-12. *Biochem J* **264:** 397-402

Apel K, Santel HJ, Redlinger TE, Falk H (1980) The protochlorophyllide holochrome of barley (Hordeum vulgare L.). Isolation and characterization of the NADPH:protochlorophyllide oxidoreductase. *Eur J Biochem* **111:** 251-258

Archibald JM (2005) Jumping genes and shrinking genomes--probing the evolution of eukaryotic photosynthesis with genomics. *IUBMB Life* **57:** 539-547

Armstrong GA, Runge S, Frick G, Sperling U, Apel K (1995) Identification of NADPH:protochlorophyllide oxidoreductases A and B: a branched pathway for light-dependent chlorophyll biosynthesis in Arabidopsis thaliana. *Plant Physiol* **108:** 1505-1517

Astner I, Schulze JO, van den Heuvel J, Jahn D, Schubert WD, Heinz DW (2005) Crystal structure of 5-aminolevulinate synthase, the first enzyme of heme biosynthesis, and its link to XLSA in humans. *EMBO J* **24:** 3166-3177

Axelsson E, Lundqvist J, Sawicki A, Nilsson S, Schroder I, Al-Karadaghi S, Willows RD, Hansson M (2006) Recessiveness and dominance in barley mutants deficient in Mg-chelatase subunit D, an AAA protein involved in chlorophyll biosynthesis. *Plant Cell* **18:** 3606-3616

Azzouzi A, Steunou AS, Durand A, Khalfaoui-Hassani B, Bourbon ML, Astier C, Bollivar DW, Ouchane S (2013) Coproporphyrin III excretion identifies the anaerobic coproporphyrinogen III oxidase HemN as a copper target in the Cu(+)-ATPase mutant copA(-) of Rubrivivax gelatinosus. *Mol Microbiol* **88:** 339-351

Bang WY, Jeong IS, Kim DW, Im CH, Ji C, Hwang SM, Kim SW, Son YS, Jeong J, Shiina T, Bahk JD (2008) Role of Arabidopsis CHL27 protein for photosynthesis, chloroplast development and gene expression profiling. *Plant Cell Physiol* **49:** 1350-1363

Battersby AR, Fookes CJR, Gustafson-Potter KE, Matcham GWJ, McDonald E (1979a) Proof by synthesis that unrearranged hydroxymethylbilane is the product from deaminase and the substrate for cosynthetase in the biosynthesis of uro'gen-III. *J Chem Soc Chem Commun*: 1155-1158

Battersby AR, Fookes CJR, Matcham GWJ, McDonald E (1979b) Order of assembly of the four pyrrole rings during biosynthesis of the natural porphyrins. *J Chem Soc Chem Commun*: 539-541

Battersby AR, Fookes CJR, Matcham GWJ, McDonald E, Hollenstein R (1983) Biosynthesis of porphyrins and related macrocycles. Part 20. Purification of deaminase and studies on its mode of action. *J Chem Soc Perkin Trans*: 3031-3040

Battersby AR, McDonald E, Wurziger HKW, James KJ (1975) Stereochemistry of biosynthesis of the vinyl groups of protoporphyrin-IX: a short synthesis of porphobilinogen. *J Chem Soc Chem Commun*: 493-494

Bauer CE, Bird TH (1996) Regulatory Circuits Controlling Photosynthesis Gene Expression. *Cell* **85:** 5-8

Beale SI (1999) Enzymes of chlorophyll biosynthesis. *Photosynth Res* **60:** 43-73

Beale SI, Castelfranco PA (1974) The Biosynthesis of delta-Aminolevulinic Acid in Higher Plants: II. Formation of C-delta-Aminolevulinic Acid from Labeled Precursors in Greening Plant Tissues. *Plant Physiol* **53:** 297-303

Beale SI, Gough SP, Granick S (1975) Biosynthesis of delta-aminolevulinic acid from the intact carbon skeleton of glutamic acid in greening barley. *Proc Natl Acad Sci U S A* **72:** 2719-2723

Begley TP, Young H (1989) Protochlorophyllide reductase. 1. Determination of the regiochemistry and the stereochemistry of the reduction of protochlorophyllide to chlorophyllide. *J Am Chem Soc* **111:** 3095-3096

Benli M, Schulz R, Apel K (1991) Effect of light on the NADPH-protochlorophyllide oxidoreductase of Arabidopsis thaliana. *Plant Mol Biol* **16:** 615-625

Benz J, Rüdiger W. (1981) Chlorophyll Biosynthesis: Various Chlorophyllides as Exogenous Substrates for Chlorophyll Synthetase. *Zeitschrift für Naturforschung C*, Vol. 36, p. 51.

Benz J, Wolf C, Rüdiger W (1980) Chlorophyll biosynthesis: Hydrogenation of geranylgeraniol. *Plant Sci Lett* **19:** 225-230

Berthold DA, Stenmark P (2003) Membrane-bound diiron carboxylate proteins. *Annu Rev Plant Biol* **54:** 497-517

Biel SW, Wright MS, Biel AJ (1988) Cloning of the Rhodobacter capsulatus hemA gene. *J Bacteriol* **170:** 4382-4384

Bishop DF, Henderson AS, Astrin KH (1990) Human delta-aminolevulinate synthase: assignment of the housekeeping gene to 3p21 and the erythroid-specific gene to the X chromosome. *Genomics* **7:** 207-214

Blankenship RE (2014) *Molecular Mechanisms of Photosynthesis*. 2*nd ed*. Oxford, UK: Wiley-Blackwell

Blankenship RE, Olson JM, Miller M (1995) Antenna Complexes from Green Photosynthetic Bacteria. In *Anoxygenic Photosynthetic Bacteria*, Blankenship RE, Madigan MT, Bauer CE (eds), pp 399-435. Dordrecht: Springer Netherlands

Block MA, Tewari AK, Albrieux C, Marechal E, Joyard J (2002) The plant S-adenosyl-L-methionine:Mg-protoporphyrin IX methyltransferase is located in both envelope and thylakoid chloroplast membranes. *Eur J Biochem* **269:** 240-248

Bogorad L (1958) The Enzymatic Synthesis of Porphyrins from Porphobilinogen: II. UROPORPHYRIN III. *J Biol Chem* **233:** 510-515

Boldareva-Nuianzina EN, Blahova Z, Sobotka R, Koblizek M (2013) Distribution and origin of oxygen-dependent and oxygen-independent forms of Mg-protoporphyrin monomethylester cyclase among phototrophic proteobacteria. *Appl Environ Microbiol* **79:** 2596-2604

Bollivar D, Braumann I, Berendt K, Gough SP, Hansson M (2014) The Ycf54 protein is part of the membrane component of Mg-protoporphyrin IX monomethyl ester cyclase from barley (Hordeum vulgare L.). *FEBS J* **281:** 2377-2386

Bollivar DW (2006) Recent advances in chlorophyll biosynthesis. *Photosynth Res* **90:** 173-194

Bollivar DW, Beale SI (1995) Formation of the isocyclic ring of chlorophyll by isolated Chlamydomonas reinhardtii chloroplasts. *Photosynth Res* **43:** 113-124

Bollivar DW, Beale SI (1996) The Chlorophyll Biosynthetic Enzyme Mg-Protoporphyrin IX Monomethyl Ester (Oxidative) Cyclase (Characterization and Partial Purification from Chlamydomonas reinhardtii and Synechocystis sp. PCC 6803). *Plant Physiol* **112:** 105-114

Bollivar DW, Clauson C, Lighthall R, Forbes S, Kokona B, Fairman R, Kundrat L, Jaffe EK (2004) Rhodobacter capsulatus porphobilinogen synthase, a high activity metal ion independent hexamer. *BMC Biochem* **5:** 17

Bollivar DW, Jiang ZY, Bauer CE, Beale SI (1994a) Heterologous expression of the bchM gene product from Rhodobacter capsulatus and demonstration that it encodes S-adenosyl-L-methionine:Mg-protoporphyrin IX methyltransferase. *J Bacteriol* **176:** 5290-5296

Bollivar DW, Suzuki JY, Beatty JT, Dobrowolski JM, Bauer CE (1994b) Directed mutational analysis of bacteriochlorophyll a biosynthesis in Rhodobacter capsulatus. *J Mol Biol* **237:** 622-640

Bollivar DW, Wang S, Allen JP, Bauer CE (1994c) Molecular genetic analysis of terminal steps in bacteriochlorophyll a biosynthesis: characterization of a Rhodobacter capsulatus strain that synthesizes

geranylgeraniol-esterified bacteriochlorophyll a. *Biochemistry* **33:** 12763-12768

Boratyn GM, Schaffer AA, Agarwala R, Altschul SF, Lipman DJ, Madden TL (2012) Domain enhanced lookup time accelerated BLAST. *Biol Direct* **7:** 12

Boynton TO, Daugherty LE, Dailey TA, Dailey HA (2009) Identification of Escherichia coli HemG as a novel, menadione-dependent flavodoxin with protoporphyrinogen oxidase activity. *Biochemistry* **48:** 6705-6711

Boynton TO, Gerdes S, Craven SH, Neidle EL, Phillips JD, Dailey HA (2011) Discovery of a gene involved in a third bacterial protoporphyrinogen oxidase activity through comparative genomic analysis and functional complementation. *Appl Environ Microbiol* **77:** 4795-4801

Breckau D, Mahlitz E, Sauerwald A, Layer G, Jahn D (2003) Oxygen-dependent coproporphyrinogen III oxidase (HemF) from Escherichia coli is stimulated by manganese. *J Biol Chem* **278:** 46625-46631

Brindley AA, Adams NB, Hunter CN, Reid JD (2015) Five glutamic acid residues in the C-terminal domain of the ChlD subunit play a major role in conferring Mg(2+) cooperativity upon magnesium chelatase. *Biochemistry* **54:** 6659-6662

Brocker MJ, Virus S, Ganskow S, Heathcote P, Heinz DW, Schubert WD, Jahn D, Moser J (2008) ATP-driven reduction by dark-operative protochlorophyllide oxidoreductase from Chlorobium tepidum mechanistically resembles nitrogenase catalysis. *J Biol Chem* **283:** 10559-10567

Bryant DA, Costas AM, Maresca JA, Chew AG, Klatt CG, Bateson MM, Tallon LJ, Hostetler J, Nelson WC, Heidelberg JF, Ward DM (2007) Candidatus Chloracidobacterium thermophilum: an aerobic phototrophic Acidobacterium. *Science* **317:** 523-526

Buhr F, El Bakkouri M, Valdez O, Pollmann S, Lebedev N, Reinbothe S, Reinbothe C (2008) Photoprotective role of NADPH:protochlorophyllide oxidoreductase A. *Proc Natl Acad Sci U S A* **105:** 12629-12634

Burke DH, Alberti M, Hearst JE (1993a) bchFNBH bacteriochlorophyll synthesis genes of Rhodobacter capsulatus and identification of the third subunit of

light-independent protochlorophyllide reductase in bacteria and plants. *J Bacteriol* **175:** 2414-2422

Burke DH, Alberti M, Hearst JE (1993b) The Rhodobacter capsulatus chlorin reductase-encoding locus, bchA, consists of three genes, bchX, bchY, and bchZ. *J Bacteriol* **175:** 2407-2413

Burke DH, Hearst JE, Sidow A (1993c) Early evolution of photosynthesis: clues from nitrogenase and chlorophyll iron proteins. *Proc Natl Acad Sci U S A* **90:** 7134-7138

Burton G, Fagerness PE, Hosozawa S, Jordan PM, Scott AI (1979) 13C n.m.r. evidence for a new intermediate, pre-uroporphyrinogen, in the enzymic transformation of porphobilinogen into uroporphyrinogens I and III. *J Chem Soc Chem Commun:* 202-204

Calderon RH, Garcia-Cerdan JG, Malnoe A, Cook R, Russell JJ, Gaw C, Dent RM, de Vitry C, Niyogi KK (2013) A conserved rubredoxin is necessary for photosystem II accumulation in diverse oxygenic photoautotrophs. *J Biol Chem* **288:** 26688-26696

Camadro JM, Labbe P (1996) Cloning and characterization of the yeast HEM14 gene coding for protoporphyrinogen oxidase, the molecular target of diphenyl ether-type herbicides. *J Biol Chem* **271:** 9120-9128

Camadro JM, Thome F, Brouillet N, Labbe P (1994) Purification and properties of protoporphyrinogen oxidase from the yeast Saccharomyces cerevisiae. Mitochondrial location and evidence for a precursor form of the protein. *J Biol Chem* **269:** 32085-32091

Canniffe DP (2010) *Engineering the Haem and Chlorophyll Biosynthetic Pathways*. PhD thesis, University of Sheffield, UK

Canniffe DP, Chidgey JW, Hunter CN (2014) Elucidation of the preferred routes of C8-vinyl reduction in chlorophyll and bacteriochlorophyll biosynthesis. *Biochem J* **462:** 433-440

Canniffe DP, Jackson PJ, Hollingshead S, Dickman MJ, Hunter CN (2013) Identification of an 8-vinyl reductase involved in bacteriochlorophyll biosynthesis in Rhodobacter sphaeroides and evidence for the existence of a third distinct class of the enzyme. *Biochem J* **450:** 397-405

Cavaleiro JAS, Kenner GW, Smith KM (1974) Pyrroles and related compounds. Part XXXII. Biosynthesis of protoporphyrin-IX from coproporphyrinogen-III. *J Chem Soc Perkin Trans 1:* 1188-1194

Chandler LE, Bartsevich VV, Pakrasi HB (2003) Regulation of manganese uptake in Synechocystis 6803 by RfrA, a member of a novel family of proteins containing a repeated five-residues domain. *Biochemistry* **42:** 5508-5514

Chelstowska A, Zoladek T, Garey J, Kushner J, Rytka J, Labbe-Bois R (1992) Identification of amino acid changes affecting yeast uroporphyrinogen decarboxylase activity by sequence analysis of hem12 mutant alleles. *Biochem J* **288 (Pt 3):** 753-757

Chen GE, Canniffe DP, Martin EC, Hunter CN (2016a) Absence of the cbb3 Terminal Oxidase Reveals an Active Oxygen-Dependent Cyclase Involved in Bacteriochlorophyll Biosynthesis in Rhodobacter sphaeroides. *J Bacteriol* **198:** 2056-2063

Chen GE, Hitchcock A, Jackson PJ, Chaudhuri RR, Dickman MJ, Hunter CN, Canniffe DP (2016b) Two Unrelated 8-Vinyl Reductases Ensure Production of Mature Chlorophylls in Acaryochloris marina. *J Bacteriol* **198:** 1393-1400

Chen M (2014) Chlorophyll modifications and their spectral extension in oxygenic photosynthesis. *Annu Rev Biochem* **83:** 317-340

Chen X, Pu H, Fang Y, Wang X, Zhao S, Lin Y, Zhang M, Dai HE, Gong W, Liu L (2015a) Crystal structure of the catalytic subunit of magnesium chelatase. *Nat Plants* **1:** 15125

Chen X, Pu H, Wang X, Long W, Lin R, Liu L (2015b) Crystal Structures of GUN4 in Complex with Porphyrins. *Mol Plant* **8:** 1125-1127

Chen X, Wang X, Feng J, Chen Y, Fang Y, Zhao S, Zhao A, Zhang M, Liu L (2014) Structural insights into the catalytic mechanism of Synechocystis magnesium protoporphyrin IX O-methyltransferase (ChlM). *J Biol Chem* **289:** 25690-25698

Chereskin BM, Castelfranco PA (1982) Effects of Iron and Oxygen on Chlorophyll Biosynthesis : ii. Observations on the biosynthetic pathway in isolated etiochloroplasts. *Plant Physiol* **69:** 112-116

Chereskin BM, Wong YS, Castelfranco PA (1982) In Vitro Synthesis of the Chlorophyll Isocyclic Ring : Transformation of Magnesium-Protoporphyrin IX and Magnesium-Protoporphyrin IX Monomethyl Ester into Magnesium-2,4-Divinyl Pheoporphyrin A(5). *Plant Physiol* **70:** 987-993

Chew AG, Bryant DA (2007a) Characterization of a plant-like protochlorophyllide a divinyl reductase in green sulfur bacteria. *J Biol Chem* **282:** 2967-2975

Chew AG, Bryant DA (2007b) Chlorophyll biosynthesis in bacteria: the origins of structural and functional diversity. *Annu Rev Microbiol* **61:** 113-129

Chidgey JW, Linhartova M, Komenda J, Jackson PJ, Dickman MJ, Canniffe DP, Konik P, Pilny J, Hunter CN, Sobotka R (2014) A cyanobacterial chlorophyll synthase-HliD complex associates with the Ycf39 protein and the YidC/Alb3 insertase. *Plant Cell* **26:** 1267-1279

Chisholm SW, Frankel SL, Goericke R, Olson RJ, Palenik B, Waterbury JB, West-Johnsrud L, Zettler ER (1992) Prochlorococcus marinus nov. gen. nov. sp.: an oxyphototrophic marine prokaryote containing divinyl chlorophyll a and b. *Arch Microbiol* **157:** 297-300

Chu GC, Katakura K, Zhang X, Yoshida T, Ikeda-Saito M (1999) Heme degradation as catalyzed by a recombinant bacterial heme oxygenase (Hmu O) from Corynebacterium diphtheriae. *J Biol Chem* **274:** 21319-21325

Cingolani P, Platts A, Wang le L, Coon M, Nguyen T, Wang L, Land SJ, Lu X, Ruden DM (2012) A program for annotating and predicting the effects of single nucleotide polymorphisms, SnpEff: SNPs in the genome of Drosophila melanogaster strain w1118; iso-2; iso-3. *Fly (Austin)* **6:** 80-92

Coates L, Beaven G, Erskine PT, Beale SI, Avissar YJ, Gill R, Mohammed F, Wood SP, Shoolingin-Jordan P, Cooper JB (2004) The X-ray structure of the plant like 5-aminolaevulinic acid dehydratase from Chlorobium vibrioforme complexed with the inhibitor laevulinic acid at 2.6 A resolution. *J Mol Biol* **342:** 563-570

Contestabile R, Angelaccio S, Maytum R, Bossa F, John RA (2000) The contribution of a conformationally mobile, active site loop to the reaction catalyzed by glutamate semialdehyde aminomutase. *J Biol Chem* **275:** 3879-3886

Coomber SA, Chaudhri M, Connor A, Britton G, Hunter CN (1990) Localized transposon Tn5 mutagenesis of the photosynthetic gene cluster of Rhodobacter sphaeroides. *Mol Microbiol* **4:** 977-989

Coomber SA, Jones RM, Jordan PM, Hunter CN (1992) A putative anaerobic coproporphyrinogen III oxidase in Rhodobacter sphaeroides. I. Molecular cloning, transposon mutagenesis and sequence analysis of the gene. *Mol Microbiol* **6:** 3159-3169

Corradi HR, Corrigall AV, Boix E, Mohan CG, Sturrock ED, Meissner PN, Acharya KR (2006) Crystal structure of protoporphyrinogen oxidase from Myxococcus xanthus and its complex with the inhibitor acifluorfen. *J Biol Chem* **281:** 38625-38633

Corrigall AV, Siziba KB, Maneli MH, Shephard EG, Ziman M, Dailey TA, Dailey HA, Kirsch RE, Meissner PN (1998) Purification of and kinetic studies on a cloned protoporphyrinogen oxidase from the aerobic bacterium Bacillus subtilis. *Arch Biochem Biophys* **358:** 251-256

Curtis PD (2016) Essential Genes Predicted in the Genome of Rubrivivax gelatinosus. *J Bacteriol* **198:** 2244-2250

Dailey HA, Dailey TA (1996) Protoporphyrinogen oxidase of Myxococcus xanthus. Expression, purification, and characterization of the cloned enzyme. *J Biol Chem* **271:** 8714-8718

Dailey TA, Dailey HA (1998) Identification of an FAD superfamily containing protoporphyrinogen oxidases, monoamine oxidases, and phytoene desaturase. Expression and characterization of phytoene desaturase of Myxococcus xanthus. *J Biol Chem* **273:** 13658-13662

Darrah PM, Kay SA, Teakle GR, Griffiths WT (1990) Cloning and sequencing of protochlorophyllide reductase. *Biochem J* **265:** 789-798

Davison PA, Schubert HL, Reid JD, Iorg CD, Heroux A, Hill CP, Hunter CN (2005) Structural and biochemical characterization of Gun4 suggests a mechanism for its role in chlorophyll biosynthesis. *Biochemistry* **44:** 7603-7612

de Lorenzo V, Eltis L, Kessler B, Timmis KN (1993) Analysis of Pseudomonas gene products using lacIq/Ptrp-lac plasmids and transposons that confer conditional phenotypes. *Gene* **123:** 17-24

de Verneuil H, Sassa S, Kappas A (1983) Purification and properties of uroporphyrinogen decarboxylase from human erythrocytes. A single enzyme catalyzing the four sequential decarboxylations of uroporphyrinogens I and III. *J Biol Chem* **258:** 2454-2460

Dehesh K, Ryberg M (1985) The NADPH-protochlorophyllide oxidoreductase is the major protein constituent of prolamellar bodies in wheat (Triticum aestivum L.). *Planta* **164:** 396-399

del Batlle AM, Benson A, Rimington C (1965) Purification and properties of coproporphyrinogenase. *Biochem J* **97:** 731-740

Demerec M, Adelberg EA, Clark AJ, Hartman PE (1966) A proposal for a uniform nomenclature in bacterial genetics. *Genetics* **54:** 61-76

DePristo MA, Banks E, Poplin R, Garimella KV, Maguire JR, Hartl C, Philippakis AA, del Angel G, Rivas MA, Hanna M, McKenna A, Fennell TJ, Kernytsky AM, Sivachenko AY, Cibulskis K, Gabriel SB, Altshuler D, Daly MJ (2011) A framework for variation discovery and genotyping using next-generation DNA sequencing data. *Nat Genet* **43:** 491-498

Ding Q, Chen G, Wang Y, Wei D (2015) Identification of Specific Variations in a Non-Motile Strain of Cyanobacterium Synechocystis sp. PCC 6803 Originated from ATCC 27184 by Whole Genome Resequencing. *Int J Mol Sci* **16:** 24081-24093

Ducey TF, Dyer DW (2002) Rapid identification of EZ::TN™ transposon insertion sites in the genome of *Neisseria gonorrhoeae*. *Epicentre Forum* **9:** 6-7

Duggan J, Gassman M (1974) Induction of porphyrin synthesis in etiolated bean leaves by chelators of iron. *Plant Physiol* **53:** 206-215

Eckhardt U, Grimm B, Hörtensteiner S (2004) Recent advances in chlorophyll biosynthesis and breakdown in higher plants. *Plant Mol Biol* **56:** 1-14

Elder GH, Evans JO, Jackson JR, Jackson AH (1978) Factors determining the sequence of oxidative decarboxylation of the 2- and 4-propionate substituents of coproporphyrinogen III by coproporphyrinogen oxidase in rat liver. *Biochem J* **169:** 215-223

Elmlund H, Lundqvist J, Al-Karadaghi S, Hansson M, Hebert H, Lindahl M (2008) A new cryo-EM single-particle ab initio reconstruction method visualizes secondary structure elements in an ATP-fueled AAA+ motor. *J Mol Biol* **375:** 934-947

Erskine PT, Norton E, Cooper JB, Lambert R, Coker A, Lewis G, Spencer P, Sarwar M, Wood SP, Warren MJ, Shoolingin-Jordan PM (1999) X-ray structure of 5-aminolevulinic acid dehydratase from Escherichia coli complexed with the inhibitor levulinic acid at 2.0 A resolution. *Biochemistry* **38:** 4266-4276

Erskine PT, Senior N, Awan S, Lambert R, Lewis G, Tickle IJ, Sarwar M, Spencer P, Thomas P, Warren MJ, Shoolingin-Jordan PM, Wood SP, Cooper JB (1997) X-ray structure of 5-aminolaevulinate dehydratase, a hybrid aldolase. *Nat Struct Biol* **4:** 1025-1031

Estevez JM, Cantero A, Reindl A, Reichler S, Leon P (2001) 1-Deoxy-D-xylulose-5-phosphate synthase, a limiting enzyme for plastidic isoprenoid biosynthesis in plants. *J Biol Chem* **276:** 22901-22909

Fan J, Liu Q, Hao Q, Teng M, Niu L (2007) Crystal structure of uroporphyrinogen decarboxylase from Bacillus subtilis. *J Bacteriol* **189:** 3573-3580

Fanica-Gaignier M, Clement-Metral J (1973a) 5-Aminolevulinic-acid synthetase of Rhodopseudomonas spheroides Y. Kinetic mechanism and inhibition by ATP. *Eur J Biochem* **40:** 19-24

Fanica-Gaignier M, Clement-Metral J (1973b) 5-Aminolevulinic-acid synthetase of Rhodopseudomonas spheroides Y. Purification and some properties. *Eur J Biochem* **40:** 13-18

Ferreira GC, Dailey HA (1988) Mouse protoporphyrinogen oxidase. Kinetic parameters and demonstration of inhibition by bilirubin. *Biochem J* **250:** 597-603

Fischer HM, Velasco L, Delgado MJ, Bedmar EJ, Scharen S, Zingg D, Gottfert M, Hennecke H (2001)

One of two hemN genes in Bradyrhizobium japonicum is functional during anaerobic growth and in symbiosis. *J Bacteriol* **183:** 1300-1311

Fleischer EB, Choi EI, Hambright P, Stone A (1964) Porphyrin Studies: Kinetics of Metalloporphyrin Formation. *Inorg Chem* **3:** 1284-1287

Fodje MN, Hansson A, Hansson M, Olsen JG, Gough S, Willows RD, Al-Karadaghi S (2001) Interplay between an AAA module and an integrin I domain may regulate the function of magnesium chelatase. *J Mol Biol* **311:** 111-122

Formighieri C, Ceol M, Bonente G, Rochaix JD, Bassi R (2012) Retrograde signaling and photoprotection in a gun4 mutant of Chlamydomonas reinhardtii. *Mol Plant* **5:** 1242-1262

Frankenberg N, Erskine PT, Cooper JB, Shoolingin-Jordan PM, Jahn D, Heinz DW (1999) High resolution crystal structure of a Mg^{2+}-dependent porphobilinogen synthase. *J Mol Biol* **289:** 591-602

Frigaard N-U, Bryant DA (2006) Chlorosomes: Antenna Organelles in Photosynthetic Green Bacteria. In *Complex Intracellular Structures in Prokaryotes*, Shively JM (ed), pp 79-114. Berlin, Heidelberg: Springer Berlin Heidelberg

Frigaard NU, Dahl C (2009) Sulfur metabolism in phototrophic sulfur bacteria. *Adv Microb Physiol* **54:** 103-200

Fuchs G, Stupperich E, Eden G (1980a) Autotrophic CO2 fixation in Chlorobium limicola. Evidence for the operation of a reductive tricarboxylic acid cycle in growing cells. *Arch Microbiol* **128:** 64-71

Fuchs G, Stupperich E, Jaenchen R (1980b) Autotrophic CO2 fixation in Chlorobium limicola. Evidence against the operation of the Calvin cycle in growing cells. *Arch Microbiol* **128:** 56-63

Fuesler TP, Wong YS, Castelfranco PA (1984) Localization of Mg-Chelatase and Mg-Protoporphyrin IX Monomethyl Ester (Oxidative) Cyclase Activities within Isolated, Developing Cucumber Chloroplasts. *Plant Physiol* **75:** 662-664

Fujita Y, Bauer CE (2000) Reconstitution of light-independent protochlorophyllide reductase from purified bchl and BchN-BchB subunits. In vitro

confirmation of nitrogenase-like features of a bacteriochlorophyll biosynthesis enzyme. *J Biol Chem* **275:** 23583-23588

Garcia Costas AM, Tsukatani Y, Rijpstra WI, Schouten S, Welander PV, Summons RE, Bryant DA (2012) Identification of the bacteriochlorophylls, carotenoids, quinones, lipids, and hopanoids of "Candidatus Chloracidobacterium thermophilum". *J Bacteriol* **194:** 1158-1168

Ge H, Lv X, Fan J, Gao Y, Teng M, Niu L (2010) Crystal structure of glutamate-1-semialdehyde aminotransferase from Bacillus subtilis with bound pyridoxamine-5'-phosphate. *Biochem Biophys Res Commun* **402:** 356-360

Gest H, Favinger JL (1983) Heliobacterium chlorum, an anoxygenic brownish-green photosynthetic bacterium containing a "new" form of bacteriochlorophyll. *Arch Microbiol* **136:** 11-16

Gibson KD, Laver WG, Neuberger A (1958) Initial stages in the biosynthesis of porphyrins. 2. The formation of delta-aminolaevulic acid from glycine and succinyl-coenzyme A by particles from chicken erythrocytes. *Biochem J* **70:** 71-81

Gibson KD, Neuberger A, Tait GH (1963) Studies on the biosynthesis of porphyrin and bacteriochlorophyll by rhodopseudomonas spheroides. 4. *S*-adenosylmethionine-magnesium protoporphyrin methyltransferase. *Biochem J* **88:** 325-334

Gibson LC, Hunter CN (1994) The bacteriochlorophyll biosynthesis gene, bchM, of Rhodobacter sphaeroides encodes S-adenosyl-L-methionine: Mg protoporphyrin IX methyltransferase. *FEBS Lett* **352:** 127-130

Gibson LC, Jensen PE, Hunter CN (1999) Magnesium chelatase from Rhodobacter sphaeroides: initial characterization of the enzyme using purified subunits and evidence for a BchI-BchD complex. *Biochem J* **337 (Pt 2):** 243-251

Gibson LC, Willows RD, Kannangara CG, von Wettstein D, Hunter CN (1995) Magnesium-protoporphyrin chelatase of Rhodobacter sphaeroides: reconstitution of activity by combining the products of the bchH, -I, and -D genes expressed in Escherichia coli. *Proc Natl Acad Sci U S A* **92:** 1941-1944

Gill R, Kolstoe SE, Mohammed F, Al DBA, Mosely JE, Sarwar M, Cooper JB, Wood SP, Shoolingin-Jordan PM (2009) Structure of human porphobilinogen deaminase at 2.8 A: the molecular basis of acute intermittent porphyria. *Biochem J* **420:** 17-25

Gomelsky L, Sram J, Moskvin OV, Horne IM, Dodd HN, Pemberton JM, McEwan AG, Kaplan S, Gomelsky M (2003) Identification and in vivo characterization of PpaA, a regulator of photosystem formation in Rhodobacter sphaeroides. *Microbiology* **149:** 377-388

Gorchein A (1972) Magnesium protoporphyrin chelatase activity in Rhodopseudomonas spheroides. Studies with whole cells. *Biochem J* **127:** 97-106

Gorchein A (1973) Control of magnesium-protoporphyrin chelatase activity in Rhodopseudomonas spheroides. Role of light, oxygen, and electron and energy transfer. *Biochem J* **134:** 833-845

Gorchein A (1997) Cell-free activity of magnesium chelatase in Rhodobacter spheroides and Rhodobacter capsulatus. *Biochem Soc Trans* **25:** 82S

Gorchein A, Gibson LC, Hunter CN (1993) Gene expression and control of enzymes for synthesis of magnesium protoporphyrin monomethyl ester in Rhodobacter sphaeroides. *Biochem Soc Trans* **21:** 201S

Goto T, Aoki R, Minamizaki K, Fujita Y (2010) Functional differentiation of two analogous coproporphyrinogen III oxidases for heme and chlorophyll biosynthesis pathways in the cyanobacterium Synechocystis sp. PCC 6803. *Plant Cell Physiol* **51:** 650-663

Gough S (1972) Defective synthesis of porphyrins in barley plastids caused by mutation in nuclear genes. *Biochim Biophys Acta* **286:** 36-54

Gough SP, Petersen BO, Duus JO (2000) Anaerobic chlorophyll isocyclic ring formation in Rhodobacter capsulatus requires a cobalamin cofactor. *Proc Natl Acad Sci U S A* **97:** 6908-6913

Granick S (1948) The structural and functional relationships between heme and chlorophyll. *Harvey Lect* **Series 44:** 220-245

Gregor J, Klug G (1999) Regulation of bacterial photosynthesis genes by oxygen and light. *FEMS Microbiol Lett* **179:** 1-9

Griffiths WT (1975) Characterization of the terminal stages of chlorophyll (ide) synthesis in etioplast membrane preparations. *Biochem J* **152:** 623-635

Griffiths WT (1978) Reconstitution of chlorophyllide formation by isolated etioplast membranes. *Biochem J* **174:** 681-692

Griffiths WT, McHugh T, Blankenship RE (1996) The light intensity dependence of protochlorophyllide photoconversion and its significance to the catalytic mechanism of protochlorophyllide reductase. *FEBS Lett* **398:** 235-238

Grigorieva G, Shestakov S (1982) Transformation in the cyanobacterium Synechocystis sp. 6803. *FEMS Microbiol Lett* **13:** 367-370

Hambright P (1975) Dynamic coordination chemistry of metalloporphyrins. In: *Porphyrins and Metalloporphyrins,*Smith KM (ed) pp 233-278. Amsterdam,The Netherlands: Elsevier Scientific Publishing Co.

Hanada S, Pierson BK (2006) The Family Chloroflexaceae. In *The Prokaryotes: Volume 7: Proteobacteria: Delta, Epsilon Subclass*, Dworkin M, Falkow S, Rosenberg E, Schleifer K-H, Stackebrandt E (eds), pp 815-842. New York, NY: Springer New York

Hansson M, Hederstedt L (1994) Bacillus subtilis HemY is a peripheral membrane protein essential for protoheme IX synthesis which can oxidize coproporphyrinogen III and protoporphyrinogen IX. *J Bacteriol* **176:** 5962-5970

Harker M, Bramley PM (1999) Expression of prokaryotic 1-deoxy-D-xylulose-5-phosphatases in Escherichia coli increases carotenoid and ubiquinone biosynthesis. *FEBS Lett* **448:** 115-119

Hart GJ, Battersby AR (1985) Purification and properties of uroporphyrinogen III synthase (co-synthetase) from Euglena gracilis. *Biochem J* **232:** 151-160

Hart GJ, Miller AD, Leeper FJ, Battersby AR (1987) Biosynthesis of the natural porphyrins: proof that

hydroxymethylbilane synthase (porphobilinogen deaminase) uses a novel binding group in its catalytic action. *J Chem Soc Chem Commun*: 1762-1765

Hartwich G, Fiedor L, Simonin I, Cmiel E, Schäfer W, Noy D, Scherz A, Scheer H (1998) Metal-Substituted Bacteriochlorophylls. 1. Preparation and Influence of Metal and Coordination on Spectra. *J Am Chem Soc* **120:** 3675-3683

Hedlund J, Jornvall H, Persson B (2010) Subdivision of the MDR superfamily of medium-chain dehydrogenases/reductases through iterative hidden Markov model refinement. *BMC Bioinformatics* **11:** 534

Heinemann IU, Jahn M, Jahn D (2008) The biochemistry of heme biosynthesis. *Arch Biochem Biophys* **474:** 238-251

Heinnickel M, Golbeck JH (2007) Heliobacterial photosynthesis. *Photosynth Res* **92:** 35-53

Hennig M, Grimm B, Contestabile R, John RA, Jansonius JN (1997) Crystal structure of glutamate-1-semialdehyde aminomutase: an alpha2-dimeric vitamin B6-dependent enzyme with asymmetry in structure and active site reactivity. *Proc Natl Acad Sci U S A* **94:** 4866-4871

Heyes DJ, Heathcote P, Rigby SE, Palacios MA, van Grondelle R, Hunter CN (2006) The first catalytic step of the light-driven enzyme protochlorophyllide oxidoreductase proceeds via a charge transfer complex. *J Biol Chem* **281:** 26847-26853

Heyes DJ, Hunter CN (2004) Identification and characterization of the product release steps within the catalytic cycle of protochlorophyllide oxidoreductase. *Biochemistry* **43:** 8265-8271

Heyes DJ, Hunter CN (2005) Making light work of enzyme catalysis: protochlorophyllide oxidoreductase. *Trends Biochem Sci* **30:** 642-649

Heyes DJ, Hunter CN, van Stokkum IH, van Grondelle R, Groot ML (2003a) Ultrafast enzymatic reaction dynamics in protochlorophyllide oxidoreductase. *Nat Struct Biol* **10:** 491-492

Heyes DJ, Martin GE, Reid RJ, Hunter CN, Wilks HM (2000) NADPH:protochlorophyllide oxidoreductase

from Synechocystis: overexpression, purification and preliminary characterisation. *FEBS Lett* **483:** 47-51

Heyes DJ, Menon BR, Sakuma M, Scrutton NS (2008) Conformational events during ternary enzyme-substrate complex formation are rate limiting in the catalytic cycle of the light-driven enzyme protochlorophyllide oxidoreductase. *Biochemistry* **47:** 10991-10998

Heyes DJ, Neil Hunter C (2009) Biosynthesis of Chlorophyll and Barteriochlorophyll. In *Tetrapyrroles: Birth, Life and Death*, pp 235-249. New York, NY: Springer New York

Heyes DJ, Ruban AV, Hunter CN (2003b) Protochlorophyllide oxidoreductase: "dark" reactions of a light-driven enzyme. *Biochemistry* **42:** 523-528

Heyes DJ, Ruban AV, Wilks HM, Hunter CN (2002) Enzymology below 200 K: the kinetics and thermodynamics of the photochemistry catalyzed by protochlorophyllide oxidoreductase. *Proc Natl Acad Sci U S A* **99:** 11145-11150

Hinchigeri SB, Hundle B, Richards WR (1997) Demonstration that the BchH protein of Rhodobacter capsulatus activates S-adenosyl-L-methionine:magnesium protoporphyrin IX methyltransferase. *FEBS Lett* **407:** 337-342

Hitchcock A, Jackson PJ, Chidgey JW, Dickman MJ, Hunter CN, Canniffe DP (2016) Biosynthesis of Chlorophyll a in a Purple Bacterial Phototroph and Assembly into a Plant Chlorophyll-Protein Complex. *ACS Synth Biol*

Ho SN, Hunt HD, Horton RM, Pullen JK, Pease LR (1989) Site-directed mutagenesis by overlap extension using the polymerase chain reaction. *Gene* **77:** 51-59

Hollingshead S (2014) *Investigating Protein-Protein Interactions in the Chlorophyll Biosynthesis Pathway*. PhD thesis (eThesis), University of Sheffield, UK

Hollingshead S, Kopecna J, Armstrong DR, Bucinska L, Jackson PJ, Chen GE, Dickman MJ, Williamson MP, Sobotka R, Hunter CN (2016) Synthesis of Chlorophyll-Binding Proteins in a Fully Segregated Deltaycf54 Strain of the Cyanobacterium Synechocystis PCC 6803. *Front Plant Sci* **7:** 292

Hollingshead S, Kopecna J, Jackson PJ, Canniffe DP, Davison PA, Dickman MJ, Sobotka R, Hunter CN (2012) Conserved chloroplast open-reading frame ycf54 is required for activity of the magnesium protoporphyrin monomethylester oxidative cyclase in Synechocystis PCC 6803. *J Biol Chem* **287:** 27823-27833

Holtorf H, Reinbothe S, Reinbothe C, Bereza B, Apel K (1995) Two routes of chlorophyllide synthesis that are differentially regulated by light in barley (Hordeum vulgare L.). *Proc Natl Acad Sci U S A* **92:** 3254-3258

Huang DD, Wang WY, Gough SP, Kannangara CG (1984) delta-Aminolevulinic acid-synthesizing enzymes need an RNA moiety for activity. *Science* **225:** 1482-1484

Huang I, Eaton-Rye J (2001) Mutagenesis of histidine-469 in the photosystem II chlorophyll a-binding protein CP47 in Synechocystis sp. PCC 6803. *Sci Access* **3:** -

Huang L, McCluskey MP, Ni H, LaRossa RA (2002) Global gene expression profiles of the cyanobacterium Synechocystis sp. strain PCC 6803 in response to irradiation with UV-B and white light. *J Bacteriol* **184:** 6845-6858

Hudson A, Carpenter R, Doyle S, Coen ES (1993) Olive: a key gene required for chlorophyll biosynthesis in Antirrhinum majus. *EMBO J* **12:** 3711-3719

Hunter CN, Coomber SA (1988) Cloning and Oxygen-regulated Expression of the Bacteriochlorophyll Biosynthesis Genes bch E, B, A and C of Rhodobacter sphaeroides. *Microbiology* **134:** 1491-1497

Hunter CN, Turner G (1988) Transfer of Genes Coding for Apoproteins of Reaction Centre and Light-harvesting LH1 Complexes to Rhodobacter sphaeroides. *Microbiology* **134:** 1471-1480

Hunter WN (2007) The non-mevalonate pathway of isoprenoid precursor biosynthesis. *J Biol Chem* **282:** 21573-21577

Islam MR, Aikawa S, Midorikawa T, Kashino Y, Satoh K, Koike H (2008) slr1923 of Synechocystis sp. PCC6803 is essential for conversion of 3,8-divinyl(proto)chlorophyll(ide) to 3-monovinyl(proto)chlorophyll(ide). *Plant Physiol* **148:** 1068-1081

Ito H, Yokono M, Tanaka R, Tanaka A (2008) Identification of a novel vinyl reductase gene essential for the biosynthesis of monovinyl chlorophyll in Synechocystis sp. PCC6803. *J Biol Chem* **283:** 9002-9011

Jackson AH, Jones DM, Philip G, Lash TD, Batlle AM, Smith SG (1980) Synthetic and biosynthetic studies of porphyrins, Part IV. Further studies of the conversion of corporporhyrinogen-III to protoporphyrin-IX: mass spectrometric investigations of the incubation of specifically deuteriated coproporhyringen-III with chicken red cell haemolysates. *Int J Biochem* **12:** 681-688

Jackson AH, Sancovich HA, Ferramola AM, Evans N, Games DE, Matlin SA (1976) Macrocyclic Intermediates in the Biosynthesis of Porphyrins. *Philos Trans R Soc Lond B* **273:** 191-206

Jackson RJ, Elvers KT, Lee LJ, Gidley MD, Wainwright LM, Lightfoot J, Park SF, Poole RK (2007) Oxygen reactivity of both respiratory oxidases in Campylobacter jejuni: the cydAB genes encode a cyanide-resistant, low-affinity oxidase that is not of the cytochrome bd type. *J Bacteriol* **189:** 1604-1615

Jacobs JM, Jacobs NJ (1987) Oxidation of protoporphyrinogen to protoporphyrin, a step in chlorophyll and haem biosynthesis. Purification and partial characterization of the enzyme from barley organelles. *Biochem J* **244:** 219-224

Jacobs NJ, Jacobs JM (1975) Fumarate as alternate electron acceptor for the late steps of anaerobic heme synthesis in Escherichia coli. *Biochem Biophys Res Commun* **65:** 435-441

Jacobs NJ, Jacobs JM (1976) Nitrate, fumarate, and oxygen as electron acceptors for a late step in microbial heme synthesis. *Biochim Biophys Acta* **449:** 1-9

Jacobs NJ, Jacobs JM (1981) Protoporphyrinogen oxidation in Rhodopseudomonas spheroides, a step in heme and bacteriochlorophyll synthesis. *Arch Biochem Biophys* **211:** 305-311

Jacobs NJ, Jacobs JM, Brent P (1970) Formation of protoporphyrin from coproporphyrinogen in extracts of various bacteria. *J Bacteriol* **102:** 398-403

Jacobs NJ, Jacobs JM, Brent P (1971) Characterization of the late steps of microbial heme synthesis: conversion of coproporphyrinogen to protoporphyrin. *J Bacteriol* **107:** 203-209

Jaffe EK, Ali S, Mitchell LW, Taylor KM, Volin M, Markham GD (1995) Characterization of the role of the stimulatory magnesium of Escherichia coli porphobilinogen synthase. *Biochemistry* **34:** 244-251

Jaschke PR, Beatty JT (2007) The photosystem of Rhodobacter sphaeroides assembles with zinc bacteriochlorophyll in a bchD (magnesium chelatase) mutant. *Biochemistry* **46:** 12491-12500

Jaschke PR, Hardjasa A, Digby EL, Hunter CN, Beatty JT (2011) A BchD (magnesium chelatase) mutant of rhodobacter sphaeroides synthesizes zinc bacteriochlorophyll through novel zinc-containing intermediates. *J Biol Chem* **286:** 20313-20322

Jensen PE, Gibson LC, Henningsen KW, Hunter CN (1996a) Expression of the chlI, chlD, and chlH genes from the Cyanobacterium synechocystis PCC6803 in Escherichia coli and demonstration that the three cognate proteins are required for magnesium-protoporphyrin chelatase activity. *J Biol Chem* **271:** 16662-16667

Jensen PE, Gibson LC, Hunter CN (1998) Determinants of catalytic activity with the use of purified I, D and H subunits of the magnesium protoporphyrin IX chelatase from Synechocystis PCC6803. *Biochem J* **334 (Pt 2):** 335-344

Jensen PE, Gibson LC, Hunter CN (1999) ATPase activity associated with the magnesium-protoporphyrin IX chelatase enzyme of Synechocystis PCC6803: evidence for ATP hydrolysis during Mg2+ insertion, and the MgATP-dependent interaction of the ChlI and ChlD subunits. *Biochem J* **339 (Pt 1):** 127-134

Jensen PE, Reid JD, Hunter CN (2000) Modification of cysteine residues in the ChlI and ChlH subunits of magnesium chelatase results in enzyme inactivation. *Biochem J* **352 Pt 2:** 435-441

Jensen PE, Willows RD, Petersen BL, Vothknecht UC, Stummann BM, Kannangara CG, von Wettstein D, Henningsen KW (1996b) Structural genes for Mg-chelatase subunits in barley: Xantha-f, -g and -h. *Mol Gen Genet* **250:** 383-394

Johnson ET, Schmidt-Dannert C (2008) Characterization of three homologs of the large subunit of the magnesium chelatase from Chlorobaculum tepidum and interaction with the magnesium protoporphyrin IX methyltransferase. *J Biol Chem* **283:** 27776-27784

Jones DT, Taylor WR, Thornton JM (1992) The rapid generation of mutation data matrices from protein sequences. *Comput Appl Biosci* **8:** 275-282

Jones RM, Jordan PM (1993) Purification and properties of the uroporphyrinogen decarboxylase from Rhodobacter sphaeroides. *Biochem J* **293 (Pt 3):** 703-712

Jordan PM, Berry A (1981) Mechanism of action of porphobilinogen deaminase. The participation of stable enzyme substrate covalent intermediates between porphobilinogen and the porphobilinogen deaminase from Rhodopseudomonas spheroides. *Biochem J* **195:** 177-181

Jordan PM, Burton G, Nordlov H, Schneider MM, Pryde L, Scott AI (1979) Pre-uroporphyrinogen: a substrate for uroporphyrinogen III cosynthetase. *J Chem Soc Chem Commun***:** 204-205

Jordan PM, Gibbs PN (1985) Mechanism of action of 5-aminolaevulinate dehydratase from human erythrocytes. *Biochem J* **227:** 1015-1020

Jordan PM, Seehra JS (1979) The biosynthesis of uroporphyrinogen III: order of assembly of the four porphobilinogen molecules in the formation of the tetrapyrrole ring. *FEBS Lett* **104:** 364-366

Jordan PM, Warren MJ (1987) Evidence for a dipyrromethane cofactor at the catalytic site of E. coli porphobilinogen deaminase. *FEBS Lett* **225:** 87-92

Jordan PM, Warren MJ, Williams HJ, Stolowich NJ, Roessner CA, Grant SK, Scott AI (1988) Identification of a cysteine residue as the binding site for the dipyrromethane cofactor at the active site of Escherichia coli porphobilinogen deaminase. *FEBS Lett* **235:** 189-193

Jordan PM, Woodcock SC (1991) Mutagenesis of arginine residues in the catalytic cleft of Escherichia coli porphobilinogen deaminase that affects dipyrromethane cofactor assembly and tetrapyrrole chain initiation and elongation. *Biochem J* **280 (Pt 2):** 445-449

Kaneko T, Nakamura Y, Sasamoto S, Watanabe A, Kohara M, Matsumoto M, Shimpo S, Yamada M, Tabata S (2003) Structural analysis of four large plasmids harboring in a unicellular cyanobacterium, Synechocystis sp. PCC 6803. *DNA Res* **10:** 221-228

Kaneko T, Sato S, Kotani H, Tanaka A, Asamizu E, Nakamura Y, Miyajima N, Hirosawa M, Sugiura M, Sasamoto S, Kimura T, Hosouchi T, Matsuno A, Muraki A, Nakazaki N, Naruo K, Okumura S, Shimpo S, Takeuchi C, Wada T, Watanabe A, Yamada M, Yasuda M, Tabata S (1996) Sequence analysis of the genome of the unicellular cyanobacterium Synechocystis sp. strain PCC6803. II. Sequence determination of the entire genome and assignment of potential protein-coding regions (supplement). *DNA Res* **3:** 185-209

Kanesaki Y, Shiwa Y, Tajima N, Suzuki M, Watanabe S, Sato N, Ikeuchi M, Yoshikawa H (2012) Identification of substrain-specific mutations by massively parallel whole-genome resequencing of Synechocystis sp. PCC 6803. *DNA Res* **19:** 67-79

Kanesaki Y, Suzuki I, Allakhverdiev SI, Mikami K, Murata N (2002) Salt stress and hyperosmotic stress regulate the expression of different sets of genes in Synechocystis sp. PCC 6803. *Biochem Biophys Res Commun* **290:** 339-348

Kannangara CG, Vothknecht UC, Hansson M, von Wettstein D (1997) Magnesium chelatase: association with ribosomes and mutant complementation studies identify barley subunit Xantha-G as a functional counterpart of Rhodobacter subunit BchD. *Mol Gen Genet* **254:** 85-92

Karger GA, Reid JD, Hunter CN (2001) Characterization of the binding of deuteroporphyrin IX to the magnesium chelatase H subunit and spectroscopic properties of the complex. *Biochemistry* **40:** 9291-9299

Kaschner M, Loeschcke A, Krause J, Minh BQ, Heck A, Endres S, Svensson V, Wirtz A, von Haeseler A, Jaeger KE, Drepper T, Krauss U (2014) Discovery of the first light-dependent protochlorophyllide

oxidoreductase in anoxygenic phototrophic bacteria. *Mol Microbiol* **93:** 1066-1078

Kato K, Tanaka R, Sano S, Tanaka A, Hosaka H (2010) Identification of a gene essential for protoporphyrinogen IX oxidase activity in the cyanobacterium Synechocystis sp. PCC6803. *Proc Natl Acad Sci U S A* **107:** 16649-16654

Kauss D, Bischof S, Steiner S, Apel K, Meskauskiene R (2012) FLU, a negative feedback regulator of tetrapyrrole biosynthesis, is physically linked to the final steps of the Mg(++)-branch of this pathway. *FEBS Lett* **586:** 211-216

Kawanishi S, Seki Y, Sano S (1983) Uroporphyrinogen decarboxylase. Purification, properties, and inhibition by polychlorinated biphenyl isomers. *J Biol Chem* **258:** 4285-4292

Keithly JH, Nadler KD (1983) Protoporphyrin formation in Rhizobium japonicum. *J Bacteriol* **154:** 838-845

Keller Y, Bouvier F, d'Harlingue A, Camara B (1998) Metabolic compartmentation of plastid prenyllipid biosynthesis--evidence for the involvement of a multifunctional geranylgeranyl reductase. *Eur J Biochem* **251:** 413-417

Kiesel S, Watzlich D, Lange C, Reijerse E, Brocker MJ, Rüdiger W, Lubitz W, Scheer H, Moser J, Jahn D (2015) Iron-sulfur cluster-dependent catalysis of chlorophyllide a oxidoreductase from Roseobacter denitrificans. *J Biol Chem* **290:** 1141-1154

Kim EJ, Kim H, Lee JK (2016) The Photoheterotrophic Growth of Bacteriochlorophyll Synthase-Deficient Mutant of Rhodobacter sphaeroides Is Restored by I44F Mutant Chlorophyll Synthase of Synechocystis sp. PCC 6803. *J Microbiol Biotechnol* **26:** 959-966

Kim EJ, Kim JS, Lee IH, Rhee HJ, Lee JK (2008) Superoxide generation by chlorophyllide a reductase of Rhodobacter sphaeroides. *J Biol Chem* **283:** 3718-3730

Kim EJ, Kim JS, Rhee HJ, Lee JK (2009) Growth arrest of Synechocystis sp. PCC6803 by superoxide generated from heterologously expressed Rhodobacter sphaeroides chlorophyllide a reductase. *FEBS Lett* **583:** 219-223

Kim EJ, Lee JK (2010) Competitive inhibitions of the chlorophyll synthase of Synechocystis sp. strain PCC 6803 by bacteriochlorophyllide a and the bacteriochlorophyll synthase of Rhodobacter sphaeroides by chlorophyllide a. *J Bacteriol* **192:** 198-207

Kim SJ, Kim MD, Choi JH, Kim SY, Ryu YW, Seo JH (2006) Amplification of 1-deoxy-D-xyluose 5-phosphate (DXP) synthase level increases coenzyme Q10 production in recombinant Escherichia coli. *Appl Microbiol Biotechnol* **72:** 982-985

Kim SW, Keasling JD (2001) Metabolic engineering of the nonmevalonate isopentenyl diphosphate synthesis pathway in Escherichia coli enhances lycopene production. *Biotechnol Bioeng* **72:** 408-415

Kim YJ, Ko IJ, Lee JM, Kang HY, Kim YM, Kaplan S, Oh JI (2007) Dominant role of the cbb3 oxidase in regulation of photosynthesis gene expression through the PrrBA system in Rhodobacter sphaeroides 2.4.1. *J Bacteriol* **189:** 5617-5625

Kikuchi G, Kumar A, Talmage P, Shemin D (1958) The enzymatic synthesis of delta-aminolevulinic acid. *J Biol Chem* **233:** 1214-1219

Klement H, Helfrich M, Oster U, Schoch S, Rüdiger W (1999) Pigment-free NADPH:protochlorophyllide oxidoreductase from Avena sativa L. Purification and substrate specificity. *Eur J Biochem* **265:** 862-874

Knaust R, Seyfried B, Schmidt L, Schulz R, Senger H (1993) Phototransformation of monovinyl and divinyl protochlorophyllide by NADPH:protochlorophyllide oxidoreductase of barley expressed in Escherichia coli. *J Photochem Photobiol B* **20:** 161-166

Kobayashi M, Oh-Oka H, Akutsu S, Akiyama M, Tominaga K, Kise H, Nishida F, Watanabe T, Amesz J, Koizumi M, Ishida N, Kano H (2000) The primary electron acceptor of green sulfur bacteria, bacteriochlorophyll 663, is chlorophyll a esterified with Delta2,6-phytadienol. *Photosynth Res* **63:** 269-280

Kobayashi M, Okada K, Ikeuchi M (2005) A suppressor mutation in the alpha-phycocyanin gene in the light/glucose-sensitive phenotype of the psbK-disruptant of the cyanobacterium Synechocystis sp. PCC 6803. *Plant Cell Physiol* **46:** 1561-1567

Koch HG, Hwang O, Daldal F (1998) Isolation and characterization of Rhodobacter capsulatus mutants affected in cytochrome cbb3 oxidase activity. *J Bacteriol* **180:** 969-978

Koch M, Breithaupt C, Kiefersauer R, Freigang J, Huber R, Messerschmidt A (2004) Crystal structure of protoporphyrinogen IX oxidase: a key enzyme in haem and chlorophyll biosynthesis. *EMBO J* **23:** 1720-1728

Kohashi M, Clement RP, Tse J, Piper WN (1984) Rat hepatic uroporphyrinogen III co-synthase. Purification and evidence for a bound folate coenzyme participating in the biosynthesis of uroporphyrinogen III. *Biochem J* **220:** 755-765

Kohno H, Furukawa T, Tokunaga R, Taketani S, Yoshinaga T (1996) Mouse coproporphyrinogen oxidase is a copper-containing enzyme: expression in Escherichia coli and site-directed mutagenesis. *Biochim Biophys Acta* **1292:** 156-162

Kolossov VL, Rebeiz CA (2001) Chloroplast biogenesis 84: solubilization and partial purification of membrane-bound [4-vinyl]chlorophyllide a reductase from etiolated barley leaves. *Anal Biochem* **295:** 214-219

Komenda J, Lupinkova L, Kopecky J (2002) Absence of the psbH gene product destabilizes photosystem II complex and bicarbonate binding on its acceptor side in Synechocystis PCC 6803. *Eur J Biochem* **269:** 610-619

Koncz C, Mayerhofer R, Koncz-Kalman Z, Nawrath C, Reiss B, Redei GP, Schell J (1990) Isolation of a gene encoding a novel chloroplast protein by T-DNA tagging in Arabidopsis thaliana. *EMBO J* **9:** 1337-1346

Kontur WS, Schackwitz WS, Ivanova N, Martin J, Labutti K, Deshpande S, Tice HN, Pennacchio C, Sodergren E, Weinstock GM, Noguera DR, Donohue TJ (2012) Revised sequence and annotation of the Rhodobacter sphaeroides 2.4.1 genome. *J Bacteriol* **194:** 7016-7017

Kopecna J, Komenda J, Bucinska L, Sobotka R (2012) Long-term acclimation of the cyanobacterium Synechocystis sp. PCC 6803 to high light is accompanied by an enhanced production of chlorophyll that is preferentially channeled to

trimeric photosystem I. *Plant Physiol* **160:** 2239-2250

Kopecna J, Sobotka R, Komenda J (2013) Inhibition of chlorophyll biosynthesis at the protochlorophyllide reduction step results in the parallel depletion of Photosystem I and Photosystem II in the cyanobacterium Synechocystis PCC 6803. *Planta* **237:** 497-508

Labbe P (1997) Purification and properties of coproporphyrinogen III oxidase from yeast. *Methods Enzymol* **281:** 367-378

Lander M, Pitt AR, Alefounder PR, Bardy D, Abell C, Battersby AR (1991) Studies on the mechanism of hydroxymethylbilane synthase concerning the role of arginine residues in substrate binding. *Biochem J* **275 (Pt 2):** 447-452

Lange C, Kiesel S, Peters S, Virus S, Scheer H, Jahn D, Moser J (2015) Broadened Substrate Specificity of 3-Hydroxyethyl Bacteriochlorophyllide a Dehydrogenase (BchC) Indicates a New Route for the Biosynthesis of Bacteriochlorophyll a. *J Biol Chem* **290:** 19697-19709

Larkin RM, Alonso JM, Ecker JR, Chory J (2003) GUN4, a regulator of chlorophyll synthesis and intracellular signaling. *Science* **299:** 902-906

Lash TD (1991) Action of uroporphyrinogen decarboxylase on uroporphyrinogen-III: a reassessment of the clockwise decarboxylation hypothesis. *Biochem J* **278 (Pt 3):** 901-903

Lash TD (2005) The enigma of coproporphyrinogen oxidase: how does this unusual enzyme carry out oxidative decarboxylations to afford vinyl groups? *Bioorg Med Chem Lett* **15:** 4506-4509

Layer G, Grage K, Teschner T, Schunemann V, Breckau D, Masoumi A, Jahn M, Heathcote P, Trautwein AX, Jahn D (2005) Radical S-adenosylmethionine enzyme coproporphyrinogen III oxidase HemN: functional features of the [4Fe-4S] cluster and the two bound S-adenosyl-L-methionines. *J Biol Chem* **280:** 29038-29046

Layer G, Moser J, Heinz DW, Jahn D, Schubert WD (2003) Crystal structure of coproporphyrinogen III oxidase reveals cofactor geometry of Radical SAM enzymes. *EMBO J* **22:** 6214-6224

Layer G, Pierik AJ, Trost M, Rigby SE, Leech HK, Grage K, Breckau D, Astner I, Jansch L, Heathcote P, Warren MJ, Heinz DW, Jahn D (2006) The substrate radical of Escherichia coli oxygen-independent coproporphyrinogen III oxidase HemN. *J Biol Chem* **281:** 15727-15734

Layer G, Reichelt J, Jahn D, Heinz DW (2010) Structure and function of enzymes in heme biosynthesis. *Protein Sci* **19:** 1137-1161

Layer G, Verfurth K, Mahlitz E, Jahn D (2002) Oxygen-independent coproporphyrinogen-III oxidase HemN from Escherichia coli. *J Biol Chem* **277:** 34136-34142

Lebedev N, Timko MP (1998) Protochlorophyllide photoreduction. *Photosynth Res* **58:** 5-23

Lebedev N, Timko MP (1999) Protochlorophyllide oxidoreductase B-catalyzed protochlorophyllide photoreduction in vitro: insight into the mechanism of chlorophyll formation in light-adapted plants. *Proc Natl Acad Sci U S A* **96:** 9954-9959

Lee DS, Flachsova E, Bodnarova M, Demeler B, Martasek P, Raman CS (2005) Structural basis of hereditary coproporphyria. *Proc Natl Acad Sci U S A* **102:** 14232-14237

Lee HJ, Ball MD, Parham R, Rebeiz CA (1992) Chloroplast Biogenesis 65 : Enzymic Conversion of Protoporphyrin IX to Mg-Protoporphyrin IX in a Subplastidic Membrane Fraction of Cucumber Etiochloroplasts. *Plant Physiol* **99:** 1134-1140

Legnaioli T, Cuevas J, Mas P (2009) TOC1 functions as a molecular switch connecting the circadian clock with plant responses to drought. *EMBO J* **28:** 3745-3757

Letunic I, Bork P (2011) Interactive Tree Of Life v2: online annotation and display of phylogenetic trees made easy. *Nucleic Acids Res* **39:** W475-478

Li H, Durbin R (2010) Fast and accurate long-read alignment with Burrows-Wheeler transform. *Bioinformatics* **26:** 589-595

Lieb C, Siddiqui RA, Hippler B, Jahn D, Friedrich B (1998) The Alcaligenes eutrophus hemN gene encoding the oxygen-independent

coproporphyrinogen III oxidase, is required for heme biosynthesis during anaerobic growth. *Arch Microbiol* **169:** 52-60

Liljenberg C (1974) Characterization and Properties of a Protochlorophyllide Ester in Leaves of Dark Grown Barley with Geranylgeraniol as Esterifying Alcohol. *Physiol Plant* **32:** 208-213

Louie GV, Brownlie PD, Lambert R, Cooper JB, Blundell TL, Wood SP, Malashkevich VN, Hadener A, Warren MJ, Shoolingin-Jordan PM (1996) The three-dimensional structure of Escherichia coli porphobilinogen deaminase at 1.76-A resolution. *Proteins* **25:** 48-78

Louie GV, Brownlie PD, Lambert R, Cooper JB, Blundell TL, Wood SP, Warren MJ, Woodcock SC, Jordan PM (1992) Structure of porphobilinogen deaminase reveals a flexible multidomain polymerase with a single catalytic site. *Nature* **359:** 33-39

Luer C, Schauer S, Mobius K, Schulze J, Schubert WD, Heinz DW, Jahn D, Moser J (2005) Complex formation between glutamyl-tRNA reductase and glutamate-1-semialdehyde 2,1-aminomutase in Escherichia coli during the initial reactions of porphyrin biosynthesis. *J Biol Chem* **280:** 18568-18572

Lundqvist J, Elmlund H, Wulff RP, Berglund L, Elmlund D, Emanuelsson C, Hebert H, Willows RD, Hansson M, Lindahl M, Al-Karadaghi S (2010) ATP-induced conformational dynamics in the AAA+ motor unit of magnesium chelatase. *Structure* **18:** 354-365

Luo J, Lim CK (1993) Order of uroporphyrinogen III decarboxylation on incubation of porphobilinogen and uroporphyrinogen III with erythrocyte uroporphyrinogen decarboxylase. *Biochem J* **289 (Pt 2):** 529-532

Mackenzie C, Choudhary M, Larimer FW, Predki PF, Stilwagen S, Armitage JP, Barber RD, Donohue TJ, Hosler JP, Newman JE, Shapleigh JP, Sockett RE, Zeilstra-Ryalls J, Kaplan S (2001) The home stretch, a first analysis of the nearly completed genome of Rhodobacter sphaeroides 2.4.1. *Photosynth Res* **70:** 19-41

Madigan MT, Jung DO (2009) An overview of purple bacteria: systematic, physiology, and habitats. In *The Purple Phototrophic Bacteria*, Hunter CN, Daldal F, Thurnauer MC, Beatty JT (eds) pp 1-15. Dordrecht, The Netherlands: Springer

Marchler-Bauer A, Bryant SH (2004) CD-Search: protein domain annotations on the fly. *Nucleic Acids Res* **32:** W327-331

Marchler-Bauer A, Derbyshire MK, Gonzales NR, Lu S, Chitsaz F, Geer LY, Geer RC, He J, Gwadz M, Hurwitz DI, Lanczycki CJ, Lu F, Marchler GH, Song JS, Thanki N, Wang Z, Yamashita RA, Zhang D, Zheng C, Bryant SH (2015) CDD: NCBI's conserved domain database. *Nucleic Acids Res* **43:** D222-226

Martin GE, Timko MP, Wilks HM (1997) Purification and kinetic analysis of pea (Pisum sativum L.) NADPH:protochlorophyllide oxidoreductase expressed as a fusion with maltose-binding protein in Escherichia coli. *Biochem J* **325 (Pt 1):** 139-145

Martins BM, Grimm B, Mock HP, Huber R, Messerschmidt A (2001) Crystal structure and substrate binding modeling of the uroporphyrinogen-III decarboxylase from Nicotiana tabacum. Implications for the catalytic mechanism. *J Biol Chem* **276:** 44108-44116

Masuda T (2008) Recent overview of the Mg branch of the tetrapyrrole biosynthesis leading to chlorophylls. *Photosynth Res* **96:** 121-143

Masuda T, Inoue K, Masuda M, Nagayama M, Tamaki A, Ohta H, Shimada H, Takamiya K (1999) Magnesium insertion by magnesium chelatase in the biosynthesis of zinc bacteriochlorophyll a in an aerobic acidophilic bacterium Acidiphilium rubrum. *J Biol Chem* **274:** 33594-33600

Masuda T, Takamiya K (2004) Novel Insights into the Enzymology, Regulation and Physiological Functions of Light-dependent Protochlorophyllide Oxidoreductase in Angiosperms. *Photosynth Res* **81:** 1-29

Mathews MA, Schubert HL, Whitby FG, Alexander KJ, Schadick K, Bergonia HA, Phillips JD, Hill CP (2001) Crystal structure of human uroporphyrinogen III synthase. *EMBO J* **20:** 5832-5839

Mathewson JH, Corwin AH (1961) Biosynthesis of Pyrrole Pigments: A Mechanism for Porphobilinogen Polymerization1. *J Am Chem Soc* **83:** 135-137

Mauzerall D, Granick S (1958) Porphyrin biosynthesis in erythrocytes. III. Uroporphyrinogen and its decarboxylase. *J Biol Chem* **232:** 1141-1162

McGlynn P, Hunter CN (1993) Genetic analysis of the bchC and bchA genes of Rhodobacter sphaeroides. *Mol Gen Genet* **236:** 227-234

McGoldrick HM, Roessner CA, Raux E, Lawrence AD, McLean KJ, Munro AW, Santabarbara S, Rigby SE, Heathcote P, Scott AI, Warren MJ (2005) Identification and characterization of a novel vitamin B12 (cobalamin) biosynthetic enzyme (CobZ) from Rhodobacter capsulatus, containing flavin, heme, and Fe-S cofactors. *J Biol Chem* **280:** 1086-1094

McKenna A, Hanna M, Banks E, Sivachenko A, Cibulskis K, Kernytsky A, Garimella K, Altshuler D, Gabriel S, Daly M, DePristo MA (2010) The Genome Analysis Toolkit: a MapReduce framework for analyzing next-generation DNA sequencing data. *Genome Res* **20:** 1297-1303

McLean S, Hunter CN (2009) An enzyme-coupled continuous spectrophotometric assay for magnesium protoporphyrin IX methyltransferases. *Anal Biochem* **394:** 223-228

Medlock AE, Dailey HA (1996) Human coproporphyrinogen oxidase is not a metalloprotein. *J Biol Chem* **271:** 32507-32510

Minamizaki K, Mizoguchi T, Goto T, Tamiaki H, Fujita Y (2008) Identification of two homologous genes, chlAI and chlAII, that are differentially involved in isocyclic ring formation of chlorophyll a in the cyanobacterium Synechocystis sp. PCC 6803. *J Biol Chem* **283:** 2684-2692

Miroux B, Walker JE (1996) Over-production of proteins in Escherichia coli: mutant hosts that allow synthesis of some membrane proteins and globular proteins at high levels. *J Mol Biol* **260:** 289-298

Mitchell LW, Jaffe EK (1993) Porphobilinogen synthase from Escherichia coli is a Zn(II) metalloenzyme stimulated by Mg(II). *Arch Biochem Biophys* **300:** 169-177

Mochizuki N, Brusslan JA, Larkin R, Nagatani A, Chory J (2001) Arabidopsis genomes uncoupled 5 (GUN5) mutant reveals the involvement of Mg-chelatase H subunit in plastid-to-nucleus signal transduction. *Proc Natl Acad Sci U S A* **98:** 2053-2058

Moseley J, Quinn J, Eriksson M, Merchant S (2000) The Crd1 gene encodes a putative di-iron enzyme required for photosystem I accumulation in copper deficiency and hypoxia in Chlamydomonas reinhardtii. *EMBO J* **19:** 2139-2151

Moseley JL, Page MD, Alder NP, Eriksson M, Quinn J, Soto F, Theg SM, Hippler M, Merchant S (2002) Reciprocal expression of two candidate di-iron enzymes affecting photosystem I and light-harvesting complex accumulation. *Plant Cell* **14:** 673-688

Moser J, Lorenz S, Hubschwerlen C, Rompf A, Jahn D (1999) Methanopyrus kandleri glutamyl-tRNA reductase. *J Biol Chem* **274:** 30679-30685

Moser J, Schubert WD, Beier V, Bringemeier I, Jahn D, Heinz DW (2001) V-shaped structure of glutamyl-tRNA reductase, the first enzyme of tRNA-dependent tetrapyrrole biosynthesis. *EMBO J* **20:** 6583-6590

Muller AH, Hansson M (2009) The barley magnesium chelatase 150-kd subunit is not an abscisic acid receptor. *Plant Physiol* **150:** 157-166

Murakami S, Yamada N, Nagano M, Osumi M (1985) Three-dimensional structure of the prolamellar body in squash etioplasts. *Protoplasma* **128:** 147-156

Muraki N, Nomata J, Ebata K, Mizoguchi T, Shiba T, Tamiaki H, Kurisu G, Fujita Y (2010) X-ray crystal structure of the light-independent protochlorophyllide reductase. *Nature* **465:** 110-114

Nagashima KV, Shimada K, Matsuura K (1996) Shortcut of the photosynthetic electron transfer in a mutant lacking the reaction center-bound cytochrome subunit by gene disruption in a purple bacterium, Rubrivivax gelatinosus. *FEBS Lett* **385:** 209-213

Nagashima S, Kamimura A, Shimizu T, Nakamura-Isaki S, Aono E, Sakamoto K, Ichikawa N, Nakazawa H, Sekine M, Yamazaki S, Fujita N, Shimada K, Hanada S, Nagashima KV (2012) Complete genome sequence of phototrophic betaproteobacterium Rubrivivax gelatinosus IL144. *J Bacteriol* **194:** 3541-3542

Nagata N, Tanaka R, Satoh S, Tanaka A (2005) Identification of a vinyl reductase gene for chlorophyll synthesis in Arabidopsis thaliana and implications for the evolution of Prochlorococcus species. *Plant Cell* **17**: 233-240

Nakanishi H, Nozue H, Suzuki K, Kaneko Y, Taguchi G, Hayashida N (2005) Characterization of the Arabidopsis thaliana mutant pcb2 which accumulates divinyl chlorophylls. *Plant Cell Physiol* **46**: 467-473

Nandi DL (1978) Delta-aminolevulinic acid synthase of rhodopseudomonas spheroides. Binding of pyridoxal phosphate to the enzyme. *Arch Biochem Biophys* **188**: 266-271

Nandi DL, Baker-Cohen KF, Shemin D (1968) Delta-aminolevulinic acid dehydratase of Rhodopseudomonas spheroides. *J Biol Chem* **243**: 1224-1230

Nandi DL, Shemin D (1968a) Delta-aminolevulinic acid dehydratase of Rhodopseudomonas spheroides. 3. Mechanism of porphobilinogen synthesis. *J Biol Chem* **243**: 1236-1242

Nandi DL, Shemin D (1968b) Delta-aminolevulinic acid dehydratase of Rhodopseudomonas spheroides. II. Association to polymers and dissociation to subunits. *J Biol Chem* **243**: 1231-1235

Nandi DL, Shemin D (1973) -Aminolevulinic acid dehydratase of Rhodopseudomonas capsulata. *Arch Biochem Biophys* **158**: 305-311

Nasrulhaq-Boyce A, Griffiths WT, Jones OT (1987) The use of continuous assays to characterize the oxidative cyclase that synthesizes the chlorophyll isocyclic ring. *Biochem J* **243**: 23-29

Naylor GW, Addlesee HA, Gibson LCD, Hunter CN (1999) The photosynthesis gene cluster of Rhodobacter sphaeroides. *Photosynth Res* **62**: 121-139

Neidle EL, Kaplan S (1993a) 5-Aminolevulinic acid availability and control of spectral complex formation in hemA and hemT mutants of Rhodobacter sphaeroides. *J Bacteriol* **175**: 2304-2313

Neidle EL, Kaplan S (1993b) Expression of the Rhodobacter sphaeroides hemA and hemT genes, encoding two 5-aminolevulinic acid synthase isozymes. *J Bacteriol* **175**: 2292-2303

Neuberger A, Scott JJ (1953) Aminolevulinic acid and porphyrin biosynthesis. *Nature* **172**: 1093-1094

Neuwald AF, Aravind L, Spouge JL, Koonin EV (1999) AAA+: A class of chaperone-like ATPases associated with the assembly, operation, and disassembly of protein complexes. *Genome Res* **9**: 27-43

Nishijima Y, Kanesaki Y, Yoshikawa H, Ogawa T, Sonoike K, Nishiyama Y, Hihara Y (2015) Analysis of spontaneous suppressor mutants from the photomixotrophically grown pmgA-disrupted mutant in the cyanobacterium Synechocystis sp. PCC 6803. *Photosynth Res* **126**: 465-475

Nogaj LA, Srivastava A, van Lis R, Beale SI (2005) Cellular levels of glutamyl-tRNA reductase and glutamate-1-semialdehyde aminotransferase do not control chlorophyll synthesis in Chlamydomonas reinhardtii. *Plant Physiol* **139**: 389-396

Nomata J, Kitashima M, Inoue K, Fujita Y (2006) Nitrogenase Fe protein-like Fe-S cluster is conserved in L-protein (BchL) of dark-operative protochlorophyllide reductase from Rhodobacter capsulatus. *FEBS Lett* **580**: 6151-6154

Nomata J, Ogawa T, Kitashima M, Inoue K, Fujita Y (2008) NB-protein (BchN-BchB) of dark-operative protochlorophyllide reductase is the catalytic component containing oxygen-tolerant Fe-S clusters. *FEBS Lett* **582**: 1346-1350

Nomata J, Swem LR, Bauer CE, Fujita Y (2005) Overexpression and characterization of dark-operative protochlorophyllide reductase from Rhodobacter capsulatus. *Biochim Biophys Acta* **1708**: 229-237

Nott A, Jung HS, Koussevitzky S, Chory J (2006) Plastid-to-nucleus retrograde signaling. *Annu Rev Plant Biol* **57**: 739-759

O'Brian MR, Thony-Meyer L (2002) Biochemistry, regulation and genomics of haem biosynthesis in prokaryotes. *Adv Microb Physiol* **46**: 257-318

O'Gara JP, Eraso JM, Kaplan S (1998) A redox-responsive pathway for aerobic regulation of photosynthesis gene expression in Rhodobacter sphaeroides 2.4.1. *J Bacteriol* **180:** 4044-4050

O'Gara JP, Kaplan S (1997) Evidence for the role of redox carriers in photosynthesis gene expression and carotenoid biosynthesis in Rhodobacter sphaeroides 2.4.1. *J Bacteriol* **179:** 1951-1961

Ogawa T, Bovey F, Shibata K (1975) An intermediate in the phytylation of chlorophyllide a in vivo. *Plant Cell Physiol* **16:** 199-202

Oh-hama T (1997) Evolutionary consideration on 5-aminolevulinate synthase in nature. *Orig Life Evol Biosph* **27:** 405-412

Oh JI, Kaplan S (1999) The cbb3 terminal oxidase of Rhodobacter sphaeroides 2.4.1: structural and functional implications for the regulation of spectral complex formation. *Biochemistry* **38:** 2688-2696

Oh JI, Kaplan S (2000) Redox signaling: globalization of gene expression. *EMBO J* **19:** 4237-4247

Ohta H, Shibata Y, Haseyama Y, Yoshino Y, Suzuki T, Kagasawa T, Kamei A, Ikeuchi M, Enami I (2005) Identification of genes expressed in response to acid stress in Synechocystis sp. PCC 6803 using DNA microarrays. *Photosynth Res* **84:** 225-230

Oliver RP, Griffiths WT (1980) Identification of the polypeptides of NADPH--protochlorophyllide oxidoreductase. *Biochem J* **191:** 277-280

Oliver RP, Griffiths WT (1982) Pigment-protein complexes of illuminated etiolated leaves. *Plant Physiol* **70:** 1019-1025

Olson JM (2004) The FMO Protein. *Photosynth Res* **80:** 181-187

Oosawa N, Masuda T, Awai K, Fusada N, Shimada H, Ohta H, Takamiya K (2000) Identification and light-induced expression of a novel gene of NADPH-protochlorophyllide oxidoreductase isoform in Arabidopsis thaliana. *FEBS Lett* **474:** 133-136

Osanai T, Imashimizu M, Seki A, Sato S, Tabata S, Imamura S, Asayama M, Ikeuchi M, Tanaka K (2009) ChlH, the H subunit of the Mg-chelatase, is an anti-sigma factor for SigE in Synechocystis sp. PCC 6803. *Proc Natl Acad Sci U S A* **106:** 6860-6865

Osanai T, Kanesaki Y, Nakano T, Takahashi H, Asayama M, Shirai M, Kanehisa M, Suzuki I, Murata N, Tanaka K (2005) Positive regulation of sugar catabolic pathways in the cyanobacterium Synechocystis sp. PCC 6803 by the group 2 sigma factor sigE. *J Biol Chem* **280:** 30653-30659

Oster U, Bauer CE, Rüdiger W (1997) Characterization of chlorophyll a and bacteriochlorophyll a synthases by heterologous expression in Escherichia coli. *J Biol Chem* **272:** 9671-9676

Oster U, Rüdiger W (1997) The G4 Gene of Arabidopsis thaliana Encodes a Chlorophyll Synthase of Etiolated Plants. *Bot Acta* **110:** 420-423

Ouchane S, Picaud M, Reiss-Husson F, Vernotte C, Astier C (1996) Development of gene transfer methods for Rubrivivax gelatinosus S1: construction, characterization and complementation of a puf operon deletion strain. *Mol Gen Genet* **252:** 379-385

Ouchane S, Steunou AS, Picaud M, Astier C (2004) Aerobic and anaerobic Mg-protoporphyrin monomethyl ester cyclases in purple bacteria: a strategy adopted to bypass the repressive oxygen control system. *J Biol Chem* **279:** 6385-6394

Ozaki H, Ikeuchi M, Ogawa T, Fukuzawa H, Sonoike K (2007) Large-scale analysis of chlorophyll fluorescence kinetics in Synechocystis sp. PCC 6803: identification of the factors involved in the modulation of photosystem stoichiometry. *Plant Cell Physiol* **48:** 451-458

Panek H, O'Brian MR (2002) A whole genome view of prokaryotic haem biosynthesis. *Microbiology* **148:** 2273-2282

Papenbrock J, Grafe S, Kruse E, Hanel F, Grimm B (1997) Mg-chelatase of tobacco: identification of a Chl D cDNA sequence encoding a third subunit, analysis of the interaction of the three subunits with the yeast two-hybrid system, and reconstitution of the enzyme activity by co-expression of recombinant CHL D, CHL H and CHL I. *Plant J* **12:** 981-990

Pardo AD, Chereskin BM, Castelfranco PA, Franceschi VR, Wezelman BE (1980) ATP

requirement for mg chelatase in developing chloroplasts. *Plant Physiol* **65:** 956-960

Parham R, Rebeiz CA (1992) Chloroplast biogenesis: [4-vinyl] chlorophyllide a reductase is a divinyl chlorophyllide a-specific, NADPH-dependent enzyme. *Biochemistry* **31:** 8460-8464

Parham R, Rebeiz CA (1995) Chloroplast biogenesis 72: a [4-vinyl]chlorophyllide a reductase assay using divinyl chlorophyllide a as an exogenous substrate. *Anal Biochem* **231:** 164-169

Pekgöz G, Gündüz U, Eroğlu I, Yücel M, Kovács K, Rákhely G (2011) Effect of inactivation of genes involved in ammonium regulation on the biohydrogen production of Rhodobacter capsulatus. *International Journal of Hydrogen Energy* **36:** 13536-13546

Peter E, Grimm B (2009) GUN4 is required for posttranslational control of plant tetrapyrrole biosynthesis. *Mol Plant* **2:** 1198-1210

Peter E, Salinas A, Wallner T, Jeske D, Dienst D, Wilde A, Grimm B (2009) Differential requirement of two homologous proteins encoded by sll1214 and sll1874 for the reaction of Mg protoporphyrin monomethylester oxidative cyclase under aerobic and micro-oxic growth conditions. *Biochim Biophys Acta* **1787:** 1458-1467

Petersen BL, Jensen PE, Gibson LC, Stummann BM, Hunter CN, Henningsen KW (1998) Reconstitution of an active magnesium chelatase enzyme complex from the bchI, -D, and -H gene products of the green sulfur bacterium Chlorobium vibrioforme expressed in Escherichia coli. *J Bacteriol* **180:** 699-704

Petersen BL, Møller MG, Jensen PE, Henningsen KW (1999) Identification of the Xan-g Gene and Expression of the Mg-chelatase Encoding Genes Xan-f, -g and -h in Mutant and Wild Type Barley (Hordeum Vulgare L.). *Hereditas* **131:** 165-170

Pfaffl MW (2001) A new mathematical model for relative quantification in real-time RT-PCR. *Nucleic Acids Res* **29:** e45

Pfaffl MW, Horgan GW, Dempfle L (2002) Relative expression software tool (REST) for group-wise comparison and statistical analysis of relative expression results in real-time PCR. *Nucleic Acids Res* **30:** e36

Phillips JD, Warby CA, Whitby FG, Kushner JP, Hill CP (2009) Substrate shuttling between active sites of uroporphyrinogen decarboxylase is not required to generate coproporphyrinogen. *J Mol Biol* **389:** 306-314

Phillips JD, Whitby FG, Kushner JP, Hill CP (2003) Structural basis for tetrapyrrole coordination by uroporphyrinogen decarboxylase. *EMBO J* **22:** 6225-6233

Phillips JD, Whitby FG, Warby CA, Labbe P, Yang C, Pflugrath JW, Ferrara JD, Robinson H, Kushner JP, Hill CP (2004) Crystal structure of the oxygen-dependant coproporphyrinogen oxidase (Hem13p) of Saccharomyces cerevisiae. *J Biol Chem* **279:** 38960-38968

Pierson BK, Castenholz RW (1974) A phototrophic gliding filamentous bacterium of hot springs, Chloroflexus aurantiacus, gen. and sp. nov. *Arch Microbiol* **100:** 5-24

Pinta V, Picaud M, Reiss-Husson F, Astier C (2002) Rubrivivax gelatinosus acsF (previously orf358) codes for a conserved, putative binuclear-iron-cluster-containing protein involved in aerobic oxidative cyclization of Mg-protoporphyrin IX monomethylester. *J Bacteriol* **184:** 746-753

Porra RJ, Falk JE (1961) Protein-bound porphyrins associated with protoporphyrin biosynthesis. *Biochem Biophys Res Commun* **5:** 179-184

Porra RJ, Falk JE (1964) The enzymic conversion of coproporphyrinogen 3 into protoporphyrin 9. *Biochem J* **90:** 69-75

Porra RJ, Schafer W, Gad'on N, Katheder I, Drews G, Scheer H (1996) Origin of the two carbonyl oxygens of bacteriochlorophyll a. Demonstration of two different pathways for the formation of ring E in Rhodobacter sphaeroides and Roseobacter denitrificans, and a common hydratase mechanism for 3-acetyl group formation. *Eur J Biochem* **239:** 85-92

Porra RJ, Thompson WA, Kriedemann PE (1989) Determination of accurate extinction coefficients and simultaneous equations for assaying chlorophylls a and b extracted with four different solvents: verification of the concentration of chlorophyll standards by atomic absorption spectroscopy. *Biochim Biophys Acta* **975:** 384-394

Porra RJ, Urzinger M, Winkler J, Bubenzer C, Scheer H (1998) Biosynthesis of the 3-acetyl and 13(1)-oxo groups of bacteriochlorophyll a in the facultative aerobic bacterium, Rhodovulum sulfidophilum--the presence of both oxygenase and hydratase pathways for isocyclic ring formation. *Eur J Biochem* **257**: 185-191

Poulson R, Polglase WJ (1974) Aerobic and anaerobic coproporphyrinogenase activities in extracts from Saccharomyces cerevisiae. *J Biol Chem* **249**: 6367-6371

Preisig O, Zufferey R, Thony-Meyer L, Appleby CA, Hennecke H (1996) A high-affinity cbb3-type cytochrome oxidase terminates the symbiosis-specific respiratory chain of Bradyrhizobium japonicum. *J Bacteriol* **178**: 1532-1538

Pudek MR, Richards WR (1975) A possible alternate pathway of bacteriochlorophyll biosynthesis in a mutant of Rhodopseudomonas sphaeroides. *Biochemistry* **14**: 3132-3137

Pugh CE, Harwood JL, John RA (1992) Mechanism of glutamate semialdehyde aminotransferase. Roles of diamino- and dioxo-intermediates in the synthesis of aminolevulinate. *J Biol Chem* **267**: 1584-1588

Qian P, Marklew CJ, Viney J, Davison PA, Brindley AA, Soderberg C, Al-Karadaghi S, Bullough PA, Grossmann JG, Hunter CN (2012) Structure of the cyanobacterial Magnesium Chelatase H subunit determined by single particle reconstruction and small-angle X-ray scattering. *J Biol Chem* **287**: 4946-4956

Qin X, Sun L, Wen X, Yang X, Tan Y, Jin H, Cao Q, Zhou W, Xi Z, Shen Y (2010) Structural insight into unique properties of protoporphyrinogen oxidase from Bacillus subtilis. *J Struct Biol* **170**: 76-82

Radmer RJ, Bogorad L (1967) (Minus) S-adenosyl-L-methionine-magnesium protoporphyrin methyltransferase, an enzyme in the biosynthetic pathway of chlorophyll in Zea mays. *Plant Physiol* **42**: 463-465

Ralf G, Repeta DJ (1992) The pigments of Prochlorococcus marinus: The presence of divinylchlorophyll a and b in a marine procaryote. *Limnol Oceanogr* **37**: 425-433

Rand K, Noll C, Schiebel HM, Kemken D, Dulcks T, Kalesse M, Heinz DW, Layer G (2010) The oxygen-independent coproporphyrinogen III oxidase HemN utilizes harderoporphyrinogen as a reaction intermediate during conversion of coproporphyrinogen III to protoporphyrinogen IX. *Biol Chem* **391**: 55-63

Rebeiz CA, Parham R, Fasoula DA, Ioannides IM (1994) Chlorophyll a biosynthetic heterogeneity. *Ciba Found Symp* **180**: 177-189; discussion 190-173

Reid JD, Hunter CN (2004) Magnesium-dependent ATPase activity and cooperativity of magnesium chelatase from Synechocystis sp. PCC6803. *J Biol Chem* **279**: 26893-26899

Reid JD, Siebert CA, Bullough PA, Hunter CN (2003) The ATPase activity of the ChlI subunit of magnesium chelatase and formation of a heptameric AAA+ ring. *Biochemistry* **42**: 6912-6920

Reinbothe C, El Bakkouri M, Buhr F, Muraki N, Nomata J, Kurisu G, Fujita Y, Reinbothe S (2010) Chlorophyll biosynthesis: spotlight on protochlorophyllide reduction. *Trends Plant Sci* **15**: 614-624

Richards WR, Lascelles J (1969) The biosynthesis of bacteriochlorophyll. The characterization of latter stage intermediates from mutants of Rhodopseudomonas spheroides. *Biochemistry* **8**: 3473-3482

Richter ML, Rienits KG (1982) The synthesis of magnesium-protoporphyrin IX by etiochloroplast membrane preparations. *Biochim Biophys Acta* **717**: 255-264

Rippka R, Deruelles J, Waterbury JB, Herdman M, Stanier RY (1979) Generic Assignments, Strain Histories and Properties of Pure Cultures of Cyanobacteria. *Microbiology* **111**: 1-61

Roessner CA, Ponnamperuma K, Scott AI (2002) Mutagenesis identifies a conserved tyrosine residue important for the activity of uroporphyrinogen III synthase from Anacystis nidulans. *FEBS Lett* **525**: 25-28

Rüdiger W (1987) Chlorophyll Synthetase and its Implication for Regulation of Chlorophyll Biosynthesis. In *Progress in Photosynthesis Research: Volume 4 Proceedings of the VIIth International*

Congress on Photosynthesis Providence, Rhode Island, USA, August 10–15, 1986*, Biggins J (ed), pp 461-467. Dordrecht: Springer Netherlands

Rüdiger W, Benz J, Guthoff C (1980) Detection and partial characterization of activity of chlorophyll synthetase in etioplast membranes. *Eur J Biochem* **109:** 193-200

Rzeznicka K, Walker CJ, Westergren T, Kannangara CG, von Wettstein D, Merchant S, Gough SP, Hansson M (2005) Xantha-l encodes a membrane subunit of the aerobic Mg-protoporphyrin IX monomethyl ester cyclase involved in chlorophyll biosynthesis. *Proc Natl Acad Sci U S A* **102:** 5886-5891

Sancar GB, Sancar A (1987) Structure and function of DNA photolyases. *Trends in Biochemical Sciences* **12:** 259-261

Sanchez-Perez G, Mira A, Nyiro G, Pasic L, Rodriguez-Valera F (2008) Adapting to environmental changes using specialized paralogs. *Trends Genet* **24:** 154-158

Sano S, Granick S (1961) Mitochondrial coproporphyrinogen oxidase and protoporphyrin formation. *J Biol Chem* **236:** 1173-1180

Sarma R, Barney BM, Hamilton TL, Jones A, Seefeldt LC, Peters JW (2008) Crystal structure of the L protein of Rhodobacter sphaeroides light-independent protochlorophyllide reductase with MgADP bound: a homologue of the nitrogenase Fe protein. *Biochemistry* **47:** 13004-13015

Sasarman A, Chartrand P, Lavoie M, Tardif D, Proschek R, Lapointe C (1979) Mapping of a new hem gene in Escherichia coli K12. *J Gen Microbiol* **113:** 297-303

Sasarman A, Letowski J, Czaika G, Ramirez V, Nead MA, Jacobs JM, Morais R (1993) Nucleotide sequence of the hemG gene involved in the protoporphyrinogen oxidase activity of Escherichia coli K12. *Can J Microbiol* **39:** 1155-1161

Saunders AH, Golbeck JH, Bryant DA (2013) Characterization of BciB: a ferredoxin-dependent 8-vinyl-protochlorophyllide reductase from the green sulfur bacterium Chloroherpeton thalassium. *Biochemistry* **52:** 8442-8451

Schäfer A, Tauch A, Jager W, Kalinowski J, Thierbach G, Puhler A (1994) Small mobilizable multi-purpose cloning vectors derived from the Escherichia coli plasmids pK18 and pK19: selection of defined deletions in the chromosome of Corynebacterium glutamicum. *Gene* **145:** 69-73

Schmid HC, Oster U, Kogel J, Lenz S, Rüdiger W (2001) Cloning and characterisation of chlorophyll synthase from Avena sativa. *Biol Chem* **382:** 903-911

Schoefs B, Franck F (2003) Protochlorophyllide reduction: mechanisms and evolutions. *Photochem Photobiol* **78:** 543-557

Schubert HL, Phillips JD, Heroux A, Hill CP (2008) Structure and mechanistic implications of a uroporphyrinogen III synthase-product complex. *Biochemistry* **47:** 8648-8655

Schulz R, Steinmuller K, Klaas M, Forreiter C, Rasmussen S, Hiller C, Apel K (1989) Nucleotide sequence of a cDNA coding for the NADPH-protochlorophyllide oxidoreductase (PCR) of barley (Hordeum vulgare L.) and its expression in Escherichia coli. *Mol Gen Genet* **217:** 355-361

Schulze JO, Schubert WD, Moser J, Jahn D, Heinz DW (2006) Evolutionary relationship between initial enzymes of tetrapyrrole biosynthesis. *J Mol Biol* **358:** 1212-1220

Scott AI, Clemens KR, Stolowich NJ, Santander PJ, Gonzalez MD, Roessner CA (1989) Reconstitution of apo-porphobilinogen deaminase: structural changes induced by cofactor binding. *FEBS Lett* **242:** 319-324

Seehra JS, Jordan PM, Akhtar M (1983) Anaerobic and aerobic coproporphyrinogen III oxidases of Rhodopseudomonas spheroides. Mechanism and stereochemistry of vinyl group formation. *Biochem J* **209:** 709-718

Shang Y, Yan L, Liu ZQ, Cao Z, Mei C, Xin Q, Wu FQ, Wang XF, Du SY, Jiang T, Zhang XF, Zhao R, Sun HL, Liu R, Yu YT, Zhang DP (2010) The Mg-chelatase H subunit of Arabidopsis antagonizes a group of WRKY transcription repressors to relieve ABA-responsive genes of inhibition. *Plant Cell* **22:** 1909-1935

Shemin D, Kumin S (1952) The mechanism of porphyrin formation; the formation of a succinyl

intermediate from succinate. *J Biol Chem* **198:** 827-837

Shemin D, Russell CS (1953) δ-Aminolevulinic acid, its role in the biosynthesis of porphyrins and purines1. *J Am Chem Soc* **75:** 4873-4874

Shen YY, Wang XF, Wu FQ, Du SY, Cao Z, Shang Y, Wang XL, Peng CC, Yu XC, Zhu SY, Fan RC, Xu YH, Zhang DP (2006) The Mg-chelatase H subunit is an abscisic acid receptor. *Nature* **443:** 823-826

Shepherd M, Hunter CN (2004) Transient kinetics of the reaction catalysed by magnesium protoporphyrin IX methyltransferase. *Biochem J* **382:** 1009-1013

Shepherd M, McLean S, Hunter CN (2005) Kinetic basis for linking the first two enzymes of chlorophyll biosynthesis. *FEBS J* **272:** 4532-4539

Shepherd M, Reid JD, Hunter CN (2003) Purification and kinetic characterization of the magnesium protoporphyrin IX methyltransferase from Synechocystis PCC6803. *Biochem J* **371:** 351-360

SHIBATA K (1957) Spectroscopic studies on chlorophyll formation in intact leaves. *J Biochem* **44:** 147-173

Shioi Y, Sasa T (1984) Terminal steps of bacteriochlorophyll a phytol formation in purple photosynthetic bacteria. *J Bacteriol* **158:** 340-343

Shioi Y, Takamiya K (1992) Monovinyl and divinyl protochlorophyllide pools in etiolated tissues of higher plants. *Plant Physiol* **100:** 1291-1295

Shoolingin-Jordan PM (1995) Porphobilinogen deaminase and uroporphyrinogen III synthase: structure, molecular biology, and mechanism. *J Bioenerg Biomembr* **27:** 181-195

Shoumskaya MA, Paithoonrangsarid K, Kanesaki Y, Los DA, Zinchenko VV, Tanticharoen M, Suzuki I, Murata N (2005) Identical Hik-Rre systems are involved in perception and transduction of salt signals and hyperosmotic signals but regulate the expression of individual genes to different extents in synechocystis. *J Biol Chem* **280:** 21531-21538

Shpilyov AV, Zinchenko VV, Grimm B, Lokstein H (2013) Chlorophyll a phytylation is required for the stability of photosystems I and II in the cyanobacterium Synechocystis sp. PCC 6803. *Plant J* **73:** 336-346

Shpilyov AV, Zinchenko VV, Shestakov SV, Grimm B, Lokstein H (2005) Inactivation of the geranylgeranyl reductase (ChlP) gene in the cyanobacterium Synechocystis sp. PCC 6803. *Biochim Biophys Acta* **1706:** 195-203

Siepker LJ, Ford M, de Kock R, Kramer S (1987) Purification of bovine protoporphyrinogen oxidase: immunological cross-reactivity and structural relationship to ferrochelatase. *Biochim Biophys Acta* **913:** 349-358

Silva PJ, Ramos MJ (2008a) A comparative density-functional study of the reaction mechanism of the O2-dependent coproporphyrinogen III oxidase. *Bioorg Med Chem* **16:** 2726-2733

Silva PJ, Ramos MJ (2008b) Comparative density functional study of models for the reaction mechanism of uroporphyrinogen III synthase. *J Phys Chem B* **112:** 3144-3148

Simon R, Priefer U, Puhler A (1983) A Broad Host Range Mobilization System for In Vivo Genetic Engineering: Transposon Mutagenesis in Gram Negative Bacteria. *Nat Biotech* **1:** 784-791

Singh AK, Summerfield TC, Li H, Sherman LA (2006) The heat shock response in the cyanobacterium Synechocystis sp. Strain PCC 6803 and regulation of gene expression by HrcA and SigB. *Arch Microbiol* **186:** 273-286

Sirijovski N, Lundqvist J, Rosenback M, Elmlund H, Al-Karadaghi S, Willows RD, Hansson M (2008) Substrate-binding model of the chlorophyll biosynthetic magnesium chelatase BchH subunit. *J Biol Chem* **283:** 11652-11660

Sirijovski N, Olsson U, Lundqvist J, Al-Karadaghi S, Willows RD, Hansson M (2006) ATPase activity associated with the magnesium chelatase H-subunit of the chlorophyll biosynthetic pathway is an artefact. *Biochem J* **400:** 477-484

Smith AG, Francis JE (1979) Decarboxylation of porphyrinogens by rat liver uroporphyrinogen decarboxylase. *Biochem J* **183:** 455-458

Smith BB, Rebeiz CA (1977) Chloroplast biogenesis: detection of Mg-protoporphyrin chelatase in vitro. *Arch Biochem Biophys* **180:** 178-185

Smith CA, Suzuki JY, Bauer CE (1996) Cloning and characterization of the chlorophyll biosynthesis gene chlM from Synechocystis PCC 6803 by complementation of a bacteriochlorophyll biosynthesis mutant of Rhodobacter capsulatus. *Plant Mol Biol* **30:** 1307-1314

Sobotka R (2014) Making proteins green; biosynthesis of chlorophyll-binding proteins in cyanobacteria. *Photosynth Res* **119:** 223-232

Sobotka R, Duhring U, Komenda J, Peter E, Gardian Z, Tichy M, Grimm B, Wilde A (2008) Importance of the cyanobacterial Gun4 protein for chlorophyll metabolism and assembly of photosynthetic complexes. *J Biol Chem* **283:** 25794-25802

Sobotka R, Tichy M, Wilde A, Hunter CN (2011) Functional assignments for the carboxyl-terminal domains of the ferrochelatase from Synechocystis PCC 6803: the CAB domain plays a regulatory role, and region II is essential for catalysis. *Plant Physiol* **155:** 1735-1747

Sofia HJ, Chen G, Hetzler BG, Reyes-Spindola JF, Miller NE (2001) Radical SAM, a novel protein. *Nucleic Acids Res* **29:** 1097-1106

Soll J, Schultz G, Rüdiger W, Benz J (1983) Hydrogenation of geranylgeraniol : two pathways exist in spinach chloroplasts. *Plant Physiol* **71:** 849-854

Spano AJ, He Z, Michel H, Hunt DF, Timko MP (1992) Molecular cloning, nuclear gene structure, and developmental expression of NADPH: protochlorophyllide oxidoreductase in pea (Pisum sativum L.). *Plant Mol Biol* **18:** 967-972

Spiller SC, Castelfranco AM, Castelfranco PA (1982) Effects of Iron and Oxygen on Chlorophyll Biosynthesis : I. In vivo observations on iron and oxygen-deficient plants. *Plant Physiol* **69:** 107-111

Spivey AC, Capretta A, Frampton CS, Leeper FJ, Battersby AR (1996) Biosynthesis of porphyrins and related macrocycles. Part 45. Determination by a novel X-ray method of the absolute configuration of the spiro lactam which inhibits uroporphyrinogen III synthase (cosynthetase). *J Chem Soc Perkin Trans***:** 2091-2102

Stanier RY, Kunisawa R, Mandel M, Cohen-Bazire G (1971) Purification and properties of unicellular blue-green algae (order Chroococcales). *Bacteriol Rev* **35:** 171-205

Steccanella V, Hansson M, Jensen PE (2015) Linking chlorophyll biosynthesis to a dynamic plastoquinone pool. *Plant Physiol Biochem* **97:** 207-216

Stenbaek A, Hansson A, Wulff RP, Hansson M, Dietz KJ, Jensen PE (2008) NADPH-dependent thioredoxin reductase and 2-Cys peroxiredoxins are needed for the protection of Mg-protoporphyrin monomethyl ester cyclase. *FEBS Lett* **582:** 2773-2778

Stetefeld J, Jenny M, Burkhard P (2006) Intersubunit signaling in glutamate-1-semialdehyde-aminomutase. *Proc Natl Acad Sci U S A* **103:** 13688-13693

Steunou AS, Liotenberg S, Soler MN, Briandet R, Barbe V, Astier C, Ouchane S (2013) EmbRS a new two-component system that inhibits biofilm formation and saves Rubrivivax gelatinosus from sinking. *Microbiologyopen* **2:** 431-446

Straka JG, Kushner JP (1983) Purification and characterization of bovine hepatic uroporphyrinogen decarboxylase. *Biochemistry* **22:** 4664-4672

Strand A, Asami T, Alonso J, Ecker JR, Chory J (2003) Chloroplast to nucleus communication triggered by accumulation of Mg-protoporphyrinIX. *Nature* **421:** 79-83

Strauss G, Fuchs G (1993) Enzymes of a novel autotrophic CO2 fixation pathway in the phototrophic bacterium Chloroflexus aurantiacus, the 3-hydroxypropionate cycle. *Eur J Biochem* **215:** 633-643

Strnad H, Lapidus A, Paces J, Ulbrich P, Vlcek C, Paces V, Haselkorn R (2010) Complete genome sequence of the photosynthetic purple nonsulfur bacterium Rhodobacter capsulatus SB 1003. *J Bacteriol* **192:** 3545-3546

Su Q, Frick G, Armstrong G, Apel K (2001) POR C of Arabidopsis thaliana: a third light- and NADPH-

dependent protochlorophyllide oxidoreductase that is differentially regulated by light. *Plant Mol Biol* **47:** 805-813

Surpin M, Larkin RM, Chory J (2002) Signal transduction between the chloroplast and the nucleus. *Plant Cell* **14 Suppl:** S327-338

Susek RE, Ausubel FM, Chory J (1993) Signal transduction mutants of Arabidopsis uncouple nuclear CAB and RBCS gene expression from chloroplast development. *Cell* **74:** 787-799

Suzuki JY, Bauer CE (1995a) Altered monovinyl and divinyl protochlorophyllide pools in bchJ mutants of Rhodobacter capsulatus. Possible monovinyl substrate discrimination of light-independent protochlorophyllide reductase. *J Biol Chem* **270:** 3732-3740

Suzuki JY, Bauer CE (1995b) A prokaryotic origin for light-dependent chlorophyll biosynthesis of plants. *Proc Natl Acad Sci U S A* **92:** 3749-3753

Swingley WD, Blankenship RE, Raymond J (2009) Evolutionary relationships among purple photosynthetic bacteria and the origin of proteobacterial photosynthetic systems. In *The Purple Phototrophic Bacteria*, Hunter CN, Daldal F, Thurnauer MC, Beatty JT (eds) pp 17-29. Dordrecht, The Netherlands: Springer

Tait GH (1969) Coproporphyrinogenase activity in extracts from Rhodopseudomonas spheroides. *Biochem Biophys Res Commun* **37:** 116-122

Tait GH (1972) Coproporphyrinogenase activities in extracts of Rhodopseudomonas spheroides and Chromatium strain D. *Biochem J* **128:** 1159-1169

Tait GH, Gibson KD (1961) The enzymic formation of magnesium protoporphyrin monomethyl ester. *Biochim Biophys Acta* **52:** 614-616

Tajima N, Sato S, Maruyama F, Kaneko T, Sasaki NV, Kurokawa K, Ohta H, Kanesaki Y, Yoshikawa H, Tabata S, Ikeuchi M, Sato N (2011) Genomic structure of the cyanobacterium Synechocystis sp. PCC 6803 strain GT-S. *DNA Res* **18:** 393-399

Tamura K, Stecher G, Peterson D, Filipski A, Kumar S (2013) MEGA6: Molecular Evolutionary Genetics Analysis version 6.0. *Mol Biol Evol* **30:** 2725-2729

Tan FC, Cheng Q, Saha K, Heinemann IU, Jahn M, Jahn D, Smith AG (2008) Identification and characterization of the Arabidopsis gene encoding the tetrapyrrole biosynthesis enzyme uroporphyrinogen III synthase. *Biochem J* **410:** 291-299

Tang KH, Wen J, Li X, Blankenship RE (2009) Role of the AcsF protein in Chloroflexus aurantiacus. *J Bacteriol* **191:** 3580-3587

Tank M, Bryant DA (2015) Chloracidobacterium thermophilum gen. nov., sp. nov.: an anoxygenic microaerophilic chlorophotoheterotrophic acidobacterium. *Int J Syst Evol Microbiol* **65:** 1426-1430

Teakle GR, Griffiths WT (1993) Cloning, characterization and import studies on protochlorophyllide reductase from wheat (Triticum aestivum). *Biochem J* **296 (Pt 1):** 225-230

Thompson JD, Higgins DG, Gibson TJ (1994) CLUSTAL W: improving the sensitivity of progressive multiple sequence alignment through sequence weighting, position-specific gap penalties and weight matrix choice. *Nucleic Acids Res* **22:** 4673-4680

Tichy M, Beckova M, Kopecna J, Noda J, Sobotka R, Komenda J (2016) Strain of Synechocystis PCC 6803 with Aberrant Assembly of Photosystem II Contains Tandem Duplication of a Large Chromosomal Region. *Front Plant Sci* **7:** 648

Tikh IB, Held M, Schmidt-Dannert C (2014) BioBrick compatible vector system for protein expression in Rhodobacter sphaeroides. *Appl Microbiol Biotechnol* **98:** 3111-3119

Townley HE, Griffiths WT, Nugent JP (1998) A reappraisal of the mechanism of the photoenzyme protochlorophyllide reductase based on studies with the heterologously expressed protein. *FEBS Lett* **422:** 19-22

Townley HE, Sessions RB, Clarke AR, Dafforn TR, Griffiths WT (2001) Protochlorophyllide oxidoreductase: a homology model examined by site-directed mutagenesis. *Proteins* **44:** 329-335

Trautmann D, Voss B, Wilde A, Al-Babili S, Hess WR (2012) Microevolution in cyanobacteria: re-

sequencing a motile substrain of Synechocystis sp. PCC 6803. *DNA Res* **19:** 435-448

Tripathy BC, Rebeiz CA (1986) Chloroplast biogenesis. Demonstration of the monovinyl and divinyl monocarboxylic routes of chlorophyll biosynthesis in higher plants. *J Biol Chem* **261:** 13556-13564

Tripathy BC, Rebeiz CA (1988) Chloroplast Biogenesis 60 : Conversion of Divinyl Protochlorophyllide to Monovinyl Protochlorophyllide in Green(ing) Barley, a Dark Monovinyl/Light Divinyl Plant Species. *Plant Physiol* **87:** 89-94

Troup B, Hungerer C, Jahn D (1995) Cloning and characterization of the Escherichia coli hemN gene encoding the oxygen-independent coproporphyrinogen III oxidase. *J Bacteriol* **177:** 3326-3331

Tsai SF, Bishop DF, Desnick RJ (1988) Human uroporphyrinogen III synthase: molecular cloning, nucleotide sequence, and expression of a full-length cDNA. *Proc Natl Acad Sci U S A* **85:** 7049-7053

Tsukatani Y, Romberger SP, Golbeck JH, Bryant DA (2012) Isolation and characterization of homodimeric type-I reaction center complex from Candidatus Chloracidobacterium thermophilum, an aerobic chlorophototroph. *J Biol Chem* **287:** 5720-5732

Tsuzuki T, Takahashi K, Inoue S, Okigaki Y, Tomiyama M, Hossain MA, Shimazaki K, Murata Y, Kinoshita T (2011) Mg-chelatase H subunit affects ABA signaling in stomatal guard cells, but is not an ABA receptor in Arabidopsis thaliana. *J Plant Res* **124:** 527-538

Tuboi S, Kim HJ, Kikuchi G (1970a) Differential induction of fraction I and fraction II of delta-aminolevulinate synthetase in Rhodopseudomonas spheroides under various incubation conditions. *Arch Biochem Biophys* **138:** 155-159

Tuboi S, Kim HJ, Kikuchi G (1970b) Occurrence and properes of two types of delta-aminolevulinate synthetase in Rhodopseudomonas spheroides. *Arch Biochem Biophys* **138:** 147-154

van de Meent EJ, Kobayashi M, Erkelens C, van Veelen PA, Amesz J, Watanabe T (1991) Identification of 81-hydroxychlorophyll a as a functional reaction center pigment in heliobacteria. *Biochim Biophys Acta* **1058:** 356-362

van Heukelem L, Lewitus AJ, Kana TM, Craft NE (1994) Improved separations of phytoplankton pigments using temperature-controlled high performance liquid chromatography. *Mar Ecol Prog Ser* **114:** 303-313

van Niel CB (1962) The present status of the comparative study of photosynthesis . *Ann Rev Plant Physiol* **13:** 1-26

Vanzin G, Yu J, Smolinski S, Tek V, Pennington G, Maness PC (2010) Characterization of genes responsible for the CO-linked hydrogen production pathway in Rubrivivax gelatinosus. *Appl Environ Microbiol* **76:** 3715-3722

Verdecia MA, Larkin RM, Ferrer JL, Riek R, Chory J, Noel JP (2005) Structure of the Mg-chelatase cofactor GUN4 reveals a novel hand-shaped fold for porphyrin binding. *PLoS Biol* **3:** e151

Wakao N, Yokoi N, Isoyama N, Hiraishi A, Shimada K, Kobayashi M, Kise H, Iwaki M, Itoh S, Takaichi S (1996) Discovery of Natural Photosynthesis using Zn-Containing Bacteriochlorophyll in an Aerobic Bacterium Acidiphilium rubrum. *Plant Cell Physiol* **37:** 889-893

Walker CJ, Castelfranco PA, Whyte BJ (1991) Synthesis of divinyl protochlorophyllide. Enzymological properties of the Mg-protoporphyrin IX monomethyl ester oxidative cyclase system. *Biochem J* **276 (Pt 3):** 691-697

Walker CJ, Mansfield KE, Rezzano IN, Hanamoto CM, Smith KM, Castelfranco PA (1988) The magnesium-protoporphyrin IX (oxidative) cyclase system. Studies on the mechanism and specificity of the reaction sequence. *Biochem J* **255:** 685-692

Walker CJ, Mansfield KE, Smith KM, Castelfranco PA (1989) Incorporation of atmospheric oxygen into the carbonyl functionality of the protochlorophyllide isocyclic ring. *Biochem J* **257:** 599-602

Walker CJ, Weinstein JD (1991a) Further characterization of the magnesium chelatase in isolated developing cucumber chloroplasts :

substrate specificity, regulation, intactness, and ATP requirements. *Plant Physiol* **95**: 1189-1196

Walker CJ, Weinstein JD (1991b) In vitro assay of the chlorophyll biosynthetic enzyme Mg-chelatase: resolution of the activity into soluble and membrane-bound fractions. *Proc Natl Acad Sci U S A* **88**: 5789-5793

Walker CJ, Weinstein JD (1994) The magnesium-insertion step of chlorophyll biosynthesis is a two-stage reaction. *Biochem J* **299 (Pt 1):** 277-284

Walker CJ, Willows RD (1997) Mechanism and regulation of Mg-chelatase. *Biochem J* **327 (Pt 2):** 321-333

Wang KF, Dailey TA, Dailey HA (2001) Expression and characterization of the terminal heme synthetic enzymes from the hyperthermophile Aquifex aeolicus. *FEMS Microbiol Lett* **202**: 115-119

Wang P, Gao J, Wan C, Zhang F, Xu Z, Huang X, Sun X, Deng X (2010) Divinyl chlorophyll(ide) a can be converted to monovinyl chlorophyll(ide) a by a divinyl reductase in rice. *Plant Physiol* **153**: 994-1003

Wang P, Grimm B (2015) Organization of chlorophyll biosynthesis and insertion of chlorophyll into the chlorophyll-binding proteins in chloroplasts. *Photosynth Res* **126**: 189-202

Wang P, Wan C, Xu Z, Wang P, Wang W, Sun C, Ma X, Xiao Y, Zhu J, Gao X, Deng X (2013) One divinyl reductase reduces the 8-vinyl groups in various intermediates of chlorophyll biosynthesis in a given higher plant species, but the isozyme differs between species. *Plant Physiol* **161**: 521-534

Warren MJ, Jordan PM (1988) Investigation into the nature of substrate binding to the dipyrromethane cofactor of Escherichia coli porphobilinogen deaminase. *Biochemistry* **27**: 9020-9030

Warren MJ, Scott AI (1990) Tetrapyrrole assembly and modification into the ligands of biologically functional cofactors. *Trends Biochem Sci* **15**: 486-491

Wellington CL, Beatty JT (1989) Promoter mapping and nucleotide sequence of the bchC

bacteriochlorophyll biosynthesis gene from Rhodobacter capsulatus. *Gene* **83**: 251-261

Whitby FG, Phillips JD, Kushner JP, Hill CP (1998) Crystal structure of human uroporphyrinogen decarboxylase. *EMBO J* **17**: 2463-2471

Whyte BJ, Castelfranco PA (1993) Further observations on the Mg-protoporphyrin IX monomethyl ester (oxidative) cyclase system. *Biochem J* **290 (Pt 2):** 355-359

Wilks HM, Timko MP (1995) A light-dependent complementation system for analysis of NADPH:protochlorophyllide oxidoreductase: identification and mutagenesis of two conserved residues that are essential for enzyme activity. *Proc Natl Acad Sci U S A* **92**: 724-728

Williams JGK (1988) [85] Construction of specific mutations in photosystem II photosynthetic reaction center by genetic engineering methods in Synechocystis 6803. In *Methods in Enzymology* Vol. Volume 167, pp 766-778. Academic Press

Willows RD, Beale SI (1998) Heterologous expression of the Rhodobacter capsulatus BchI, -D, and -H genes that encode magnesium chelatase subunits and characterization of the reconstituted enzyme. *J Biol Chem* **273**: 34206-34213

Willows RD, Gibson LC, Kanangara CG, Hunter CN, von Wettstein D (1996) Three separate proteins constitute the magnesium chelatase of Rhodobacter sphaeroides. *Eur J Biochem* **235**: 438-443

Willows RD, Hansson A, Birch D, Al-Karadaghi S, Hansson M (2004) EM single particle analysis of the ATP-dependent BchI complex of magnesium chelatase: an AAA+ hexamer. *J Struct Biol* **146**: 227-233

Willows RD, Kriegel AM (2009) Biosynthesis of Bacteriochlorophylls in Purple Bacteria. In *The Purple Phototrophic Bacteria*, Hunter CN, Daldal F, Thurnauer MC, Beatty JT (eds), pp 57-79. Dordrecht: Springer Netherlands

Wilson K (2001) Preparation of genomic DNA from bacteria. *Curr Protoc Mol Biol* **Chapter 2:** Unit 2 4

Wong YS, Castelfranco PA (1984) Resolution and Reconstitution of Mg-Protoporphyrin IX

Monomethyl Ester (Oxidative) Cyclase, the Enzyme System Responsible for the Formation of the Chlorophyll Isocyclic Ring. *Plant Physiol* **75:** 658-661

Wong YS, Castelfranco PA (1985) Properties of the Mg-Protoporphyrin IX Monomethyl Ester (Oxidative) Cyclase System. *Plant Physiol* **79:** 730-733

Wong YS, Castelfranco PA, Goff DA, Smith KM (1985) Intermediates in the formation of the chlorophyll isocyclic ring. *Plant Physiol* **79:** 725-729

Wu FQ, Xin Q, Cao Z, Liu ZQ, Du SY, Mei C, Zhao CX, Wang XF, Shang Y, Jiang T, Zhang XF, Yan L, Zhao R, Cui ZN, Liu R, Sun HL, Yang XL, Su Z, Zhang DP (2009) The magnesium-chelatase H subunit binds abscisic acid and functions in abscisic acid signaling: new evidence in Arabidopsis. *Plant Physiol* **150:** 1940-1954

Xu K, Delling J, Elliott T (1992) The genes required for heme synthesis in Salmonella typhimurium include those encoding alternative functions for aerobic and anaerobic coproporphyrinogen oxidation. *J Bacteriol* **174:** 3953-3963

Xu K, Elliott T (1994) Cloning, DNA sequence, and complementation analysis of the Salmonella typhimurium hemN gene encoding a putative oxygen-independent coproporphyrinogen III oxidase. *J Bacteriol* **176:** 3196-3203

Yamamoto H, Kurumiya S, Ohashi R, Fujita Y (2009) Oxygen sensitivity of a nitrogenase-like protochlorophyllide reductase from the cyanobacterium Leptolyngbya boryana. *Plant Cell Physiol* **50:** 1663-1673

Yamanashi K, Minamizaki K, Fujita Y (2015) Identification of the chlE gene encoding oxygen-independent Mg-protoporphyrin IX monomethyl ester cyclase in cyanobacteria. *Biochem Biophys Res Commun* **463:** 1328-1333

Yang ZM, Bauer CE (1990) Rhodobacter capsulatus genes involved in early steps of the bacteriochlorophyll biosynthetic pathway. *J Bacteriol* **172:** 5001-5010

Ye J, Coulouris G, Zaretskaya I, Cutcutache I, Rozen S, Madden TL (2012) Primer-BLAST: a tool to design target-specific primers for polymerase chain reaction. *BMC Bioinformatics* **13:** 134

Yen HC, Marrs B (1976) Map of genes for carotenoid and bacteriochlorophyll biosynthesis in Rhodopseudomonas capsulata. *J Bacteriol* **126:** 619-629

Yildiz FH, Gest H, Bauer CE (1991) Genetic analysis of photosynthesis in Rhodospirillum centenum. *J Bacteriol* **173:** 4163-4170

Yoshinaga T, Sano S (1980a) Coproporphyrinogen oxidase. I. Purification, properties, and activation by phospholipids. *J Biol Chem* **255:** 4722-4726

Yoshinaga T, Sano S (1980b) Coproporphyrinogen oxidase. II. Reaction mechanism and role of tyrosine residues on the activity. *J Biol Chem* **255:** 4727-4731

Yu J, Shen G, Wang T, Bryant DA, Golbeck JH, McIntosh L (2003) Suppressor mutations in the study of photosystem I biogenesis: sll0088 is a previously unidentified gene involved in reaction center accumulation in Synechocystis sp. strain PCC 6803. *J Bacteriol* **185:** 3878-3887

Zaman Z, Abboud MM, Akhtar M (1972) Mechanism and stereochemistry of vinyl group formation in haem biosynthesis. *J Chem Soc Chem Commun*: 1263-1264

Zaman Z, Akhtar M (1976) Mechanism and stereochemistry of vinyl-group formation in haem biosynthesis. *Eur J Biochem* **61:** 215-223

Zeilstra-Ryalls JH, Kaplan S (2004) Oxygen intervention in the regulation of gene expression: the photosynthetic bacterial paradigm. *Cell Mol Life Sci* **61:** 417-436

Zeng Y, Feng F, Medova H, Dean J, Koblizek M (2014) Functional type 2 photosynthetic reaction centers found in the rare bacterial phylum Gemmatimonadetes. *Proc Natl Acad Sci U S A* **111:** 7795-7800

Zhao Y, Yang J, Qin B, Li Y, Sun Y, Su S, Xian M (2011) Biosynthesis of isoprene in Escherichia coli via methylerythritol phosphate (MEP) pathway. *Appl Microbiol Biotechnol* **90:** 1915-1922

Zhou S, Sawicki A, Willows RD, Luo M (2012) C-terminal residues of oryza sativa GUN4 are required for the activation of the ChlH subunit of magnesium

chelatase in chlorophyll synthesis. *FEBS Lett* **586:** 205-210

Zsebo KM, Hearst JE (1984) Genetic-physical mapping of a photosynthetic gene cluster from R. capsulata. *Cell* **37:** 937-947